Imparting Functionality to Macromolecules for Selective Stimulus Response

Evan D. Margaretta

Dissertation submitted to the faculty of the Virginia Polytechnic Institute and State University in partial fulfillment of the requirements for the degree of

Doctor of Philosophy
In
Chemistry

Timothy E. Long, Chair
Robert B. Moore
S. Richard Turner
J. Randy Heflin

May 26, 2016
Blacksburg, VA

Keywords: ionic liquids, block copolymers, stimuli response

Imparting Functionality to Macromolecules for Selective Stimulus Response

Evan D. Margaretta

ABSTRACT

Polymeric materials with inherent stimulus response represent an ever-growing area of research. In particular, block copolymers demonstrate exciting properties owing to their enhanced mechanical strength and microphase separation. Incorporating functionality into block copolymers proves useful in enhancing their utility. Presently, synthesis and subsequent post-polymerization modification achieved this for a range of block copolymers. In particular, neutralization of acid-containing polymers readily imparted ionic functionality and yielded microphase-separated block copolymer domains, enhancing polymer thermomechanical properties and ion transport. An ABA triblock copolymer composed of mechanically reinforcing polystyrene outer blocks and ionic central poly(1-methylimidazolium acrylate) block acted as a host for ionic liquid that caused an evolution in bulk morphology, resulting in enhanced ionic conductivity. The resulting membrane also exhibited a strong electromechanical actuation response under applied potential. Adding ionic liquid doped with a corresponding lithium salt enabled evaluation of sulfonated block copolymers as components of ternary polymer electrolytes, relevant for battery applications. Modification of a sulfonic acid-containing pentablock copolymer presented photocurable functional groups to the ionic domains which enabled their UV irradiation-induced curing. This novel route of modifying ion-containing block copolymers resulted in enhanced thermomechanical properties and enabled healing of physical defects in the film, unprecedented for ion-containing block copolymers.

Covalent networks represent a relevant area of research for a wide variety of applications such as coatings, adhesives, and scaffolds. Careful design of degradable crosslinkers enables stimulus response in these networks by eliminating covalent crosslinks and affording a soluble product. Extension of poly(ethylene glycol) methacrylate-based network formation into three dimensions using microstereolithography resulted in novel acid-degradable 3D-printed parts. An additional study investigated mixtures of acrylamide-modified poly(vinyl alcohol) and poly(ethylene glycol) diacrylate as water-soluble resins for the direct formation of hydrogels from solution. Photorheology and photocalorimetry investigated the thermal and mechanical changes inherent in the curing process and evaluated the mixtures as a platform for microstereolithography.

Acknowledgments

"But the Lord stood by me and strengthened me" has been the rallying cry of my time in graduate school. Paul writes this to Timothy at the end of his life (2 Tim 4:17), and how true it has been for me as well! In the good times and in the bad, in the lean times and in the rich, in my failures and in my success, this statement hold true time and time and time and time (and time) again. I would not be where I am now without the divine guidance, discernment, wisdom, correction, and ultimately salvation I've found in Jesus Christ.

My interest in polymer science was kindled by Prof. Robert Newland at Rowan University, who was the first person to force me to think about the fact that "everything is made of something" and contemplate what that really means. His description of structure-property relationships intrigued me, and off I went. His excitement for polymer science, polymer chemistry, and all things polymers is infectious. I must also acknowledge Prof. Greg Caputo for his stark realism as a professor and instructor. Taking his classes could never be called pleasant, but they were always exceedingly beneficial and indisputably fair. I've never met an instructor who wants his students to truly learn, understand, apply, and ultimately succeed as much as he does. For all the external show of being an insensitive and grumpy person, we all know that Caputo is basically a big teddy bear. His impact on the students in Rowan's department of chemistry and biochemistry cannot be overstated. I am also appreciative of Prof. Subash Jonnalagadda for pushing and encouraging me as a student, and for always challenging us to approach organic chemistry from a fundamental perspective. He is fantastically dedicated to his students, and cares tremendously for them. Finally, I will always be indebted to Prof. Lei Yu for providing me the opportunity to take

on a very open-ended, undefined, and new research project and run with it. He introduced me to ionic liquids and to polymer synthesis, and for that I will always be grateful.

My journey of graduate research would not have been possible without my advisor, Prof. Tim Long. I'm truly grateful for the opportunity he provided me and his direction throughout these years. He holds everyone in the group to an incredibly high standard but does everything he can to ensure that we meet or exceed that standard, and we are all better for it. Where Prof. Newland kindled my interest in polymer science, Prof. Long has stoked my love for it. My advisory committee of Profs. Richard Turner, Randy Heflin and Bob Moore have provided valuable feedback to me with regards to my research and professional development, and Profs. Moore and Heflin are also excellent collaborators. Other faculty who have offered their input and lent their expertise to my research and coursework include Profs. Chris Williams, Paul Deck, Abby Whittington and Lou Madsen. I must also thank Profs. Greg Liu and Paul Carlier in particular for their open ears and willingness to listen when I've needed to talk about life as a graduate student.

I would like to acknowledge the wonderful people who make the day-in and day-out slog of graduate school more bearable. Of particular note are Ken Knott, Geno Iannoccone, Murthy Shanaiah, Mehdi Ashraf-Khorassani, and Bill Bebout in analytical services; Chris Winkler, Steve McCartney, and Andrew "Gio" Giordani at the NCFL; Joli Huynh, Laurie Good, Anna Hawthorne, Valerie Owens, Naya Sou, and particularly Sharelle Carbaugh in the department of chemistry; Tom Wertalik, who blows glass like it's nobody's business; Tammy Jo Hiner, Teresa Dickerson, Cyndy Graham, and Tiffany Carpenetti with MII; Kenny Osborne and Joey Ritenour with EHS; Claire Santos, Vicki Long, Michelle Dalton, Claudia Brodkin, David Whitt, Ingrid Rowland and all the various

work-study students who work in the teaching labs; Larry Jackson, Steve Breeding, and Donnie Neel for their computer wizardry and IT black magic; Mike from Praxair who genuinely cares and makes each delivery with an ear splitting smile; and Ronny, Patty, and Diane (in particular) who have kept the Hahn labs clean and the Hahn researchers smiling each and every day.

Entire libraries could be filled with tomes devoted to extolling the virtues of Brent Bowden and his tireless facilitation of anything and everything that happens in the Long group. He is not only a super cool guy, but his willingness to always help anyone is commendable and should be imitated by all. The number of "help!" emails he receives from the Long group is innumerable, and help he always does. He is the straw that stirs the drink, the oil in the engine, the solution-in-the-back-of-the-book to that math problem that you have no idea how to approach, and the block copolymer that compatibilizes a blend of the two corresponding immiscible homopolymers. As Brent goes, so does the group. We all owe him a debt of gratitude!

I have learned many lessons in life, but perhaps the most relevant has been that what exactly it is I happen to be doing is far less important than those with whom I am doing it. Projects, events, tasks, and jobs come and go, but the souls and spirits of friends are forever. My acknowledgments of my fellow Long group researchers must start with Keren Zhang, whose friendship has been extremely important to me. I've never met a sweeter person; her personality is like an ice-cold glass of sweet tea on a humid summer day in Blacksburg. The record should officially show that Keren is so good to me. Who knew that a bacon-wrapped chicken leg would be only the start of something even better? Ashley Nelson has been a calming and encouraging presence in my life since we met. I

will always remember our monthly dinners and chats, and the sanity and clarity imparted to me in those times. Her perspective on life is refreshing. Joe Dennis has put up more than anyone else in the group with my terrible puns, loud music, and even louder voice. His friendship is invaluable, and that has been increasingly clear to me in these last few stressful months. The Long group is better off for his presence in it, even despite the occasional pentavalent carbon. David "Dingles" Inglefield also consistently goes out of his way, even since his departure from VT, to ensure that I'm doing alright and that we keep up with developments in each other's lives. Similarly, Asem Abdulahad is one of the most genuine, straightforward people I know. His advice and willingness to listen are sincerely appreciated, and I'm glad I know him and that we've kept in touch since he moved on from the group. Allison Pekkanen has been a wonderful lab mate, lab neighbor, and collaborator. Her future is particularly bright, and she blends the right amount of sass into her levity.

I would like to also acknowledge the other Long group researchers that I have had the pleasure of overlapping with here in Blacksburg for at least a little bit: my mentor Tianyu Wu, Adam Smith, Matt Green, Shijing Cheng, Renlong Gao, Steve June, Mana Tamami, Mike Allen, Nancy Zhang, Dan Buckwalter, Sean Hemp, Chainika Jangu, Alie Schultz, Daisuke Yamamoto, Alex Fersner, John Herlihy, Zhiyang Zhang, Makito Yokoe, Mingtao Chen, Ryan Mondschein, Justin "Stin" Sirrine, Kevin Drummey, Katie Valentine, Ke "Kecao" Cao, Sachin Bobade, Nick Moon, Akanksha Kanitkar, Chuck Carfagna, Maruti Hegde, Don Aduba, Philip Scott, Alex Haring, Raouf Medimagh, Motohiro Aiba, Cam Chatham, and Mariam Badawi. I'd also like to acknowledge the undergraduate students I've been able to work with: Sachin Gangele, Mick Abrahamson, Kyle Mathena, and particularly Zane Haley, who was always on time with a smile and was thinking two

steps ahead for his projects even when I wasn't. Other undergraduate researchers whose presence around lab has been particularly appreciated include Tobin "Tobes" Weiseman, Eric "Fergie" Ferguson, El-Sheba "El" Okwei, and Josh Enokida.

Productivity and sanity in graduate school simply would not have been tenable if I had never ventured outside of my research group (however fantastic) for friendship or collaborations. To that end I would like to acknowledge my collaborators in Greg Fahs and Sam Talley from Prof. Moore's group, Dong Wang from Prof. Heflin's group, Andre Stevenson from Prof. Whittington's group, and Callie Zawaski and Nick Chartrain from Prof. Williams's group. I must also thank Carl Willis of Kraton Polymers LLC, and Travis Hodgdon, Freddy Barnabas, Corey Kenneally, and Doug Graham from Procter & Gamble for their input and technical partnership on funded projects. On a less professional note, the relationships I have formed with Rachael Parker, Nathan Carter, Kristina Roth, Lindsey Anderson, Rui Zhang, Sarah Blosch, Bruce Orler, Scott Radzinski, Jeff Foster, Jeff Two, Kyle Arrington, Chad Powell, and Lindsay Johnson-soon-to-be-Dennis have been particularly enriching and encouraging. Rachael in particular has been a voice of clarity and reason through the fog of grad school stress. A special thanks to Nate for teaching me how to roast a pig!

Just as I benefited from having friends and collaborators with diverse technical backgrounds to push and expand my knowledge and understanding as a scientist, I find it particularly beneficial to have been a part of the wider Hokie community with many who know little or nothing about science. A big thanks goes to the members of VT Ultimate Frisbee Fun and Blacksburg Ultimate for helping me get my mind off of school for an hour (almost) every week during the nice weather. In particular, I would like to acknowledge

Josh Deng and Rebecca Minnick for their efforts to bring people together. Extra props to my teammates and fellow champions on Sky City, Bomb Squad, and DISCiples in VT's Ultimate Frisbee advanced intramural brackets. Nice pull! Similarly, the staff at Bollo's Café and Bakery in Blacksburg have been wonderful, and the pumpkin chocolate chip muffins cannot be recommended highly enough!

Within the broader Hokie community, I can confidently say that I have found a second home and family in Chi Alpha Christian Fellowship (VTXA). My acknowledgement section would be woefully lacking if I were to exclude any mention of the impact on my life that Pastor Anthony Saladino and his wife Michelle have had with all of their advice, prayer, and listening. Meeting up with Anthony every other week for 3 years has been one of the truly edifying experiences I've had the privilege and honor of having during my time in graduate school. Thanks for leading by example and for holding nothing back from this community. I would also like to mention the other encouraging staff members of VTXA who have foregone various life opportunities to spread joy on this campus and to encourage and exhort the students here: Jason and Caysie Martin, Jordan and Courtney Napoli, Brittnee and Eric Willoughby, Noah and Cassy Philipson, Evan and Sara Boyle, Jill and Josh Alexander, Mark and Charity Byerly, Josh and Megan Kestner, Nick and Melanie Arakaky, Kyle and Kaitlin Van Dyke, Katie Jaberg, Shannon Wimmer, Mark Wedding, and Melissa "Melkay" Kausch.

I've met several of my closest friends in and through VTXA. Nathan Wright is one of the best people I know, full stop. His willingness to be direct but always gracious with me is one of the best qualities I've ever encountered in anyone. I'm secretly glad that he's bad at science and hates it, because that led to one of the most enriching and fulfilling

friendships I'll ever know. Caleb Brooks is a great friend with a great sense of humor. I'll always remember our near-psychic nonverbal communication after years of living together. I appreciate him and his thoughtfulness and will always be challenged by his level of introspection and self-examination. Grace Grunstra is (quite fittingly) one of the most gracious people I've ever had the privilege of knowing. Her presence brightens every room she enters, and she puts everyone around her at ease. Bradley Peterson never ceases to make me laugh, and watching him find his stride as an adult and as a person has been one of my very favorite things about my time at Tech. His friendship might be my most random, but I'm glad I have it and wouldn't trade it for anything. Monte McCarthy is the most chill, most even-keeled person I know, and his calm and steady demeanor regardless of circumstances is enviable. Dana Brink is a dear friend who enriches my life simply by being in it. Nobody lives with an attitude of gratefulness quite like she does. Alyssa Brink might just be the most selfless and humble person I know. She is thoughtful and kind in a way that too few people are, and her constant joy, persistent optimism, and continual encouragement inspire me to be a better person. Her laughter and smile are infectious. John Robertson and Lili Carrillo Cala are amazing people and friends. Thanks for always keeping me accountable, for thoughtfully exhorting me in life, for being quick with a pithy rejoinder, and for pushing the limits of buck wild. Bret and Sarah "Swills" Brooks always welcome me into their lives, and I'm thankful for it. Bret is among the most intelligent and well-spoken people I've ever known, and Sarah's sweetness is instantly evident in her interactions with everyone. Standing with them on their wedding day is one of my greatest honors. The award for Most Present Neighbor goes to Andrew Alston for being the unofficial fourth roommate. His openness and willingness to meet needs as he sees them

arise set him apart from those around him. Garrett Wilcocks pursues integrity with everything he has. Katie Jaberg is a delight and is one of the strongest people I know. Shannon Wimmer giggles at everything, and it's fantastic. I'm glad she and Katie decided to return to VTXA as staff members because our community benefits immensely from their presence. Rachel Hinduja genuinely cares for everyone she meets. Sameer Hinduja took a personal interest in my life when he didn't need to, and that has meant so much to me. The parallels between his life and mine make me excited for the future.

Nick "Goobs" Huber's integrity and desire to do the right thing are evident in how he carries himself, and I will forever be thankful for his willingness to initiate uncomfortable conversations when he knows they need to happen. He is a natural leader and connects easily to people around him. Ashley Kindervater never stops selflessly serving the people around her, and even though it frustrates me sometimes, it's from a place of conviction of my own selfishness in those moments. I appreciate her kind, gentle, and cheerful personality. Kyle Van Dyke brings it like nobody else. Kaitlin Van Dyke embodies kindness and always does what needs to be done even when nobody else wants to do it, and always does it graciously with a smile on her face. Taylor Bean once described herself as "thoughtful and transparent", and I couldn't agree more with her assessment. Her readiness to talk and write about Big Life Things is commendable and pairs well with the good head on her shoulders. Caroline Omland's zeal for life is unrivaled, and it's inspiring. "Overzealous" Chris Nellis has profound insight on everyday life and how it broadly relates to bigger themes. Jackson Maxey is the most passionate person I know. I've never seen him do anything half-heartedly. David "DB" Chung has big life goals and I will be flabbergasted if he doesn't achieve them. His desire to learn and to turn knowledge into

understanding and understanding into tangible help for people in need will serve him well in the future. Mark Wedding is one of the most interesting men in VTXA and can make orange juice with apples instead of oranges. His character is evident in his sensitivity to the emotions and feelings of others around him. Rachel Stahle's wisdom and maturity never cease to amaze me. She has an amazing innate ability to encourage people by saying what they *need* to hear in a way that makes them *want* to hear it, and that's truly a rare and precious trait. Sheng Tan and I are very different, because he's almost always doing something incredibly meaningful for somebody else. Romico "Meeks" Macatula always comes through in the clutch. Always.

I could go on and on and on about so many people, in no particular order, that I've met through VTXA who have positively impacted my life, taught me some lesson, or encouraged me in some way, even if indirectly or unknowingly: Ethan O'Connell, Jerrell Crews, Lee-Pin Shing, Justin "Stin" Kobayashi, Zach Baker, Sam Barnes, Quinton Ivey and Mel Quinones, Lauren Keating, Felicity Smith, Ryne and Jenna Noska, Hannah Vega, Rachel Nissen and Sam Lawton, Rachel Miller, Katie and Angelyn Newberger, Stephen G. Law, Elena and Travis Markham, Tina Ko, Luigi-John Santos, Courtney Bullock, Alex Boyle, Ramon Sigala, Zach Gilchrist, Grace and Irene Howell, Jacob Boston, Jeff and Laura Draudt, Ike and Jake Barnard, Monica Li, Elliot George, Yaw Ansah, Meagan Lovejoy, Yi Gao and Hannah Ulrich, Shuaiya Wang, Tim Einstein, Russell "Sprouts" Bradley, Jacque Zook, Lauren Alexander, Taylor Kroeller, Monica Fikes, Qian Wang, Collin Grant, Jordan "The Original J-Riles" Riley, Justin "The Real J-Ryals" Ryals, Ed Turner, Jamar "Jam-Wheezy" Nealy, Benjamin Thomas Knoop Ackerman, Jack and Emily Cooper, Thomas Lawson, Medi Kikoni, Nate Lawton, Jonathan Dinschel, Bernard "Nard"

Lee Hayward III, David Marshall, Alyssa “Ambush” Bushhouse, Kara Meyer, Emma Ramsis, Elissa Kim, Jordan White, David Henderson, Xikai “Sir” Zhao, Grant Spence, Alex Cumbie, Patrick Hurst, Spencer Annis, Hannah Gray, Becca Goodhart, Luke Miller, Benton Stickley, Grayson Daffron, Shem Kentish-Smith, Jia Liu, Alex DeRieux, David Cyprian Hicks, Devin Vandyke, Bethany Hartman, Brittany “BCroft” Croft, Klint Ciriaco, Wes and Morgan Childress, Patrick Lestyan, Dave Richards, Laura Sakmyster, Paul Cupp, Shannon Rodgers, Laura Ferlazzo, Hannah Rodriguez, Kendall Shafran, Eliana “El” Marrs, Ashley Yuan, Corrie Chamberlin, Sarah Turner, Mary Rose Lunde, Leah “Jean Holes” Jones, Zach Kemp, Hoy Lee, Ben Slaughter, Morgan Alexander, Bethany Lyon, Serena Blalock, Ashley and Caitlyn Hearst, Taylor Allen, Stefanie Froelich, Jordan O’Donnell, Jen Rubio, Ashley Moreno, Ariana Colligan, Andrea Kuliasha, Chris Jones, Drew and Nathan Roethlisberger, Robert Salama, Ben Lyon, Josiah Noska, Rachel Prill, Stephen Lucas, Brian Moore, David “Dandy” Anderegg, Ray Hu, Rebekah Youngk, Rob Kidane, Sue Kim, Jonathan Kerlin, Heston Anderson, Ryan “Butters” Butterfield, Jean Janvier, Luke Lapham, Ciara Craddock, Luke and Vince Loparo, Jared King, Nick Acree, E.L. Smiling, Sam Ahn, Kevin Wright, Biruk Amare, Will Newlon, Caylon Minor, Frank Taylor, Jeremy Ilang-Ilang, Michael Burton, Caleb Notheis, Olivia Grim, Erin Johnson, Amy Davis, Ayana Stukes, David Maeng, Cam Overton, Amber Messick, Travis Cruz, Brittany Sutton, Alex Ashamole, Jared Solomon, Luke DiPette, Alex Earley, Ben Anderson, Josh Kobayashi, Petey Mainardi, Joshua Worrell, “Big” John Rebman, Vamsi Dhananjay, and (who could ever forget) Jordan Halvorsen. Ann and R Brooks, Bernie and Ruth Grunstra, Tim and Lisa Wright, Tom and Theresa Huber, and Paul and Kathy Gray have not only raised wonderful children but have graciously extended their hospitality and

warmth to me over these last few years. I'm sure there are so many others. I'll always miss Darren Hankins, the meaningful and insightful conversations I had with him, and his thought-provoking questions.

I also need to acknowledge my friends "back home" in New Jersey who have offered their support to me over these last few years. Jillian Utter taught me a lot about life and relationships, and encouraged me to pursue graduate education. My friendship with her taught me a lot about myself. Joseph Diaz came into my life out of nowhere in 2014 even though he lived "just three miles down the road" from me my whole life. His doggedly optimistic pursuit of his dreams inspires me, as does his ability to shift seamlessly from the light to the weighty matters in life. Jon D'Angelo relates with people on a level rarely seen, and he has a tremendous hunger for meaningful interactions. Alex Billig embodies sass but never lets that get in the way of encouraging me. She's doing big things with her life. Shane Smith has been a dear friend and has shown his loyalty as a friend time and again. Alan Kahn reminds me of a much cooler and less nerdy version of myself. I enjoy our shared interests and picking his mind. Josh Sponring has an immensely calm and mature personality inconsistent with his young age. I walk away encouraged every time I see him. Kevin Feliciano is one of my oldest friends, and I plan to keep it that way. I'm thankful for his ability and desire to see how little circumstances fit into the bigger picture of life, and to see trends in seemingly unrelated areas. Joelle Hayes has a brilliant mind and I always enjoy her company. Sarah Moore has been on the receiving end of so many long diatribes and thought experiments from me while I was at my worst. I will forever be grateful for her grace in hearing me out and the wisdom in her replies. Connor Walsh's presence is readily welcomed in any room on account of his well-timed jokes and overall thoughtful

addition to conversation. The entire Sender family has welcomed me as one of their own, and I have always seen them as an extension of my own family. I can't remember life without them in it, and I am forever grateful for Saul and Lucy, David and Irene, and Rachel. Mike and Christine Ducane, Bill and Cindy Higgins, and Ed and Ellie Feliciano have also extended their grace and hospitality to me time and time again since my teenage years. I'm thankful for them and their children and every conversation I've ever had with them. They are role models who lead by example. Brian and Victoria Higgins are amazing friends who always check in on me. Brian has wisdom far beyond his years and I've learned so much from him in the approximately 1000 hours (not an exaggeration or hyperbole from me) we have spent together in my car. I am convinced that Tori is the friendliest person on the face of this earth. Growing up alongside Brian and watching him go from a chump teenager to a leader and influencer of people has been one of my biggest joys in life. It is an immense honor to have been a part of their wedding. David and Chelsea Ducane are similarly wonderful. David carries himself with quiet dignity that belies his goofy sense of humor. His kindness has meant so much to me. Chelsea is the best friend I've ever had: she is wise; she is gracious, she is willing to have hard conversations and tell me what I need to hear even when that isn't what I want to hear; her support is unwavering. She has been one of the constant and clearest sources of encouragement in my life since we first became friends, and my time in Blacksburg has only highlighted that.

My family also warrants acknowledging for their support and encouragement through these years. On the Margaretta side: Emmaleigh; Jesse; Hannah; Zachary; Jennifer; Lauren; Tom and Briana; Janel and Perri; Susan, Nancy, Mike, and Lily; Matt, Ruby, Kayla, Alyssa, and Jenna; Michael, Kristen, Madison, and Jordan; Uncle Rick and Aunt

Danielle; Aunt Leslie and Uncle Joe; Uncle Bill and Aunt Toni; Uncle John and Aunt Elaine; Aunt Judy and Uncle Richard; and Aunt Kathy and Uncle Robert. I will forever miss Aunt Kathy and appreciate the sense of creativity she brought to the family. On the Ambroziak side: Mike; Danny; Matt and Florencia; Bryan, who left us too soon; Uncle Lenny and Aunt Carol; and Uncle Ish and Aunt Linda. You're wonderful people who have helped shape me into the person I am today. I must also acknowledge my brother, Doug, who is the first Margaretta Hokie and one of my biggest sources of motivation. He is the smartest person I know, capable of anything he puts his mind to. His drive and desire are inspiring and watching him realize his goals as I've strived towards mine has brought me immeasurable joy. I'm proud to call him my brother and my friend. Finally, I must acknowledge my parents, Dave and Irene, who have done everything possible within their power to put me in a place where success was imminent and attainable. My parents have at times changed jobs and taken pay cuts to be able to spend more time with our family, and picked up overtime hours to make ends meet. They taught me and Doug the value of hard work and saving money, but not at the expense of enjoying life. I've always had their unwavering support and unceasing prayer. Dad taught me always to "do the right thing" from a very young age, and he has lived up to the standard he set. Mom never does anything without first considering the best interests of everyone else. She has the biggest heart of anyone I've ever known, and she bends over backwards to ensure that everything is just-so for everyone else. I'm exceedingly thankful for their steadfast presence in my life, and I love them deeply. I owe them so much of my success.

Attributions

Prof. Timothy E. Long
: Professor of Chemistry at Virginia Tech and research advisor

Dr. David L. Inglefield, Jr.
: Past graduate student in Dr. Long's research group who contributed to Chapter 4.

Dr. Chainika Jangu
: Past graduate student in Dr. Long's research group who contributed to Chapter 4.

Mingtao Chen
: Graduate student in Dr. Long's research group who contributed to Chapter 5.

Dr. Zhiyang Zhang
: Past post-doctoral researcher in Dr. Long's research group who contributed to Chapter 5.

Dr. Maruti Hegde
: Post-doctoral researcher in Dr. Long's research group who contributed to Chapter 6.

Ryan J. Mondschein
: Graduate student in Dr. Long's research group who contributed to Chapter 6.

Allison M. Pekannen
: Graduate student in Dr. Long's research group who contributed to Chapter 7.

Justin M. Sirrine
: Graduate student in Dr. Long's research group who contributed to Chapter 8.

Sachin Gangele
: Past undergraduate student in Dr. Long's research group who contributed to Chapter 6.

Robert "Zane" Haley
: Past undergraduate student in Dr. Long's research group who contributed to Chapter 7.

Prof. J. Randy Heflin
: Professor of Physics at Virginia Tech and collaborator on Chapter 4.

Dr. Dong Wang
: Past graduate student in Dr. Heflin's research group who contributed to Chapter 4.

Prof. Robert B. Moore
: Professor of Chemistry at Virginia Tech and collaborator on Chapters 4 and 6.

Gregory B. Fahs
: Graduate student in Dr. Moore's research group who contributed to Chapter 4.

Samantha J. Talley
: Graduate student in Dr. Moore's research group who contributed to Chapter 6.

Prof. Christopher B. Williams
: Assistant Professor at Virginia Tech in Mechanical Engineering and collaborator on Chapter 7.

Nicholas A. Chartrain
: Graduate student in Dr. Williams's research group who contributed on Chapter 7.

Dr. Donald C. Aduba, Jr.

Post-doctoral researcher in both Dr. Williams's and Dr. Long's research groups who contributed on Chapter 7.

Dr. Charles S. Carfagna, Jr.

Facilities manager at the Macromolecular Materials Discovery Center who contributed to Chapter 8.

Table of Contents

Chapter 1: Introduction

1.1 Dissertation overview

This dissertation focuses on the effects of incorporating functionality into macromolecular materials with an emphasis on the post-polymerization of block copolymers to selectively impart ionic groups. Chapter 2 reviews the synthetic strategies employed towards hyaluronic acid-based block- and graft- copolymers, as well as their biomedical applications. Chapter 3 provides a review of degradable covalent networks. It offers a summary of the various functional groups that enable degradation in response to an external stimulus and some of their relative advantages and disadvantages. A perspective on the future of the field suggests exploiting well-established small-molecule chemistry to investigate networks with precisely tailorable response profiles to meet the demands of emerging technology.

Chapter 4 details the synthesis, post-polymerization modification, and characterization of ABA triblock copolymers. Incorporation of ionic liquid to the ion-containing central block caused a change in polymer bulk morphology and enabled the construction of a structure-morphology-property relationship. The ionic liquid-containing polymer exhibited a mechanical response to an applied potential, establishing its potential as an electroactive device. Chapter 5 reports the composition-property relationship of sulfonated polymers and ionic liquids, as well as the composition-property relationship of an ionic liquid and its lithium salt analog. Extending these comparisons to novel compositions of a lithium sulfonate-containing ABA triblock copolymer, lithium salt, and

ionic liquid provided a platform for future evaluation of sulfonate-containing polymers for ternary polymer electrolyte applications.

Chapter 6 examines the neutralization of a sulfonic acid-containing styrenic pentablock copolymer with a UV-curable amine. Membranes formed from the resulting ion-containing polymer demonstrated enhanced thermomechanical properties and the ability to heal physical defects. Chapter 7 focuses on incorporating stimuli-labile sites into covalent network to enable chemical degradation of objects 3D-printed using microstereolithography. Chapter 8 discusses photocured acrylamide-modified poly(vinyl alcohol) as a potential platform for directly 3D-printing pre-swollen hydrogels with microstereolithography. Chapter 9 provides some overall conclusions for the dissertation and Chapter 10 details some potential future work.

Chapter 2: Hyaluronic Acid Copolymers for Emerging Biomedical Applications

2.1 Abstract

Polysaccharide block and graft copolymers display many interesting properties for use in biological settings, owing to the physical characteristics and chemical versatility of the polysaccharide segment. Researchers widely study the incorporation of hyaluronic acid, one such polysaccharide, into block and graft copolymers with numerous synthetic materials possessing diverse properties. Specifically, hyaluronic acid-containing copolymers and their self-assembled nanostructures display suitability for a variety of biomedical applications such as drug delivery, nonviral gene delivery, and tissue engineering scaffolds.

2.2 Introduction

Both the physical and chemical properties of polysaccharides prove their importance in biological settings. In addition, polysaccharides continue to play an ever increasing role in the field of polymer chemistry as researchers investigate the incorporation of naturally occurring and biodegradable polysaccharides into applications where purely synthetic materials previously dominated such as food packaging[1] and anticorrosion coatings.[2] Block and graft copolymers of polysaccharides often display properties suitable for a wide variety of applications such as controlled-release tablets,[3] nonviral gene delivery,[4,5,6] amphiphilic suspension agents,[7] anticoagulants,[8] and fluorescent nanoparticles for the study of protein-carbohydrate interactions.[9] Furthermore, when the components of block or graft copolymers have different properties, self-assembly of nanostructures becomes possible. Intermolecular forces such as hydrophobic interactions, hydrogen bonding, dipole-dipole forces, and electrostatic interactions play

key roles in the self-assembly of particles. The biocompatibility and self-assembly of block and graft polysaccharide copolymers often provide suitable properties for biomedical applications.

The polysaccharide hyaluronic acid (HA), also known as hyaluronan or hyaluronate, features a repeat unit of alternating (1→4)-β linked D-glucuronic acid and (1→3)-β linked *N*-acetyl-D-glucosamine saccharides[10,11,12] (**Figure 2.1**). HA plays multiple roles in the extracellular matrix (ECM) including steric interactions for regulating molecular motion[13] and physical support in cartilage where it forms 10^5 kDa supramolecular structures with aggregan.[14] Aggregan falls under the class of proteins called proteoglycans which feature with covalently attached oligo- or polysaccharides. These high molecular weight structures that result from the association of HA with aggregan maintain structural support in cartilage. HA provides physical support, maintains viscosity in joint synovial fluid and in the vitreous body of the eye,[11] and aids in regulation of tissue hydration.[11,14]

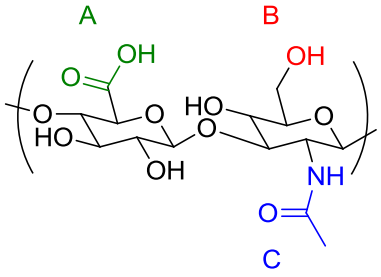

Figure 2.1. Structure of HA that highlights (A) the carboxylic acid, (B) the primary hydroxyl, and (C) the *N*-acetamide reactive groups, which allow for its chemical modification.

The wide variety of HA's molecular weight-dependent applications truly proves its versatility. For instance, HA of molecular weight 10^5-10^7 Da provides physical support and aids in immunosuppression[15] but hinders angiogenesis[16] because of its space-filling properties in the ECM. HA chains of less than 50 repeat units show anti-inflammatory properties.[17] Interestingly, chains of this size also display the ability to enhance angiogenesis,[18] which owes to the drastically reduced size of the HA fragments. Oligomeric HA containing less than 10 repeat units induces heat-shock proteins,[19] which cells express at elevated temperatures or in the presence of other stress, and also acts a cell signal.[20] More specifically, the interaction between HA and the receptor CD44 triggers a large number of widely studied transduction pathways.[20] Cancerous cells often overexpress the CD44 receptor, allowing HA-containing materials to selectively target tumors.

2.3 Chemical Modification of HA

Each repeat unit of HA features a carboxylate, a primary hydroxyl, and an *N*-acetyl group; each of these allows for chemical modification. Researchers employ a wide variety of diverse reactions to modify HA.[12] In order to perform many of the following reactions, a tetrabutyl ammonium (TBA) or similarly hydrophobic cation must act as the counterion to the carboxylate of HA. These hydrophobic cations aid HA's solubility in polar organic solvents such as dimethyl sulfoxide, in which the acidic or sodium salt forms of HA do not dissolve.

The carboxylate engages in amidation reactions with amines, often in the presence of activators such as carbodiimides,[21] triazines,[22] 1,1'-carbonyldiimidazole,[23] or 2-chloro-1-methylpyridinium iodide.[24] Esterification reactions occur with alkyl halides[25] or with primary alcohols such as methanol in the presence of a diazomethane activator.[26]

Additionally the carboxylate reacts with tosylate-modified diols[27] to yield crosslinked hydrogels with diester linkages. Another esterification reaction involves treatment with glycidyl methacrylate to yield methacrylated HA which readily undergoes photoinitiated radical crosslinking.[28] Another reaction employed in the modification of carboxylate is four-component Ugi condensation with formaldehyde, cyclohexyl isocyanide, and a diamine such as lysine.[29]

Divinyl sulfone[30,31,32] and ethylene sulfide[33] each react with the primary hydroxyl to form ethers (**Figure 2.2**). Due to the difunctionality of divinylsulfone, that reaction results in a crosslinked HA network. Epoxides may react in a fashion similar to ethylene sulfide, but changing the reaction conditions leads to esterification of the carboxylate as described above.[12] Difunctional epoxides such as butanediol diglycidyl ether lead to the formation of crosslinked networks.[34] Additionally, the primary hydroxyl also forms esters with a wide variety of compounds under varying reaction conditions.[12] Treatment with glutaraldehyde leads to hemiacetal formation,[32] reacting with cyanogen bromide forms a carbamate,[35] and sodium periodate oxidizes the alcohol to an aldehyde.[36]

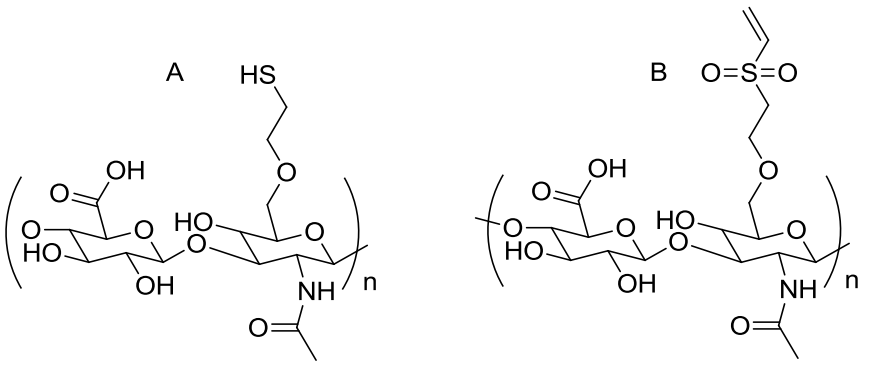

Figure 2.2. Products obtained when the primary hydroxyl of HA is reacted with (A) ethylene sulfide and (B) divinyl sulfone. The remaining vinyl group also undergoes the same reaction, leading to a crosslinked HA network.

Significantly fewer reactions that modify the *N*-acetyl group occur relative to the carboxylate and primary hydroxyl functional groups. Reduction of the amide with hydrazine yields an amine which can further react with carbodiimide-activated carboxylic acids to yield a different amide.[23] Researchers rarely employ these reactions due to both the multistep nature of the modification and the ease of performing amidation at the carboxylate. The benefit of these reactions involves the preservation of the ionic character of the HA with addition of an amide side chain.

Modified HA also self assembles into nanoparticles if the given pendant substituent possesses sufficient hydrophobicity. Examples of such pendant species include 5β-cholanic acid[37] and ceramide.[38,39] For instance, HA modified through amidation with 5β-cholanic acid, a cholesterol derivative, self-assembled through hydrophobic interactions in aqueous media to yield nanoparticles with 5β-cholanic acid cores and HA shells.[37] Further modification with the anionic fluorescent label Cy5.5 allowed tracking of cellular uptake of the HA nanoparticles. Nanoparticles synthesized with differing degrees of 5β-cholanic acid modification exhibited no real difference in cellular uptake, as expected due the responsibility of the nanoparticles' outer HA shell for uptake. However, increasing the extent of HA modification caused decreasing nanoparticle size as the pendant 5β-cholanic acid groups interacted more closely (**Figure 2.3**).[37]

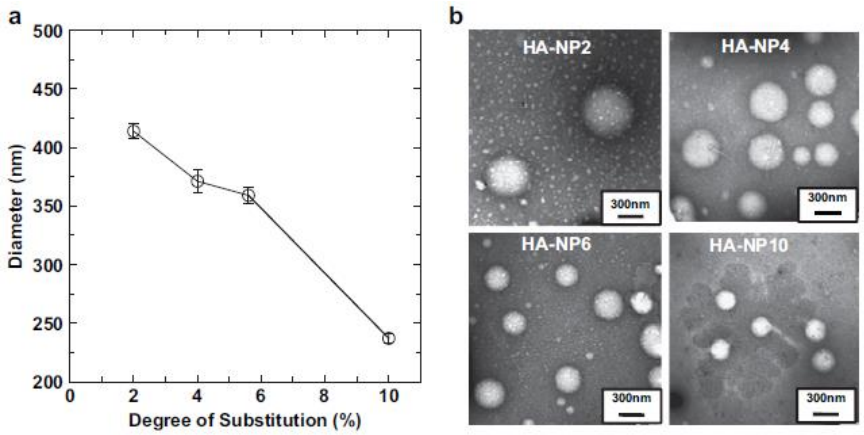

Figure 2.3. Dynamic light scattering (DLS) and transmission electron microscopy (TEM) show the decreasing diameter of HA nanoparticles with increasing degree of substitution with 5β-cholanic acid. This image was adapted from Reference 37.

Further investigation done on HA-cholanic acid nanoparticles involved mineralization with calcium nitrate and ammonium phospate and subsequent loading with doxorubicin.[40] Mineralization caused the nanoparticles to shrink from 260 nm to 140 nm; however, the nanoparticle size increased when exposed to an acidic environment, displaying pH-responsive degradation of the mineral domains.[40]

2.4 HA in Supramolecular Coacervates and Hydrogels

2.4.1 Coacervates

HA affords myriad avenues for chemical modification. Additionally, the polyanionic character of HA also allows for supramolecular chemistry through electrostatic interactions. The resulting coacervates show many interesting properties. The complex coacervation of mussel adhesive protein features prominently in literature and these marine creatures inspired a number of attempts to synthetically mimic the underwater adhesive properties of their protein coacervates. Stewart[41] wrote a broad overview of these efforts, which include attempts to form coacervates of recombinant or hybrid mussel protein with

HA.[42,43] Additionally, HA also forms coacervates with other compounds such as silk fibroin[44] and chitosan.[45,46,47]

In the case of HA-chitosan coacervates, researchers observed the formation of spherical capsules[47] and also achieved double-walled microspheres[46] through the emulsification-coacervation method. The spherical capsules possessed diameters ranging from 590-1550 μm depending on coacervation conditions such as HA concentration and environmental pH.[47] Thus, researchers synthesized gels of chitosan and HA that allowed the encapsulation of model compounds Cyclosporine A and bovine serum albumin[48] in addition to the anticoagulant heparin.[49]

Similarly, addition of HA to poly(L-lysine)-*b*-poly(lactic acid) AB diblock copolymers yielded micellar structures coated with HA.[50] PLL-*b*-PLA forms nanoscale micelles that feature a PLA core and cationic PLL shell which interacts with anionic polysaccharides such as HA, heparin, or carboxymethyl-dextran upon their addition. In this case the HA surface layer enhanced the specificity of the polyionic-complexed micelles compared to heparin or carboxymethyl-dextran surface layers, which allowed the selective targeting through CD44-mediated endocytosis of sinusoidal endothelial liver cells which transport oxygen and nutrients from the bloodstream into the liver.[50]

2.4.2 Hydrogels

Crosslinked hydrogels of HA show properties suitable for tissue engineering such as minimal toxicity, appropriate modulus, and good porosity.[51,52,53,54] Various synthetic routes employing the likes of Diels-Alder cycloaddition,[52] photoinitiated radical addition,[53] Michael-type addition to divinyl sulfone,[55] or thiol-ene[33] addition yielded HA-based hydrogels. This review focuses on HA-containing copolymers. For further reading on the

therapeutic applications of HA homopolymer-based materials and hydrogels, the author recommends the excellent reviews from Burdick,[56] Chung,[54] Allison,[57] and Balasz.[58]

Carbodiimide-activated coupling of 2,2'-ethylenedioxy-bis(ethylamine) to the carboxylates of HA provided crosslinked nanoparticles of size <110 nm.[59] Various reaction conditions such as ionic strength, pH, HA concentration, and stoichiometric ratio of crosslinker all impacted the final particle size when varied. However, dynamic light scattering (DLS) investigation of nanoparticle size showed bimodal distribution owing to the aggregation of the nanoparticles. Increased salt content in the synthesis medium more efficiently screened the electrostatic interactions and helped to prevent the formation of larger particles.[59] Additionally, increasing the amount of crosslinker from 7% to 25% stoichiometric ratio led to smaller diameters.

2.5 HA-containing Block and Graft Copolymers

Ring opening polymerization, coupling, enzymatic polymerization, and radical polymerization all afford polysaccharide-containing block copolymers.[60] Coupling of HA with pre-prepared synthetic polymers yields HA-containing block copolymers. In the case of HA-containing graft copolymers, researchers employ the grafting-to approach more commonly than the grafting-from method although examples of the latter exist. [61,62,63]

HA forms block copolymers with synthetic polymers such as poly(ethylene oxide)[64] (PEO) through oxime click, poly(2-ethyl-2-oxazoline)[65] through amine coupling, and poly(benzyl-L-glutamate)[66,67,68] (PBLG) through Huisgen alkyne-azide cycloaddition. In each case, reductive amination of HA with sodium cyanoborohydride yielded a reactive chain end which underwent subsequent modification to feature a terminal alkyne in the case of blocking with poly(benzyl-L-glutamate). Another similar block copolymer features

a poly(lactic acid-*co*-glycolide) (PLGA) block in addition to a block of HA. Again, sodium cyanoborohydride reduced the chain end of HA to yield an amine, which further reacted with *N*-hydroxysuccinimide-terminated PLGA to yield HA-*b*-PLGA.[69]

Synthetic vesicles called polymersomes display interesting characteristics and result from the self-assembly of amphiphilic block copolymers in solution. The spherical structure allows encapsulation of small molecules and therefore mimicry of vesicles such as naturally occurring endosomes and artificially prepared liposomes. As such, block copolymers containing HA prove able to form polymersomes provided sufficient hydrophobicity of the second block. For instance, HA-*b*-PBLG displayed the ability to form polymersomes[66,67,68,70] and encapsulate antitumor drugs such as doxorubicin and docetaxel. A benefit of HA-containing polymersomes for drug delivery results from the natural occurrence of HA within the body, which provides an enzymatic route for its biodegradation[70] with hyaluronidase.

Treatment of HA with ammonium persulfate allows radical addition of acrylonitrile[61] or acrylic acid[62] (AA) in a grafted-from method. The use of ceric ammonium nitrate in acidic solution allows grafting of hydroxyethyl methacrylate (HEMA) from the HA backbone.[63] Grafted-to copolymers of HA and other biocompatible polymers such as poly(L-lysine) (PLL) or poly (ethylene glycol) (PEG) feature prominently in the literature. Carbodiimide coupling affords HA-*g*-PLGA[71] and also PEG-grafted HA,[72] although the latter requires acidic conditions. Poloxamer, which consists of an ABA triblock copolymer of PEG as the hydrophilic A blocks and poly(propylene glycol) (PPG) as the hydrophobic B block, also links to HA through carbodiimide coupling when modified with terminal amines.[73] Carboxylate endcapped poly(*N*-isopropyl acrylamide) (PNIPAM) adds to amine-

modified HA through amide linkages to provide HA-g-PNIPAM.[74] Modification of poly(lactic acid) (PLA) with *N*-hydroxysuccinamide and subsequent addition to HA in the presence of diethylamine catalyst yields HA-*g*-PLA.[75,76]

Both HA-*g*-PLGA[71] and HA-*b*-PLGA[37] self-assembled into core-shell micellar nanoparticles in aqueous conditions. In both cases, hydrophobic PLGA formed the core and encapsulated the antitumoral drug doxorubicin as HA formed the outer shell. The HA-*b*-PLGA nanoparticles displayed diameters <60 nm, which increased with increasing extent of doxorubicin loading.[37]

Nanoparticles of HA-*g*-PLGA decreased in diameter with increasing graft density. Additionally, doubling the molecular weight of the PLGA grafts led to a drastically reduced diameter, owing to the increased weight percentage of PLGA in the nanoparticle composition. For instance, nanoparticles bearing 5,000 g/mol $\bar{M}_w$ PLGA grafts on 8.6% of HA repeat units displayed a diameter of 539.4±8.8 nm as determined through DLS, a nanoparticles containing 10,000 g/mol $\bar{M}_w$ PLGA grafts on 5.4% of HA repeat units displayed a diameter of just 98.4±3.7 nm.[71]

In some cases, researchers grafted HA onto a preexisting polymer backbone such as PLL[77,78] or branched poly(ethylene imine) (PEI).[79] Synthesis of PLL-*g*-HA typically consists of reductive amination with sodium cyanoborohydride of the HA reducing end and covalent coupling with the pendant primary amine of PLL[77] (**Scheme 2.1**). Synthesis of PEI-*g*-HA utilizes carbodiimide coupling.[79] These examples provide a foundation for further exploration of HA as a graft in copolymers.

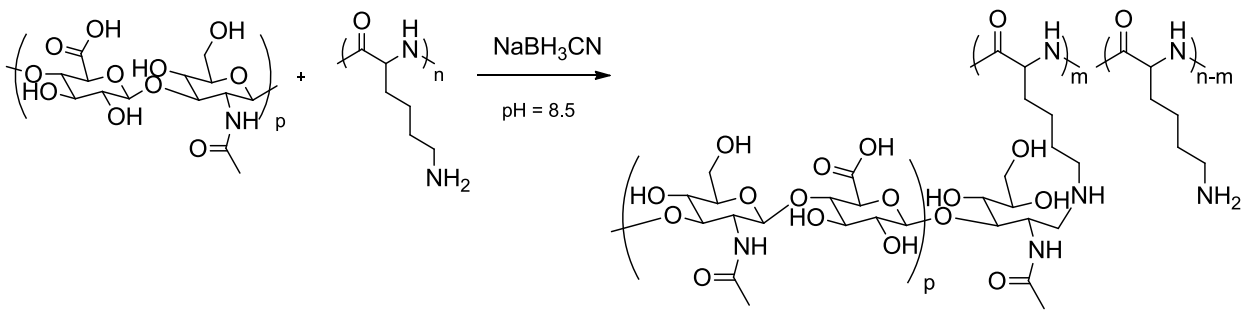

Scheme 2.1. Structure of PLL-*g*-HA prepared through sodium cyanoborohyride coupling in basic conditions.

Generic crosslinking of modified HA with a difunctional polymer yields a hydrogel. In some cases, low molecular weight modified HA acts as a crosslinker to yield a hydrogel or covalently adds to the surface of preexisting hydrogels.[80] In the case of the former, treatment of HA, gelatin, and chondroitin-6-sulfate with a carbodiimide yielded a "tri-co-polymer network", that proved suitable for tissue engineering;[81,82] in the latter, HA grafted onto the surface of a chitosan-gelatin hydrogel enhanced the degradation of the tissue scaffold compared to both the pristine hydrogel and a hydrogel prepared with HA as a crosslinker rather than as a surface modifier.[80]

2.6 Biomedical Applications of HA Copolymers

Both the variety of available synthetic methods of modification and biocompatibility of HA in addition to its ability to specifically bind to CD44 make it a natural target for use in biomedical applications such as tissue engineering and drug or gene delivery for anticancer and other therapies.

2.6.1 Drug Delivery

As mentioned previously, the self-assembly of HA-copolymer nanoparticles allows for the loading of antitumor drugs such as doxorubicin,[38, 40, 66,67,68,69,71,75] ciprofloxacin,[73]

and docetaxel.[39,70] In these cases, researchers employed materials such as HA-*b*-PBLG,[66,67,68,70] HA-*g*-PLGA[71] and its block copolymer counterpart HA-*b*-PLGA.[69] HA-*g*-poloxamer, HA-*g*-PLA,[75] mineralized HA-cholanic acid,[40] and HA-ceramide.[38]

Additionally, surface functionalization of lipid-based nanoparticles with HA allowed more efficient trafficking of mitomycin C[83] to *ex vivo* tumor cells associated with head and neck cancers but did not display typical toxicity towards noncancerous cells from the same patients. Doctors typically avoid treatment with the drug due to its considerable toxicity; however, the increased specificity as a result of CD44-HA interaction helps curtail this problem.[83]

Of these, more focus centers on doxorubicin-loaded HA-*b*-PBLG and its *in vivo* and *in vitro* properties. As mentioned previously, HA-*b*-PBLG self-assembles into polymersomes that feature antiparallel-packed PBLG segments surrounded with layers of HA.[67] These vesicles display no cytotoxicity[66] which makes them attractive candidates for drug delivery vehicles. Fluorescence microscopy tracked the cellular uptake in MCF-7 and U87 cancer cells of doxorubicin both from a doxorubicin solution and from a solution of doxorubicin-loaded micelles (**Figure 2.4**). In both cell lines, doxorubicin delivered from HA-*b*-PBLG micelles displayed better cellular uptake than doxorubicin delivered from solution, with the most notable differences evident beginning at 12 hours.[66]

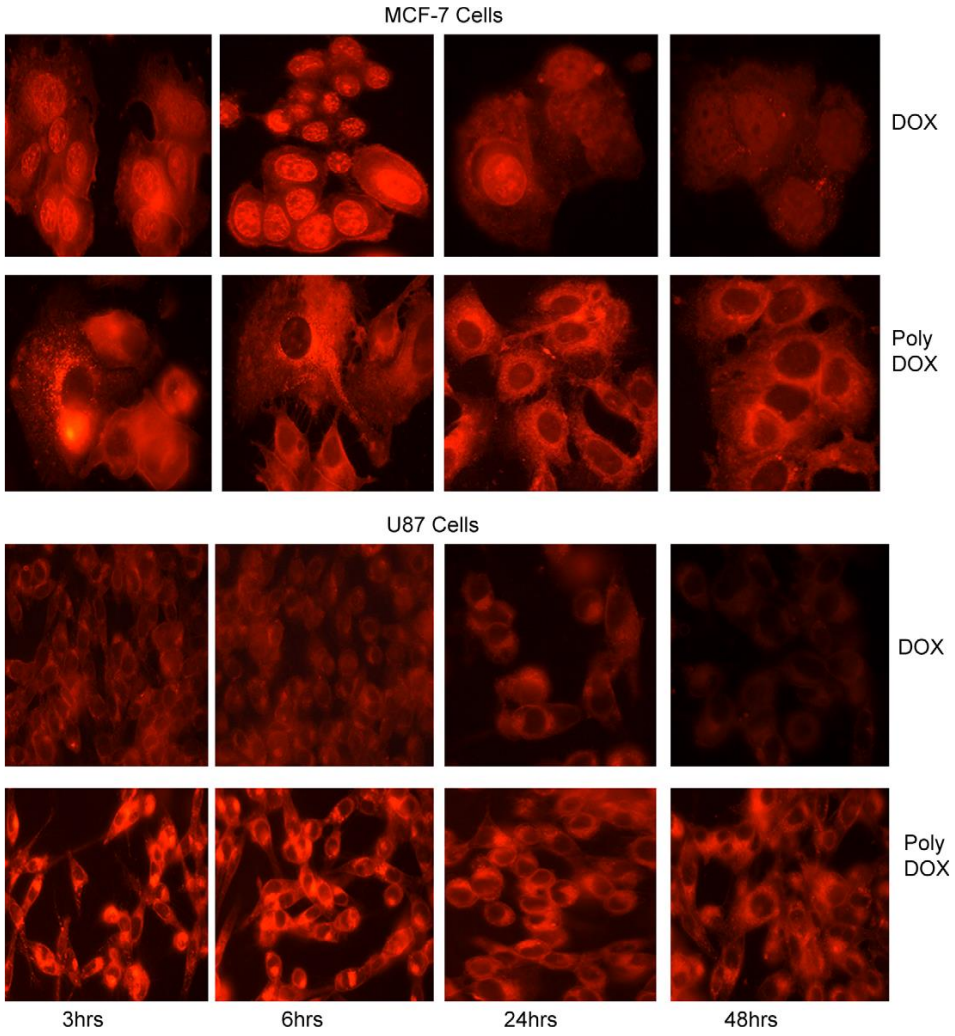

Figure 2.4. Fluorescent microscopy proves the superiority of HA-*b*-PBLG micelles for delivering doxorubicin. This image was adapted from Reference 66.

Similarly, the *in vivo* activity of HA-*b*-PBLG polymersomes loaded with doxorubicin proved effective at reducing tumor volume and extending the lifetime of mice with Ehrlich ascites tumors (EATs).[68] EATs overexpress CD44, allowing for CD44-regulated uptake of the doxorubicin-loaded HA-*b*-PBLG polymersomes. Therefore, HA-*b*-PBLG proves thus far a suitable vehicle for delivery of doxorubicin.

In addition to the mentioned drugs, HA-*g*-PEG displays the ability to entrap insulin peptides in solution.[72] In this case, comparison of graft densities established that increased PEG content helped to protect the HA backbone from hydrolytic degradation as well as to more efficiently regulate insulin leakage from the solution. However, at graft densities >10%, insulin leakage from HA-*g*-PEG proved greater than that from unmodified HA which the investigators attributed to increased phase separation as a result of PEG content. The HA-g-PEG system showed promise as a controlled-release insulin delivery system that relied on the natural enzymatic breakdown of HA over time.[72]. However, this study compared the weight percentage of PEG calculated from graft density of only one length of PEG graft (Mn = 5,000 g/mol). A more systematic study may provide more insight into the mechanism of insulin release from the HA-*g*-PEG system and whether it varies more closely with density or the weight percent of the PEG grafts.

2.6.2 Nonviral Gene Delivery

In HA-containing copolymers for nonviral DNA delivery, low molecular weight HA attaches to the backbone of PLL. Under physiological conditions, the pendant amines of the unreacted PLL chain exist as ammonium cations, which allows for binding of anionic DNA or RNA. The presence of HA served to decrease cytotoxicity and to actively target cancer cells through CD44-regulated uptake.[78] The graft copolymer readily binds DNA at a positive-to-negative charge ratio of 1.0[78] as shown through fluorescence spectroscopy with ethidium bromide and also proved efficient for gene transfection to sinusoidal endothelial liver cells. Uncomplexed DNA displayed marginal cellular uptake, and addition of HA homopolymer screened the interactions between CD44 and PLL-*g*-HA and resulted in decreased cellular uptake.[78]

Similarly, PEI-*g*-HA proves suitable for delivery of small interfering RNA (siRNA).The electrostatic interaction between anionic siRNA and the cationic PEI segment of PEI-*g*-HA allowed for condensation of particles 20 nm in diameter.[79] Once again, HA played a key role in reducing the cytotoxicity of the PEI-siRNA and allowed receptor-regulated cellular uptake. Further investigation led to the synthesis of nanoparticles prepared through crosslinking low molecular weight PEI with cystamine bisacrylamide (SS) couples to HA to form (PEI-SS)-*b*-HA that features a block of HA connected to a reducible PEI-SS nanoparticle.[84] In the presence of (PEI-SS)-*b*-HA, (siRNA) selectively complexes with the cationic PEI segment, forming clusters and leaving the HA portions to coat the outside. These clusters proved effective for efficiently delivering siRNA that inhibits expression of vascular endothelial growth factor (VEGF), therefore preventing angiogenesis and serving to kill the tumor.[84]

2.6.3 Tissue Engineering

HA-containing copolymers also show promise as cell scaffolds for tissue engineering. The naturally occurring presence of HA in the ECM proves the biocompatibility of HA for cell proliferation applications; however, a simple solution of HA homopolymer does not provide the physical support required to function as a scaffold for *in vitro* culture of tissue. Thus, researchers employ the incorporation of other polymers to tune the characteristics of the scaffold and achieve the desired mechanical, thermal, and biological properties.

The HA-gelatin-chondroitin tri-copolymer system that Chang et al introduced in 2003[81] effectively mimics the ECM in cartilage and thus proves its worth as perhaps the most important HA-containing copolymer for tissue engineering. Because cartilage tissue lacks a blood supply of its own, minor injuries to cartilage require longer healing periods

and may even lead to more serious or progressively worsening conditions. In patients with significant cartilage degeneration, doctors often employ complete joint replacement rather than attempt to repair the cartilage.[81] Thus, researchers targeted effective and efficient *in vivo* engineering of cartilage for treatment of joint injuries. The HA-gelatin-chondroitin formulation displayed the ability to promote growth of chondrocyte cells, which comprise cartilage.

Tissue engineering requires use of a porous material as the scaffold to promote uniform cell growth and allow sufficient space for cell proliferation. The HA-gelatin-chondroitin scaffold exhibited uniform pore size of 180 μm[81] as seen below in an image obtained through scanning electron microscopy (SEM) (**Figure 2.5**). This finding prompted further investigation into fine tuning the biological activity of the scaffold. The protein transforming growth factor-β1 (TGF-β1) plays a role in many cellular processes such as cell proliferation and differentiation. Surface modification of the tri-copolymer scaffold with TGF-β1 allowed for enhanced cell proliferation in *in vitro* studies as well as increased cellular expression of collagen and HA.[82]

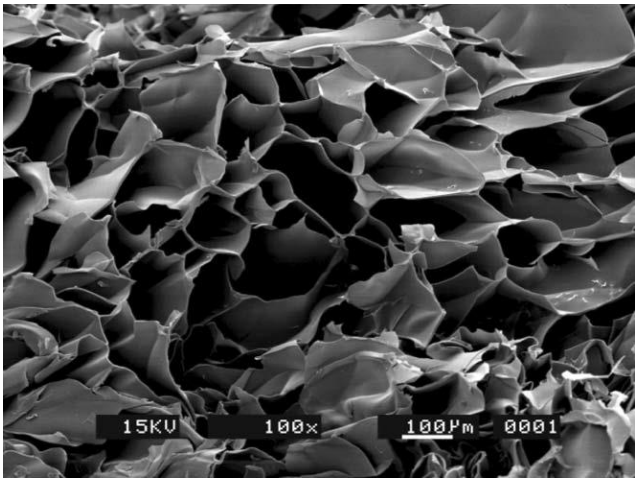

Figure 2.5. SEM demonstrates the porous nature of the HA-gelatin-chondroitin scaffold. This figure was adapted from Reference 81.

Other HA copolymers for tissue engineering include HA-*g*-PNIPAM[74] and HA-*g*-HEMA.[63] HA-*g*-PNIPAM displays thermal responsiveness, forming hydrogels when heated above 30 °C, which allows for an injectable material to gel *in situ* upon delivery to physiological conditions. *In vitro* experiments confirmed the suitability of the material for cell proliferation and *in vivo* studies confirmed its biocompatibility in mice and although these studies excluded cell delivery with the copolymer[85] the material showed promise for future investigation. HA-*g*-HEMA films also proved suitable for lung tissue culture with minimal cytotoxicity in *in vitro* studies. Rather than forming a three dimensional network, HA-*g*-HEMA forms films that swell up to 68% in water and allow cells deposited onto the surface to penetrate up to 50 μm into the film.[63] The film-forming properties of the copolymer potentially provide avenues for specific tailoring of scaffold shape.

2.7 Conclusion

The well-established validity of HA for a variety of applications led to investigation of HA-containing copolymers for various uses. The versatility and wide array of available methods of chemical modification of HA in addition to its inherent biological function prove HA copolymers to possess significant potential for emerging biomedical applications. Various HA copolymers display abilities to function as drug delivery vehicles, gene carriers for nonviral delivery, and scaffolds for tissue engineering. HA copolymers thus far show immense promise in biomedical applications and future investigation will prove crucial for unlocking the full potential of HA copolymers.

2.8 References

1. Nanda, R.; Sasmal, A.; Sasmal, S.; Nayak, P. L. *Popular Plastics & Packaging* **2009,** *54* (2), 50-57.
2. Banerjee, S.; Srivastava, V.; Singh, M. M. *Corrosion Science* **2012,** *59* (0), 35-41.
3. Goni, I.; Ferrero, M. C.; Jimenez-Castellanos, R. M.; Gurruchaga, M. *Drug Dev. Ind. Pharm.* **2002,** *28*, 1101-1115.
4. Park, J. S.; Park, J.-K.; Nam, J.-P.; Kim, W.-S.; Choi, C.; Kim, M.-Y.; Jang, M.-K.; Nah, J.-W. *Macromol. Res.* **2012,** *20*, 667-672.
5. Yu, H.; Chen, X.; Lu, T.; Sun, J.; Tian, H.; Hu, J.; Wang, Y.; Zhang, P.; Jing, X. *Biomacromolecules* **2007,** *8*, 1425-1435.
6. Schatz, C.; Louguet, S.; Le Meins, J.-F.; Lecommandoux, S. *Angewandte Chemie International Edition* **2009,** *48* (14), 2572-2575.
7. Narumi, A.; Otsuka, I.; Matsuda, T.; Miura, Y.; Satoh, T.; Kaneko, N.; Kaga, H.; Kakuchi, T. *J. Polym. Sci., Part A: Polym. Chem.* **2006,** *44*, 3978-3985.
8. Pawlaczyk, I.; Czerchawski, L.; Pilecki, W.; Lamer-Zarawska, E.; Gancarz, R. *Carbohydrate Polymers* **2009,** *77* (3), 568-575.
9. Aissou, K.; Pfaff, A.; Giacomelli, C.; Travelet, C.; Mueller, A. H. E.; Borsali, R. *Macromol. Rapid Commun.* **2011,** *32*, 912-916.
10. Volpi, N.; Schiller, J.; Stern, R.; Soltes, L. *Curr. Med. Chem.* **2009,** *16*, 1718-1745.
11. Kogan, G.; Šoltés, L.; Stern, R.; Schiller, J.; Mendichi, R., Hyaluronic Acid: Its Function and Degradation in in vivo Systems. In *Studies in Natural Products Chemistry*, Atta ur, R., Ed. Elsevier: 2008; Vol. Volume 34, pp 789-882.
12. Schanté, C. E.; Zuber, G.; Herlin, C.; Vandamme, T. F. *Carbohydrate Polymers* **2011,** *85* (3), 469-489.
13. Klein, J.; Meyer, F. A. *Biochim. Biophys. Acta, Gen. Subj.* **1983,** *755*, 400-11.
14. Scott, J. E. *Int. J. Biol. Macromol.* **1991,** *13*, 157-61.
15. McBride, W. H.; Bard, J. B. *J Exp Med* **1979,** *149*, 507-15.
16. Feinberg, R. N.; Beebe, D. C. *Science* **1983,** *220*, 1177-9.
17. Noble, P. W. *Matrix Biol.* **2002,** *21*, 25-29.
18. West, D. C.; Hampson, I. N.; Arnold, F.; Kumar, S. *Science* **1985,** *228*, 1324-6.
19. Xu, H.; Ito, T.; Tawada, A.; Maeda, H.; Yamanokuchi, H.; Isahara, K.; Yoshida, K.; Uchiyama, Y.; Asari, A. *J. Biol. Chem.* **2002,** *277*, 17308-17314.
20. Turley, E. A.; Noble, P. W.; Bourguignon, L. Y. W. *J. Biol. Chem.* **2002,** *277*, 4589-4592.
21. Kuo, J. W.; Swann, D. A.; Prestwich, G. D. *Bioconjugate Chemistry* **1991,** *2* (4), 232-241.
22. Bergman, K.; Elvingson, C.; Hilborn, J.; Svensk, G.; Bowden, T. *Biomacromolecules* **2007,** *8*, 2190-2195.
23. Bellini, D.; Topai, A. Preparation and use of hyaluronic acid amides or other derivatives. WO2000001733A1, 2000.
24. Magnani, A.; Rappuoli, R.; Lamponi, S.; Barbucci, R. *Polymers for Advanced Technologies* **2000,** *11* (8-12), 488-495.
25. Della, V. F.; Romeo, A. Hyaluronic acid esters and their medical and cosmetic uses and formulations. EP216453A2, 1987.
26. Jeanloz, R. W.; Forchielli, E. *J Biol Chem* **1950,** *186*, 495-511.
27. Huin-Amargier, C.; Marchal, P.; Payan, E.; Netter, P.; Dellacherie, E. *J. Biomed. Mater. Res., Part A* **2006,** *76A*, 416-424.

28. Prata, J. E.; Barth, T. A.; Bencherif, S. A.; Washburn, N. R. *Biomacromolecules* **2010,** *11*, 769-775.
29. Crescenzi, V.; Francescangeli, A.; Capitani, D.; Mannina, L.; Renier, D.; Bellini, D. *Carbohydrate Polymers* **2003,** *53* (3), 311-316.
30. Balazs, E. A.; Leshchiner, A. Crosslinked gels of hyaluronic acid and products containing these gels for cosmetics and pharmaceuticals. US4582865A, 1986.
31. Ramamurthi, A.; Vesely, I. *J. Biomed. Mater. Res.* **2002,** *60*, 196-205.
32. Collins, M. N.; Birkinshaw, C. *J. Appl. Polym. Sci.* **2007,** *104*, 3183-3191.
33. Serban, M. A.; Yang, G.; Prestwich, G. D. *Biomaterials* **2008,** *29*, 1388-1399.
34. Guarise, C.; Pavan, M.; Pirrone, L.; Renier, D. *Carbohydr. Polym.* **2012,** *88*, 428-434.
35. Mlcochova, P.; Bystricky, S.; Steiner, B.; Machova, E.; Koos, M.; Velebny, V.; Krcmar, M. *Biopolymers* **2006,** *82*, 74-79.
36. Jia, X.; Colombo, G.; Padera, R.; Langer, R.; Kohane, D. S. *Biomaterials* **2004,** *25*, 4797-4804.
37. Choi, K. Y.; Chung, H.; Min, K. H.; Yoon, H. Y.; Kim, K.; Park, J. H.; Kwon, I. C.; Jeong, S. Y. *Biomaterials* **2009,** *31*, 106-114.
38. Jin, Y.-J.; Termsarasab, U.; Ko, S.-H.; Shim, J.-S.; Chong, S.; Chung, S.-J.; Shim, C.-K.; Cho, H.-J.; Kim, D.-D. *Pharm. Res.*, Ahead of Print.
39. Cho, H.-J.; Yoon, H. Y.; Koo, H.; Ko, S.-H.; Shim, J.-S.; Lee, J.-H.; Kim, K.; Kwon, I. C.; Kim, D.-D. *Biomaterials* **2011,** *32*, 7181-7190.
40. Han, S.-Y.; Han, H. S.; Lee, S. C.; Kang, Y. M.; Kim, I.-S.; Park, J. H. *J. Mater. Chem.* **2011,** *21*, 7996-8001.
41. Stewart, R. J.; Wang, C. S.; Shao, H. *Advances in Colloid and Interface Science* **2011,** *167* (1–2), 85-93.
42. Lim, S.; Choi, Y. S.; Kang, D. G.; Song, Y. H.; Cha, H. J. *Biomaterials* **2010,** *31* (13), 3715-3722.
43. Hwang, D. S.; Zeng, H.; Srivastava, A.; Krogstad, D. V.; Tirrell, M.; Israelachvili, J. N.; Waite, J. H. *Soft Matter* **2010,** *6* (14), 3232-3236.
44. Malay, Ö.; Bayraktar, O.; Batıgün, A. *International Journal of Biological Macromolecules* **2007,** *40* (4), 387-393.
45. Matthew, H. W.; Salley, S. O.; Peterson, W. D.; Klein, M. D. *Biotechnology progress* **1993,** *9* (5), 510-519.
46. Liu, F.; Liu, L.; Li, X.; Zhang, Q. *Journal of materials science. Materials in medicine* **2007,** *18* (11), 2215-2224.
47. Vasiliu, S.; Popa, M.; Rinaudo, M. *European Polymer Journal* **2005,** *41* (5), 923-932.
48. de, l. F. M.; Seijo, B.; Alonso, M. J. *Macromol. Biosci.* **2008,** *8*, 441-450.
49. Oyarzun-Ampuero, F. A.; Brea, J.; Loza, M. I.; Torres, D.; Alonso, M. J. *Int. J. Pharm.* **2009,** *381*, 122-129.
50. Ohya, Y.; Takeda, S.; Shibata, Y.; Ouchi, T.; Kano, A.; Iwata, T.; Mochizuki, S.; Taniwaki, Y.; Maruyama, A. *Journal of Controlled Release* **2011,** *155* (1), 104-110.
51. Kim, I. L.; Mauck, R. L.; Burdick, J. A. *Biomaterials* **2011,** *32* (34), 8771-8782.
52. Nimmo, C. M.; Owen, S. C.; Shoichet, M. S. *Biomacromolecules* **2011,** *12* (3), 824-830.

53. Leach, J. B.; Bivens, K. A.; Patrick, C. W., Jr.; Schmidt, C. E. *Biotechnol. Bioeng.* **2003,** *82*, 578-589.
54. Chung, H. J.; Park, T. G. *Nano Today* **2009,** *4* (5), 429-437.
55. Kim, J.-T.; Choi, J.-H.; Lee, D.-Y. *Nat. Sci.* **2010,** *2*, 764-768.
56. Burdick, J. A.; Prestwich, G. D. *Advanced Materials* **2011,** *23* (12), H41-H56.
57. Allison, D. D.; Grande-Allen, K. J. *Tissue Eng.* **2006,** *12*, 2131-2140.
58. Balazs, E. A.; Band, P. A. In *Therapeutic use of hyaluronan-based products*, Elsevier Ltd.: 2008; pp 311-332.
59. Maroda, M.; Bodnar, M.; Berko, S.; Bako, J.; Eros, G.; Csanyi, E.; Szabo-Revesz, P.; Hartmann, J. F.; Kemeny, L.; Borbely, J. *Carbohydr. Polym.* **2011,** *83*, 1322-1329.
60. Schatz, C.; Lecommandoux, S. *Macromol. Rapid Commun.* **2010,** *31*, 1664-1684.
61. Hosseinzadeh, H. *Asian J. Chem.* **2012,** *24*, 2537-2540.
62. Hosseinzadeh, H. *Res. J. Pharm., Biol. Chem. Sci.* **2012,** *3*, 756-761.
63. Radhakumary, C.; Nandkumar, A. M.; Nair, P. D. *Carbohydr. Polym.* **2011,** *85*, 439-445.
64. Novoa-Carballal, R.; Muller, A. H. E. *Chemical Communications* **2012,** *48* (31), 3781-3783.
65. Yang, Y.; Kataoka, K.; Winnik, F. M. *Macromolecules* **2005,** *38* (6), 2043-2046.
66. Upadhyay, K. K.; Bhatt, A. N.; Mishra, A. K.; Dwarakanath, B. S.; Jain, S.; Schatz, C.; Le Meins, J.-F.; Farooque, A.; Chandraiah, G.; Jain, A. K.; Misra, A.; Lecommandoux, S. *Biomaterials* **2010,** *31* (10), 2882-2892.
67. Upadhyay, K. K.; Meins, J. F. L.; Misra, A.; Voisin, P.; Bouchaud, V.; Ibarboure, E.; Schatz, C.; Lecommandoux, S. *Biomacromolecules* **2009,** *10* (10), 2802-2808.
68. Upadhyay, K. K.; Mishra, A. K.; Chuttani, K.; Kaul, A.; Schatz, C.; Le Meins, J.-F.; Misra, A.; Lecommandoux, S. *Nanomedicine: Nanotechnology, Biology and Medicine* **2012,** *8* (1), 71-80.
69. Jeong, Y.-I.; Kim, D. H.; Chung, C.-W.; Yoo, J. J.; Choi, K. H.; Kim, C. H.; Ha, S. H.; Kang, D. H. *Colloids Surf., B* **2012,** *90*, 28-35.
70. Upadhyay, K. K.; Bhatt, A. N.; Castro, E.; Mishra, A. K.; Chuttani, K.; Dwarakanath, B. S.; Schatz, C.; Le, M. J.-F.; Misra, A.; Lecommandoux, S. *Macromol. Biosci.* **2010,** *10*, 503-512.
71. Lee, H.; Ahn, C.-H.; Park, T. G. *Macromolecular Bioscience* **2009,** *9* (4), 336-342.
72. Moriyama, K.; Ooya, T.; Yui, N. *Journal of Controlled Release* **1999,** *59* (1), 77-86.
73. Cho, K. Y.; Chung, T. W.; Kim, B. C.; Kim, M. K.; Lee, J. H.; Wee, W. R.; Cho, C. S. *International Journal of Pharmaceutics* **2003,** *260* (1), 83-91.
74. Tan, H.; Ramirez, C. M.; Miljkovic, N.; Li, H.; Rubin, J. P.; Marra, K. G. *Biomaterials* **2009,** *30*, 6844-6853.
75. Pitarresi, G.; Palumbo, F. S.; Albanese, A.; Fiorica, C.; Picone, P.; Giammona, G. *Journal of Drug Targeting* **2010,** *18* (4), 264-276.
76. Palumbo, F. S.; Pitarresi, G.; Mandracchia, D.; Tripodo, G.; Giammona, G. *Carbohydrate Polymers* **2006,** *66* (3), 379-385.
77. Asayama, S.; Nogawa, M.; Takei, Y.; Akaike, T.; Maruyama, A. *Bioconjugate Chemistry* **1998,** *9* (4), 476-481.

78. Takei, Y.; Maruyama, A.; Ferdous, A.; Nishimura, Y.; Kawano, S.; Ikejima, K.; Okumura, S.; Asayama, S.; Nogawa, M.; Hashimoto, M.; Makino, Y.; Kinoshita, M.; Watanabe, S.; Akaike, T.; Lemasters, J. J.; Sato, N. *FASEB J.* **2004,** *18*, 699-701.
79. Jiang, G.; Park, K.; Kim, J.; Kim, K. S.; Oh, E. J.; Kang, H.; Han, S.-E.; Oh, Y.-K.; Park, T. G.; Hahn, S. K. *Biopolymers* **2008,** *89*, 635-642.
80. Mao, J. S.; liu, H. F.; Yin, Y. J.; Yao, K. D. *Biomaterials* **2003,** *24* (9), 1621-1629.
81. Chang, C.-H.; Liu, H.-C.; Lin, C.-C.; Chou, C.-H.; Lin, F.-H. *Biomaterials* **2003,** *24*, 4853-4858.
82. Chou, C.-H.; Cheng, W. T. K.; Lin, C.-C.; Chang, C.-H.; Tsai, C.-C.; Lin, F.-H. *J. Biomed. Mater. Res., Part B* **2006,** *77B*, 338-348.
83. Bachar, G.; Cohen, K.; Hod, R.; Feinmesser, R.; Mizrachi, A.; Shpitzer, T.; Katz, O.; Peer, D. *Biomaterials* **2011,** *32* (21), 4840-4848.
84. Park, K.; Lee, M.-Y.; Kim, K. S.; Hahn, S. K. *Biomaterials* **2010,** *31*, 5258-5265.
85. Tan, H.; Ramirez, C. M.; Miljkovic, N.; Li, H.; Rubin, J. P.; Marra, K. G. *Biomaterials* **2009,** *30* (36), 6844-6853.

Chapter 3: A Perspective on Degradable Covalent Networks

(*In preparation* for submission)

Evan Margaretta and Timothy E. Long*

Department of Chemistry, Macromolecules Innovation Institute
Virginia Tech, Blacksburg, VA 24061

*To whom correspondence should be addressed
E-mail: telong@vt.edu
TEL: (540)231-2480
FAX: (540)231-8517

Keywords: polymer networks, stimulus response, chemical degradation

3.1 Abstract:

Polymer networks exhibit broadly applicable properties across a wide range of applications. Networks with incorporated degradability prove an attractive target as researchers investigate polymeric materials that exhibit a chemical response to an external stimulus for smart materials. Borrowing from established small molecule and protecting group chemistry enables rational design of cleavable networks in response to stimuli such as water, pH, or other chemical signals. This perspective highlights advances in polymer networks that feature degradable functional groups upon exposure to various stimuli and also discusses further potential avenues of exploration in the field.

3.2 Introduction

Polymer scientists often aim to produce materials with enhanced stability for broad applicability and extended use in increasingly harsh environments. To achieve this, researchers investigate crosslinked polymers that feature robust mechanical properties and solvent resistance. However, it is increasingly apparent that fine control of network stability represents a powerful and underused synthetic strategy. Crosslinked materials that

degrade under a well-defined set of conditions represent a major target towards stimuli-responsive smart materials with tunable properties, and towards environmentally-friendly recyclable materials.[1-9]

Network materials result from incorporation of multifunctional monomers that enable bridging between polymer chains. Difunctional components lead to crosslinking in the chain-growth polymerization of vinyl-containing compounds. Trifunctional or even tetrafunctional vinyl compounds further tune the curing process and the properties of the final product. In step-growth reactions, addition of trifunctional or greater monomers enables crosslinking. Implementation of cleavable sites into these multifunctional crosslinkers yields exploitable degradation properties inherent in the resulting material (**Figure 3.1**).

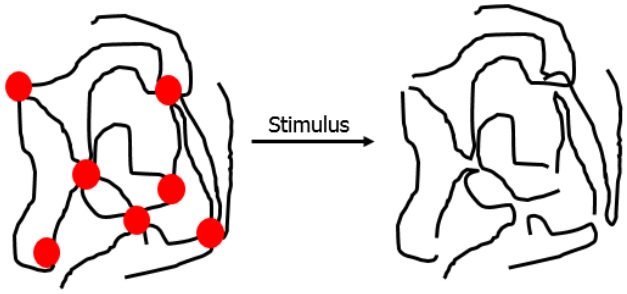

Figure 3.1. Representation of a network featuring crosslink sites (red circles) that degrade upon exposure to a stimulus.

This paper provides an overview of degradable covalent networks with an emphasis on recent examples of stimuli-triggered degradation. These examples are arranged according to the cleavable functional group, with respective sections devoted to hydrolyzable networks featuring esters or anhydrides, acetals, disulfide groups, tertiary alkyl esters, base-cleavable esters, silyl ethers, poly(benzyl ether)s, and polyhexahydrotriazines. Finally, the manuscript discusses potential areas of exploration in

the field with regards to greater signal sensitivity and selectivity, wider variety of trigger degradation, and utilization of established degradation chemistry into crosslinked materials.

3.3 Degradable Networks

3.3.1 Esters

Polymers such as poly(ε-caprolactone) (PCL), poly(D/L lactide) (PLA), polyglycolide (PGA), and poly(lactide-*co*-glycolide) (PLGA) (**Figure 2**) represent polyesters commonly used in biomedical applications due to their hydrolytic sensitivity.[10-12] PLGA and PLA, in particular, find use because of their low glass transition temperatures (T_g) and melting temperatures (T_m). Furthermore, some compositions of PLGA exhibit no crystallinity as irregularities inhibit chain packing.[13] Semicrystalline polymers degrade much more slowly than do amorphous analogs, due to relative impermeability of polymer crystallites to water. Hydrolysis of polyesters remains especially attractive because the liberated carboxylic acid byproduct catalyzes further ester degradation.

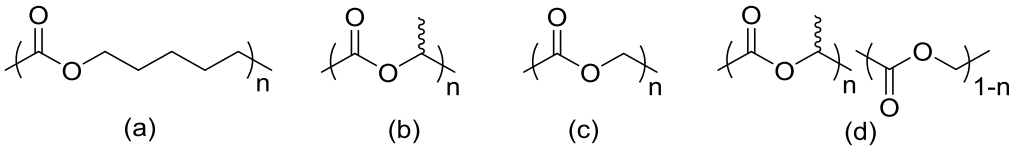

Figure 3.2. Structures of (a) PCL, (b) PLA, (c) PGA, and (d) PLGA.

Anseth *et al* demonstrated the usefulness of PCL- and PLA-based dimethacrylates for tissue scaffolding.[14] Diethylene glycol-initiated ring-opening polymerization (ROP) of caprolactone, lactide, or a series of comonomer mixtures afforded polyester diol oligomers, and subsequent methacrylation generated photocurable macromers. The networks proved

cell viable, and also degraded under physiological conditions in phosphate-buffered saline solutions at pH 7.4 and 37 °C, although the fastest observed time was 105 days.

Other work in the same group used poly(ethylene glycol) (PEG) to initiate ROP of D,L-lactide.[15] Acrylation and subsequent photocuring of the diols yielded PEG-based hydrogel networks with hydrolyzable esters, which served as hosts for high molecular weight solutes such as lysozyme, bovine serum albumin, or fluorescently-labeled dextrin. The swelling, mesh size, and release profiles of the networks were examined as molecular weight of the crosslinker changed, enabling a detailed study of degradation on network structure and solute release. Although Hubbell previously studied PEG-based, lactide-containing networks for their cell adhesion properties and degradation, Anseth's lactide-containing networks improved on Hubbell's earlier work by featuring more readily-hydrolyzed esters.[16-18] In this case, Anseth's networks containing the highest PEG spacer size and a low relative incorporation of ester units exhibited full degradation in under 1 day.

Anseth's synthesis also provided a route towards methacrylate-containing PLA-grafted poly(vinyl alcohol) (PVOH), which generated a highly functional PVOH-*g*-PLA crosslinker.[19] When mixed with PLA-*b*-PEG-*b*-PLA diacrylate and photocured, the resulting networks exhibited tunable swelling, release, and degradation behavior under physiological conditions. Also, these networks demonstrated suitability for tissue engineering applications. Photocuring the components in the presence of chondrocytes afforded a network with uniformly encapsulated cells, which remained alive and functioning throughout the 8 week duration of the experiment. Others directly crosslinked acrylate-containing PVOH-*g*-PLA and achieved similar results.[20-21]

Research from the Bowman group investigated similar PLA-*b*-PEG-*b*-PLA diacrylates which underwent curing with multifunctional thiols.[22] Varying the relative ratios of mono-, di-, and tetrafunctional thiols and the overall thiol concentration generated a detailed study of crosslinker effects on the molecular weight between crosslinked sites, which correlated well to theoretically predicted results.[23] Bowman's earlier research established a novel kinetic model to aid in the description of multivinyl network formation during photocuring.[24]

3.3.2 Anhydrides

Anhydrides undergo hydrolysis more rapidly than esters as a result of increased electron withdrawing effect of the second carbonyl, making them attractive groups for targeted degradation.[25-26] Since their first introduction into degradable networks in 1998, several investigations further explored the feasibility of anhydride-containing networks for biomedical applications.[27-28] Early examples in the literature greatly detailed the degradation mechanism and pathway of anhydride-containing containing networks through analysis of the degradation products with MALDI-TOF mass spectrometry.[29-30]

Recently, reports investigated polyesters with terminal methacrylate-containing anhydride functionalities.[31-33] Linear or star-shaped PCL-based polymers were end-functionalized with succinic anhydride-based compounds to yield terminal carboxylic acids, which were further modified with methacrylic anhydride. These networks were evaluated for their water sorption and controlled release of propranolol HCl.[31,34] Another notable example of a polyanhydride network used multifunctional thiol crosslinkers with 4-pentenoic anhydride to produce gels with tunable hydrophobicity and thermal

properties.[35] These and other anhydride-containing gels degraded through surface erosion and corroborated earlier examples.[36-38]

One drawback inherent with networks that employ star-shaped crosslinkers is the ratio of crosslinkable functional groups to the cleavable groups. For instance, with these anhydride-containing crosslinkers, the synthetic strategy placed the anhydride groups at the chain ends prior to crosslinking. Because of this, each labile linkage only liberates one chain from the crosslinked site. Thus, a tetrafunctional crosslinker requires three degradation events to fully free the crosslinked chains from that crosslinked site. While advantageous for controlled release over longer periods of time, this type of network architecture lacks precise control and quick response to the degradation trigger.

3.3.3 Acetals and ketals

Integrating a more finely-tunable degradation mechanism represents a logical advance in the development of stimulus-responsive networks. While pH serves as just one example of an exploitable trigger, it plays a well-defined and understood role in biological systems allowing the targeting of environment-specific stability and properties in synthetic networks. For instance, the pH differences between the extracellular matrix (pH 7.4), endosomes (pH ~ 5.5) and lysosomes (pH ~ 4.5) is well-documented and represents the difference between a slightly basic environment and a decidedly acidic one.[39-40] The acetal and ketal functionalities prove particularly susceptible to degradation in acidic environments, and therefore typify such stimulus-responsive linkages.

An early example employed direct reaction of proteins with an acetal-containing hetero-bifunctional crosslinker featuring maleimide and NHS-ester functionalities.[41] The acetal-crosslinked bioconjugate exhibited a half-life ($t_{1/2}$) of 139 h at pH 5.5. However, the

authors discussed the potential advantages of tuning the electronic environment around the acetal to facilitate rapid degradation. This study also investigated crosslinkers that featured ortho-ester acid-labile groups, but these compounds exhibited inherent hydrolytic sensitivity over a wide pH range which rendering them unsuitable for selectively pH-triggered degradation.

In this vein, Frechet *et al.* detailed the synthesis and characterization of various acetal-containing networks for biomedical applications.[42-44] Acetal-containing, acrylamide-based hydrogels (**Figure 3**) exhibited a $t_{1/2}$ of 24 h at pH 7.4, while reducing the pH to 5.5 caused a marked drop to a $t_{1/2}$ of 5.5 min.[42] The crosslinker also permitted synthesis of microgels on the order of 1-10 μm in size featuring encapsulated fluorescently-labeled albumin to show feasibility of therapeutic protein delivery. Further work highlighted the tunability of acetal-containing linkages to investigate the stability of drug-polymer conjugates and drug-loaded micelles.[43,45] Many other reports detail the inclusion of acetal or acylal linkages into networks for pH-sensitive degradation. Applications of these crosslinked networks included step-and-flash imprint lithography, tissue engineering, and delivery of therapeutics.[46-57] Degradation of the acetal linkages occurred on timescales ranging from under a minute to over three weeks, indicating the wide window of degradation timescales.[47-48]

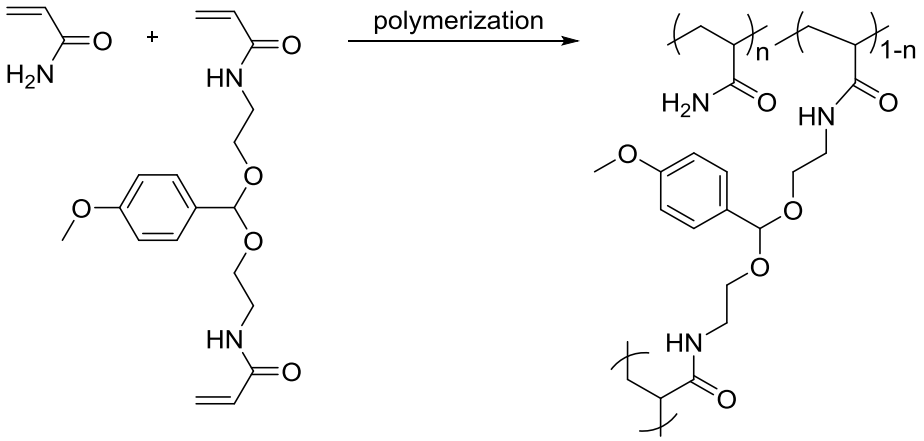

Figure 3.3. pH-degradable, acetal-containing poly(acrylamide)-based networks.

The potential for fine-tuning the cleavage of acetal groups enables judicious and careful design on the molecular level to affect the degradability of the bulk material in ways that ester and anhydride linkages simply do not offer. Tuning the reactivity of the acetal group affects its lability over a range of pH values due to the first order rate dependence of degradation on pH.[43] As a result, engineered acetal linkages that exhibit remarkably fast degradation in acidic environments also often exhibit relative hydrolytic instability in more mild conditions, rendering them impractical for many other applications. However, careful design of acetal and chemically similar ketal and formal linkages can enhance the hydrolytic stability under common usage conditions while still providing a route towards chemical degradation.

An exciting area of recently emerging research with these acid-degradable groups lies in acid-cleavable organic compounds for use in carbon fiber composite matrix resins. Carbon fiber composites featuring degradable matrices exhibit similar robust mechanical properties compared to those with traditional permanent epoxide resins. Several examples of these engineered crosslinkers degrade into their respective starting materials, affording true chemical recyclability.[58-63] One example used acetal-containing diisocyanates for synthesis of degradable polyurethanes, which also found use as carbon fiber matrix resins.

Degradation of the polyurethane led to near complete recovery of the carbon fibers.[59] Crosslinkers comprising an acid-degradable group and multiple amine functionalities found use in chemically-degradable epoxide resins.[60-63] When used in carbon fiber composites, treatment with strong acid served to cleave the labile groups, which enabled recovery of the carbon fibers and subsequent reuse in composites.[58]

3.3.4 Disulfides

Sulfur-sulfur bonds form in oxidizing environments, while reducing environments favor the breaking of the disulfide bond into two corresponding thiols. As discussed previously, pH generally requires treatment of the network material with a solution to begin degradation, while disulfide bonds prove susceptible to reducing environments that include the presence of reducing gases such as hydrogen, carbon monoxide or hydrogen sulfide. However, the majority of reductive cleavage of disulfide bonds is performed in the presence of reducing agents such as dithiothreitol (DTT), the peptide glutathione (GSH), or phosphine compounds. Because disulfide bonds between cysteine residues play a major role in dictating protein structure, much of the literature in the area of disulfide bond-containing networks revolves around biomedical applications.[58-64]

Pan *et al.* employed Michael addition of polyethyleimine (PEI) to N,N'-bis(acryloyl)cystamine (**Figure 3.4**) to synthesize hydrogels for evaluation of their encapsulation and release properties of ceftriaxone sodium.[65] A detailed study established structure-property relationships for kinetics and extent of water uptake, morphology, surface area, and degradation. In general, the degradation rate, pore size, and water uptake all decreased with increasing crosslink density. Upon treatment with DTT, the gels released all sequestered drug as quickly as 48 h, and completely degraded after two weeks.

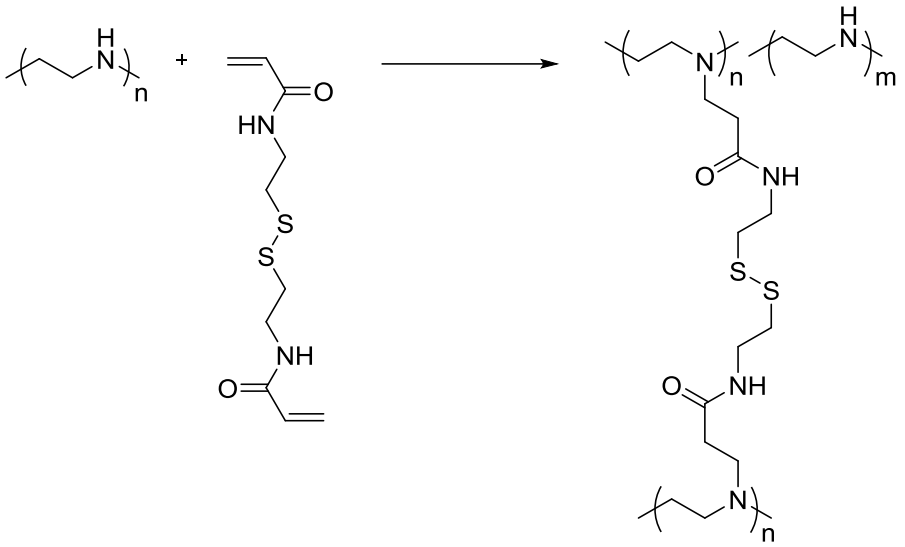

Figure 3.4. Structure of a reductively cleavable disulfide-containing, PEI-based Michael addition network.

3.3.5 Tertiary alkyl esters

Various other kinds of crosslinkers demonstrate capability of stimulus-triggered degradation. Diacrylates and dimethacrylates of tertiary diols (**Figure 5**) display acid lability in networks and in core-crosslinked star polymers.[47,72-73] Cleavage of these esters generally requires treatment with a strong acid such as trifluoroacetic acid or *p*-toluenesulfonic acid and mild heating to achieve full degradation of the cleavable groups. These tertiary alkyl esters also display well-characterized thermal degradation.[74-75] While not as responsive as acetals, these tertiary esters prove resistant to undesired degradation at neutral pH.

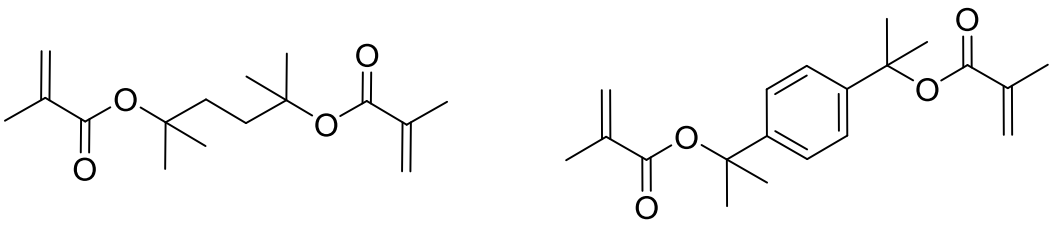

Figure 3.5. Examples of tertiary alkyl esters that degrade upon exposure to heat or acid.

3.3.6 Base-labile crosslinkers

To this point, literature largely detailed acid-cleavable linkages rather than base-labile functionalities. However, some recent investigations explored the synthesis and characterization of base-degradable crosslinkers (**Figure 3.6**).[76-78] In one case, Patrickios *et al.* borrowed from established protecting group chemistry to develop a novel, symmetric dimethacrylate compound based on 2,6-pyridinediethanol (**Figure 3.6a**).[76] Upon treatment with 0.4 M NaOD, the 2-(pyridin-2-yl)ethyl groups readily degraded in 10 min to liberate 2,6-divinylpyridine. While the crosslinker was synthesized in poor overall yield, limiting the usefulness of this particular strategy, the degradation proceeded on the same timescale as the fastest reported acid-labile acetals. The networks also proved hydrotically stable in neutral and acidic environments, demonstrating the selectivity of the stimulus response.

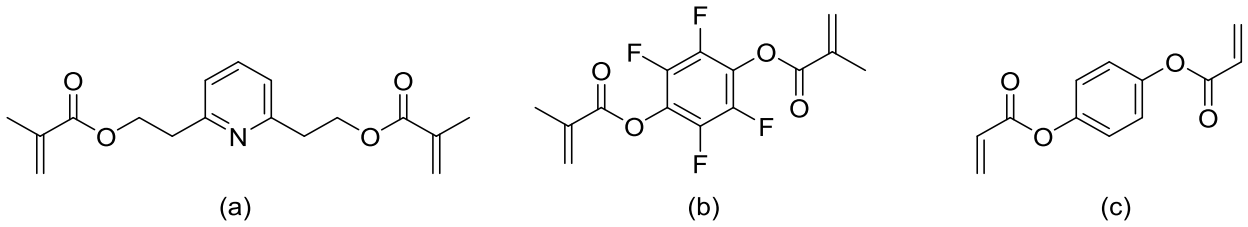

Figure 3.6. Structures of base-cleavable crosslinkers.

Other notable examples of alkaline-labile crosslinkers feature *para*-substituted phenyl diesters. Metz and Theato synthesized a tetrafluorohydroquinone (TFHQ) dimethacrylate (**Figure 3.6b**) for formation of poly(N-isopropyl acrylamide) (PNIPAM)-based hydrogels.[77] Treatment of the networks with ispropylamine yielded linear PNIPAM chains as the phenolic esters underwent nucleophilic acyl substitution to form the corresponding amide and liberate TFHQ. UV-visible spectroscopy tracked the progress of the reaction. Full network degradation occurred over a range from 5 min to 3 h depending

on the crosslinker concentration. However, the release of toxic TFHQ inhibits the use of this crosslinker in many applications.

Chang *et al.* eliminated this concern when they synthesized a nonfluorinated phenyl diacrylate and generated networks of hydroquinone diacrylate (**Figure 3.6c**) with *t*-butyl acrylate.[78] The networks degraded upon exposure to $NaHCO_3$ in methanol at mild temperatures over a 36 h time period. Importantly, the phenolic diester proved stable when TFA removed the tertiary esters of poly(*t*-butyl acrylate)-containing networks to yield poly(acrylic acid)-based gels. These acid-containing networks then cleaved under similar exposure to aqueous $NaHCO_3$. Furthermore, the authors also prepared a triblock copolymer with poly(glycidyl methacrylate) (PGMA) terminal blocks using a phenolic diester initiator. Crosslinking of the self-assembled PGMA phases and subsequent cleavage of the phenolic esters in the main chain afforded crosslinked PGMA nanospheres. This study in particular elegantly highlighted the usefulness of selectively degradable linkages in preparing various stimuli-responsive network materials.

3.3.7 Silyl Ethers

Silyl ethers also degrade under acidic conditions and exhibit tunable degradation properties. Themistou and Patrickios reported in 2004 the hydrolytic instability of a dimethyl silyl ether dimethacrylate-based crosslinker (**Figure 3.7a**) compared to a simple ethylene glycol dimethacrylate in network and star polymer synthesis.[79] DeSimone *et al.* employed a diacrylic version of a similar crosslinker (**Figure 3.7b**) and compared its degradation properties to those of a di-*t*-butyl silyl ether analog, which remained stable under similar degradative conditions.[80] Most recently, silyl ether-containing thiol-ene networks showed tunable degradation resulting from the functionality and hydrophobicity

of the selected thiol and vinyl compounds.[81] These examples of labile silyl ethers further demonstrate the versatility of these networks for various manufacturing applications such as photolithography and degradable therapeutic particles.

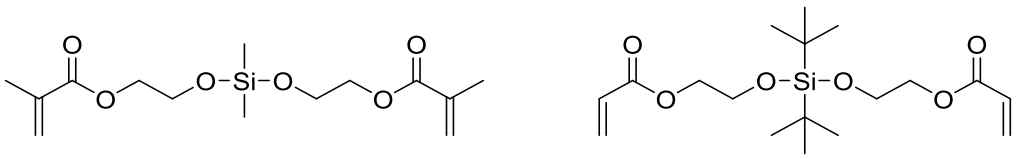

Figure 3.7. Structures of the silyl ether-based crosslinkers employed by Patrickios (a) and DeSimone (b).

3.3.8 Poly(benzyl ether)s

Self-immolative polymers, such as poly(benzyl ethers) (PBEs) degrade through a linear, head-to-tail depolymerization mechanism.[82-85] Phillips *et al.* described a norbornene-containing, protected PBE that acted as macromolecular, multifunctional crosslinker of decyl ester-containing norbornene for ROMP (**Figure 8**).[86] In this case, fluoride cleaved the protecting group and initiated the depolymerization of the PBE. The timescale of depolymerization depended on the molecular weight of the norbornene-containing PBE and ranged from 10 to 40 min. The network served as an adhesive for various substrates, and degradation of the PBE resulted in rapid debonding.

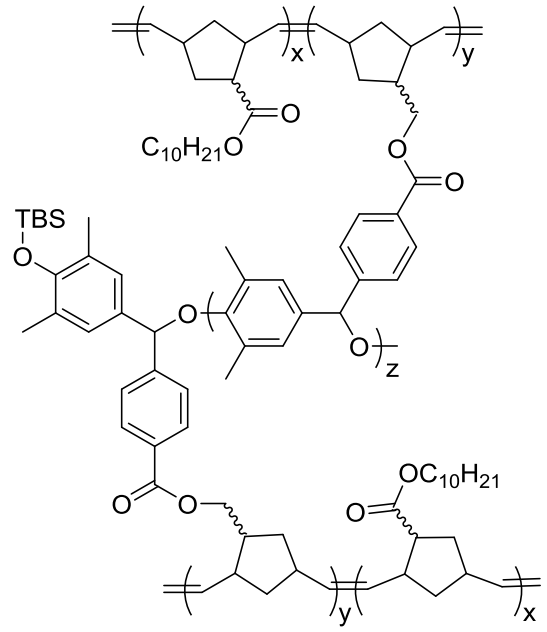

Figure 3.8. Structure of the PBE-crosslinked polynorbornene-based network.

3.3.9 Polyhexahydrotriazines

Aromatic polyhexahydrotriazines (PHTs) (**Figure 3.9**) represent a major advancement towards recyclable thermosets.[87-88] The highly crosslinked networks arise from the reaction of an aromatic diamine with paraformaldehyde to yield a hemiaminal dynamic covalent network. Dynamic covalent networks, also known as covalent adaptable networks or vitrimers, also represent an area of interest for thermoset-type materials with enhanced processability and have been well-reviewed elsewhere.[89-92] Upon thermal treatment at 200 °C, the network undergoes a chemical change from a dynamic covalent network to a traditional thermoset that features hexahydrotriazine linkages. These thermosets displayed robust thermomechanical properties with a T_g near 200 °C and Young's modulus of 10.3 GPa. While these networks also displayed excellent solvent resistance, digestion with sulfuric acid enabled recovery of the oxydianiline monomer in 86% yield. Carbon nanotube-PHT composites exhibited reinforced mechanical strength,

and degradation of the composite network resulted in high recovery yield of both the nanotubes and the PHT network components.

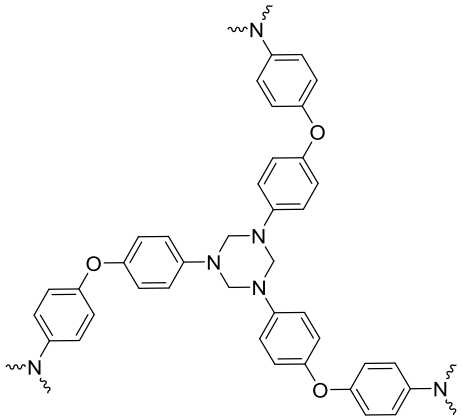

Figure 3.9. pH-reversible PHT network based on oxydianiline.

3.4 Towards the future

The PHTs described above depart from most common degradable networks due to their inherent mechanical properties. Most degradable networks covered here arise from chain growth-type monomers and mechanisms to yield primarily hydrocarbon structures with minimal or no crystallinity. Furthermore, the crosslinking functionality is truly reversible for PHTs, in stark contrast with most other degradable networks. Similarly, degradable or reformable thermosets prove especially attractive targets for researchers due to their implications for manufacturing in various industries. While PHTs form a degradable linkage in their polymerization, another rational approach is to investigate synthesis of cleavable monomers for incorporation into traditional step-growth engineering thermosets. In this area, established literature reports of degradable polymers and small molecules could prove useful as templates for designing recyclable networks.[59, 61, 93-95] In particular, degradable networks as matrix resins offer interesting and exciting possibilities for recovering carbon nanotubes, carbon fibers, and glass fibers from composites, enabling

further reuse. Composite systems that yield both matrix starting materials and the reinforcing component upon degradation, such as the PHT-based composites, prove incredibly attractive.

Thermosets that can be reformed or reprocessed with minimal changes in thermomechanical properties prove an attractive target for researchers. Vitrimers allow for reprocessing of thermoset-type materials, representing a different approach to material recyclability.[96-97] Vitrimers based on polyimines, polyesters, and polyurethanes demonstrate reprocessability in response to external stimuli such as water, heat, or strain.[98-101] These vitrimer networks therefore lend attractive processability to their applications, especially for composite applications. A critically important area of future research involves coupling the reprocessability of vitrimers with chemical degradability to enable both thermoset reforming and degradation to recapture starting materials. This kind of approach has immense implications for composite materials. One recent report explored using a polyimine vitrimer as a matrix in carbon fiber composites to enable the reforming of the entire composite without any chemical treatment steps while also allowing chemical degradation of the matrix to recover both the carbon fibers and matrix monomers.[98] A composite containing chemically recycled starting materials demonstrated similar tensile properties to the pristine composite.

There is an obvious tradeoff between designing an inherently degradable material and the range of useful environments for that material. For instance, hydrolytic properties enable many applications of degradable networks, but just as many applications exist where hydrolytic stability proves paramount. Thus, the future design of degradable networks requires exploitation of a wider variety of triggers. While signals such as pH and reducing

environments work well for systems that seek to use them, those stimuli also often interfere with other functional groups, bonds, linkages, and so on. Precise targeting of less conventional triggers offers closer control over network properties and helps ensure degradation only when desired.

Reports of triggers such as oxidizing environments, mechanical stress, and light already exist and their networks warrant further investigation. Aromatic oxalate linkages degrade in the presence of H_2O_2 to form CO_2 and the corresponding alcohols.[102] Polymers that contain mechanophores such as β-lactam groups degrade upon application of an external force such as ultrasound.[103] Examples of photolabile functional groups include *ortho*-nitrobenzyl (*o*-NB) esters, *o*-NB ethers, and cyclobutane diimides.[104-107] It is easy to imagine, for instance, a polyimide network composed of a multifunctional amine with cyclobutane dianhydride that degrades upon UV irradiation but proves stable over a wide pH range (**Figure 3.10**).

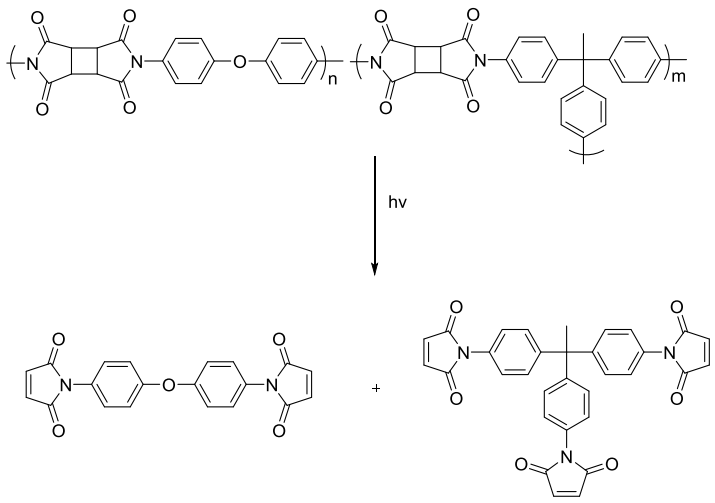

Figure 3.10. Hypothetical UV-induced degradation of a polyimide network into maleimide-containing small molecules.

Similarly, the design of stimulus-responsive covalent networks must also account for the timescale of the degradation. As a general rule, sharp transitions lend greater control

over the properties of smart materials for various application. However, other applications favor degradation mechanisms that provide a response over longer timescales. Thus, surface erosion-controlled hydrolysis of anhydride-containing networks works well for controlled release applications while rapidly-degraded acetals prove particularly useful for burst-release drug delivery. For recyclable materials, the timescale of degradation is relevant for the reducing the cost involved with the recycling process. In this case, the extent of recovery of starting components with good purity for further reuse and the efficiency and conditions inherent to the recycling process are also important from an industrial and financial perspective.

Researchers must also consider the sensitivity of the degradable linkage to the signal. Disruption of a network with a catalytic or amplified signal is preferred over stoichiometric reactions for reasons such as atom economy, cost of degradation, and minimizing the formation of undesired byproducts. For these reasons, multifunctional macromolecular crosslinkers of self-immolative polymers such as PBEs demonstrate tremendous potential. In these cases, a single interaction at the chain end results in depolymerization and degradation of several crosslinks.

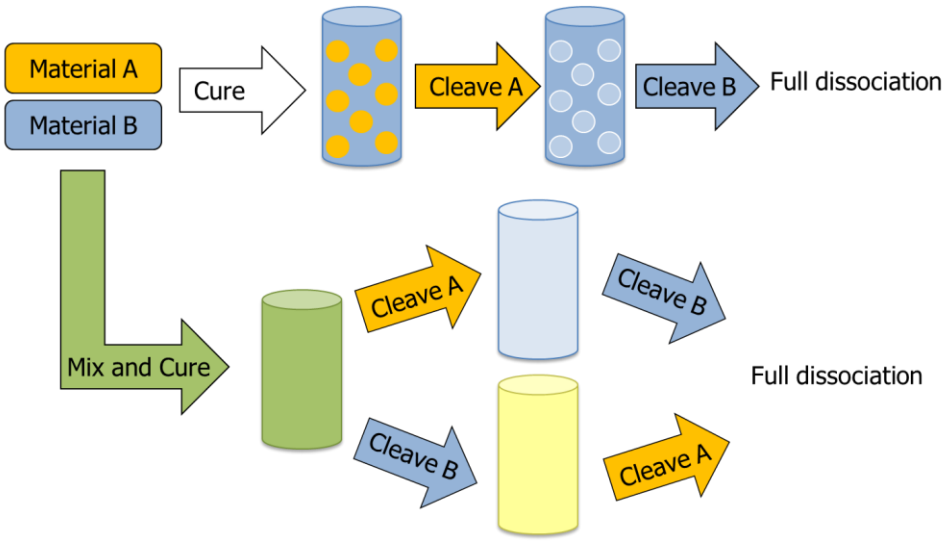

Figure 3.11. Additive manufacturing of multiply-degradable networks permits fine tuning of degradation properties, multiple routes to complete dissociation, and control of degradative properties in three dimensions.

Another exciting area of potential research lies in combining multiple kinds of crosslinkers with orthogonal cleavability to achieve step-wise degradable networks (**Figure 3.11**). For instance, employing both acid-sensitive and base-sensitive crosslinkers may enable partial degradability of the network and subsequent degradation following another step. This grants greater control over the degradation behavior of the network. Oxime sulfonate-containing polymers represent an interesting possibility, as mechanical stress causes bond scission to form a sulfonic acid group, which could potentially trigger subsequent degradation.[108] A separate but similar type of design could see the incorporation of crosslinkers that respond to the same stimulus but at different time scales, such as acid-sensitive acetals and tertiary alkyl esters. Tailoring the relative inclusion of the two crosslinking compounds might permit fine tuning of the resultant network's degradation. Excitingly, these types of dually- or multiply-degradable designs appear well-poised for

use in additive manufacturing as developments in the field grant more precise control of an object's chemical properties in three-dimensional space.

3.5 Conclusion

It remains clear that degradable networks represent an exciting area of research for a variety of applications. Several strategies generated networks with numerous diverse functional groups that feature different mechanisms and rates of degradation. However, with increasing demands for stimuli-responsive smart materials with robust properties, ample opportunity for improvement and advancement of the field still exists. Exploiting well-established chemistry empowers researchers to further explore this area and develop novel materials with precisely tailored properties.

3.6 References

1. Long, T. E., Toward Recyclable Thermosets. *Science* **2014,** *344* (6185), 706-707.
2. Ma, S.; Webster, D. C., Naturally Occurring Acids as Cross-Linkers To Yield VOC-Free, High-Performance, Fully Bio-Based, Degradable Thermosets. *Macromolecules* **2015,** *48* (19), 7127-7137.
3. Shirai, M., Photocrosslinkable polymers with degradable properties. *Polymer Journal* **2014,** *46* (12), 859-865.
4. Gallagher, J. J.; Hillmyer, M. A.; Reineke, T. M., Degradable Thermosets from Sugar-Derived Dilactones. *Macromolecules* **2014,** *47* (2), 498-505.
5. Giménez, R.; Fernández-Francos, X.; Salla, J. M.; Serra, A.; Mantecón, A.; Ramis, X., New degradable thermosets obtained by cationic copolymerization of DGEBA with an s(γ-butyrolactone). *Polymer* **2005,** *46* (24), 10637-10647.
6. González, L.; Ramis, X.; Salla, J. M.; Mantecón, A.; Serra, A., The degradation of new thermally degradable thermosets obtained by cationic curing of mixtures of DGEBA and 6,6-dimethyl (4,8-dioxaspiro[2.5]octane-5,7-dione). *Polymer Degradation and Stability* **2007,** *92* (4), 596-604.
7. Halpern, J. M.; Urbanski, R.; Weinstock, A. K.; Iwig, D. F.; Mathers, R. T.; von Recum, H. A., A biodegradable thermoset polymer made by esterification of citric acid and glycerol. *Journal of Biomedical Materials Research Part A* **2014,** *102* (5), 1467-1477.
8. Lei, Y.-Q.; He, Z.-X.; Luo, Y.; Lu, S.-N.; Li, C.-J., Chemical degradation of bisphenol A diglycidyl ether/methyl tetrahydrophthalic anhydride networks by p-Toluenesulfonic-acetic anhydride. *Polymer Degradation and Stability* **2016,** *123*, 115-120.

9. Lakhera, N.; Laursen, C. M.; Safranski, D. L.; Frick, C. P., Biodegradable thermoset shape-memory polymer developed from poly(β-amino ester) networks. *Journal of Polymer Science Part B: Polymer Physics* **2012,** *50* (11), 777-789.
10. John, G.; Morita, M., Synthesis and Characterization of Photo-Cross-Linked Networks Based on l-Lactide/Serine Copolymers. *Macromolecules* **1999,** *32* (6), 1853-1858.
11. Nagata, M.; Yamamoto, Y., Photocurable Shape-Memory Copolymers of ε-Caprolactone and L-Lactide. *Macromolecular Chemistry and Physics* **2010,** *211* (16), 1826-1835.
12. Davis, K. A.; Anseth, K. S., Controlled Release from Crosslinked Degradable Networks. **2002,** *19* (4-5), 39.
13. Gilding, D. K.; Reed, A. M., Biodegradable polymers for use in surgery—polyglycolic/poly(actic acid) homo- and copolymers: 1. *Polymer* **1979,** *20* (12), 1459-1464.
14. Davis, K. A.; Burdick, J. A.; Anseth, K. S., Photoinitiated crosslinked degradable copolymer networks for tissue engineering applications. *Biomaterials* **2003,** *24* (14), 2485-2495.
15. Lu, S.; Anseth, K. S., Release Behavior of High Molecular Weight Solutes from Poly(ethylene glycol)-Based Degradable Networks. *Macromolecules* **2000,** *33* (7), 2509-2515.
16. Han, D. K.; Hubbell, J. A., Synthesis of Polymer Network Scaffolds from l-Lactide and Poly(ethylene glycol) and Their Interaction with Cells. *Macromolecules* **1997,** *30* (20), 6077-6083.
17. Sawhney, A. S.; Pathak, C. P.; Hubbell, J. A., Bioerodible hydrogels based on photopolymerized poly(ethylene glycol)-co-poly(.alpha.-hydroxy acid) diacrylate macromers. *Macromolecules* **1993,** *26* (4), 581-587.
18. Cruise, G. M.; Scharp, D. S.; Hubbell, J. A., Characterization of permeability and network structure of interfacially photopolymerized poly(ethylene glycol) diacrylate hydrogels. *Biomaterials* **1998,** *19* (14), 1287-1294.
19. Anseth, K. S.; Metters, A. T.; Bryant, S. J.; Martens, P. J.; Elisseeff, J. H.; Bowman, C. N., In situ forming degradable networks and their application in tissue engineering and drug delivery. *Journal of Controlled Release* **2002,** *78* (1–3), 199-209.
20. Mawad, D.; Martens, P. J.; Odell, R. A.; Poole-Warren, L. A., The effect of redox polymerisation on degradation and cell responses to poly (vinyl alcohol) hydrogels. *Biomaterials* **2007,** *28* (6), 947-955.
21. Nuttelman, C. R.; Henry, S. M.; Anseth, K. S., Synthesis and characterization of photocrosslinkable, degradable poly(vinyl alcohol)-based tissue engineering scaffolds. *Biomaterials* **2002,** *23* (17), 3617-3626.
22. Rydholm, A. E.; Held, N. L.; Bowman, C. N.; Anseth, K. S., Gel Permeation Chromatography Characterization of the Chain Length Distributions in Thiol−Acrylate Photopolymer Networks. *Macromolecules* **2006,** *39* (23), 7882-7888.
23. Lovestead, T. M.; Burdick, J. A.; Anseth, K. S.; Bowman, C. N., Understanding multivinyl monomer photopolymerization kinetics through modeling and GPC investigation of degradable networks. *Polymer* **2005,** *46* (16), 6226-6234.

24. Martens, P. J.; Bowman, C. N.; Anseth, K. S., Degradable networks formed from multi-functional poly(vinyl alcohol) macromers: comparison of results from a generalized bulk-degradation model for polymer networks and experimental data. *Polymer* **2004,** *45* (10), 3377-3387.
25. Uhrich, K. E.; Cannizzaro, S. M.; Langer, R. S.; Shakesheff, K. M., Polymeric Systems for Controlled Drug Release. *Chemical Reviews* **1999,** *99* (11), 3181-3198.
26. Carbone, A. L.; Uhrich, K. E., Design and Synthesis of Fast-Degrading Poly(anhydride-esters). *Macromolecular Rapid Communications* **2009,** *30* (12), 1021-1026.
27. Muggli, D. S.; Burkoth, A. K.; Keyser, S. A.; Lee, H. R.; Anseth, K. S., Reaction Behavior of Biodegradable, Photo-Cross-Linkable Polyanhydrides. *Macromolecules* **1998,** *31* (13), 4120-4125.
28. Burkoth, A. K.; Anseth, K. S., A review of photocrosslinked polyanhydrides:: in situ forming degradable networks. *Biomaterials* **2000,** *21* (23), 2395-2404.
29. Burkoth, A. K.; Anseth, K. S., MALDI-TOF Characterization of Highly Cross-Linked, Degradable Polymer Networks. *Macromolecules* **1999,** *32* (5), 1438-1444.
30. Anseth, K. S.; Quick, D. J., Polymerizations of Multifunctional Anhydride Monomers to Form Highly Crosslinked Degradable Networks. *Macromolecular Rapid Communications* **2001,** *22* (8), 564-572.
31. Hakala, R. A.; Korhonen, H.; Meretoja, V. V.; Seppälä, J. V., Photo-Cross-Linked Biodegradable Poly(Ester Anhydride) Networks Prepared from Alkenylsuccinic Anhydride Functionalized Poly(ε-caprolactone) Precursors. *Biomacromolecules* **2011,** *12* (7), 2806-2814.
32. Hakala, R. A.; Korhonen, H.; Seppälä, J. V., Hydrolysis behaviour of crosslinked poly(ester anhydride) networks prepared from functionalised poly(ε-caprolactone) precursors. *Reactive and Functional Polymers* **2013,** *73* (1), 11-17.
33. Poetz, K. L.; Mohammed, H. S.; Shipp, D. A., Surface Eroding, Semicrystalline Polyanhydrides via Thiol–Ene "Click" Photopolymerization. *Biomacromolecules* **2015,** *16* (5), 1650-1659.
34. Mönkäre, J.; Hakala, R. A.; Vlasova, M. A.; Huotari, A.; Kilpeläinen, M.; Kiviniemi, A.; Meretoja, V.; Herzig, K. H.; Korhonen, H.; Seppälä, J. V.; Järvinen, K., Biocompatible photocrosslinked poly(ester anhydride) based on functionalized poly(ε-caprolactone) prepolymer shows surface erosion controlled drug release in vitro and in vivo. *Journal of Controlled Release* **2010,** *146* (3), 349-355.
35. Rutherglen, B. G.; McBath, R. A.; Huang, Y. L.; Shipp, D. A., Polyanhydride Networks from Thiol−Ene Polymerizations. *Macromolecules* **2010,** *43* (24), 10297-10303.
36. Liu, X.; Pan, D.; Guo, Q.; Zhao, Y.; Wang, Z., The dominant role of polymer erosion in paclitaxel release from folate-modified poly(ether-anhydride) nanocarrier. *Journal of Applied Polymer Science* **2013,** *129* (2), 748-755.
37. Watkins, A. W.; Anseth, K. S., Copolymerization of photocrosslinkable anhydride monomers for use as a biodegradable bone cement. *Journal of Biomaterials Science - Polymer Edition* **2003,** *14* (3), 267-278.
38. Shastri, V. P.; Padera, R. F.; Tarcha, P.; Langer, R., A preliminary report on the biocompatibility of photopolymerizable semi-interpenetrating anhydride networks. *Biomaterials* **2004,** *25* (4), 715-721.

39. Sorkin, A.; von Zastrow, M., Signal transduction and endocytosis: close encounters of many kinds. *Nature Reviews Molecular Cell Biology* **2002,** *3* (8), 600-614.
40. Mellman, I.; Fuchs, R.; Helenius, A., Acidification of the endocytic and exocytic pathways. *Annual Review of Biochemistry* **1986,** *55* (1), 663-700.
41. Srinivasachar, K.; Neville, D. M., New protein crosslinking reagents that are cleaved by mild acid. *Biochemistry* **1989,** *28* (6), 2501-2509.
42. Murthy, N.; Thng, Y. X.; Schuck, S.; Xu, M. C.; Fréchet, J. M. J., A Novel Strategy for Encapsulation and Release of Proteins: Hydrogels and Microgels with Acid-Labile Acetal Cross-Linkers. *Journal of the American Chemical Society* **2002,** *124* (42), 12398-12399.
43. Gillies, E. R.; Goodwin, A. P.; Fréchet, J. M. J., Acetals as pH-Sensitive Linkages for Drug Delivery. *Bioconjugate Chemistry* **2004,** *15* (6), 1254-1263.
44. Kwon, Y. J.; Standley, S. M.; Goodwin, A. P.; Gillies, E. R.; Fréchet, J. M. J., Directed Antigen Presentation Using Polymeric Microparticulate Carriers Degradable at Lysosomal pH for Controlled Immune Responses. *Molecular Pharmaceutics* **2005,** *2* (1), 83-91.
45. Gillies, E. R.; Fréchet, J. M. J., pH-Responsive Copolymer Assemblies for Controlled Release of Doxorubicin. *Bioconjugate Chemistry* **2005,** *16* (2), 361-368.
46. Heath, W. H.; Palmieri, F.; Adams, J. R.; Long, B. K.; Chute, J.; Holcombe, T. W.; Zieren, S.; Truitt, M. J.; White, J. L.; Willson, C. G., Degradable Cross-Linkers and Strippable Imaging Materials for Step-and-Flash Imprint Lithography. *Macromolecules* **2008,** *41* (3), 719-726.
47. Palmieri, F.; Adams, J.; Long, B.; Heath, W.; Tsiartas, P.; Willson, C. G., Design of Reversible Cross-Linkers for Step and Flash Imprint Lithography Imprint Resists. *ACS Nano* **2007,** *1* (4), 307-312.
48. Yin, R.; Zhang, N.; Wu, W.; Wang, K., Poly(ethylene glycol)-grafted cyclic acetals based polymer networks with non-water-swellable, biodegradable and surface hydrophilic properties. *Materials Science and Engineering: C* **2016,** *62*, 137-143.
49. Bulmus, V.; Chan, Y.; Nguyen, Q.; Tran, H. L., Synthesis and Characterization of Degradable p(HEMA) Microgels: Use of Acid-Labile Crosslinkers. *Macromolecular Bioscience* **2007,** *7* (4), 446-455.
50. Knorr, V.; Russ, V.; Allmendinger, L.; Ogris, M.; Wagner, E., Acetal Linked Oligoethylenimines for Use As pH-Sensitive Gene Carriers. *Bioconjugate Chemistry* **2008,** *19* (8), 1625-1634.
51. Li, Y.; Du, W.; Sun, G.; Wooley, K. L., pH-Responsive Shell Cross-Linked Nanoparticles with Hydrolytically Labile Cross-Links. *Macromolecules* **2008,** *41* (18), 6605-6607.
52. Themistou, E.; Patrickios, C. S., Synthesis and Characterization of Polymer Networks and Star Polymers Containing a Novel, Hydrolyzable Acetal-Based Dimethacrylate Cross-Linker. *Macromolecules* **2006,** *39* (1), 73-80.
53. Kim, S.; Linker, O.; Garth, K.; Carter, K. R., Degradation kinetics of acid-sensitive hydrogels. *Polymer Degradation and Stability* **2015,** *121*, 303-310.
54. Themistou, E.; Patrickios, C. S., Star Polymers and Polymer Networks Containing a Novel, Hydrolyzable Diacetal-Based Dimethacrylate Cross-Linker: Synthesis, Characterization, and Hydrolysis Kinetics. *Macromolecules* **2007,** *40* (14), 5231-5234.

55. Themistou, E.; Patrickios, C. S., A Cleavable Network Based on Crosslinked Star Polymers Containing Acid-Labile Diacetal Crosslinks: Synthesis, Characterization and Hydrolysis. *Macromolecular Chemistry and Physics* **2008,** *209* (10), 1021-1028.
56. Chan, Y.; Bulmus, V.; Zareie, M. H.; Byrne, F. L.; Barner, L.; Kavallaris, M., Acid-cleavable polymeric core–shell particles for delivery of hydrophobic drugs. *Journal of Controlled Release* **2006,** *115* (2), 197-207.
57. Themistou, E.; Kanari, A.; Patrickios, C. S., Thermolyzable polymer networks and star polymers containing a novel, compact, degradable acylal-based dimethacrylate cross-linker: Synthesis, characterization, and thermolysis. *Journal of Polymer Science Part A: Polymer Chemistry* **2007,** *45* (24), 5811-5823.
58. Liang, B.; Qin, B.; Pastine, S.; Li, X. Reinforced composite and method for recycling the same. WO2013007128A1, 2013.
59. Qin, B.; Li, X.; Liang, B. Degradable Isocyanate Compounds and Applications Thereof. WO2015081610A1, 2015.
60. Qin, B.; Li, X.; Liang, B. Novel curing agents and degradable polymers and composites based thereon. WO2014169847A1, 2014.
61. Qin, B.; Li, X.; Liang, B. Novel cyclic acetal, cyclic ketal diamines epoxy curing agents and degradable polymers and composites based thereon. WO2014169846A1, 2014.
62. Pastine, S. Sterically hindered aliphatic polyamine cross-linking agents, compositions containing and uses thereof. WO2015054698A1, 2015.
63. Pastine, S. Processes for the preparation of di-(2-aminoethyl) formal, di-(3-aminopropyl) formal, and related molecules. US20130324764A1, 2013.
64. Petros, R. A.; Ropp, P. A.; DeSimone, J. M., Reductively Labile PRINT Particles for the Delivery of Doxorubicin to HeLa Cells. *Journal of the American Chemical Society* **2008,** *130* (15), 5008-5009.
65. Bilalis, P.; Varlas, S.; Kiafa, A.; Velentzas, A.; Stravopodis, D.; Iatrou, H., Preparation of hybrid triple-stimuli responsive nanogels based on poly(L-histidine). *Journal of Polymer Science Part A: Polymer Chemistry* **2015**, n/a-n/a.
66. Huang, X.; Appelhans, D.; Formanek, P.; Simon, F.; Voit, B., Tailored Synthesis of Intelligent Polymer Nanocapsules: An Investigation of Controlled Permeability and pH-Dependent Degradability. *ACS Nano* **2012,** *6* (11), 9718-9726.
67. Ulasan, M.; Yavuz, E.; Bagriacik, E. U.; Cengeloglu, Y.; Yavuz, M. S., Biocompatible thermoresponsive PEGMA nanoparticles crosslinked with cleavable disulfide-based crosslinker for dual drug release. *Journal of Biomedical Materials Research Part A* **2015,** *103* (1), 243-251.
68. Grant, N.; Wu, H.; Zhang, H., Reduction-Controlled Release of Organic Nanoparticles from Disulfide Cross-linked Porous Polymer. *Industrial & Engineering Chemistry Research* **2014,** *53* (1), 246-252.
69. Oh, J. K.; Tang, C.; Gao, H.; Tsarevsky, N. V.; Matyjaszewski, K., Inverse Miniemulsion ATRP: A New Method for Synthesis and Functionalization of Well-Defined Water-Soluble/Cross-Linked Polymeric Particles. *Journal of the American Chemical Society* **2006,** *128* (16), 5578-5584.
70. Bonner, D. K.; Zhao, X.; Buss, H.; Langer, R.; Hammond, P. T., Crosslinked linear polyethylenimine enhances delivery of DNA to the cytoplasm. *Journal of Controlled Release* **2013,** *167* (1), 101-107.

71. Han, S.-C.; He, W.-D.; Li, J.; Li, L.-Y.; Sun, X.-L.; Zhang, B.-Y.; Pan, T.-T., Reducible polyethylenimine hydrogels with disulfide crosslinkers prepared by michael addition chemistry as drug delivery carriers: Synthesis, properties, and in vitro release. *Journal of Polymer Science Part A: Polymer Chemistry* **2009,** *47* (16), 4074-4082.
72. Kilian, L.; Wang, Z.-H.; Long, T. E., Synthesis and cleavage of core-labile poly(alkyl methacrylate) star polymers. *Journal of Polymer Science Part A: Polymer Chemistry* **2003,** *41* (19), 3083-3093.
73. Mather, B. D.; Williams, S. R.; Long, T. E., Synthesis of an Acid-Labile Diacrylate Crosslinker for Cleavable Michael Addition Networks. *Macromolecular Chemistry and Physics* **2007,** *208* (18), 1949-1955.
74. Rudy, C. E.; Fugassi, P., The Thermal Decomposition of Tertiary Butyl Acetate. *Journal of Physical and Colloid Chemistry* **1948,** *52* (2), 357-363.
75. Ogino, K.; Chen, J.-S.; Ober, C. K., Synthesis and Characterization of Thermally Degradable Polymer Networks. *Chemistry of Materials* **1998,** *10* (12), 3833-3838.
76. Elladiou, M.; Patrickios, C. S., A dimethacrylate cross-linker cleavable under thermolysis or alkaline hydrolysis conditions: synthesis, polymerization, and degradation. *Chemical Communications* **2016,** *52* (15), 3135-3138.
77. Metz, N.; Theato, P., Synthesis and Characterization of Base Labile Poly(N-isopropylacrylamide) Networks Utilizing a Reactive Cross-Linker. *Macromolecules* **2009,** *42* (1), 37-39.
78. Chang, R.; Li, N.; Qin, J.; Wang, H., Easy degradable polymeric gel with extremely base-labile cross-linking. *Polymer* **2015,** *60*, 62-68.
79. Themistou, E.; Patrickios, C. S., Synthesis and Characterization of Star Polymers and Cross-Linked Star Polymer Model Networks Containing a Novel, Silicon-Based, Hydrolyzable Cross-Linker. *Macromolecules* **2004,** *37* (18), 6734-6743.
80. Parrott, M. C.; Luft, J. C.; Byrne, J. D.; Fain, J. H.; Napier, M. E.; DeSimone, J. M., Tunable Bifunctional Silyl Ether Cross-Linkers for the Design of Acid-Sensitive Biomaterials. *Journal of the American Chemical Society* **2010,** *132* (50), 17928-17932.
81. Ware, T.; Jennings, A. R.; Bassampour, Z. S.; Simon, D.; Son, D. Y.; Voit, W., Degradable, silyl ether thiol-ene networks. *RSC Advances* **2014,** *4* (75), 39991-40002.
82. Olah, M. G.; Robbins, J. S.; Baker, M. S.; Phillips, S. T., End-Capped Poly(benzyl ethers): Acid and Base Stable Polymers That Depolymerize Rapidly from Head-to-Tail in Response to Specific Applied Signals. *Macromolecules* **2013,** *46* (15), 5924-5928.
83. Lewis, G. G.; Robbins, J. S.; Phillips, S. T., Phase-Switching Depolymerizable Poly(carbamate) Oligomers for Signal Amplification in Quantitative Time-Based Assays. *Macromolecules* **2013,** *46* (13), 5177-5183.
84. Yeung, K.; Kim, H.; Mohapatra, H.; Phillips, S. T., Surface-Accessible Detection Units in Self-Immolative Polymers Enable Translation of Selective Molecular Detection Events into Amplified Responses in Macroscopic, Solid-State Plastics. *Journal of the American Chemical Society* **2015,** *137* (16), 5324-5327.

85. Liu, G.; Wang, X.; Hu, J.; Zhang, G.; Liu, S., Self-Immolative Polymersomes for High-Efficiency Triggered Release and Programmed Enzymatic Reactions. *Journal of the American Chemical Society* **2014,** *136* (20), 7492-7497.
86. Kim, H.; Mohapatra, H.; Phillips, S. T., Rapid, On-Command Debonding of Stimuli-Responsive Cross-Linked Adhesives by Continuous, Sequential Quinone Methide Elimination Reactions. *Angewandte Chemie International Edition* **2015,** *127* (44), 13255-13259.
87. García, J. M.; Jones, G. O.; Virwani, K.; McCloskey, B. D.; Boday, D. J.; ter Huurne, G. M.; Horn, H. W.; Coady, D. J.; Bintaleb, A. M.; Alabdulrahman, A. M. S.; Alsewailem, F.; Almegren, H. A. A.; Hedrick, J. L., Recyclable, Strong Thermosets and Organogels via Paraformaldehyde Condensation with Diamines. *Science* **2014,** *344* (6185), 732-735.
88. Fevre, M.; Wojtecki, R. J.; Hedrick, J.; García, J. M.; Hedrick, J. L., Tailorable Thermal Properties Through Reactive Blending Using Orthogonal Chemistries and Layer-by-Layer Deposition of Poly(1,3,5-hexahydro-1,3,5-triazine) Networks. *Advanced Functional Materials* **2016**, n/a-n/a.
89. Montarnal, D.; Capelot, M.; Tournilhac, F.; Leibler, L., Silica-Like Malleable Materials from Permanent Organic Networks. *Science* **2011,** *334* (6058), 965-968.
90. Bowman, C. N.; Kloxin, C. J., Covalent Adaptable Networks: Reversible Bond Structures Incorporated in Polymer Networks. *Angewandte Chemie International Edition* **2012,** *51* (18), 4272-4274.
91. Kloxin, C. J.; Bowman, C. N., Covalent adaptable networks: smart, reconfigurable and responsive network systems. *Chemical Society Reviews* **2013,** *42* (17), 7161-7173.
92. Kloxin, C. J.; Scott, T. F.; Adzima, B. J.; Bowman, C. N., Covalent Adaptable Networks (CANs): A Unique Paradigm in Cross-Linked Polymers. *Macromolecules* **2010,** *43* (6), 2643-2653.
93. Dingels, C.; Frey, H., From Biocompatible to Biodegradable: Poly(Ethylene Glycol)s with Predetermined Breaking Points. *Advanced Polymer Science* **2013,** *262* (Hierarchical Macromolecular Structures: 60 Years after the Staudinger Nobel Prize II), 167-190.
94. Kaitz, J. A.; Lee, O. P.; Moore, J. S., Depolymerizable polymers: preparation, applications, and future outlook. *MRS Communications* **2015,** *5* (02), 191-204.
95. Li, J.; Nagamani, C.; Moore, J. S., Polymer Mechanochemistry: From Destructive to Productive. *Accounts of Chemical Research* **2015,** *48* (8), 2181-2190.
96. Imbernon, L.; Norvez, S.; Leibler, L., Stress Relaxation and Self-Adhesion of Rubbers with Exchangeable Links. *Macromolecules* **2016,** *49* (6), 2172-2178.
97. Capelot, M.; Unterlass, M. M.; Tournilhac, F.; Leibler, L., Catalytic Control of the Vitrimer Glass Transition. *ACS Macro Letters* **2012,** *1* (7), 789-792.
98. Taynton, P.; Ni, H.; Zhu, C.; Yu, K.; Loob, S.; Jin, Y.; Qi, H. J.; Zhang, W., Repairable Woven Carbon Fiber Composites with Full Recyclability Enabled by Malleable Polyimine Networks. *Advanced Materials* **2016,** *28* (15), 2904-2909.
99. Taynton, P.; Yu, K.; Shoemaker, R. K.; Jin, Y.; Qi, H. J.; Zhang, W., Heat- or Water-Driven Malleability in a Highly Recyclable Covalent Network Polymer. *Advanced Materials* **2014,** *26* (23), 3938-3942.

100. Brutman, J. P.; Delgado, P. A.; Hillmyer, M. A., Polylactide Vitrimers. *ACS Macro Letters* **2014,** *3* (7), 607-610.
101. Fortman, D. J.; Brutman, J. P.; Cramer, C. J.; Hillmyer, M. A.; Dichtel, W. R., Mechanically Activated, Catalyst-Free Polyhydroxyurethane Vitrimers. *Journal of the American Chemical Society* **2015,** *137* (44), 14019-14022.
102. Kim, S.; Park, H.; Song, Y.; Hong, D.; Kim, O.; Jo, E.; Khang, G.; Lee, D., Reduction of oxidative stress by p-hydroxybenzyl alcohol-containing biodegradable polyoxalate nanoparticulate antioxidant. *Biomaterials* **2011,** *32* (11), 3021-3029.
103. Robb, M. J.; Moore, J. S., A Retro-Staudinger Cycloaddition: Mechanochemical Cycloelimination of a β-Lactam Mechanophore. *Journal of the American Chemical Society* **2015,** *137* (34), 10946-10949.
104. June, S. M.; Suga, T.; Heath, W. H.; Lin, Q.; Puligadda, R.; Yan, L.; Dillard, D.; Long, T. E., Photoactive Polyesters Containing o-Nitro Benzyl Ester Functionality for Photodeactivatable Adhesion. *The Journal of Adhesion* **2013,** *89* (7), 548-558.
105. June, S. M.; Suga, T.; Heath, W. H.; Long, T. E.; Lin, Q.; Puligadda, R., Photo-Reactive Polyimides and Poly(siloxane imide)s as Reversible Polymeric Interfaces. *The Journal of Adhesion* **2010,** *86* (10), 1012-1028.
106. Radl, S.; Kreimer, M.; Manhart, J.; Griesser, T.; Moser, A.; Pinter, G.; Kalinka, G.; Kern, W.; Schlögl, S., Photocleavable epoxy based materials. *Polymer* **2015,** *69*, 159-168.
107. Kevwitch, R. M.; McGrath, D. V., Synthesis and degradation of photolabile dendrimers based on o-nitrobenzyl ether photolabile cores. *New Journal of Chemistry* **2007,** *31* (7), 1332-1336.
108. Nagamani, C.; Liu, H.; Moore, J. S., Mechanogeneration of Acid from Oxime Sulfonates. *Journal of the American Chemical Society* **2016,** *138* (8), 2540-2543.

Chapter 4: Imidazolium-containing ABA Triblock Copolymers as Electroactive Devices

(Published in *ACS Applied Materials and Interfaces*, **2016**, *8*, 1280-1288.)

Evan Margaretta[a], Gregory B. Fahs[a], David L. Inglefield, Jr.[a], Chainika Jangu[a], Dong Wang[b], James R. Heflin[b], Robert B. Moore[a], Timothy E. Long[a*]

[a]*Department of Chemistry, Macromolecules and Interfaces Institute,* [b]*Department of Physics*
Virginia Tech, Blacksburg, VA 24061

*To whom correspondence should be addressed
E-mail: telong@vt.edu
TEL: (540)231-2480
FAX: (540)231-8517

Keywords: controlled polymerization, block copolymers, ionic liquids, self-assembly, electromechanical actuators

4.1 Abstract

Two-step reversible addition-fragmentation chain transfer (RAFT) polymerization and two subsequent post-polymerization modification steps afforded well-defined ABA triblock copolymers featuring mechanically reinforcing polystyrene outer blocks and 1-methylimidazole-neutralized poly(acrylic acid)-based central blocks. Size exclusion chromatography and ^{1}H NMR spectroscopy confirmed predictable molecular weights and narrow distributions. The ionic liquid (IL) 1-ethyl-3-methylimidazolium trifluoromethanesulfonate ([EMIm][OTf]) was incorporated at 30 wt % into polymeric films. Thermogravimetric analysis, differential scanning calorimetry, and dynamic mechanical analysis determined the thermomechanical properties of the polymers and polymer-IL composites. Atomic force microscopy, small angle X-ray scattering (SAXS), and transmission electron microscopy (TEM) determined surface and bulk morphologies,

and poly(Sty-*b*-AA(MeIm)-*b*-Sty) exhibited a change from packed cylindrical to lamellar morphology in SAXS upon IL incorporation. Electrochemical impedance spectroscopy determined the in-plane ionic conductivities of the polymer-IL membranes ($\sigma \sim 10^{-4}$ S/cm). A device fabricated from poly(Sty-*b*-AA(MeIm)-*b*-Sty) with 30 wt % incorporated IL demonstrated mechanical actuation under a low applied voltage of 4 V.

4.2 Introduction

Polymer-ionic liquid composites represent an emerging field of study owing to their synergy of thermomechanical and conductive properties.[1,2] In particular, polymers in conjunction with ionic liquid (IL) demonstrate suitability for various applications including sensors, artificial muscle, devices for energy harvesting, and gas separation membranes.[3,4,5,6] Electromechanical actuators based on ionic liquid-containing polymeric membranes offer robust mechanical integrity, greater design versatility, and enhanced response at low applied potential (< 10 V).[4,5, 7]

The use of block copolymers in ion-polymer transducers offers greater control over actuator properties. Block copolymers offer the advantage of tailored microphase-separated morphology, which greatly affects ionic conductivity in block copolymer films. Mahanthappa *et al.* showed the change in ionic conductivity as AB diblock copolymer morphology changed from hexagonally-packed cylinders to lamellar, and they compared these values to the corresponding homopolymer.[8] Elabd *et al.* also demonstrated the superior ionic conductivities on the scale of two-orders of magnitude for weakly microphase-separated AB diblock copolymers over their random copolymer analogues despite the absence of long-range periodicity.[9]

ABA triblock copolymers exhibit superior mechanical properties over AB diblock copolymers of similar composition, resulting from physical crosslinking at on each end of the low-T_g central block. Variation of block length and relative block incorporation enables precise tailoring of thermomechanical, morphological, and conductive properties of the final electromechanical transducer.[7, 10,11] For instance, Long *et al.* recently demonstrated ionic conductivity dependence on relative block lengths for ABA triblock copolymers with charged central blocks.[10] Several studies also report the preferential interaction of IL with polar phases of block copolymer matrices, demonstrating further suitability of block copolymers for electroactive devices.[12,13,14]

Eisenberg *et al.* reported extensively on the self-assembling nature of polystyrene (PS) and poly(acrylic acid) (PAA) AB diblock copolymers.[15,16,17,18,19] An additional report studied PS-*b*-PAA-*b*-PS and demonstrated self-assembly in IL 1-butyl-3-methylimidazolium hexafluorophosphate (BMIm PF_6).[20] Transmission electron microscopy (TEM) revealed a change from vesicles to micelles with increased molecular weight of PAA central block. Another study investigated an AB diblock copolymer of PS and poly(sodium acrylate) (PNaA) in the presence of varying amounts of 1-cetylpyridinium surfactant.[21] In the solid state, these materials contained cetyl chain crystalline domains with amorphous PS and PNaA domains, depending on the level of surfactant loading. Previous work also established the suitability of imidazolium-containing polymers for electromechanical actuators due to their inherent thermal stability and excellent ionic conductivity.[10, 22,23,24] Vinylbenzylimidazole (VBIm)-based triblock copolymers synthesized with nitroxide-mediated polymerization yielded actuators with response behaviors comparable to industry benchmark Nafion® when incorporated with IL.[10] In this

case, the imidazolium cation was covalently bound to the polymer backbone. In our other work, alkylimidazole neutralization of a sulfonated symmetric pentablock copolymer and subsequent swelling with IL provided an actuator with mobile imidazolium counterion.[24]

In the present work, neutralization of PS-*b*-PAA-*b*-PS-based triblock copolymers with 1-methylimidazole (MeIm) presents the imidazolium functionality in novel poly(Sty--*b*-AA(MeIm)-*b*-Sty) and poly(Sty-*b*-[nBA$_{4\%}$-*co*-AA(MeIm)$_{96\%}$]-*b*-Sty) ABA triblock copolymers. This manuscript details the RAFT synthesis and thermomechanical properties of these novel ABA triblock copolymers. Furthermore, the present study examines the incorporation of 1-ethyl-3-methylimidazolium trifluoromethanesulfonate ([EMIm][OTf]) to yield polymer-IL composite with ionic conductivity on the order of 10^{-4} S/cm and demonstrates actuation behavior of the resulting fabricated electromechanical transducer.

4.3 Experimental

4.3.1 Materials. Styrene (Sty, >99%), *n*-butyl acrylate (nBA, 99%), and *t*-butyl acrylate (tBA, >98%) were purchased from Sigma Aldrich and passed through a basic alumina column to remove inhibitor. 2,2'-Azobis(isobutyronitrile) (AIBN, Aldrich, 99%) was recrystallized twice from methanol. 1-Methylimidazole (MeIm, ≥99%) was purchased from Sigma Aldrich and distilled prior to use. 1-Ethyl-3-methylimidazolium trifluoromethanesulfonate ([EMIm][OTf], >99%) was purchased from Sigma Aldrich and dried *in vacuo* at 100 °C for 18 h prior to use. Carbon disulfide (≥99%), tetrabutyl ammonium hydrogen sulfate (TBA HSO_4, ≥99%), sodium hydroxide (NaOH, ≥97%), anhydrous 1,4-dioxane, HCl (4.0 M in 1,4-dioxane), and phenolphthalein (ACS grade) were purchased from Sigma Aldrich and used as received. All other solvents were purchased from Spectrum Chemical and used without further purification.

4.3.2 Synthesis of polystyrene (PS) precursor

2-(1-carboxy-1-methylsulfanylthiocarbonylsulfanyl)-2-methylpropionic acid (CMP) was synthesized in accordance with previously established literature.[25] In a typical RAFT polymerization, AIBN (16.4 mg, 0.1 mmol), CMP (282 mg, 1 mmol), and Sty (220 mL, 1.92 mol) were added to a 500-mL, round-bottomed flask equipped with magnetic stirring. The solution was sparged with argon for 30 min, and the reaction was subsequently immersed in a mineral oil bath thermostated at 65 °C. Monomer conversion was monitored with ^{1}H NMR spectroscopy in $CDCl_3$ as the reaction proceeded, while THF SEC provided molecular weight data. The reaction was terminated after 48 h at 25% monomer conversion through the introduction of air and removal from heat. To ensure complete monomer removal, the product was precipitated into methanol and collected with vacuum filtration, then subsequently reprecipitated into methanol from a 30 wt % THF solution, collected with vacuum filtration, and dried at 60 °C *in vacuo* for 18 h.

4.3.3 Synthesis of ABA triblock copolymers

In a typical RAFT polymerization, a 100 mL, round-bottomed flask equipped with a magnetic stir bar was charged with AIBN (17.6 mg, 107 μmol), PS precursor (10 g, 216 μmol), butyl acrylate (16.6 g, 130 mmol), and *N*,*N*-dimethylformamide (DMF, 64 mL). The relative ratios of tBA and nBA incorporated into the central block of the ABA triblock copolymer was varied, with central block compositions of 0 and 5 mol % nBA targeted. The polymerization reaction was sparged with argon for 20 minutes to remove air, and submerged in a thermostated 70 °C mineral oil bath. The reaction was terminated after 10 h through the introduction of air and removal from heat. The product was precipitated into CH_3OH:H_2O mixture (4:1, v:v) and vacuum filtration was employed to collect the solids.

^{1}H NMR spectroscopy provided M_n data for the central block consistent with the molecular weight data as determined through THF SEC, and also determined the relative incorporation of tBA and nBA in the central block to be consistent with the charged values. Films of poly(Sty-*b*-tBA-*b*-Sty) and poly(Sty-*b*-[nBA$_{4\%}$-*co*-tBA$_{96\%}$]-*b*-Sty) were cast from 10 wt % in THF. The films were annealed at 110 °C for 8 h, then 110 °C *in vacuo* for 8 h.

4.3.4 Acid cleavage of t-butyl esters

t-Butyl esters were selectively cleaved through an adapted acidolysis procedure.[26] ABA triblock copolymer was added to a round-bottomed flask equipped with a magnetic stir bar. HCl (4.0 M in 1,4-dioxane) was added to achieve five equivalents of acid per *t*-butyl ester. Additional 1,4-dioxane was added to afford a final polymer concentration of 75 g/L. The reaction flask was sealed and allowed to stir at 25 °C for 48 h. The product was precipitated into hexanes and collected through decantation of the supernatant. The solids were then redissolved in THF at 30 wt % and reprecipitated into hexanes. Vacuum filtration isolated the product, which was washed thoroughly with diethyl ether and collected in quantitative yield. The product was dried at 40 °C *in vacuo* for 18 h. ^{1}H NMR spectroscopy indicated the quantitative selective cleavage of *t*-butyl esters. Films of poly(Sty-*b*-AA-*b*-Sty) and poly(Sty-*b*-[nBA$_{4\%}$-*co*-AA$_{96\%}$]-*b*-Sty) were cast onto Si-coated PET from 10 wt % solutions in 9:2 THF:CH_3OH mixture. The films were dried at 40 °C for 8 h, then 40 °C *in vacuo* for 8 h.

4.3.5 Neutralization of carboxylic acid-containing copolymers

To introduce imidazolium groups to the polymer, the acrylic acid units were neutralized with MeIm according to the following procedure. Acid-containing triblock copolymers were dissolved in a round-bottomed flask equipped with a magnetic stir bar at

10 wt % in THF:CH_3OH mixture (9:2, v:v). MeIm was added dropwise in the presence of phenolphthalein indicator until the persistence of a slight pink color, and the solution was allowed to stir for 16 h at 25 °C. The reaction was then dialyzed against THF, and solvent was subsequently removed under rotary evaporation to afford the product in quantitative yield. The product was dried at 40 °C *in vacuo* for 18 h. Films of poly(Sty-*b*-AA(MeIm)-*b*-Sty) and poly(Sty-*b*-[$nBA_{4\%}$-*co*-$AA(MeIm)_{96\%}$]-*b*-Sty) were cast onto Si-coated PET from 10 wt % solutions in THF:CH_3OH mixture (9:2, v:v). The films were further dried at 40 °C for 8 h, then 40 °C *in vacuo* for 8 h.

4.3.6 Ionic liquid incorporation

The ionic liquid (IL) [EMIm][OTf] was incorporated to the imidazolium-containing triblock copolymers in the following fashion. The polymer was dissolved at 10 wt % in THF:CH_3OH mixture (9:2, v:v). [EMIm][OTf] was added by micropipette at 30 wt % IL relative to the polymer. The solution was subjected to magnetic stirring for 24 h at 25 °C. Films were cast directly from solution onto a PTFE substrate and subsequently annealed at 110 °C for 8 h, then 110 °C *in vacuo* for 8 h. Dried films were stored in a vacuum desiccator until immediately prior to further characterization to eliminate potential water uptake.

4.3.7 Synthesis of random copolymer control

To determine polymer microstructure effect on properties, the random copolymer analogue of poly(Sty-*b*-tBA-*b*-Sty) was synthesized. Sty (5.00 mL, 43.6 mmol), tBA (7.66 mL, 52.3 mmol), AIBN (16.4 mg, 0.1 mmol) and DMF (56.3 mL) were charged to a 100-mL, round-bottomed flask equipped with a magnetic stir bar. The solution was sparged with argon for 20 min and subsequently immersed in a thermostated 65 °C mineral oil bath

and allowed to stir for 24 h. The polymer product was precipitated in 4:1 CH_3OH:H_2O, collected by vacuum filtration, and dried at 50 °C *in vacuo* for 18 h. ^{1}H NMR spectroscopy determined the polymer composition of 61:39 molar ratio of Sty:tBA. THF SEC provided the molecular weight data. Poly(Sty-*co*-tBA) was then subjected to the same acid cleavage and MeIm neutralization modification steps as detailed above. Poly(Sty-*co*-AA(MeIm)) was cast with 30 wt% [EMIm][OTf] from 10 wt% THF solution and annealed for 8 h at 80 °C, then at 80 °C *in vacuo* for an additional 18 h. The dried film was stored in a vacuum desiccator until immediately prior to further characterization to eliminate potential water uptake.

4.3.8 Analytical Methods

^{1}H NMR spectroscopy (Varian Unity, 400 MHz, $CDCl_3$, DMSO-d_6) confirmed structure of monomer and polymer in addition to monomer conversion. Melting points were recorded on an Electrothermal 1101D Mel-Temp melting point apparatus operating at 10 °C/min. Tetrahydrofuran (THF) size exclusion chromatography (SEC) at 30 ºC using a flow rate of 1.0 mL/min through three Polymer Laboratories PLgel 5 µm MIXED-C columns determined the molecular weights of the obtained polymers. SEC instrumentation included a Waters717plus autosampler equipped with Waters 515 HPLC pump, Waters 2414 refractive index detector, and Wyatt miniDawn MALLS detector operating at 690 nm. Differential scanning calorimetry (DSC, TA Instruments Q2000) determined thermal transitions using a standard heat/cool/heat method with 10 °C/min heating rate and 100 °C/min cooling rate under constant N_2 purge. All glass transition temperature (T_g) values are reported from the second heats. Thermogravimetric analysis (TGA, TA Instruments Q50) recorded the 5%-weight loss temperature ($T_{d,5\%}$) of the polymers when subjected to

a 10 °C/min temperature ramp under constant N_2 purge. Dynamic mechanical analysis (DMA, TA Instruments Q800) was performed in oscillatory tension mode at 1 Hz with temperature ramp of 3 °C/min. Electrochemical impedance spectroscopy (EIS, Autolab PGSTAT 302N) was performed using a four-point electrode sample cell at 10% ± 0.1% relative humidity in an ESPEC BTL-433 environmental chamber which controls temperature to 0.1 °C. Alternating sine-wave potential (0.2 V) was applied over 0.1-10^6 Hz frequency range. The high *x*-axis intercept of the Nyquist plot of imaginary impedance as a function of real impedance gave the resistance value.

4.3.9 Morphological analysis

A Veeco MultiMode scanning microscope yielded atomic force microscopy (AFM) images. Triblock copolymer films were imaged with in tapping mode with a set point ratio of 0.78 using a nano-sensor silicon tip with spring constant of 42 N m^{-1}. Samples for transmission electron microscopy were cryomicrotomed, vapor stained for 1 h with OsO_4, and subsequently imaged with a Phillips EM420 transmission electron micrograph operating at 120 kV acceleration voltage. Images were processed with the profile feature in Gatan Digital Micrograph software, and domain sizes are reported as the average of 50 domains from five images of varied magnification.

Small angle X-ray scattering (SAXS) experiments were performed using a Rigaku S-Max 3000 3 pinhole SAXS system, equipped with a rotating anode emitting X-rays with a wavelength of 0.154 nm (Cu Kα). The sample-to-detector distance was 1603 mm, and q-range was calibrated using a silver behenate standard. Two-dimensional SAXS patterns were obtained using a fully integrated 2D multiwire, proportional counting, gas-filled detector, with an exposure time of 1 hour. The SAXS data have been corrected for sample

thickness, sample transmission and background scattering. All the SAXS data were analyzed using the SAXSGUI software package to obtain radially integrated SAXS intensity versus scattering vector q, where q=($4\pi/\lambda$)sin(θ), θ is one half of the scattering angle, and λ is the wavelength of X-ray.

Peak positions were determined from an exponential least squares fit of the 1-D scattering profiles. The fits were performed using a sum of Gaussian distributions. In order to accurately determine the Gaussian fit parameters, a second-order polynomial removed the Bonart thermal background, and Porod's Law accounted for the scattering contribution from the phase boundaries. The intensity is defined as follows:

$I(q) = \sum_i G_i(q) + P_2(q) + \frac{K}{q^4}$, where

$P_2(q) = a + b\,q + c\,q^2$ and $G_i(q) = A_i\,Exp[-\frac{(q-q_{0,i})^2}{2\sigma_i^2}]$

4.3.10 Actuation behavior

The electromechanical device was fabricated and tested as follows: a gold foil leaf (120 nm thick, L.A. Gold Leaf Wholesaler) electrode was hot pressed on each side of the membrane with 700 lb. force at 90 °C for 20 sec. Subsequently the membrane was cut into strips (1 mm by 1 cm) for actuation tests.

The tests were performed on a custom built probe station which clamps one end of fabricated device between two electrodes while permitting free movement at the other end. A DC step voltage (4.0 V, HP 6218A power supply) was applied to the actuator. A SONY HXR-MC1 high-definition video camera recorded the bending at 30 FPS for further analysis. The actuation curvature (inverse radius) was determined by the relationships: I=2rsin(θ/2) and a=rθ, where I is the distance between the free tip and fixed end of the bend actuator, r is the radius of the curve, a is the arc length, and θ is the arc angle. Positive

curvature was arbitrarily assigned when the actuator bent toward the cathode, with negative curvature indicating bending towards the anode.

4.4 Results and Discussion

4.4.1 Synthesis and thermomechanical characterization

RAFT polymerization afforded precise triblock copolymers using the convergent CTA CMP in two steps (**Scheme 4.1**). First, bulk polymerization of styrene yielded the PS precursor used for subsequent central block additions. Then, the controlled central block addition yielded poly(Sty-*b*-tBA-*b*-Sty) and poly(Sty-*b*-[nBA$_{4\%}$-*co*-tBA$_{96\%}$]-*b*-Sty). **Table 4.1** contains the molecular weight data as obtained from THF SEC and ^{1}H NMR spectroscopy, and calculated molecular weights of the post-modified polymers (**Scheme 4.2**) based on quantitative conversion. The polymer products exhibited no change in molecular weight or PDI in the acid hydrolysis step owing to the chemical stability of the trithiocarbonate functionality under the reaction conditions. Previous literature also established the electrochemical and thermal stability of trithiocarbonate-containing RAFT agents.[27,28] PDI values near 1.2 for the triblocks represented good control for acrylate polymerization given the well-known presence of intra- and intermolecular chain transfer to acrylic backbone.[29] T_g and $T_{d,5\%}$ values as determined with DSC and TGA, respectively, are reported as well.

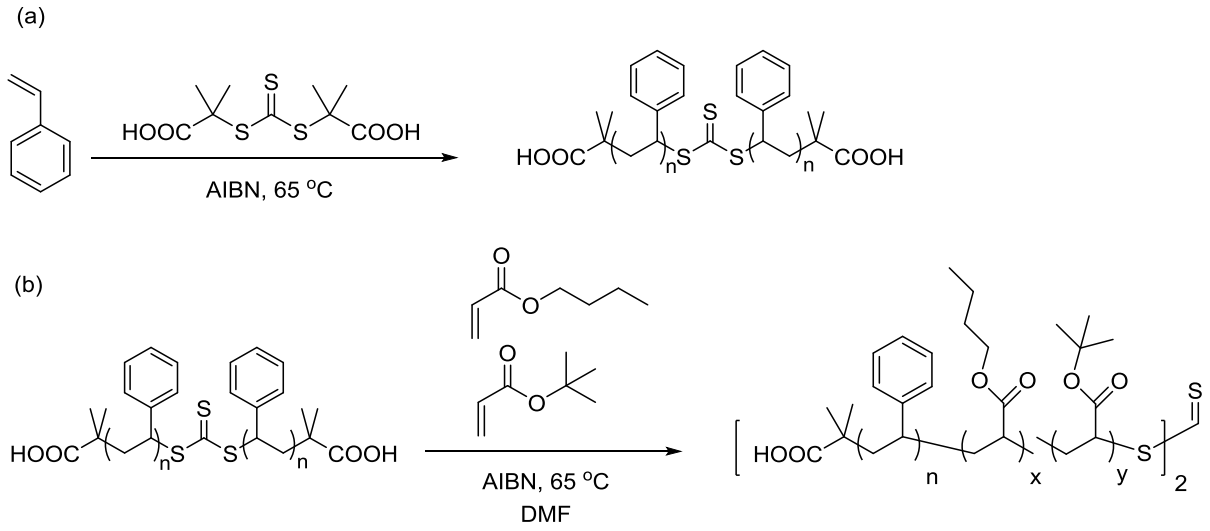

Scheme 4.1. Synthesis of (a) polystyrene precursor and (b) poly(styrene-*b*-(*n*BA-*co*-*t*BA)-*b*-styrene) ABA triblock copolymer.

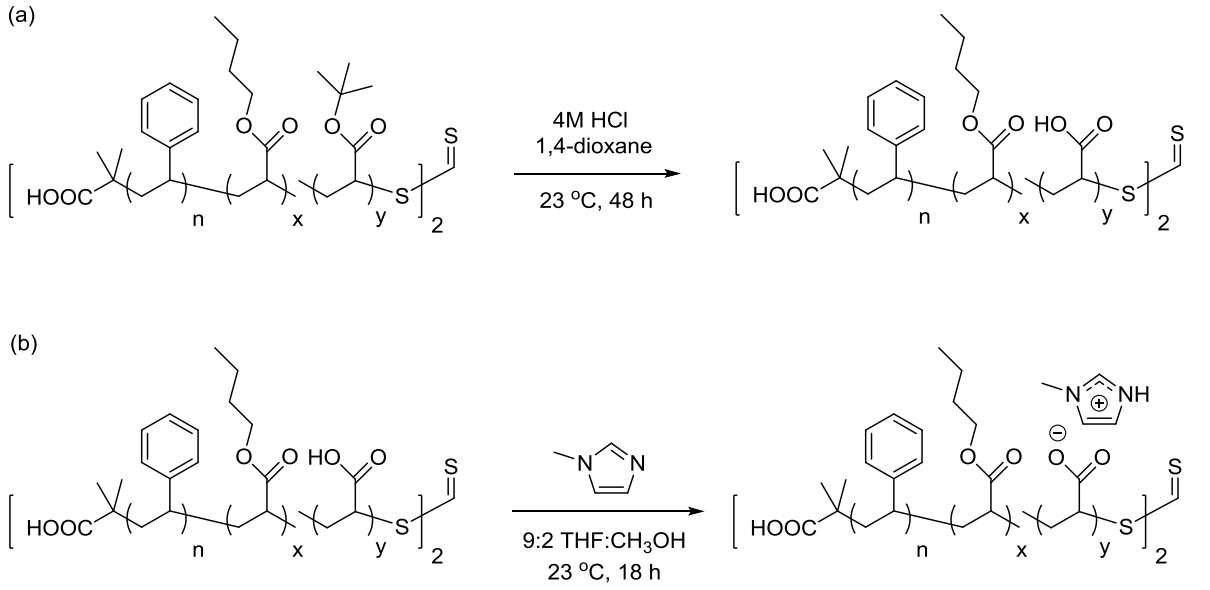

Scheme 4.2. Postpolymerization modification (a) of poly(styrene-*b*-(*n*BA-*co*-*t*BA)-*b*-styrene) to yield poly(styrene-*b*-(*n*BA-*co*-AA)-*b*-styrene) and (b) subsequent neutralization with 1-methylimidazole.

TGA (**Table 4.1**) data demonstrated clear trends. Degradation of poly(Sty-*b*-tBA-*b*-Sty) and poly(Sty-*b*-[nBA$_{4\%}$-*co*-tBA$_{96\%}$]-*b*-Sty) near 220-230 °C correlated with *t*-butyl ester thermolysis to liberate isobutylene.[30,31] This observed weight loss agreed with incorporation of tBA determined through ^{1}H NMR spectroscopy. Similarly, $T_{d,5\%}$ values observed for poly(Sty-*b*-AA(MeIm)-*b*-Sty) and poly(Sty-*b*-[nBA$_{4\%}$-*co*-AA(MeIm)$_{96\%}$]-*b*-

Sty) agreed well with the boiling point of 1-methylimidazole (198 °C), indicating the evolution of 1-methylimidazole following the reverse acid-base reaction.

Table 4.1. Polymer molecular weight and thermal properties.

Polymer	M_n (kg/mol)	M_w (kg/mol)	PDI	$T_{g,1}$ (°C)	$T_{g,2}$ (°C)	$T_{d,5\%}$ (°C)
PS precursor	46.4	48.7	1.05	100	--	331
Poly(Sty-*b*-tBA-*b*-Sty)	114	136	1.19	101	48	226
Poly(Sty-*b*-AA-*b*-Sty)	84.9*	101*		99	ND	254
Poly(Sty-*b*-AA(MeIm)-*b*-Sty)	128*	152*		98	70	190
with 30 wt% incorporated [EMIm][OTf]				100	8	189
Poly(Sty-b-[$nBA_{4\%}$-*co*-$tBA_{96\%}$]-b-Sty)	119	144	1.21	101	42	231
Poly(Sty-b-[$nBA_{4\%}$-*co*-$AA_{96\%}$]-b-Sty)	88.6*	107*		100	ND	251
Poly(Sty-b-[$nBA_{4\%}$-*co*-$AA(MeIm)_{96\%}$]-b-Sty)	133*	160*		100	65	196
with 30 wt% incorporated [EMIm][OTf]				106	-15	192
Poly(Sty-*co*-tBA)	78.6	128	1.64	77	--	235
Poly(Sty-*co*-AA)	66.1*	108*		100	--	269
Poly(Sty-*co*-AA(MeIm))	119*	195*		103	--	152
with 30 wt% incorporated [EMIm][OTf]				67	--	201

ND = not determined; *calculated based on quantitative postpolymerization modification steps

Observation of two T_gs in DSC (**Table 4.1**) indicated the microphase-separated morphology of the triblock copolymers. Copolymerization of nBA and tBA in the central block insertion step yielded a random copolymer central block displaying a T_g at 42 °C, consistent with Fox equation's prediction of 44 °C. Incorporation of nBA imparted greater central block flexibility through decreasing central block T_g. In the case of each triblock copolymer, T_g at or near 100 °C suggested the presence of a PS phase. For poly(Sty-*b*-AA-*b*-Sty) and poly(Sty-*b*-[$nBA_{4\%}$-*co*-$AA_{96\%}$]-*b*-Sty), no second T_g was observed below the $T_{d,5\%}$, likely due to AA dehydration prior to onset of segmental motion. Neutralization to yield poly(Sty-*b*-AA(MeIm)-*b*-Sty) and poly(Sty-*b*-[$nBA_{4\%}$-*co*-$AA(MeIm)_{96\%}$]-*b*-Sty) lead to central block T_g values of 70 °C and 65 °C, respectively, as a result of decreased hydrogen bonding, suppression of anhydride formation, and increase in free volume concomitant with incorporation of bulkier MeIm counterion. Upon 30 wt% incorporation

of the [EMIm][OTf], the central block T_g values for poly(Sty-*b*-AA(MeIm)-*b*-Sty) and poly(Sty-*b*-[nBA$_{4\%}$-*co*-AA(MeIm)$_{96\%}$]-*b*-Sty) dropped to 8 °C and -15 °C, respectively. The T_gs of the mechanically reinforcing PS outer blocks remained unchanged, demonstrating selective incorporation of IL to the imidazolium-containing central blocks. The absence of IL melting endotherm at -13°C in the DSC thermograms confirmed complete uptake of the IL into the polymer and indicated the absence of free IL in the membranes.

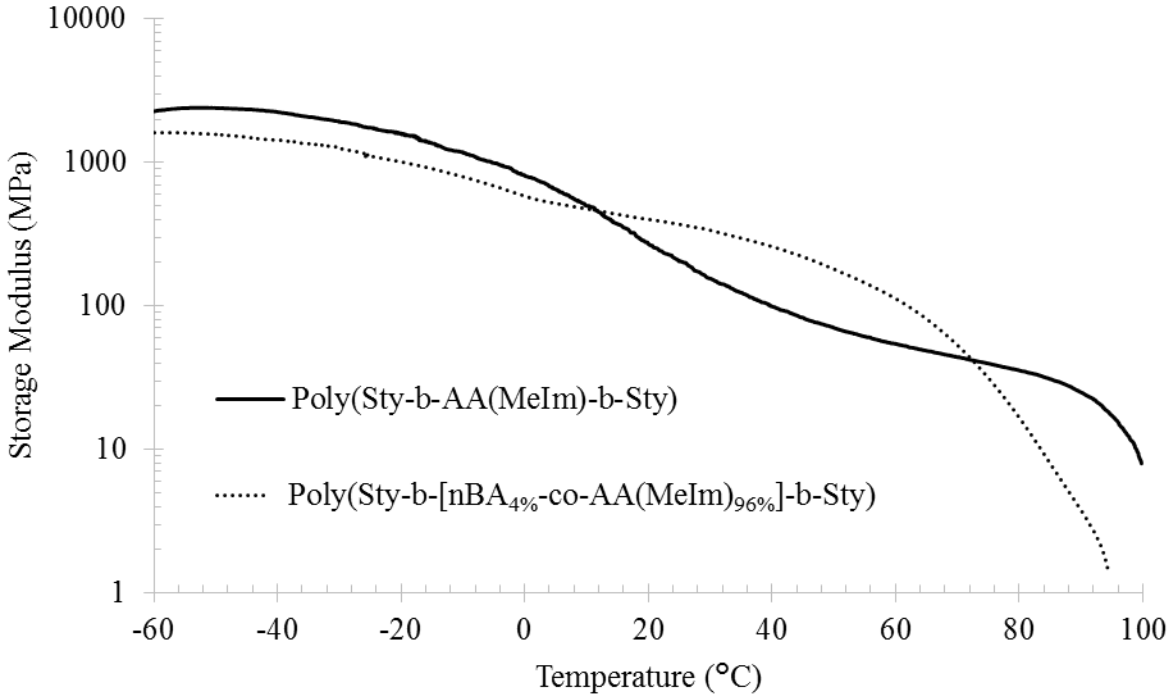

Figure 4.1. DMA elucidates the thermomechanical properties of the obtained triblock copolymers with 30 wt% incorporated IL.

The brittle nature of poly(Sty-*b*-AA(MeIm)-*b*-Sty) and poly(Sty-*b*-[nBA$_{4\%}$-*co*-AA(MeIm)$_{96\%}$]-*b*-Sty) prevented determination of thermomechanical properties using DMA. Incorporation of IL through a "cast with" procedure sufficiently plasticized the ion-containing central blocks to yield flexible films suitable for such analysis (**Figure 4.1**).

DMA demonstrated the microphase separation observed with DSC with two clear transitions evident in each curve. The first decrease in storage moduli occurred at temperatures that corresponded well with central block T_gs, while the flow temperatures near 100 °C related to PS T_g. While the IL-containing membrane of poly(Sty-*b*-[nBA$_{4\%}$-*co*-AA(MeIm)$_{96\%}$]-*b*-Sty) displayed the lower central block T_g in both DMA and DSC, its plateau modulus remained significantly higher than that observed for poly(Sty-*b*-AA(MeIm)-*b*-Sty). A plateau modulus ~100 MPa at room temperature demonstrated the robust mechanical integrity and sufficient flexibility required for electroactive device applications.[22]

4.4.2 Ionic conductivity

EIS (**Figure 4.2**) highlighted the conductive nature of the IL-containing membranes with in-plane ionic conductivities on the order of 10^{-4} S/cm. Poly(Sty-*b*-AA(MeIm)-*b*-Sty) exhibited similar ionic conductivity to poly(Sty-*b*-[nBA$_{4\%}$-*co*-AA(MeIm)$_{96\%}$]-*b*-Sty) over the same temperature range when each membrane possessed 30 wt % [EMIm][OTf]. The brittle nature of the films in the absence of IL prohibited EIS for those samples. When comparing poly(Sty-*b*-AA(MeIm)-*b*-Sty) with its random copolymer analogue poly(Sty-*co*-AA(MeIm)), the importance of microphase-separated morphology was evident, as the random copolymer exhibited conductivities on the order of 10^{-5} S/cm, representing an order of magnitude gain in conductivity upon the introduction of well-defined microphase separation. The increase observed for the in-plane ionic conductivity proves consistent with previous literature observation.[9]

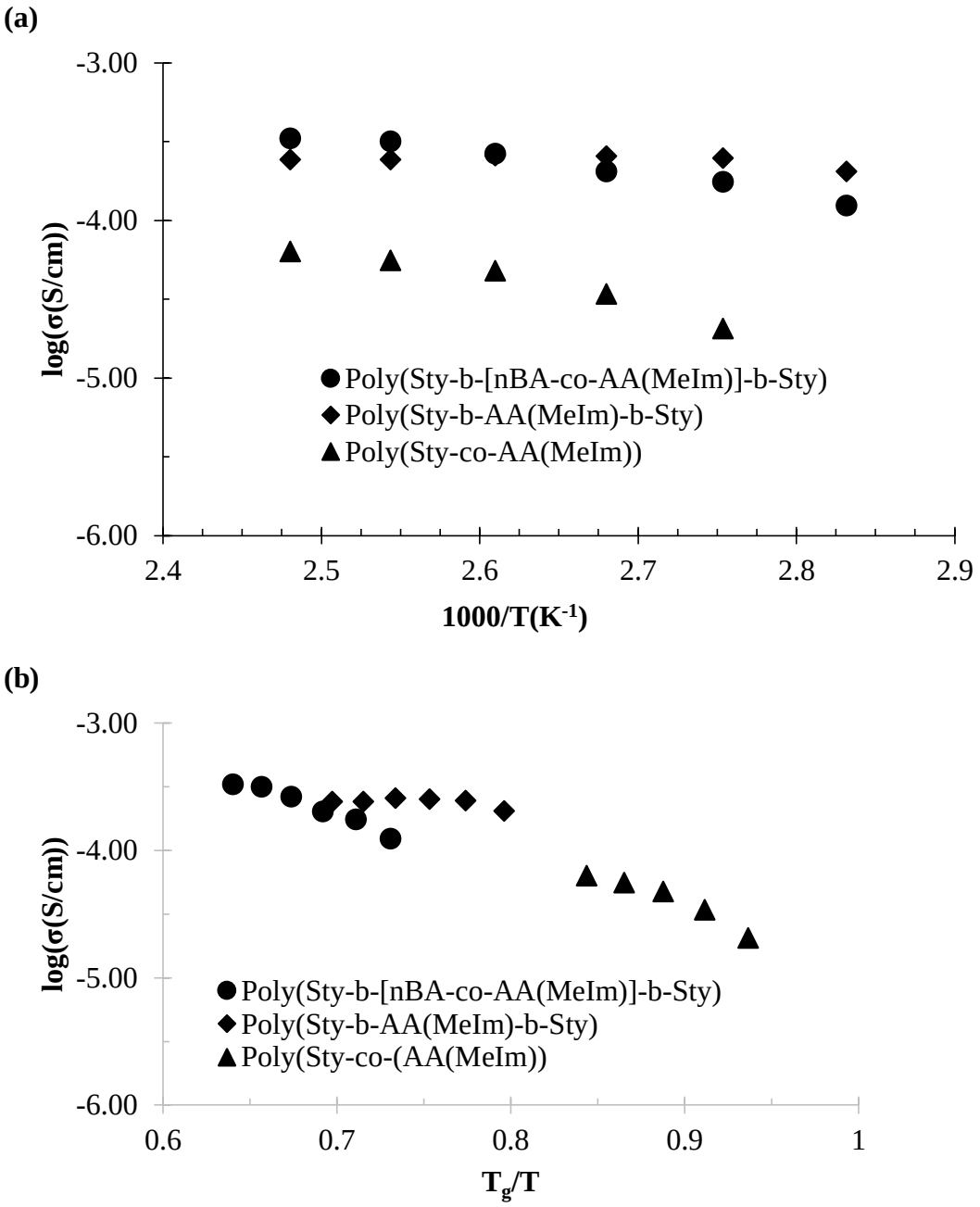

Figure 4.2. Impedance spectroscopy confirms the superior conductivity in the absence of *n*BA with (a) change in temperature and (b) when normalized by T_g.

The ionic conductivity values observed here compare well with those previously reported for ionic ABA triblock copolymers as well as fabricated electromechanical devices.[10,22,23] Frisbie, Lodge *et al.* reported ionic conductivities on the order of 10^{-4} S/cm

in the same temperature range for ion gels comprised of 50 wt % PS-*b*-PMMA-*b*-PS (30 wt % PS) in [EMIm][Tf_2N].[12] Watanabe then reported the actuation of PS-*b*-PMMA-*b*-PS (48 wt % PS) ion gels comprised of 30 wt % polymer in [EMIm][Tf_2N].[13] While Frisbie and Lodge did not comment on the morphology of the ion gels, AFM demonstrated the presence of PS spheres distributed in IL-PMMA continuous phase in Watanabe's similar ion gels, which also displayed ionic conductivity ~10^{-3} S/cm. The ionic conductivity for poly(Sty-*b*-AA(MeIm)-*b*-Sty) proved within an order of magnitude even at significantly reduced ionic liquid loading, indicating the competitive nature of the polymers with current literature benchmarks, especially given the absence of free IL in the polymer-IL membranes.

4.4.3 Morphological characterization

AFM (**Figure 4.3a-b)** revealed the surface morphologies of poly(Sty-*b*-AA(MeIm)-*b*-Sty) and poly(Sty-*b*-[$nBA_{4\%}$-*co*-$AA(MeIm)_{96\%}$]-*b*-Sty) in the absence of IL and confirmed the phase separated nature of the materials suggested with DSC. Poly(Sty-*b*-AA(MeIm)-*b*-Sty) exhibits hexagonally packed cylinders on the surface of the membrane and poly(Sty-*b*-[$nBA_{4\%}$-*co*-$AA(MeIm)_{96\%}$]-*b*-Sty) displays well-defined lamellar surface morphology. In particular, SAXS (**Figure 4.3c**, **Table 4.2**) indicated the presence of an ordered morphology, consistent with packed cylinders rather than spheres in poly(Sty-*b*-AA(MeIm)-*b*-Sty), with broad scattering peaks at $q^*:\sqrt{3}:3$. The SAXS profile of poly(Sty-*b*-[$nBA_{4\%}$-*co*-$AA(MeIm)_{96\%}$]-*b*-Sty) illustrates the presence of reflections indicative of microphase separation but in contrast with the AFM results (**Figure 4.3b**) it does not conclusively reveal any long range order in the bulk. Because central block molecular weights remained similar, nBA incorporation into the central block

likely affected the Flory-Huggins interaction parameter χ sufficiently enough to induce significant change in morphology. However, the present investigation did not include determination of this parameter.

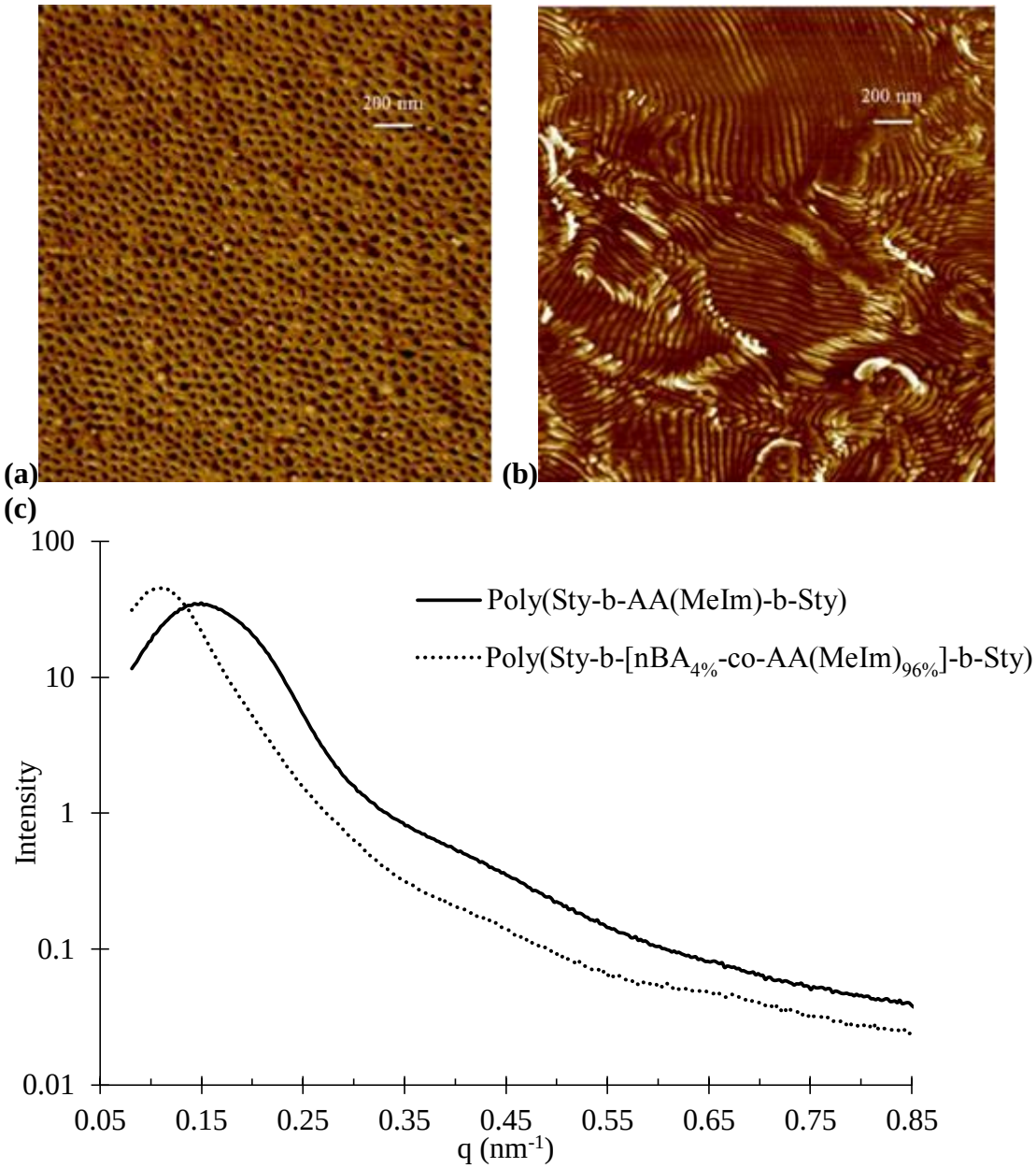

Figure 4.3. AFM phase images of (a) Poly(Sty-b-AA(MeIm)-b-Sty), (b) Poly(Sty-b-[$nBA_{4\%}$-co-$AA(MeIm)_{96\%}$]-b-Sty) reveal differences in surface morphologies, and (c) SAXS profiles indicate bulk morphologies similar to those observed in AFM.

Table 4.2. Summary of SAXS analysis

Sample	Scattering Peaks	Morphology
Poly(Sty-*b*-AA(MeIm)-*b*-Sty)	$q^*, \sqrt{3}q, 3q$	cylindrical
with 30 wt % IL	$q^*, 3q, 5q$	lamellar
Poly(Sty-*b*-[nBA$_{4\%}$-*co*-AA(MeIm)$_{96\%}$]-*b*-Sty)	q^*	ND
with 30 wt % IL	$q^*, \sqrt{3}q, \sqrt{8}q$	ND

ND = not determined

SAXS also probed bulk morphology of IL-containing membranes (**Figure 4.4**), further confirming the phase separation indicated in DMA and DSC. Scattering peaks at ratios *q*:3:5* suggest lamellar morphology upon the incorporation of IL into poly(Sty-*b*-AA(MeIm)-*b*-Sty) (**Table 4.2**). Microphase structure critically affects ionic conductivity of membranes, with films possessing lamellar morphology exhibiting higher ionic conductivity than those having hexagonally-packed cylinders.[8] When polymer samples approach 50:50 vol %, structure and form factors in the scattering may overlay and reduce peak intensity at even integral reflections.[32,33] The primary scattering peak position at 0.125 nm^{-1} correlated to d-spacing of 50.3 nm. The change from packed cylinders to lamellae ostensibly resulted from varying both χ and volume fraction of the central block. Meanwhile, the SAXS profile for poly(Sty-*b*-[nBA$_{4\%}$-*co*-AA(MeIm)$_{96\%}$]-*b*-Sty) cast with 30 wt% IL indicates microphase-separated bulk morphology with some degree of long-range order; however, the broad secondary scattering peaks of $q^*:\sqrt{3}:\sqrt{8}$ do not directly correlate to geometries commonly observed for ABA triblock copolymers.

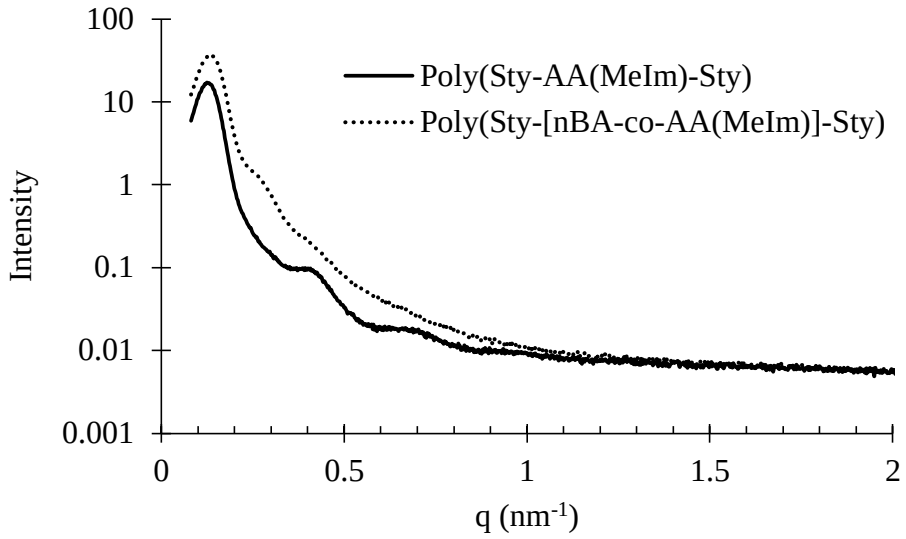

Figure 4.4. SAXS profiles of poly(Sty-*b*-AA(MeIm)-*b*-Sty) (solid) and poly(Sty-*b*-[$nBA_{4\%}$-co-$AA(MeIm)_{96\%}$]-*b*-Sty) (dotted) reveal microphase separation when cast with 30 wt% [EMIm][OTf] ionic liquid.

TEM clearly revealed the bulk morphologies of poly(Sty-*b*-AA(MeIm)-*b*-Sty) and poly(Sty-*b*-[$nBA_{4\%}$-*co*-$AA(MeIm)_{96\%}$]-*b*-Sty), further confirming the SAXS data. (**Figure 4.5**). The micrographs clearly showed the lamellar bulk morphology of poly(Sty-*b*-AA(MeIm)-*b*-Sty). The images revealed interlamellar spacing of 51.15 ± 4.79 nm, which correlated well with the d-spacing as determined using SAXS. **Figure 4.5a** demonstrates the small grain size of the lamellar domains, which explains the broad nature of the peaks in the SAXS profiles. Increasing the magnification (**Figure 4.5b**) better reveals the well-defined order of the lamellar domains. The small grain size may provide some explanation for the conductivity of the film. Balsara demonstrated the inverse correlation of lamellar domain grain size with ionic conductivity in block copolymer electrolyte samples.[34]

(a)

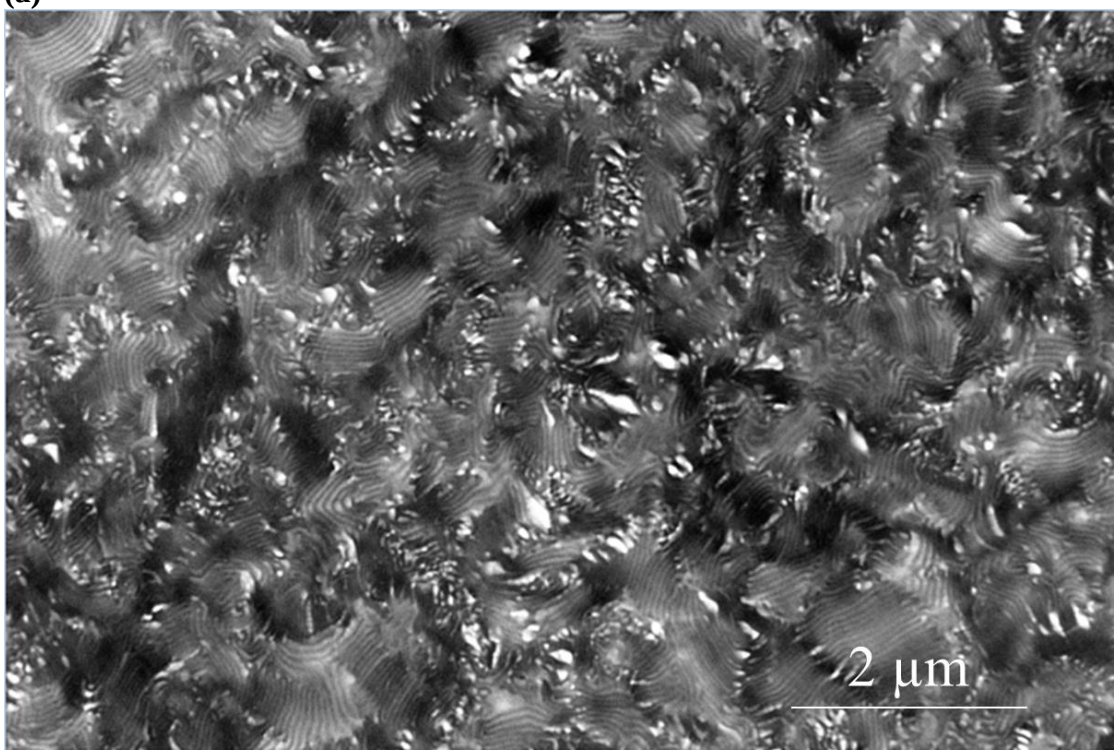

(b)

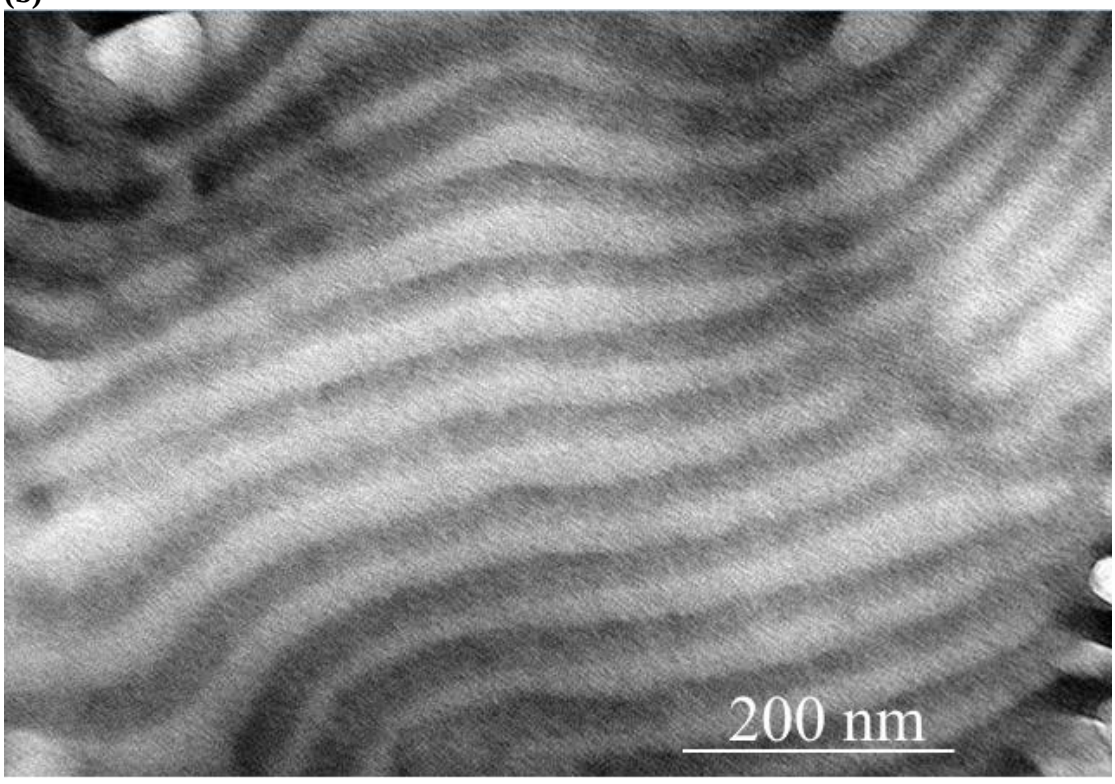

(c) 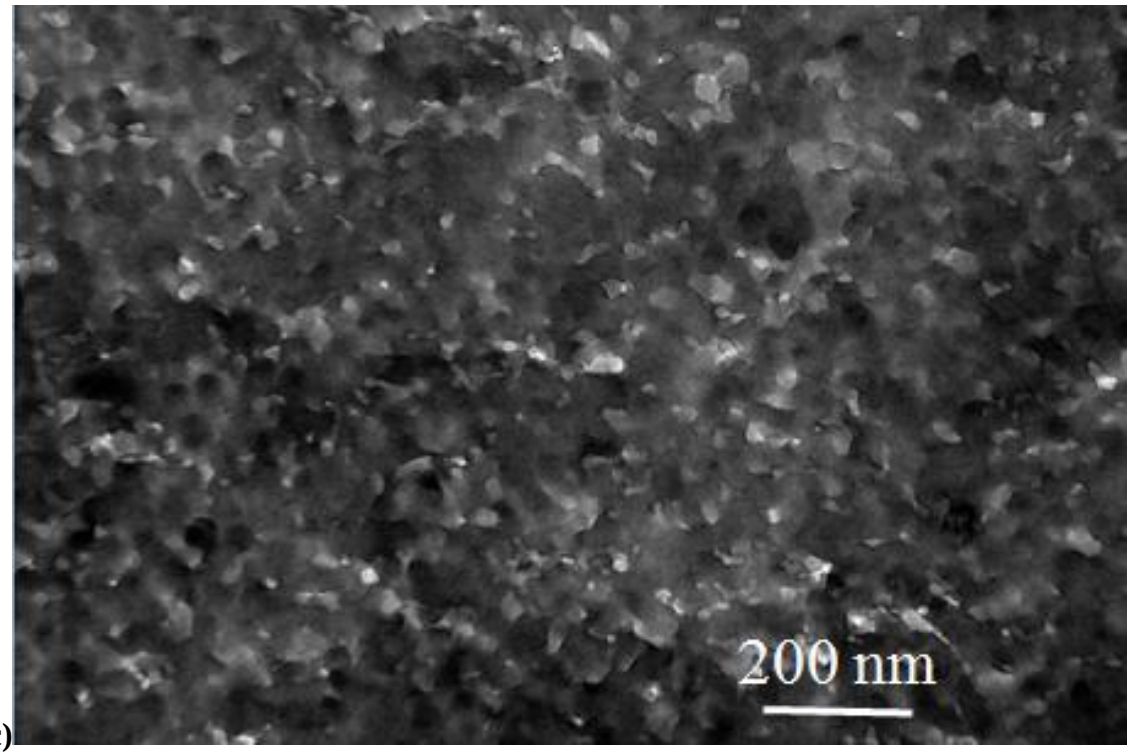

Figure 4.5. Transmission electron micrographs of OsO_4-stained poly(Sty-*b*-AA(MeIm)-*b*-Sty) at (a) 7,500x and (b) 96,000x magnification and (c) poly(Sty-*b*-[$nBA_{4\%}$-*co*-$AA(MeIm)_{96\%}$]-*b*-Sty) at 96,000x magnification. All samples have 30 wt% [EMIm][OTf] incorporated.

4.4.4 Actuation behavior

Poly(Sty-*b*-AA(MeIm)-*b*-Sty) proved especially attractive for further investigation of actuation behavior due to its robust thermomechanical properties, superior room temperature ionic conductivity, and lamellar morphology upon incorporation of IL. The fabricated actuator does not include conductive nanocomposite (CNC) layers between the polymer-IL membrane and the gold electrodes. The layer-by-layer (LbL) assembly process involves repeated sequential immersion of the polymer-IL film into solutions of cationic poly(allyl amine) hydrochloride (PAH) and anionic gold nanoparticles.[10,24] CNC layers impart enhanced ion transport properties and offer

increased surface area at the electrode interface.[1,10,22,24] Cationic PAH solution proves sufficiently acidic (pH = 4.0) to protonate PAA central block (pK_a = 4.7) causing rapid leeching of IL from the membrane, likely a result of MeIm-polymer dissociation in the central block. PAH solutions with pH > 5.0 reduced the rate of – but did not prevent – IL leeching. Therefore, the fabrication process removed CNC LbL assembly in favor of directly hot pressing the gold foil electrodes to each side of the polymer-IL membrane.

Figure 4.6a illustrates the mechanical deformation response to electric potential stimulus. The membrane initially bent towards the cathode before reversing towards the anode. The bidirectional bending resulted from the time difference between accumulation of mobile cations at the anode and mobile anions at the cathode and typifies polymer-IL transducer actuation.[10, 35] These observations proved consistent with Madsen *et al.*'s diffusion measurements for [EMIm][OTf] in Nafion® membranes wherein the larger cation moved up to three times faster at low levels of hydration.[36]

(a)

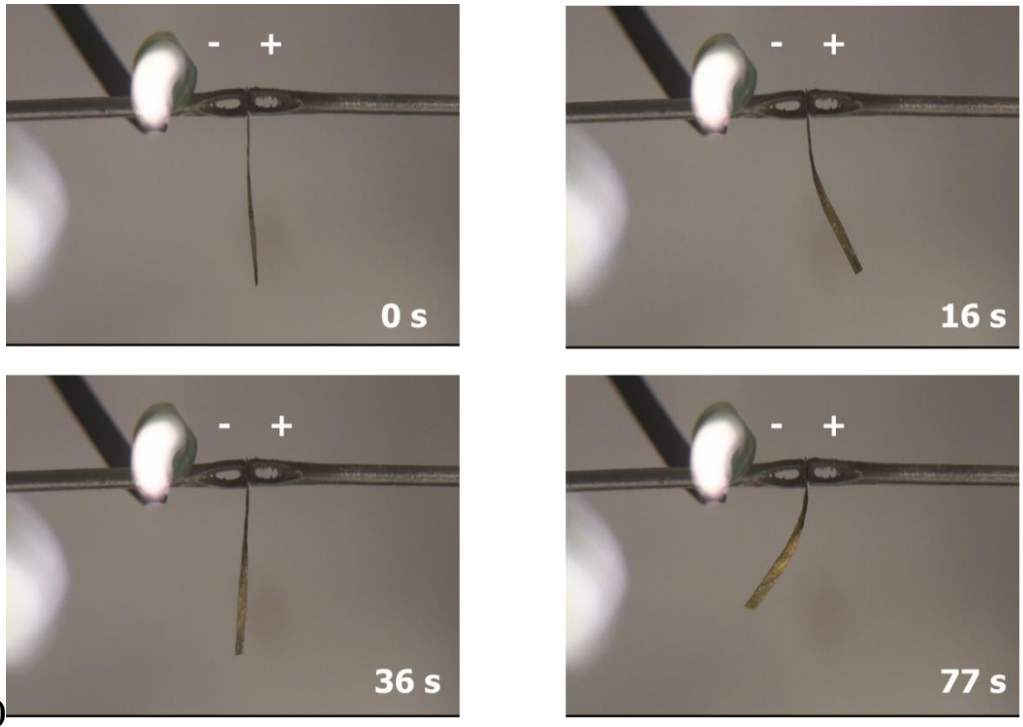

(b)

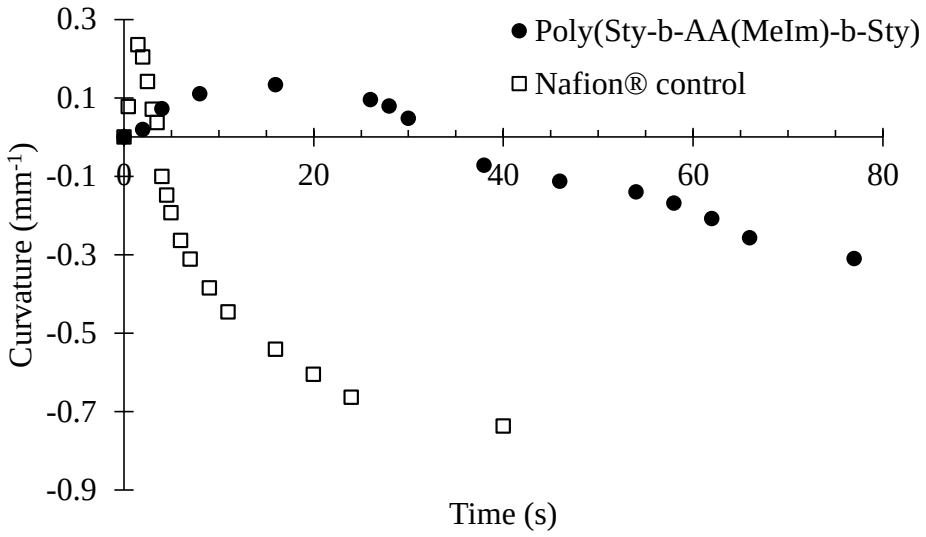

Figure 4.6. (a) Actuation behavior and (b) curvature of Poly(Sty-*b*-AA(MeIm)-*b*-Sty) with 30 wt% EMIm OTf incorporated (●) and Nafion® membrane with 29.5 wt% EMIm OTf incorporated (□).

Figure 4.6b displays the curvature of the device as a function of time during application of electric potential compared to a Nafion® control. The actuator exhibited initial forward curvature similar to previously studied imidazolium sulfonated pentablock copolymer, although the presently investigated membrane displays a faster response time, even in the absence of CNC layers.[24] The ionic conductivity on the order of 10^{-4} S/cm for poly(Sty-*b*-AA(MeIm)-*b*-Sty) with 30 wt % [EMIm][OTf] as a result of lamellar bulk morphology explains the actuation performance of the fabricated device.

4.5 Conclusion

For the first time, we prepared an electromechanical transducer using anionic ABA triblock copolymer poly(Sty-*b*-AA(MeIm)-*b*-Sty) and ionic liquid [EMIm][OTf]. RAFT polymerization yielded ABA triblock copolymers poly(Sty-*b*-tBA-*b*-Sty) and poly(Sty-*b*-

[nBA$_{4\%}$-*co*-tBA$_{96\%}$]-*b*-Sty) with PDI approximately 1.20. Two subsequent postpolymerization modification steps yielded novel ion-containing polymers poly(Sty-*b*-AA(MeIm)-*b*-Sty) and poly(Sty-*b*-[nBA$_{4\%}$-*co*-AA(MeIm)$_{96\%}$]-*b*-Sty). The synthesized polymers exhibited microphase separation as observed using DMA and DSC. SAXS and AFM further confirmed the polymer films' self-assembly. Upon the incorporation of 30 wt % [EMIm][OTf], poly(Sty-*b*-AA(MeIm)-*b*-Sty) demonstrated a plateau modulus ~100 MPa in DMA, desirable for electromechanical transducer fabrication. EIS determined in-plane conductivity values for poly(Sty-*b*-AA(MeIm)-*b*-Sty) and poly(Sty-*b*-[nBA$_{4\%}$-*co*-AA(MeIm)$_{96\%}$]-*b*-Sty) membranes containing 30 wt % IL on the order of 10^{-4} S/cm, representing an order of magnitude increase over a random copolymer analogue. Given the absence of free IL, these conductivity values compete with current literature benchmarks. For the first time, SAXS investigated the bulk morphologies of these polymer-IL membranes, revealing lamellar morphology in poly(Sty-*b*-AA(MeIm)-*b*-Sty) and packed cylinders in poly(Sty-*b*-[nBA$_{4\%}$-*co*-AA(MeIm)$_{96\%}$]-*b*-Sty). Poly(Sty-*b*-AA(MeIm)-*b*-Sty) exhibited lamellar morphology, thermomechanical properties, and noteworthy ionic conductivity upon [EMIm][OTf] incorporation, and proved suitable as an electromechanical actuator, with a fabricated transducer demonstrating initial response time and bending magnitude comparable to literature examples, even in the absence of CNC.

4.6 Acknowledgments

This material is based on work supported by the U.S. Army Research Office under Grant W911NF-07-1-0452 Ionic Liquids in Electro-Active Devices (ILEAD) MURI. The

authors acknowledge the staff and facilities of the Virginia Tech Nanoscale Characterization and Fabrication Laboratory (NCFL).

4.7 References

1. Duncan, A. J.; Leo, D. J.; Long, T. E., Beyond Nafion: Charged Macromolecules Tailored for Performance as Ionic Polymer Transducers. *Macromolecules* **2008,** *41* (21), 7765-7775.
2. Lodge, T. P., A Unique Platform for Materials Design. *Science* **2008,** *321* (5885), 50-51.
3. Akle, B. J.; Donald, J. L., Characterization and Modeling of Extensional and Bending Actuation in Ionomeric Polymer Transducers. *Smart Mater. Struct.* **2007,** *16* (4), 1348.
4. Akle, B. J.; Bennett, M. D.; Leo, D. J.; Wiles, K. B.; McGrath, J. E., Direct Assembly Process: A Novel Fabrication Technique for Large Strain Ionic Polymer Transducers. *J. Mater. Sci.* **2007,** *42* (16), 7031-7041.
5. Pelrine, R.; Kornbluh, R.; Pei, Q.; Joseph, J., High-Speed Electrically Actuated Elastomers with Strain Greater Than 100%. *Science* **2000,** *287* (5454), 836-839.
6. Gu, Y.; Cussler, E. L.; Lodge, T. P., ABA-Triblock Copolymer Ion Gels for CO2 Separation Applications. *J. Membr. Sci.* **2012,** *423–424* (0), 20-26.
7. Wu, T.; Wang, D.; Zhang, M.; Heflin, J. R.; Moore, R. B.; Long, T. E., RAFT Synthesis of ABA Triblock Copolymers as Ionic Liquid-Containing Electroactive Membranes. *ACS Appl. Mater. Interfaces* **2012,** *4* (12), 6552-6559.
8. Weber, R. L.; Ye, Y.; Schmitt, A. L.; Banik, S. M.; Elabd, Y. A.; Mahanthappa, M. K., Effect of Nanoscale Morphology on the Conductivity of Polymerized Ionic Liquid Block Copolymers. *Macromolecules* **2011,** *44* (14), 5727-5735.
9. Ye, Y.; Choi, J.-H.; Winey, K. I.; Elabd, Y. A., Polymerized Ionic Liquid Block and Random Copolymers: Effect of Weak Microphase Separation on Ion Transport. *Macromolecules* **2012,** *45* (17), 7027-7035.
10. Jangu, C.; Wang, J.-H. H.; Wang, D.; Sharick, S.; Heflin, J. R.; Winey, K. I.; Colby, R. H.; Long, T. E., Well-Defined Imidazolium ABA Triblock Copolymers as Ionic-Liquid-Containing Electroactive Membranes. *Macromol. Chem. Phys.* **2014,** *215* (13), 1319-1331.
11. Cheng, S.; Beyer, F. L.; Mather, B. D.; Moore, R. B.; Long, T. E., Phosphonium-Containing ABA Triblock Copolymers: Controlled Free Radical Polymerization of Phosphonium Ionic Liquids. *Macromolecules* **2011,** *44* (16), 6509-6517.
12. Zhang, S.; Lee, K. H.; Frisbie, C. D.; Lodge, T. P., Ionic Conductivity, Capacitance, and Viscoelastic Properties of Block Copolymer-Based Ion Gels. *Macromolecules* **2011,** *44* (4), 940-949.
13. Imaizumi, S.; Kokubo, H.; Watanabe, M., Polymer Actuators Using Ion-Gel Electrolytes Prepared by Self-Assembly of ABA-Triblock Copolymers. *Macromolecules* **2011,** *45* (1), 401-409.
14. He, Y.; Li, Z.; Simone, P.; Lodge, T. P., Self-Assembly of Block Copolymer Micelles in an Ionic Liquid. *J. Am. Chem. Soc.* **2006,** *128* (8), 2745-2750.

15. Burke, S. E.; Eisenberg, A., Effect of Sodium Dodecyl Sulfate on the Morphology of Polystyrene-b-Poly(acrylic acid) Aggregates in Dioxane−Water Mixtures. *Langmuir* **2001,** *17* (26), 8341-8347.
16. Luo, L.; Eisenberg, A., Thermodynamic Size Control of Block Copolymer Vesicles in Solution. *Langmuir* **2001,** *17* (22), 6804-6811.
17. Shen, H.; Eisenberg, A., Block Length Dependence of Morphological Phase Diagrams of the Ternary System of PS-b-PAA/Dioxane/H2O. *Macromolecules* **2000,** *33* (7), 2561-2572.
18. Yu, Y.; Zhang, L.; Eisenberg, A., Morphogenic Effect of Solvent on Crew-Cut Aggregates of Amphiphilic Diblock Copolymers. *Macromolecules* **1998,** *31* (4), 1144-1154.
19. Zhang, L.; Shen, H.; Eisenberg, A., Phase Separation Behavior and Crew-Cut Micelle Formation of Polystyrene-b-poly(acrylic acid) Copolymers in Solutions. *Macromolecules* **1997,** *30* (4), 1001-1011.
20. Zheng, L.; Chai, Y.; Liu, Y.; Zhang, P., Controlled RAFT Synthesis of Polystyrene-b-poly(acrylic acid)-b-polystyrene Block Copolymers and their Self-assembly in an Ionic Liquid [BMIM][PF6]. *e-Polym.* **2011,** *11* (1), 436-443.
21. Lysenko, E. A.; Bronich, T. K.; Eisenberg, A.; Kabanov, V. A.; Kabanov, A. V., Block Ionomer Complexes from Polystyrene-block-polyacrylate Anions and N-Cetylpyridinium Cations. *Macromolecules* **1998,** *31* (14), 4511-4515.
22. Green, M. D.; Choi, J.-H.; Winey, K. I.; Long, T. E., Synthesis of Imidazolium-Containing ABA Triblock Copolymers: Role of Charge Placement, Charge Density, and Ionic Liquid Incorporation. *Macromolecules* **2012,** *45* (11), 4749-4757.
23. Green, M. D.; Wang, D.; Hemp, S. T.; Choi, J.-H.; Winey, K. I.; Heflin, J. R.; Long, T. E., Synthesis of Imidazolium ABA triblock Copolymers for Electromechanical Transducers. *Polymer* **2012,** *53* (17), 3677-3686.
24. Gao, R.; Wang, D.; Heflin, J. R.; Long, T. E., Imidazolium Sulfonate-containing Pentablock Copolymer-Ionic Liquid Membranes for Electroactive Actuators. *J. Mater. Chem.* **2012,** *22* (27), 13473-13476.
25. Lai, J. T.; Filla, D.; Shea, R., Functional Polymers from Novel Carboxyl-Terminated Trithiocarbonates as Highly Efficient RAFT Agents. *Macromolecules* **2002,** *35* (18), 6754-6756.
26. Colombani, O.; Ruppel, M.; Schubert, F.; Zettl, H.; Pergushov, D. V.; Müller, A. H. E., Synthesis of Poly(n-butyl acrylate)-block-poly(acrylic acid) Diblock Copolymers by ATRP and Their Micellization in Water. *Macromolecules* **2007,** *40* (12), 4338-4350.
27. Li, Q.; Hu, X.; Bai, R., Synthesis of Photodegradable Polystyrene with Trithiocarbonate as Linkages. *Macromol. Rapid Commun.* **2015,** *36* (20), 1810-1815.
28. de Freitas, A. G. O.; Trindade, S. G.; Muraro, P. I. R.; Schmidt, V.; Satti, A. J.; Villar, M. A.; Ciolino, A. E.; Giacomelli, C., Controlled One-Pot Synthesis of Polystyrene-block-Polycaprolactone Copolymers by Simultaneous RAFT and ROP. *Macromol. Chem. Phys.* **2013,** *214* (20), 2336-2344.
29. Ahmad, N. M.; Charleux, B.; Farcet, C.; Ferguson, C. J.; Gaynor, S. G.; Hawkett, B. S.; Heatley, F.; Klumperman, B.; Konkolewicz, D.; Lovell, P. A.; Matyjaszewski, K.; Venkatesh, R., Chain Transfer to Polymer and Branching in

Controlled Radical Polymerizations of n-Butyl Acrylate. *Macromol. Rapid. Commun.* **2009,** *30* (23), 2002-2021.
30. Rudy, C. E.; Fugassi, P., The Thermal Decomposition of Tertiary Butyl Acetate. *J. Phys. Colloid Chem.* **1948,** *52* (2), 357-363.
31. Dugas, V.; Chevalier, Y., Chemical Reactions in Dense Monolayers: In Situ Thermal Cleavage of Grafted Esters for Preparation of Solid Surfaces Functionalized with Carboxylic Acids. *Langmuir* **2011,** *27* (23), 14188-14200.
32. Roe, R. J., *Methods of X-Ray and Neutron Scattering in Polymer Science*. Oxford University Press: 2000.
33. Honeker, C. C.; Thomas, E. L.; Albalak, R. J.; Hajduk, D. A.; Gruner, S. M.; Capel, M. C., Perpendicular Deformation of a Near-Single-Crystal Triblock Copolymer with a Cylindrical Morphology. 1. Synchrotron SAXS. *Macromolecules* **2000,** *33* (25), 9395-9406.
34. Chintapalli, M.; Chen, X. C.; Thelen, J. L.; Teran, A. A.; Wang, X.; Garetz, B. A.; Balsara, N. P., Effect of Grain Size on the Ionic Conductivity of a Block Copolymer Electrolyte. *Macromolecules* **2014,** *47* (15), 5424-5431.
35. Yang, L.; Sheng, L.; Junhong, L.; Dong, W.; Jain, V.; Montazami, R.; Heflin, J. R.; Jing, L.; Madsen, L.; Zhang, Q. M., Ion Transport and Storage of Ionic Liquids in Ionic Polymer Conductor Network Composites. *Appl. Phys. Lett.* **2010,** *96* (22), 223503.
36. Hou, J.; Zhang, Z.; Madsen, L. A., Cation/Anion Associations in Ionic Liquids Modulated by Hydration and Ionic Medium. *J. Phys. Chem. B* **2011,** *115* (16), 4576-4582.

Chapter 5: Properties of Ionic Liquid-Containing Sulfonated Copolymer Ternary Electrolytes

(*In preparation* for submission)

Evan Margaretta, Zhiyang Zhang, Mingtao Chen, Sachin Gangele, Timothy E. Long*

Department of Chemistry, Macromolecules Innovation Institute
Virginia Tech, Blacksburg, VA 24061

*To whom correspondence should be addressed
E-mail: telong@vt.edu
TEL: (540)231-2480
FAX: (540)231-8517

Keywords: controlled polymerization, block copolymers, ionic liquids, battery electrolytes, post-polymerization modification

5.1 Abstract

Researchers commonly address enhanced battery performance through optimization of binary electrolyte mixtures of polymer and ionic liquid (IL) or IL and lithium salt. Recently, ternary polymer electrolytes that contain all three components emerged as a viable and attractive target. Constructing composition-property relationships for IL-sulfonated copolymer binary mixtures established the plasticizing effect of IL on sulfonic acid-containing polymers. When the cation was exchanged to Li^+, ILs exhibited slight antiplasticization at low incorporations before demonstrating an overall general trend of plasticization. Furthermore, viscosity, conductivity, and diffusion measurements for binary mixtures of 1-ethyl-3-methylimidazolium bis(trifluoromethyl)sulfonylimide (EMIm Tf_2N) and $LiTf_2N$ enabled a greater understanding of the temperature-dependent properties of the mixtures in addition to the overall effects of adding $LiTf_2N$ to the IL. Investigation of properties for binary IL-Li salt mixtures and IL-sulfonated polymer

mixtures enabled rational design of a sulfonated ABA-triblock copolymer featuring a sulfonated polystyrene central block with mechanically reinforcing outer poly(*t*-butylstyrene) outer blocks. Sequential anionic polymerization and subsequent sulfonation and neutralization to the lithium sulfonate yielded a polymeric host for binary mixtures of $LiTf_2N$-containing EMIm Tf_2N, which depressed the central block T_g to ~150 °C regardless of $LiTf_2N$ content.

5.2 Introduction

Ternary ionic liquid (IL)-based polymer electrolytes represent an interesting and emerging area of research for lithium ion battery applications.[1] These ternary electrolytes generally consist of an ion-conducting polymer, a lithium salt, and an IL diluent. When ILs are utilized to solvate the Li salt, the two compounds usually share a common counteranion. ILs in particular impart advantageous properties for battery applications, such as nonvolatility, greater electrochemical stability, and reduced flammability.[2] To date, most work in battery research focused on the charge dissociation and transport in lithium salt-ionic liquid binary electrolytes or in polymer-salt binary electrolytes.[3-15] For ternary polymer electrolytes, researchers seek to build upon previously established research in the field of binary electrolytes and extend those findings to determine safe and effective formulations for enhanced battery performance.

In polymer-salt binary electrolytes, researchers generally exploit the crown ether-like interaction of ethylene oxide units and metal cations.[16,17] Most commonly, the polymeric component of the mixture is crosslinked poly(ethylene glycol) (PEG) or high molecular weight poly(ethylene oxide) (PEO). The addition of oligo(ethylene oxide) to binary mixtures of an ionic liquid and its Li salt greatly increased Li^+ solvation.[18] However,

in the absence of crosslinking, PEG-containing polymer electrolytes often suffer from poor mechanical properties. Balsara *et al.* often employed polystyrene-*b*-poly(ethylene oxide) (PS-*b*-PEO) to induce microphase-separated morphology wherein the glassy PS phases also impart mechanical strength.[12] The microphase-separation further enables investigation of the effects of bulk morphological arrangement on binary electrolyte performance.[19,20] Polymer-salt mixtures featuring polyphosphazenes with ethylene oxide side groups, such as poly[bis(methoxyethoxy)ethoxy)phosphazene] (MEEP), also demonstrate high ionic conductivity at room temperature.[21,22] Blending a MEEP-salt binary electrolyte with a reinforcing polymer enhanced its electrochemical and thermal stability, while using $LiAlCl_4$ salt enabled free-standing films even without the reinforcing polymer.[23] Other reports of phosphazene-based electrolytes incorporated organic carbonate solvents in battery applications.[24,25]

When extended to IL-containing ternary systems, little has evolved with respect to polymer choice. While one study used crosslinked cyclic phosphazene as the macromolecular component, PEO-based ternary polymer electrolytes are far more common in the literature.[26-29] Simulations also aided in understanding the complex dynamics of these ternary systems. Diddens and Heuer presented a systematic molecular dynamics study on ternary electrolytes composed of PEO, lithium bis(trifluoromethyl)sulfonylimide ($LiTf_2N$), and N-methyl-N-propylpyrrolidinium (C_3mpyr) Tf_2N.[30] They established that the addition of C_3mpyr Tf_2N to the PEO/$LiTf_2N$ electrolyte plasticized the electrolyte and led to greater conductivity. However, as the IL replaced the PEO in the system rather than simple addition, the reduction in ether oxygens relative to $LiTf_2N$ marginalized the benefits of the plasticizing effect. Additional

simulation studies from Diddens and Heuer also confirmed the importance of segmental motion to drive the transport of Li^+ cations in the ternary electrolyte.[31] These theoretical findings helped explain experimental results from Passerini *et al.* regarding Li^+ transport in binary and ternary IL-based electrolytes.[5,6,26-28]

Sulfonate-containing polymers or block copolymers demonstrate usefulness for a variety of applications owing to their favorable properties for charge transport.[32-37] The ionic interactions of the sulfonate-containing groups often lead to ion clusters in random copolymers and to well-defined bulk morphology arising from microphase-separation in block copolymers.[38-40] However, sulfonated copolymers have yet to be explored as the polymeric component of ternary polymer electrolytes. Many reports established the plasticization of ion-containing block copolymers with ILs, indicating the potential for the IL component of the ternary polymer electrolyte to depress polymer T_g and therefore enhance performance.[41-43] Incorporation of non-ionic, mechanically reinforcing blocks to the polymer would likely lend superior thermomechanical properties to the ternary polymer electrolyte. Therefore, examining the thermal effects of IL and Li-salt incorporation to sulfonated block copolymers represents a crucial and fundamental initial step for exploration of these systems for potential use as ternary polymer electrolytes.

This manuscript details the thermal effects resulting from IL incorporation to sulfonate-containing copolymers for binary mixtures of IL and sulfonated polymers, establishes composition-property relationships for binary mixtures of EMIm Tf_2N and $LiTf_2N$, and finally investigates the thermal properties of ternary polymer electrolytes composed of a lithium sulfonate-containing ABA triblock copolymer, $LiTf_2N$ salt , and ionic liquid EMIm Tf_2N. Both sulfonic acid and lithium sulfonate-containing polymers

served as hosts for a variety of ionic liquids, and served to establish the effects of the IL structure and content on thermal properties. Furthermore, doping EMIm Tf_2N with $LiTf_2N$ affected the viscosity, ionic conductivity, and thermal transitions of the IL mixtures. Pulsed-gradient stimulated echo (PGSTE) experiments in nuclear magnetic resonance (NMR) spectroscopy determined the bulk self-diffusion values and apparent Stokes radii of the Tf_2N^-, $EMIm^+$, and Li^+ ionic species. Addition of the Li-doped EMIm Tf_2N into the sulfonated block copolymer changed its thermal properties and provided a platform for further research into sulfonated copolymers as ternary polymer electrolytes.

5.3 Experimental

5.3.1 Materials

Styrene (Sty) and 4-*t*-butylstyrene (tBS) were purchased from Sigma Aldrich and distilled from calcium hydride first and then freshly from di-*n*-butylmagnesium prior to use. 1-Ethyl-3-methylimidazolium bromide (EMIm Br, ≥97%), *sec*-butyllithium (1.4 M solution in cyclohexane), acetic anhydride (≥99%), 1,2-dichloroethane (DCE, anhydrous, 99.8%), lithium hydroxide (LiOH, ≥99%), poly(4-styrenesulfonic acid) (PSSA, 18 wt% in water) and sodium sulfate (Na_2SO_4, ≥99%) were purchased from Sigma Aldrich and used as received. Lithium bis(trifluoromethylmethane)sulfonimide ($LiTf_2N$, ≥99%) was supplied by Solvay. Dichloromethane (DCM), methanol, and concentrated H_2SO_4 were purchased from Spectrum Chemicals and used as received. ILs other than EMIm Tf_2N were purchased from Sigma Aldrich and dried *in vacuo* at 100 °C for 18 h prior to use.

5.3.2 Analytical Methods

^1H and ^{19}F NMR spectroscopies were performed using a Varian Unity 400 MHz spectrometer at ambient temperature in DMSO-d_6, $CDCl_3$, or CD_3OD. THF size exclusion

chromatography (SEC) at 35 ºC using a flow rate of 1.0 mL/min through three Polymer Laboratories PLgel 5 µm MIXED-C columns determined the molecular weights of the obtained polymers. SEC instrumentation included a Waters717plus autosampler equipped with Waters 515 HPLC pump, Waters 2414 refractive index detector, and Wyatt miniDawn MALLS detector operating at 690 nm. Thermogravimetic analysis (TGA) was performed on a TA Instruments Q500 under nitrogen atmosphere with heating ramp of 10 °C/min to determine 5% weight loss temperatures ($T_{d,5\%}$). Differential scanning calorimetry (DSC) determined thermal transitions using standard heat/cool/heat procedure under helium atmosphere with heating rate of 10 °C/min and quench cool on a TA Instruments Q1000. Glass transition temperatures (T_gs) were determined on the second heating cycle. Temperature-dependent viscosities and conductivities of ionic liquid and lithium-containing ionic liquids were determined according to previous literature.[44]

Samples were inserted into 5 mm NMR tubes after drying in a vacuum chamber for 24 hours at 100 °C. ^{7}Li, ^{1}H and ^{19}F self-diffusion measurements were performed using the pulsed-gradient stimulated echo sequence (PGSTE) on a Bruker Avance III 9.4 T widebore spectrometer equipped with a Diff60 diffusion probe, a 5 mm ^{7}Li coil and a 8 mm double resonance (^{1}H/^{2}H) RF coil. The NMR signal attenuation due to diffusion is described by the Stejskal-Tanner equation:

$$I = I_0 e^{-D\gamma^2 g^2 \delta^2 (\Delta - \delta/3)} \quad (1)$$

where I is the spin-echo signal intensity, I_0 is the signal intensity at zero gradient, γ is the gyromagnetic ratio of the nucleus (rad s^{-1} T^{-1}), g is the magnitude of the gradient pulse (T m^{-1}), and D is the self-diffusion coefficient of lithium ions in the samples derived by fitting Equation 1. Δ is the duration (100-300 ms in this work) between the leading edges of the

two gradient pulses and δ is the duration (1 ms in this work) of the gradient pulse, depending on the corresponding relaxation times of the membranes. A 16-step variation of gradient strength (*g)* was employed with 64 scans taken at each step to yield sufficient signal-to-noise ratio (SNR). Errors in *D* are generally < ± 10%. All diffusion experiments were conducted at various temperatures ranging from 25 °C to 75°C.

5.3.3 Synthesis of EMIm Tf_2N

In a typical synthesis, $LiTf_2N$ (30 g, 104 mmol) and EMIm Br (19.9 g, 104 mmol) were measured into a clean, dry 500-mL, round-bottomed flask equipped with a magnetic stir bar and dissolved in 250 mL deionized (DI) H_2O. 50 mL DCM was added, and the contents of the flask were stirred at ambient temperature for 24 h, after which the contents of the flask were transferred to a separatory funnel. The product was extracted with 20 mL DCM five times, and the combined DCM phase was washed ten times with DI H_2O. The product solution was dried over Na_2SO_4, and the DCM was removed under rotary evaporation. After further drying at 100 °C *in vacuo* for 18 h, the product 1-ethyl-3-methylimidazolium bis(trifluoromethyl)sulfonylimide (EMIm Tf_2N) was isolated as a clear, viscous liquid with an isolated yield of > 90%. Silver nitrate test indicated quantitative anion exchange.

5.3.4 Preparation of $LiTf_2N$-doped EMIm Tf_2N

$LiTf_2N$ and EMIm Tf_2N were dried overnight at 100 °C *in vacuo*. $LiTf_2N$ was added to EMIm Tf_2N to yield solutions of $LiTf_2N$-doped IL having concentrations of 11 and 33 wt% $LiTf_2N$. The solutions were heated to 80 °C to aid dissolution of the solids. All IL samples were dried at 100 °C *in vacuo* for 18 h prior to use.

5.3.5 Incorporation of ionic liquids into sulfonated polystyrene

PSSA solution was titrated with LiOH in the presence of a phenolphthalein indicator, dialyzed against DI H_2O, and lyophilized to provide poly(lithium 4-styrenesulfonate) (PSSLi) in quantitative yield. PSSA solution was lyophilized to afford the neat homopolymer. Ionic liquids were incorporated to PSSA and PSSLi by adding the desired amount of ionic liquid to a 50 wt% solution of PSSA (in methanol) or PSSLi (in water). The ionic liquid-containing polymer solutions were stirred at room temperature for 24 h, and solvent was slowly removed on a hot plate at 40 °C. Samples were then further dried at 80 °C *in vacuo* to constant weight, and stored in a vacuum desiccator until immediately prior to further experiments.

5.3.6 Synthesis of block copolymer

In a representative synthesis, a flame-dried, nitrogen-purged 100-mL round-bottomed flask was equipped with a magnetic stir bar and charged with 60 mL cyclohexane and 3 g (3.3 mL) tBS and immersed in a 50 °C thermostated oil bath. The polymerization reaction was initiated with sec-butyllithium solution (0.1 mL) and allowed to proceed for 45 min, at which time 6 g (6.6 mL) styrene was added by syringe under nitrogen. Upon addition of styrene, the reaction color turned from orange to red. After 45 min, additional 3 g (3.3 mL) tBS was added and permitted to polymerize. The color of the reaction returned to orange upon the addition of tBS. After the final 45 min reaction time, the polymerization reaction was terminated with degassed methanol. The polymer was precipitated in methanol, collected with vacuum filtration, redissolved in THF (30% by weight), precipitated into methanol, collected with vacuum filtration, and dried *in vacuo* at 70 °C.

5.3.7 Sulfonation of block copolymer

Styrenic block copolymers were sulfonated using a literature procedure.[38] Briefly, the styrenic block copolymer was added to a clean, dry, 250-mL round-bottomed flask equipped with magnetic stir bar and purged for 30 min with nitrogen. Then, DCE was added such that the polymer concentration was 20 wt%, and the flask was immersed in a thermostated oil bath at 50 °C. In a separate flask under nitrogen atmosphere, acetic anhydride was added to 20 mL DCE and cooled in an ice bath for 90 min. Then, one equivalent of concentrated sulfuric acid relative to acetic anhydride was added to the acetic anhydride solution. The flask was shaken vigorously, returned to the ice bath, and immediately cannulated into the warmed polymer solution. The reaction was terminated with isopropanol after 24 h. The crude reaction mixture was dialyzed against methanol and the sulfonated polymer product was isolated with rotary evaporation. Titration of polymer solution in methanol with aqueous LiOH in the presence of phenolphthalein indicator determined the ion exchange capacity (IEC) of the sulfonated polymer to be 3.2 meq/g. The titrated solution was then dialyzed against methanol and the lithium sulfonate-containing polymer was isolated by rotary evaporation at 80 °C and dried *in vacuo* at 100 °C for 48 h.

5.3.8 Incorporation of ILs to sulfonated block copolymer

Sulfonated block copolymer was dispersed at 10 wt% in methanol depending on extent of sulfonation. A calculated amount of IL was added to achieve a concentration of 30 wt% relative to the sulfonated block. Mixtures were stirred for 18 h and then solvent was removed by rotary evaporation. IL-containing polymer samples were dried for 18 h at 100 °C *in vacuo* before use and removed to a desiccator until immediately prior to further experiments to mitigate water uptake.

5.4 Results and Discussion

5.4.1 Thermal effects of IL addition to PSSA and PSSLi

Ionic liquids featuring the 1-ethyl-3-methylimidazolium (EMIm) or 1-butyl-3-methylimidazolium (BMIm) cations and various anions such as triflate (OTf), tetrafluoroborate (BF_4), ethyl sulfate ($EtSO_4$), or bis(trifluoromethyl)sulfonylimide (Tf_2N) often plasticize ion-containing polymers. Incorporating the ionic liquids EMIm OTf, EMIm $EtSO_4$, EMIm BF_4, BMIm BF_4, and EMIm Tf_2N in 5 wt% increments up to 25% caused a drop in T_g for PSSA (**Figure 5.1**). Although PSSA exhibits a 5% weight loss temperature ($T_{d,5\%}$) of 172 °C, below any observed T_g, incorporation of the ILs to PSSA increased its thermal stability and enabled observation of T_g using DSC. While the EMIm OTf-, EMIm $EtSO_4$-, and EMIm Tf_2N-containing samples all demonstrated a linear decrease in T_g with increasing wt% IL, the samples that featured the BF_4^- anion showed a gradual reduction in T_g up to 15 wt% IL content, after which subsequent addition of IL caused a greater change in T_g. None of the thermograms displayed endotherms corresponding to the T_m of the added IL, indicating well-mixed, homogenous addition.

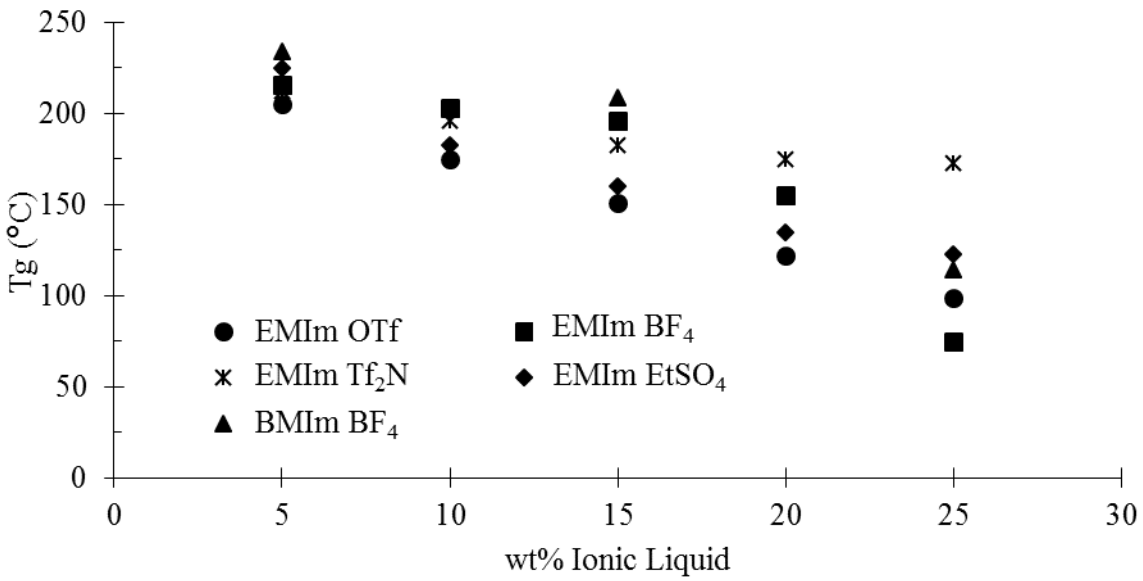

Figure 5.1. Effect of incorporating ionic liquids in increasing wt% on PSSA T_g.

Neutralizing the sulfonic acid groups of PSSA to their lithium salts using simple titration yielded PSSLi in quantitative yield. ILs were incorporated in a fashion similar to PSSA, permitting observation of the change in T_g as a function of extent of IL content. Because PSSLi only dissolves in water and EMIm Tf_2N is not water miscible, attempts at obtaining a homogenous mixture of EMIm Tf_2N in PSSLi proved difficult and yielded inconsistent results. **Figure 5.2** shows the change in T_g for PSSLi upon the addition of increasing wt% IL. All ILs show the same general trend of decreasing T_g at greater IL content. However, at low incorporations of IL, the T_g slightly increased. This effect potentially arose from screening of polyelectrolyte ionic aggregations and partial filling of free volume, as described in previous literature.[45-47] In all cases, the T_g of the IL-containing PSSLi sample exceeded that of the corresponding IL-containing PSSA sample. This resulted from the exchange from the sulfonic acid to the more strongly aggregating lithium sulfonate.

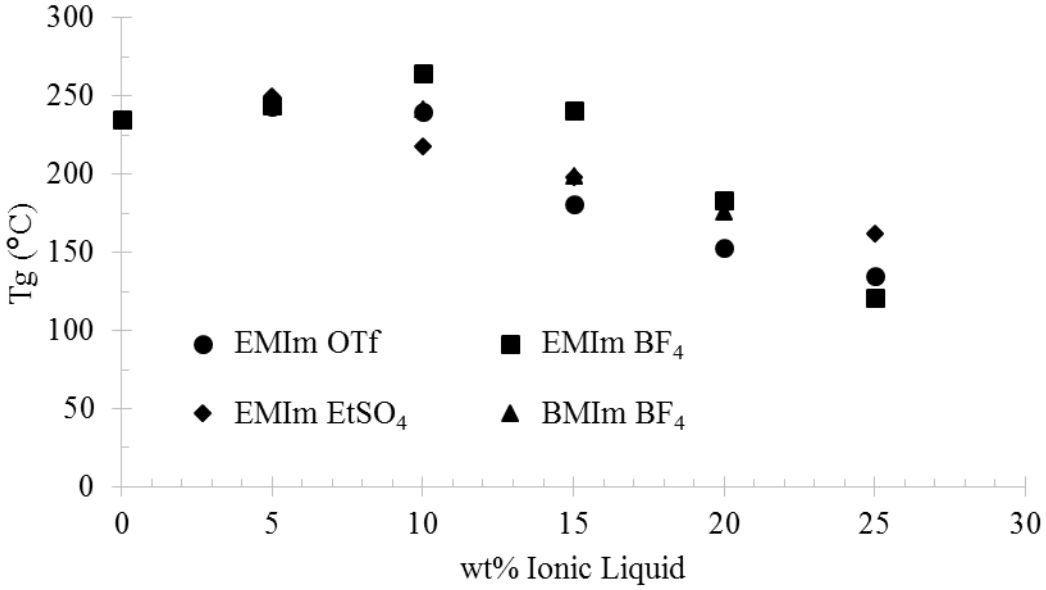

Figure 5.2. Effect of incorporation ionic liquids in increasing wt% on PSSLi T_g.

5.4.2 Effects of adding $LiTf_2N$ to EMIm Tf_2N

Addition of $LiTf_2N$ to corresponding EMIm-based ionic liquid enabled further evaluation for use in ternary polymer electrolytes. DSC revealed the effects of $LiTf_2N$ addition on the thermal transitions of EMIm Tf_2N (**Figure 5.3**). The pure IL exhibits a T_g at -91 °C and a T_m at -11 °C. Upon addition of $LiTf_2N$ in an 8:1 (w:w) ratio of EMIm Tf_2N:$LiTf_2N$, the T_g increased only slightly to -89 °C and the T_m decreased to -23 °C. In addition to the change in these transition temperatures, the enthalpy of melting clearly decreased, which suggested a less ordered and defined crystal structure upon the incorporation of $LiTf_2N$. Further increasing the relative incorporation of $LiTf_2N$ raised the T_g to -82 °C. This amount of $LiTf_2N$ content suppressed crystallinity to below the detection limit of the instrument. The suppression of T_m with increasing $LiTf_2N$ proved consistent with the general theory of melting point depression.

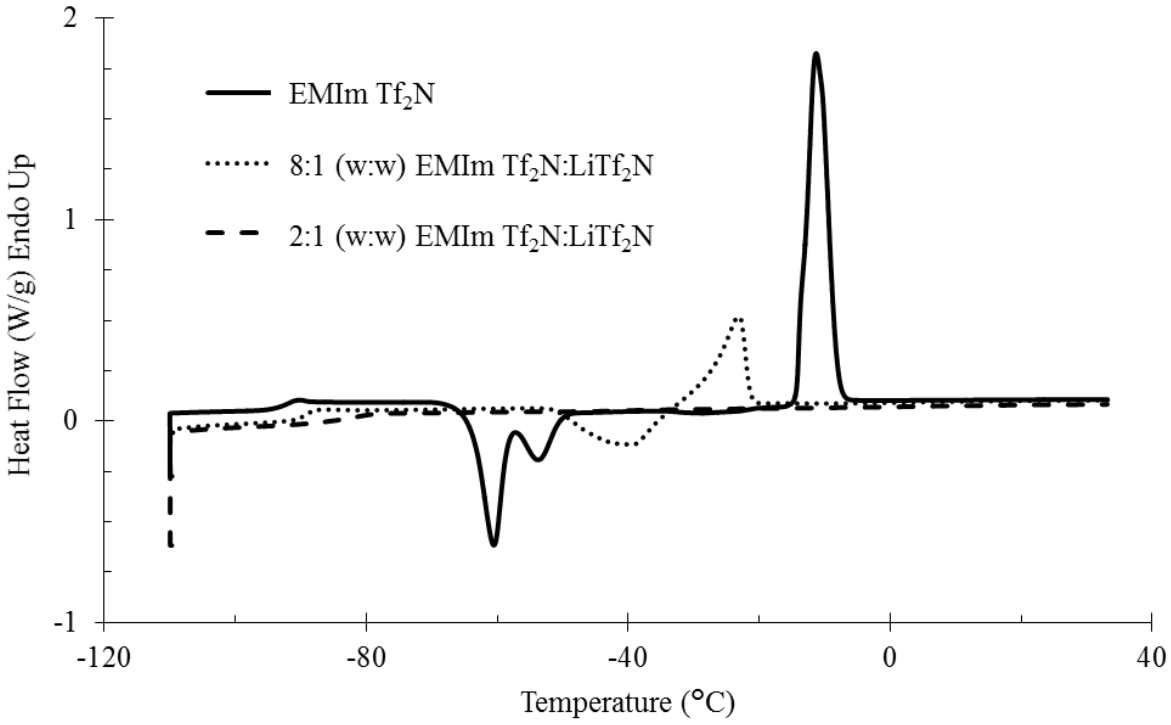

Figure 5.3. DSC thermograms of EMIm Tf_2N with added $LiTf_2N$.

Probing the temperature-dependent conductivity and viscosity (**Figure 5.4**) allowed for investigation into the effects of adding lithium cations into the IL. Dissolving $LiTf_2N$ into EMIm Tf_2N yielded solutions of 8:1 and 2:1 (w:w) of EMIm Tf_2N:$LiTf_2N$. Solution conductivity (**Figure 5.4a**) demonstrated increasing conductivity of the solutions with increasing temperature. Purging the solutions with dry argon in a sealed glass assembly ensured the IL samples remained moisture-free. Furthermore, the ionic conductivity of the samples decreased with increasing $LiTf_2N$ content. The pure EMIm Tf_2N sample exhibited ionic conductivity on the order of $\sigma = 10^{-2}$ S/cm, which was nearly twice the 8:1 (w:w) EMIm Tf_2N:$LiTf_2N$ solution, and about 7 times greater than 2:1 (w:w) EMIm Tf_2N:$LiTf_2N$ solution. A rheometer equipped with concentric cylinder geometry further investigated the temperature-dependent viscosity (**Figure 5.4b**) of the EMIm Tf_2N-based samples. A custom-designed glass enclosure facilitated a constant, gentle flow of dry

argon over the geometry throughout the duration of the experiment and mitigated atmospheric water uptake. The results clearly demonstrated the decreasing viscosity as temperature increased. While conductivity followed the trend of EMIm Tf_2N > 8:1 (w:w) EMIm Tf_2N:$LiTf_2N$ > 2:1 (w:w) EMIm Tf_2N:$LiTf_2N$, the viscosity values followed the reverse trend. 2:1 (w:w) EMIm Tf_2N:$LiTf_2N$ demonstrated viscosity roughly an order of magnitude greater than EMIm Tf_2N. As the concentration of $LiTf_2N$ increased, viscosity increased and conductivity decreased, indicating that viscosity likely governed ionic conductivity. These observations corresponded well with previous literature reports of other binary mixtures of ionic liquids with corresponding lithium salts.[6,7]

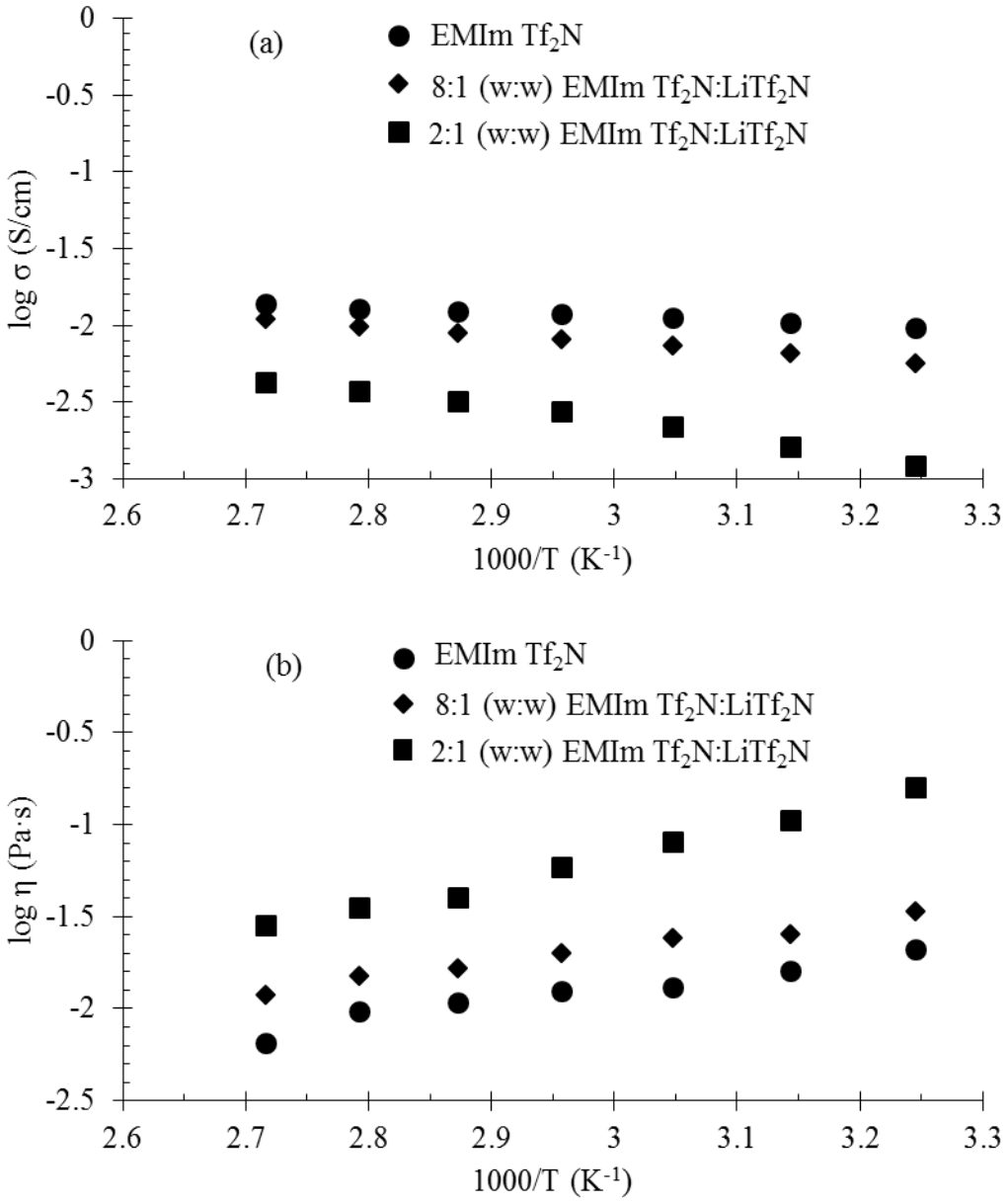

Figure 5.4. Temperature-dependent conductivity (a) and viscosity (b) of pure IL (circles), 8:1 IL:Li Salt (diamonds) and 2:1 IL:Li Salt (squares) samples.

The fractional Walden rule relates molar conductivity to viscosity using the following relationship:

$$\log \lambda_m = \log C' + \alpha \log \eta^{-1} \quad (2)$$

where λ_m is the molar conductivity of the sample and η is the viscosity measured at the same temperature. In this expression, C' is a vertical shift factor related to ion radius and α relates to ion dissociation. When α is unity, it roughly represents completely dissociated ions analogous to 0.1 M aqueous KCl.[48] Plotting the molar conductivity as a function of inverse viscosity according to this relationship (**Figure 5.5**) revealed the C' and α values for the EMIm Tf_2N-based IL samples. EMIm Tf_2N, 8:1 (w:w) EMIm Tf_2N:$LiTf_2N$, and 2:1 (w:w) EMIm Tf_2N:$LiTf_2N$ exhibited C' values of 0.10 S cm^2 mol^{-1}, 0.27 S cm^2 mol^{-1}, and 0.22 S cm^2 mol^{-1}, respectively. The same respective samples had α values of 0.32, 0.67, and 0.73. The departure of the α values from unity likely resulted from the difference in interaction with Tf_2N^- anion of the Li^+ cation and $EMIm^+$ cation.

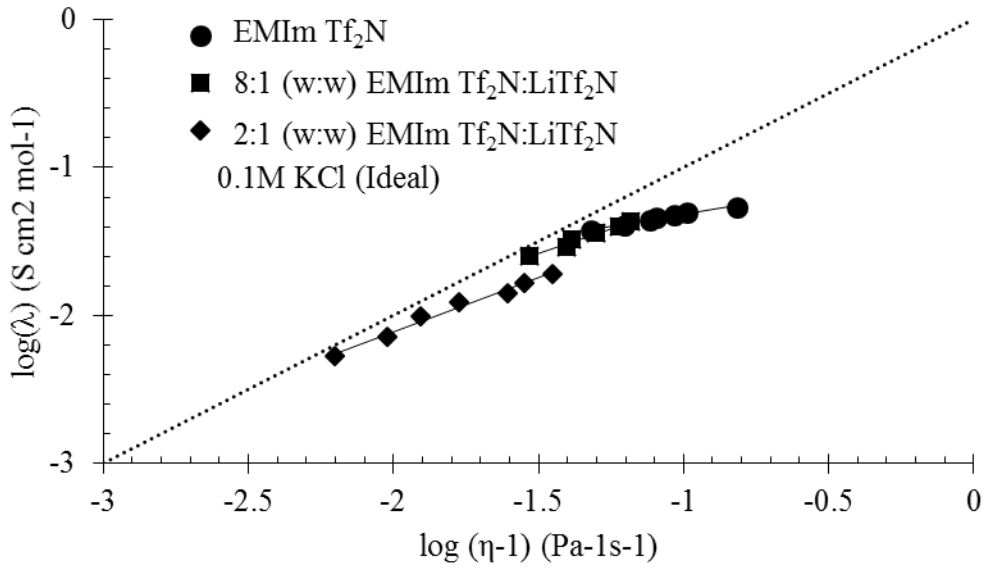

Figure 5.5. Fractional Walden plots of pure EMIm Tf_2N (circles), 8:1 (w:w) EMIm Tf_2N:$LiTf_2N$ (diamonds), and 2:1 (w:w) EMIm Tf_2N:$LiTf_2N$ (squares) samples. Linear fits are included to provide a visual comparison to 0.1 M KCl ideal electrolyte.

PGSTE NMR spectroscopy experiments measured the temperature-dependent diffusion coefficient of the various ionic species present in the $LiTf_2N$-doped EMIm Tf_2N

liquids (**Figure 5.6**). PGSTE NMR spectroscopy offers enhanced accuracy and precision of diffusion measurements relative to the pulsed gradient spin echo (PGSE) NMR spectroscopy technique, and proves particularly effective for more complex mixtures.[49] Here, PGSTE NMR spectroscopy exploited the well-resolved chemical signals of the ions, as the $EMIm^+$ cation was the only ion present to yield a ^1H signal, the ^{19}F signal was restricted to the Tf_2N^- anion, and the Li^+ cation was the only species that had an active ^7Li signal. For all the ions investigated, the diffusion coefficients increased as temperature increased, as expected. The observed decrease in viscosity at increasing temperatures further intuitively supported this trend. The $EMIm^+$ cation demonstrated highest diffusion values in the pure ionic liquid EMIm Tf_2N, and displayed reduced values of diffusion upon increasing incorporation of $LiTf_2N$ (**Figure 5.6a**). The same trend held for Tf_2N^- diffusion (**Figure 5.6b**) as well as for Li^+ cation diffusion (**Figure 5.6c**). In all cases, increased $LiTf_2N$ content resulted in reduced ion diffusion, which also followed the increased viscosity of the ionic liquids as a result of adding $LiTf_2N$.

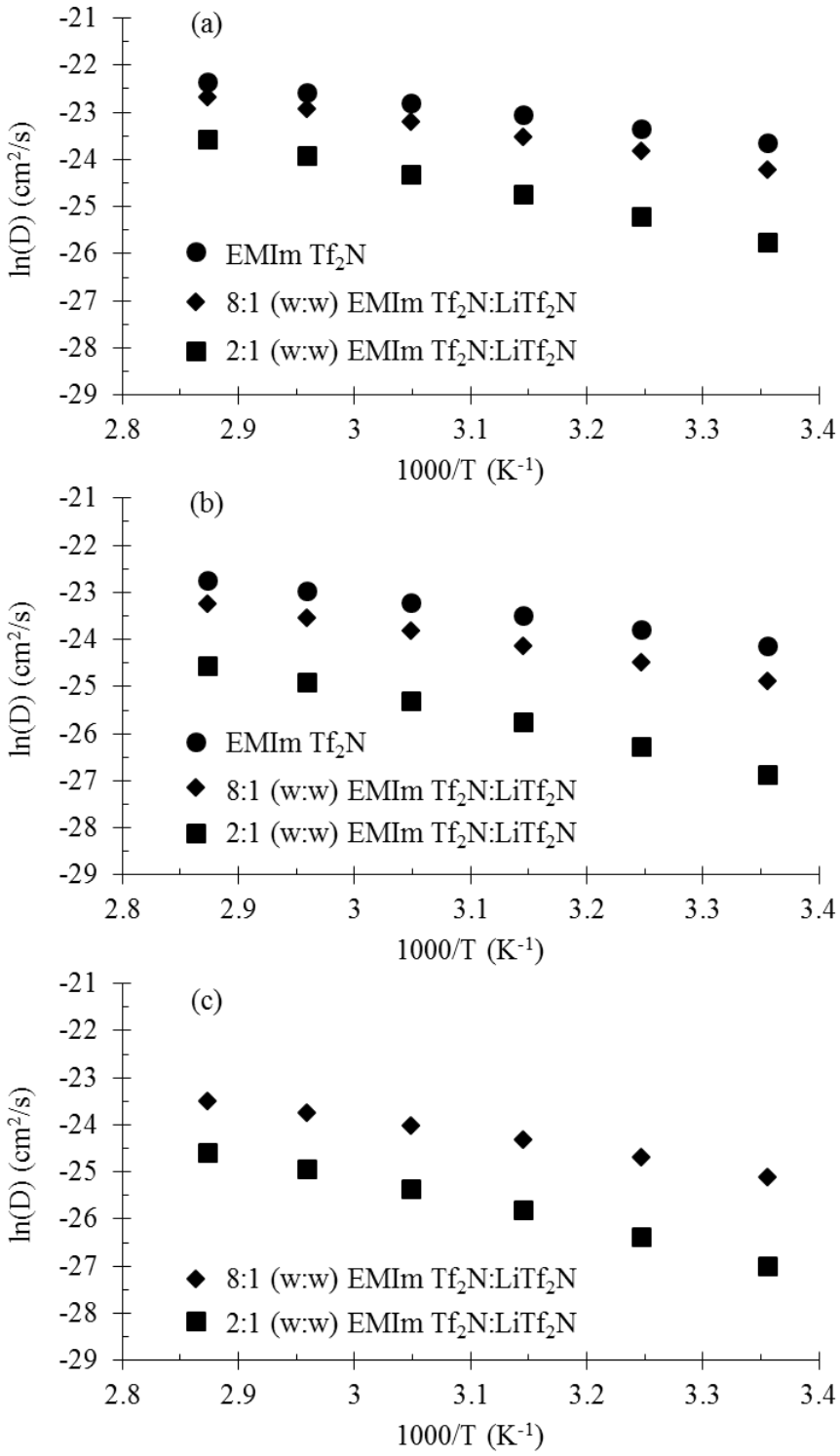

Figure 5.6. Temperature dependent diffusion values for (a) $EMIm^+$ cation (b) Tf_2N^- anion, and (c) Li^+ cation from PGSTE NMR spectroscopy.

Evaluating the activation energies (E_a) of diffusion for the ions aids in grasping a more complete picture of the effects of lithium salt doping on ionic liquid properties. The Arrhenius equation yielded E_a values (**Table 5.1**) for $EMIm^+$, Tf_2N^-, and Li^+ diffusion according to:

$$\ln D = \frac{-E_a}{RT} + \ln A \quad (3)$$

where D is the diffusion of the ionic species, R is the ideal gas constant, T is the temperature, and A is the Arrhenius pre-exponential factor. E_a drastically increased upon $LiTf_2N$ incorporation for both $EMIm^+$ and Tf_2N^-, and then further increased with additional $LiTf_2N$ incorporation. While no E_a was calculated for Li^+ diffusion in EMIm Tf_2N because the pure ionic liquid contained no Li^+, the E_a increased when $LiTf_2N$ content increased from 8:1 (w:w) $EMImTf_2N$:$LiTf_2N$ to 2:1 (w:w) $EMImTf_2N$:$LiTf_2N$. The increased E_a of diffusion for the ionic species in the IL mixtures as $LiTf_2N$ content increased correlated well to their reduced values of diffusion. Thus, as the E_a barrier for diffusion increased, the measured diffusion of the ions decreased.

Table 5.1. Activation energies for diffusion of the different ionic species in $LiTf_2N$-doped EMIm Tf_2N.

Sample	**E_a of ^1H Diffusion (kJ/mol)**	**E_a of ^{19}F Diffusion (kJ/mol)**	**E_a of ^7Li Diffusion (kJ/mol)**
EMIm Tf_2N	22	23	--
8:1 (w:w) EMIm Tf_2N: $LiTf_2N$	26	27	26
2:1 (w:w) EMIm Tf_2N: $LiTf_2N$	36	37	38

Using measured diffusion and viscosity values at a given temperature further permits calculation of apparent ionic radii of the diffusing particle through the Stokes-Einstein equation, as follows:

$$D = \frac{k_B T}{4\pi\eta r} \quad (4)$$

where D is the diffusion, k_B is Boltzmann's constant, T is temperature, η is solution viscosity, and r is the so-called apparent Stokes radius. The constant 4 in the denominator was chosen to better approximate the diffusion of a particle through a medium comprised of particles of similar size that can interact with the diffusing species.[50,51] Determining the apparent ionic radius of the diffusing species granted greater understanding of the effects of $LiTf_2N$ incorporation on a molecular level. The apparent Stokes radii of the Tf_2N^--containing and $EMIm^+$-containing diffusing particles showed a nonlinear temperature dependence, with two regimes. The temperature required to change the size of the Tf_2N^--containing clusters showed no clear trend with increasing $LiTf_2N$ content. However, the apparent Stokes radius of the Tf_2N^--containing ionic particles increased with increasing $LiTf_2N$ content, indicating a preferential interaction of the Tf_2N^- anion with Li^+ cation that resulted in larger clusters. When more $EMIm^+$ cations were present in the binary IL mixture, they served to partially screen the interaction of Li^+ and Tf_2N^-. The apparent Stokes radii of the $EMIm^+$-containing ionic species decreased with increasing $LiTf_2N$ content, which also supported the conclusions from the data determined for Tf_2N^--containing clusters. In pure $EMImTf_2N$, the only cation-anion interaction present exists between $EMIm^+$ and Tf_2N^-. Thus, the $EMIm^+$-containing clusters readily contain bulky Tf_2N^- anions. However, when $LiTf_2N$ is added to create a binary mixture, the stronger association of Li^+ to with Tf_2N^- relative to the $EMIm^+$ interaction with Tf_2N^- attracts a greater number of Tf_2N^- anions to the Li^+ containing cluster. Thus, with increasing Li^+ content, the ionic clusters present in the binary mixture favored Li^+ Tf_2N^- interactions and

caused the increase in apparent Stokes radius for Tf_2N^--containing clusters, while $EMIm^+$-containing clusters became smaller.

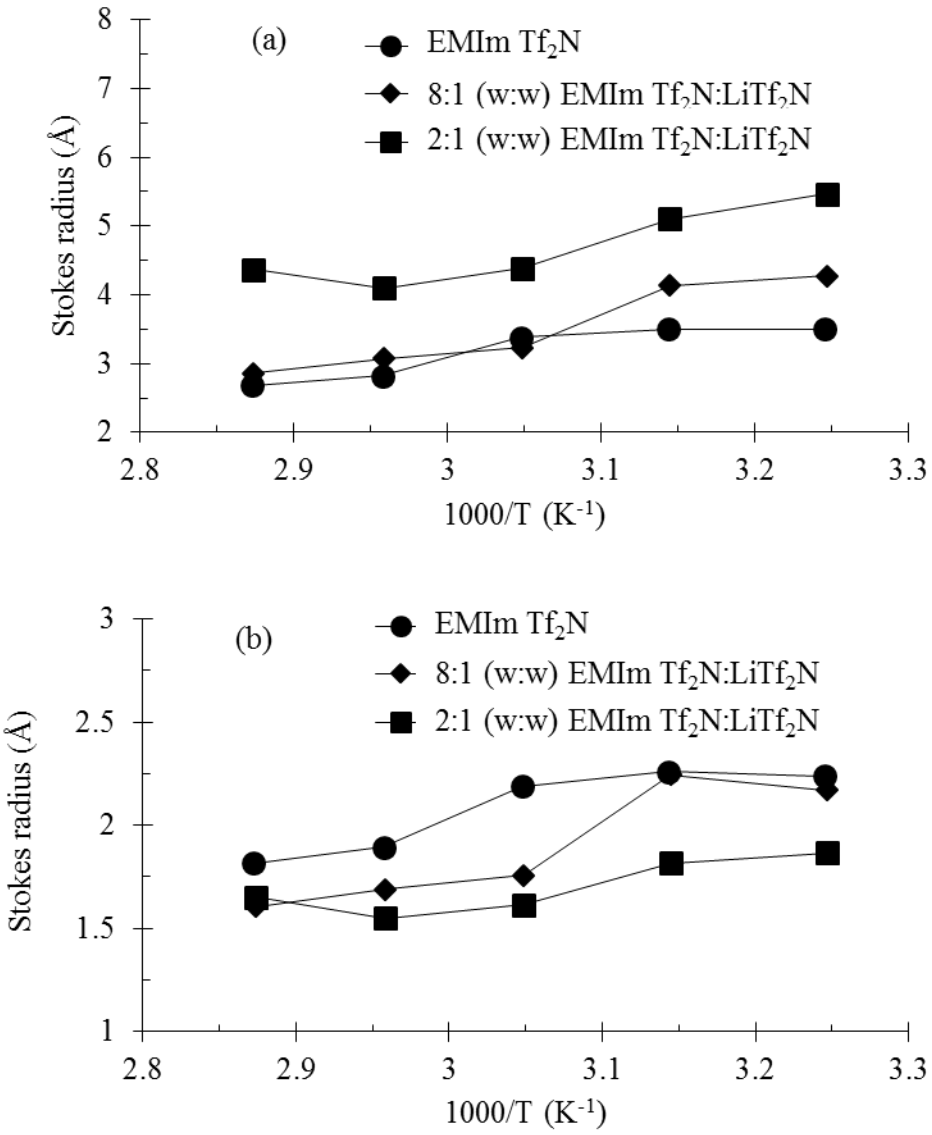

Figure 5.7. Stokes radius of ionic species containing (a) Tf_2N^- and (b) EMIm as $LiTf_2N$ content increases. Lines serve to guide the eye.

5.4.3 Ternary polymer electrolytes

Adding the Li-doped EMIm Tf_2N solutions to a polymer resulted in a ternary polymer electrolyte. Rather than employing crosslinked PEO that is common to the literature, a sulfonated triblock copolymer acted as a host for the ILs. Sequential living anionic polymerization (Scheme 1) of *t*-butyl styrene, styrene, and *t*-butyl styrene in cyclohexane yielded the ABA styrenic triblock copolymer PtBS-*b*-PS-*b*-PtBS. SEC (Figure 9) in THF revealed the molecular weight and polydispersity index of the synthesized polymer. The monomodal trace indicated the absence of premature termination during the course of the reaction. The polymer had M_n = 38.7 kg mol^{-1}, M_w = 42.2 kg mol^{-1}, and PDI = 1.09 which indicated control over the polymerization reaction and the well-defined nature of the triblock copolymer product. The composition of the obtained block copolymer matched the charged monomer composition, and corresponded to PtBS terminal blocks with 16.5 kg mol^{-1} molecular weight and PS central block of 9.3 kg mol^{-1} molecular weight.

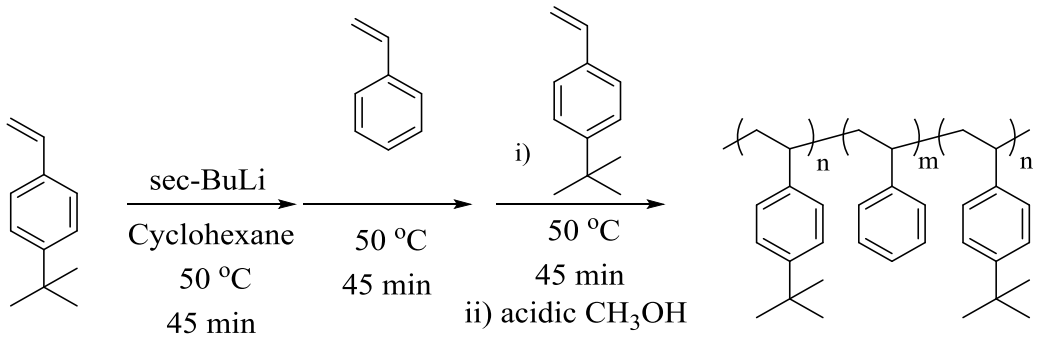

Scheme 5.1. Sequential anionic polymerization of styrenic ABA triblock copolymer.

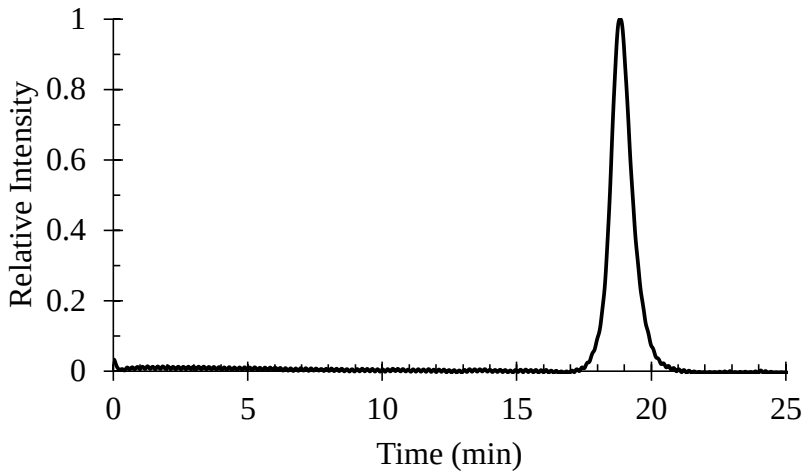

Figure 5.8. SEC trace of PtBS-*b*-PS-*b*-PtBS in THF.

Post-polymerization modification of the styrenic triblock copolymer selectively imparted lithium sulfonate functionality to the PS central block (**Scheme 5.2**). Treatment of the styrenic ABA block copolymer with acetyl sulfate presented the sulfonic acid functionality to the central block through an electrophilic aromatic substitution mechanism.[52] The *t*-butyl group on the 4-position of the outer PtBS blocks effectively blocked those phenyl rings from participating in the reaction. Good solvation of the PtBS blocks in the reaction medium prevented the reaction from rapidly turning heterogeneous, which facilitated high extent of sulfonation of the PS block. After isolation of the sulfonated block copolymer, titration of the sulfonic acid groups with LiOH determined the extent of sulfonation and provided the lithium sulfonate-containing copolymer. Titration measured an ion exchange capacity of 1.6 meq g^{-1} for the sulfonated block copolymer, which corresponded to 88 mol% sulfonation of the central PS block. The $T_{d,5\%}$ decreased upon the introduction of the sulfonate functionality to the central block, and the T_g attributed to the central PS block changed from 99 °C to above the $T_{d,5\%}$. The retention

of the T_g near 125 °C, attributed to the PtBS blocks, further indicated the selective nature of the modification.

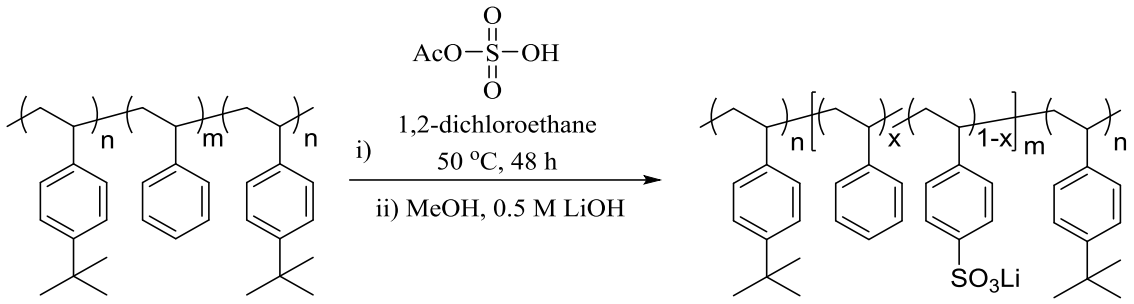

Scheme 5.2. Selective sulfonation of the central block and subsequent neutralization to lithium sulfonate.

The combination of central block sulfonation and hydrophobic outer blocks enabled the dispersion of the lithium sulfonate-containing copolymer in methanol, which permitted homogenous mixing of the charged block copolymer with EMIm Tf_2N-based IL samples, an improvement over the PSSLi homopolymer. Adding the Li-doped EMIm Tf_2N into the sulfonated block copolymer represented the first step towards evaluating these materials as novel ternary polymer electrolytes. Samples contained 30 wt% of the IL-based binary mixture relative to the ionic block weight. Above 30 wt% incorporation, the samples exhibited macrophase separation, likely due to the presence of hydrophobic PtBS blocks.. Thermograms revealed no melting endotherms when compared to the data in Figure 3, which indicated homogenous mixing of the IL-based solutions into the sulfonated copolymer. The ternary polymer electrolytes each displayed a T_g near 125 °C, consistent with the T_g of the PtBS outer blocks.

Table 5.2. Thermal properties of sulfonated block copolymers with added $LiTf_2N$-doped EMIm Tf_2N.

Sample	**$T_{d,5\%}$**	**$T_{g,1}$ (°C)**	**$T_{g,2}$ (°C)**
PtBS-*b*-PS-*b*-PtBS	407	99	125
PtBS-*b*-sPSLi-*b*-PtBS	218	ND	127
+ 30 wt% EMIm Tf_2N	319	147	126
+ 30 wt% 8:1 (w:w) EMIm Tf_2N:$LiTf_2N$	312	151	131
+ 30 wt% 2:1 (w:w) EMIm Tf_2N:$LiTf_2N$	316	148	125

Addition of the $LiTf_2N$-doped IL solutions permitted observation of the central block T_g near 150 °C, as the IL solutions plasticized the ion-containing central block. Plasticization of ionic segments proves favorable for conductive applications because segmental motion often drives ionic conductivity in polymer-containing electrolytes.[53,54] While the brittle nature of the resulting samples prohibited evaluation of the ion transport and thermomechanical properties, optimized block copolymer composition and degree of sulfonation would mitigate macrophase separation and allow for greater extent of IL incorporation and plasticization. This initial study of the thermal properties therefore proved encouraging for further investigation of these sulfonated block copolymer-containing ternary systems for electrolyte applications

5.5 Conclusions

IL addition to PSSA and PSSLi plasticized the polymers at levels relevant for polymer electrolytes. Incorporating $LiTf_2N$ into EMIm Tf_2N IL at two increasing weight fractions led to an increase in viscosity and decrease in conductivity. PGSTE experiments measured the diffusion values for the various ionic species present in the binary IL mixtures, and afforded greater insight into ion dynamics at the molecular level. To synthesize a polymeric host for the binary IL mixtures, sequential anionic polymerization,

post-polymerization sulfonation, and neutralization to the lithium sulfonate-containing polymer afforded an ABA triblock copolymer with sulfonated polystyrene central block and poly(*t*-butylstyrene) outer blocks. Addition of the binary IL mixtures to the sulfonated triblock copolymer reduced the T_g of the sulfonated block to *ca* 150 °C. These ternary polymer systems that featured sulfonated polystyrene as the host represent a novel addition to the field and a platform for further investigation as electrolytes.

5.6 Acknowledgments

The research detailed here was supported in part by Kraton Polymers, LLC. The authors acknowledge Dr. Carl Willis for his technical support and direction, as well as Prof. Lou Madsen in the VT Department of Chemistry for his expertise and insightful discussion regarding PGSTE experiments.

5.8 References

1. Osada I, de Vries H, Scrosati B and Passerini S. *Angew Chem Int Ed* **55:** 500-513 (2016).
2. Welton T. *Chem Rev* **99:** 2071-2084 (1999).
3. Andriola A, Singh K, Lewis J and Yu L. *J Phys Chem B* **114:** 11709-11714 (2010).
4. Armand M, Endres F, MacFarlane DR, Ohno H and Scrosati B. *Nat Mater* **8:** 621-629 (2009).
5. Castiglione F, Ragg E, Mele A, Appetecchi GB, Montanino M and Passerini S. *J Phys Chem Lett* **2:** 153-157 (2011).
6. Castiglione F, Famulari A, Raos G, Meille SV, Mele A, Appetecchi GB and Passerini S. *J Phys Chem B* **118:** 13679-13688 (2014).
7. Duluard S, Grondin J, Bruneel J-L, Pianet I, Grélard A, Campet G, Delville M-H and Lassègues J-C. *J Raman Spectrosc* **39:** 627-632 (2008).
8. Hayamizu K, Aihara Y, Nakagawa H, Nukuda T and Price WS. *J Phys Chem B* **108:** 19527-19532 (2004).
9. Indris S, Heinzmann R, Schulz M and Hofmann A. *J Electrochem Soc* **161:** A2036-A2041 (2014).
10. Jr. DTH and Balsara NP. *Annu Rev Mater Res* **43:** 503-525 (2013).
11. Young NP, Devaux D, Khurana R, Coates GW and Balsara NP. *Solid State Ionics* **263:** 87-94 (2014).
12. Chintapalli M, Chen XC, Thelen JL, Teran AA, Wang X, Garetz BA and Balsara NP. *Macromolecules* **47:** 5424-5431 (2014).

13. Chintapalli M, Le TNP, Venkatesan NR, Mackay NG, Rojas AA, Thelen JL, Chen XC, Devaux D and Balsara NP. *Macromolecules* **49:** 1770-1780 (2016).
14. Timachova K, Watanabe H and Balsara NP. *Macromolecules* **48:** 7882-7888 (2015).
15. Pesko DM, Jung Y, Hasan AL, Webb MA, Coates GW, Miller Iii TF and Balsara NP. *Solid State Ionics* **289:** 118-124 (2016).
16. Pedersen CJ. *J Am Chem Soc* **89:** 7017-7036 (1967).
17. Lee CH, VanHouten D, Lane O, McGrath JE, Hou J, Madsen LA, Spano J, Wi S, Cook J, Xie W, Oh HJ, Geise GM and Freeman BD. *Chem Mater* **23:** 1039-1049 (2011).
18. Bayley PM, Lane GH, Lyons LJ, MacFarlane DR and Forsyth M. *J Phys Chem C* **114:** 20569-20576 (2010).
19. Wang DR, Wujcik KH, Teran AA and Balsara NP. *Macromolecules* **48:** 4863-4873 (2015).
20. Wang X, Thelen JL, Teran AA, Chintapalli M, Nakamura I, Wang Z-G, Newstein MC, Balsara NP and Garetz BA. *Macromolecules* **47:** 5784-5792 (2014).
21. Blonsky PM, Shriver DF, Austin P and Allcock HR. *J Am Chem Soc* **106:** 6854-6855 (1984).
22. Luther TA, Stewart FF, Budzien JL, LaViolette RA, Bauer WF, Harrup MK, Allen CW and Elayan A. *J Phys Chem B* **107:** 3168-3176 (2003).
23. Abraham KM and Alamgir M. *Chemistry of Materials* **3:** 339-348 (1991).
24. Jankowsky S, Hiller MM, Fromm O, Winter M and Wiemhöfer HD. *Electrochim Acta* **155:** 364-371 (2015).
25. Jankowsky S, Hiller MM, Stolina R and Wiemhöfer HD. *J Power Sources* **273:** 574-579 (2015).
26. de Vries H, Jeong S and Passerini S. *RSC Adv* **5:** 13598-13606 (2015).
27. Joost M, Kunze M, Jeong S, Schönhoff M, Winter M and Passerini S. *Electrochim Acta* **86:** 330-338 (2012).
28. Kim GT, Appetecchi GB, Carewska M, Joost M, Balducci A, Winter M and Passerini S. *J Power Sources* **195:** 6130-6137 (2010).
29. Choi J-A, Kang Y and Kim D-W. *Electrochim Acta* **89:** 359-364 (2013).
30. Diddens D and Heuer A. *J Phys Chem B* **118:** 1113-1125 (2014).
31. Diddens D and Heuer A. *ACS Macro Lett* **2:** 322-326 (2013).
32. Ortiz-Negrón A and Suleiman D. *J Appl Polym Sci* **132:** n/a-n/a (2015).
33. Park MJ and Kim SY. *J Polym Sci, Part B: Polym Phys* **51:** 481-493 (2013).
34. Kim O, Shin TJ and Park MJ. *Nat Commun* **4:** (2013).
35. Kim O, Kim SY, Park B, Hwang W and Park MJ. *Macromolecules* **47:** 4357-4368 (2014).
36. Kim O, Kim SY, Lee J and Park MJ. *Chem Mater* **28:** 318-325 (2016).
37. Kim SY, Lee J and Park MJ. *Macromolecules* **47:** 1099-1108 (2014).
38. Weiss RA, Fitzgerald JJ and Kim D. *Macromolecules* **24:** 1071-1076 (1991).
39. Choi J-H, Willis CL and Winey KI. *J Membr Sci* **394–395:** 169-174 (2012).
40. Choi J-H, Ye Y, Elabd YA and Winey KI. *Macromolecules* **46:** 5290-5300 (2013).
41. Gao R, Wang D, Heflin JR and Long TE. *J Mater Chem* **22:** 13473-13476 (2012).
42. Jangu C, Wang J-HH, Wang D, Sharick S, Heflin JR, Winey KI, Colby RH and Long TE. *Macromol Chem Phys* **215:** 1319-1331 (2014).

43. Margaretta E, Fahs GB, Inglefield DL, Jangu C, Wang D, Heflin JR, Moore RB and Long TE. *ACS Appl Mater Interfaces* **8:** 1280-1288 (2016).
44. Green MD, Schreiner C and Long TE. *J Phys Chem A* **115:** 13829-13835 (2011).
45. Vrentas JS, Duda JL and Ling HC. *Macromolecules* **21:** 1470-1475 (1988).
46. Nolte AJ, Treat ND, Cohen RE and Rubner MF. *Macromolecules* **41:** 5793-5798 (2008).
47. Burgess SK, Lee JS, Mubarak CR, Kriegel RM and Koros WJ. *Polymer* **65:** 34-44 (2015).
48. Schreiner C, Zugmann S, Hartl R and Gores HJ. *J Chem Eng Data* **55:** 1784-1788 (2010).
49. Annat G, MacFarlane DR and Forsyth M. *J Phys Chem B* **111:** 9018-9024 (2007).
50. Shi Z, Debenedetti PG and Stillinger FH. *J Chem Phys* **138:** 12A526 (2013).
51. Sharma M and Yashonath A. *Diffusion Fundamentals* **7:** 11.11-11.15 (2007).
52. Fitzgerald JJ and Weiss RA. *J Macromol Sci, Part C* **28:** 99-185 (1988).
53. Bronstein LM, Karlinsey RL, Stein B, Yi Z, Carini J and Zwanziger JW. *Chem Mater* **18:** 708-715 (2006).
54. Inceoglu S, Rojas AA, Devaux D, Chen XC, Stone GM and Balsara NP. *ACS Macro Lett* **3:** 510-514 (2014).

Chapter 6: A Healable Photocured Ion-Containing Block Copolymer Membrane

(In preparation for submission)

Evan Margaretta, Maruti Hegde, Ryan J. Mondschein, Samantha J. Talley, Robert B. Moore, Timothy E. Long*

Department of Chemistry, Macromolecules Innovation Institute
Virginia Tech, Blacksburg, VA, 24061

*To whom correspondence should be addressed
E-mail: telong@vt.edu
TEL: (540)231-2480
FAX: (540)231-8517

Keywords: block copolymer, stimulus response, post-polymerization modification, photocuring, healable

6.1 Abstract

2-(Dimethylamino)ethyl methacrylate (DMAEMA) readily neutralized a sulfonic acid-containing pentablock copolymer. The methacrylate functionality of the DMAEMA-sulfonate ion pair readily photocured upon exposure of the film to UV irradiation. Thermogravimetric analysis (TGA), differential scanning calorimetry (DSC), and dynamic mechanical analysis (DMA) compared the thermal and mechanical properties of the modified membrane to a sulfonic acid-containing control sample and revealed the enhanced thermomechanical properties of the modified membrane. Small-angle X-ray scattering (SAXS) investigated the photocured, DMAEMA-containing film, revealing the preservation of bicontinuous bulk morphology. The photocured membrane exhibited water uptake of 17.1 ± 2.9 wt%, water vapor transport rate of 2.5 ± 0.1 kg m^{-2} day^{-1}, and NaCl permeability of 9.7 x 10^{-8} cm^2 sec^{-1}. Optical microscopy examined the ability to heal

membrane defects, and tensile testing further demonstrated the recovery of mechanical properties of the photocured, ion-containing pentablock copolymer after healing.

6.2 Introduction

Block copolymers that feature covalently bound ionic groups represent an exciting field of research within polymer science owing to their favorable thermomechanical and transport properties.[1-3] In particular, the extensive design versatility inherent with ionic block copolymers enables tuning of properties and self-assembly through variation of parameters such as ion structure, relative block lengths, charge density, bulk morphology, and charge placement *e.g.* backbone *vs* pendant charge.[4-14] Tailoring of these parameters makes ion-containing block copolymers useful for a wide variety of applications including thermoplastics, antimicrobials, nonviral gene delivery, fuel cells, gas separation, water purification, and electromechanical actuators.[15-25] In particular, sulfonated copolymers receive significant attention from researchers due to the sulfonate group's ability to aid in nanoparticle templating, ionic conductivity, and water permeability.[21, 26-34]

Random ion-containing copolymers, such as ionomers or polyelectrolytes, also demonstrate properties useful for many of these applications. Some random ionomers further display self-healing capabilities, as the noncovalent ionic interactions behave as physical crosslink sites that enable re-mending of the polymer.[35-40] Metal-neutralized poly(ethylene-*co*-methacrylic acid) (EMAA) represents a widely studied example of a healable ionomer.[41-46] Research on healable polymers also focuses on dynamic covalent bonding or nonionic physical interactions as the driving force for healing.[47-51] However, the literature strangely lacks reports of healable ion-containing block copolymers, with examples of self-healing block copolymers instead featuring metal-ligand or

complementary hydrogen bonding interactions as physical crosslinks.[52] Ionic block copolymers may exhibit advantageous properties over random ionomers due to the tunable geometry of microphase separation within the bulk, as opposed to random ionic clusters, especially in the presence of a nonionic phase that features a low glass transition temperature (T_g) to promote molecular mobility.

The Nexar family of sulfonated block copolymers features pentablock architecture arising from sequential living anionic polymerization of *t*-butyl styrene, isoprene, styrene, isoprene, and *t*-butyl styrene.[53] Hydrogenation of the polyisoprene block coupled with the alkyl group in the outer blocks enables selective sulfonation of the central polystyrene block to yield a sulfonic acid-containing, microphase-separated pentablock copolymer with general structure poly(*t*-butylstyrene-*b*-hydrogenated isoprene-*b*-sulfonated styrene-*b*-hydrogenated isoprene-*b*-*t*-butylstyrene) (tBS-HI-SS-HI-tBS). The terminal tBS blocks act as mechanically reinforcing anchors, while the HI blocks provide flexibility and toughness to the membrane in addition to a low T_g local environment surrounding the ionic phase. Previous research by Winey *et al* on Nexar focused on its micellar solution and bulk morphologies.[54-56] Geise *et al* also added several notable contributions to the literature that focused on characterizing and understanding the transport properties of Nexar.[20, 57-60] Another study exploited the excellent water transport properties to investigate pervaporative water extraction from short chain aliphatic alcohols.[61] Most recently, the sulfonated pentablock copolymer proved viable for nanofiltration of wastewater to remove heavy metal ions.[62]

Thus far, examples of Nexar modification in the academic and patent literature focused on neutralization of the sulfonic acid site with metal or ammonium cations.[60, 63-66]

Aluminum metal cations proved especially useful in tuning the water and salt transport properties in addition to enhancing the mechanical strength of the resulting membrane.[60] The multivalency of the Al^{3+} cation enabled stronger electrostatic crosslinking in the SS phases and resulted in smaller *d*-spacing in the ionic domain which led to reduced water uptake, water permeability, and coefficient of water diffusion. Similarly, another study investigated the effects of neutralizing the sulfonated styrenic pentablock copolymer with calcium, aluminum, or copper cations to influence the barrier properties of the membrane to dimethyl methylphosphonate, a nerve agent employed in chemical warfare, although the scope of the investigation did not include the morphological effects of this modification.[63]

The effects of crosslinking on polymer thermomechanical and rheological properties are widely studied. These crosslink sites exist as permanent covalent linkages, dynamic covalent linkages, or transient physical interactions. One simple route to crosslinked networks involves UV irradiation to initiate a radical reaction, often of acrylic or methacrylic species. While studies exist detailing photocrosslinked block copolymers, previous literature in ion-containing networks is largely limited to crosslinked gels containing ionic liquids or polymerizable ionic liquids.[67-70] One example exists of using UV irradiation to crosslink the ionic phase of a photonic block copolymer through excitement of the counteranion and resultant hydrogen abstraction from the polymer backbone to generate free radical crosslinking.[71] However, the literature lacks reports of ionic block copolymers where the polymer photocures through covalent linkage of the counterions to each other to provide an electrostatically crosslinked network.

This manuscript details a unique approach to the facile modification of a commercially available sulfonated styrenic pentablock copolymer with a methacrylic

tertiary amine under mild conditions and subsequent UV irradiation to covalently link through countercations. The present study investigates the effects of modification on membrane thermomechanical properties, bulk morphology, water uptake, water vapor transmission rate, salt permeability, and mechanical properties. Furthermore, we explore the effect of the ionic interactions on the capacity of the membrane to heal physical defects. To the authors' best knowledge, this represents the first example in the literature of a healable, photocured, ion-containing block copolymer.

6.3 Experimental

6.3.1 Materials

The sulfonated pentablock copolymer Nexar MD9200 (IEC = 2.0) was provided by Kraton Polymers LLC and used without further purification. 2-(Dimethylamino)ethyl methacrylate (DMAEMA, 98%) was purchased from Sigma Aldrich and inhibitor was removed by passing through an alumina plug prior to use. All solvents were purchased from Spectrum Chemicals and used as received.

6.3.2Analytical Methods

Thermogravimetric analysis (TGA) was performed on a TA Instruments Q500 under nitrogen atmosphere with a heating ramp of 10 °C/min. Differential scanning calorimetry (DSC) determined thermal transitions using standard heat/cool/heat procedure under nitrogen atmosphere with a heating rate of 10 °C/min and quench cool on a TA Instruments Q2000. Glass transition temperatures (T_gs) were determined on the second heating cycle. Dynamic mechanical analysis (DMA) was performed on a TA Instruments Q800 in film tension mode with 1 Hz oscillation, 15 μm amplitude, and 3 °C/min heating rate. Tensile testing was performed at a 5 mm/min crosshead rate on an Instron 5500R universal testing instrument using dumbbell-shaped specimens cut with a Pioneer Dietecs

die. Data was analyzed according to ASTM D638 and represents the average of five samples.

Micrographs were recorded using an Olympus BX51 optical microscope operating in transmission mode equipped with a 10x objective and connected to a Linkam Scientific Instruments TMS 94 heating stage. Indentations were made manually across the surface of the dumbbell shaped samples using a razor blade. The direction of the indentation was perpendicular to the direction of the applied strain in tensile testing. Samples were set at ambient temperature and heated to the desired temperature at a rate of 100 °C/ min. The healing capabilities of the samples were tested both with and without the application of an external shear force.

Salt permeability values were recorded using a PermeGear Side-bi-Side jacketed horizontal cells with 15 mm diameter membrane port, PermeGear H-series stirrers, and a heater/circulator operating at 25 °C. The donor cell contained 2000 ppm aqueous NaCl solution and the other contained deionized water. The conductivity of the water in the receiver cell was measured and correlated to a calibration curve to determine the concentration of NaCl. Membranes were equilibrated in 2000 ppm aqueous NaCl solution for at least 48 h prior to measurement. Salt permeability, P_s, was determined according to the relationship:

$$\ln\left[1 - 2\frac{C_R[t]}{C_D[0]}\right] = -2\frac{A}{VL}P_s t \quad (1)$$

where $C_R[t]$ is the NaCl concentration in the receiving cell at time t, $C_D[0]$ is the initial NaCl concentration in the donor cell, A is the surface area of the membrane, V is the volume of the donor and receiving cells, and L is the thickness of the membrane.[72]

Degree of swelling (DS) was determined by immersing a portion of dried film in an excess of water for one week, and was calculated according to

$$DS = \frac{M-M_0}{M_0}\ x\ 100\% \quad (2)$$

where M is the mass of the swollen membrane and M_0 is the mass of the dried film prior to immersion. Immersion studies were performed in triplicate. Water vapor transport rate (WVTR) was measured in triplicate at 50% relative humidity at 35 °C according to a previously described method.[60]

6.3.3 Morphological Analysis

Small angle X-ray scattering (SAXS) experiments were performed using a Rigaku S-Max 3000 3 pinhole SAXS system, equipped with a rotating anode emitting X-ray with a wavelength of 0.154 nm (Cu K_α). The sample-to-detector distance was 1603 mm, and the q-range was calibrated using a silver behenate standard. Two-dimensional SAXS patterns were obtained using a 2D multiwire, proportional counting, gas-filled detector, with an exposure time of 2 h. The SAXS data were corrected for sample transmission and sample thickness. All SAXS data were analyzed using the SAXSGUI software package to obtain radially integrated SAXS intensity versus the scattering vector q, where $q=(4\pi/\lambda)\sin(\theta)$, θ is one half of the scattering angle and λ is the X-ray wavelength. Primary feature spacings were determined according to the relationship

$$d = \frac{2\pi}{q^*} \quad (3)$$

where d is the spacing and q* is the maximum intensity in the scattering profile.

6.3.4 Modification of Nexar MD9200

A 10 wt% micellar solution of Nexar MD9200 in cyclohexane was added to a 100 mL, round-bottomed flask equipped with a magnetic stir bar and wrapped in aluminum

foil. A calculated amount of DMAEMA (1:1 stoichiometry) was added dropwise to the flask, similar to previous literature precedent.[66] The contents were allowed to stir at room temperature for 18 hours, at which time the solution was cast directly into PTFE dishes. Films were dried at ambient temperature *in vacuo* for 48 hours. The casting and drying process was carried out under dark conditions at ambient temperature to minimize premature photocuring or thermal curing of the methacrylic counterion. After drying, films were photocured using a Fusion Systems UV benchtop conveyor belt curing system with intensity (W/cm^2) as follows: 0.844 visible, 1.431 UVA, 1.301 UVB, and 0.240 UVC. Sequential Soxhlet extraction of the cured films was performed with water first and cyclohexane second. The membranes were annealed at 130 °C for 18 h *in vacuo*. A control sample membrane of unmodified Nexar MD9200 was prepared and annealed in similar fashion.

6.4 Results and Discussion

6.4.1 Modification and thermomechanical characterization

The methacrylic tertiary amine DMAEMA readily neutralized those sulfonic acid sites in Nexar MD9200 according to literature procedure (**Scheme 6.1**) to yield a sulfonated styrenic pentablock copolymer with photocurable countercations.[66] Casting the polymer solution afforded a free-standing, flexible membrane, and subsequent irradiation with UV cured the methacrylate countercation (**Scheme 6.2**). Sequential Soxhlet extractions of the photocured membrane with water and cyclohexane revealed negligible mass loss and yielded a gel fraction > 99%, which further indicated high efficiency of countercation photocuring within the ionic domains. The close proximity of the ammonium methacrylate

countercations within microphase-separated domains of the cast pentablock copolymer membrane likely facilitated efficient photocuring even in the solid state.

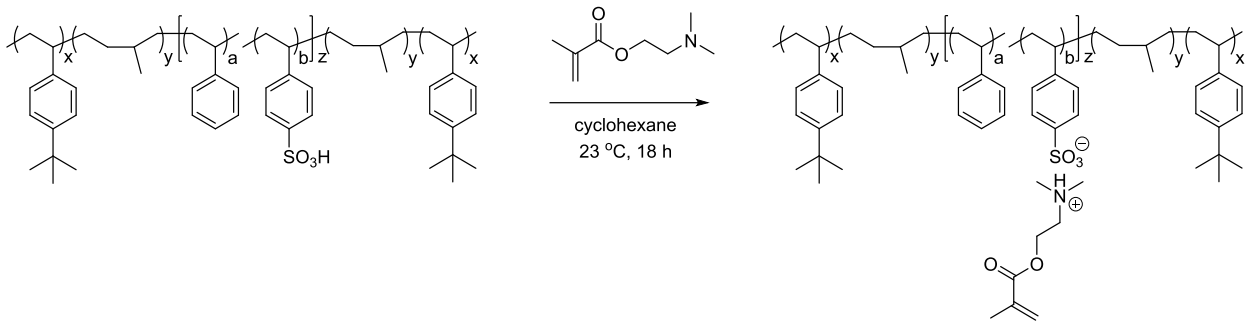

Scheme 6.1. Neutralization of Nexar MD9200 with DMAEMA.

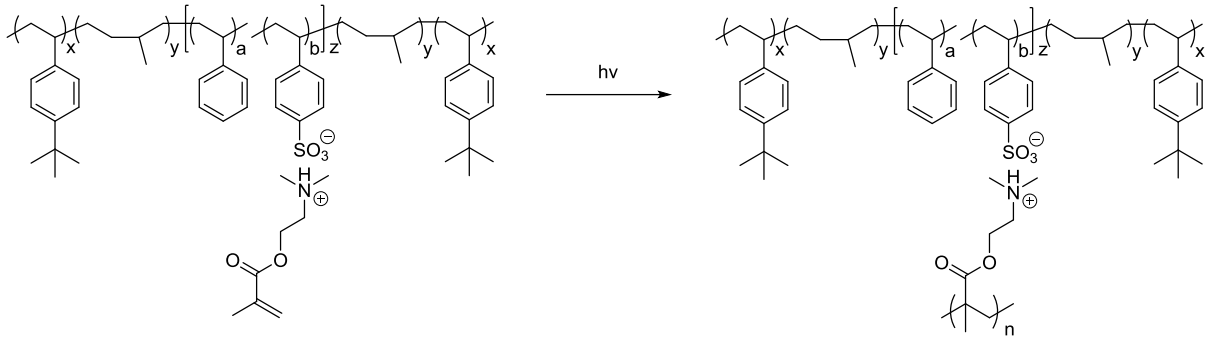

Scheme 6.2. Photocuring of DMAEMA-neutralized Nexar MD9200.

TGA investigated the weight loss profiles of the two membranes as a function of increasing temperature under a nitrogen atmosphere. The 5% weight loss temperature increased from 214 °C to 278 °C upon neutralization and subsequent photocuring. DSC revealed the glass transition temperatures (**Table 6.1**) of the films. Both samples displayed a T_g near -50 °C which corresponded to the HI blocks. Second T_gs around 115 °C related to the T_g of the terminal tBS blocks. The increased thermal stability of the modified analog enabled detection of a third transition at 186 °C that corresponded to the ionic phase.

Table 6.1. Thermal properties of Nexar MD9200 and photocured modified Nexar membranes determined using TGA and DSC.

Sample	$T_{d,5\%}$ (°C)	$T_{g,1}$ (°C)	$T_{g,2}$ (°C)	$T_{g,3}$ (°C)
Nexar MD9200	214	-52	113	ND
Photocured DMAEMA Nexar	278	-51	118	186

The strong electrostatic interaction of sulfonated polystyrene central block with cured methacrylate ammonium ions resulted in greater thermomechanical properties (**Figure 6.1**) as investigated with DMA in tension mode. In both membranes, DMA clearly revealed the T_g of the HI blocks at -35 °C. The second drops in plateau moduli at 108 °C and 113 °C corresponded to the T_g of the tBS outer blocks in the control membrane and the photocured DMAEMA-modified Nexar film, respectively. These transitions agreed reasonably well with those observed using DSC. The higher wt% content of the hard, ionic phase in the modified Nexar membrane caused an increase in storage modulus. Nexar MD9200 exhibited a final decrease in storage modulus at 126 °C which caused the film to yield. In contrast, the modified polymer film demonstrated robust thermomechanical properties up to 195 °C before flow, which revealed the effects of electrostatic crosslinking in the ionic phase. Neutralization and photocuring of the central ionic block therefore resulted in a 70 °C extension of the service window, unprecedented for sulfonated styrenic pentablock copolymers.

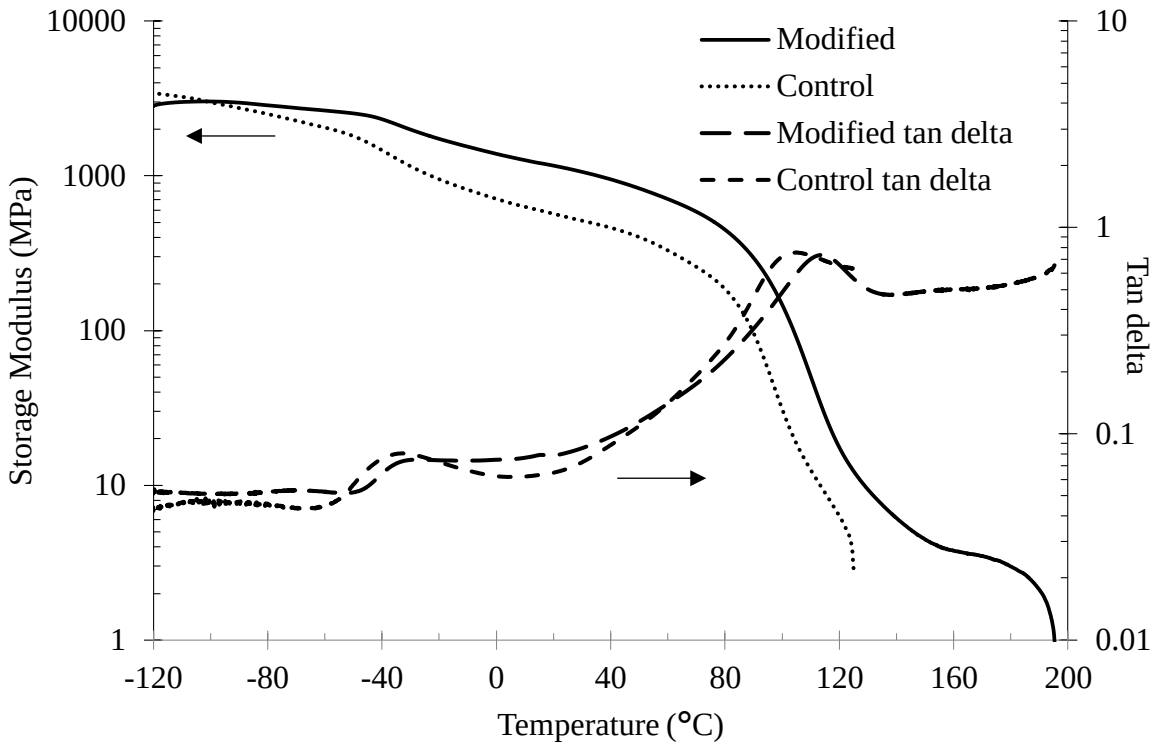

Figure 6.1. DMA revealed the enhanced thermomechanical properties as a result of photocuring DMAEMA-modified Nexar (solid line) compared to Nexar control (dotted line).

6.4.2 Morphological characterization of membranes

SAXS investigated the bulk morphology of Nexar MD9200 and its neutralized and subsequently photocured analogs (**Figure 6.2**). Winey *et al* previously studied in great detail the structure-morphology-property relationship of Nexar polymers with varied degree of sulfonation in the central block.[56] In that study, Nexar membranes with IEC ≤ 1.0 exhibited discrete SS phases existing within a matrix of HI and tBS. At higher IECs, the membranes displayed bicontinuous bulk morphologies without any well-defined long range order. The scattering profile of the unmodified Nexar control studied presently had scattering peaks at 0.24 nm^{-1} and 0.45 nm^{-1} which matched well with the previous

literature.[56] Upon neutralization of the sulfonated polystyrene phase with DMAEMA, the maxima in the scattering profile shifted to 0.15 nm^{-1} and 0.31 nm^{-1}. The shift of the principle scattering peak represented an increase in *d*-spacing from 26 nm to 42 nm, likely resulting from the significant increase in countercation size. Subsequent irradiation caused the ionic domains to decrease in size as the methacrylic counterions became covalently linked. The principle scattering peak of the resulting photocured membrane existed at 0.17 nm^{-1} and corresponded to ionic domains with *d*-spacing of 37 nm.

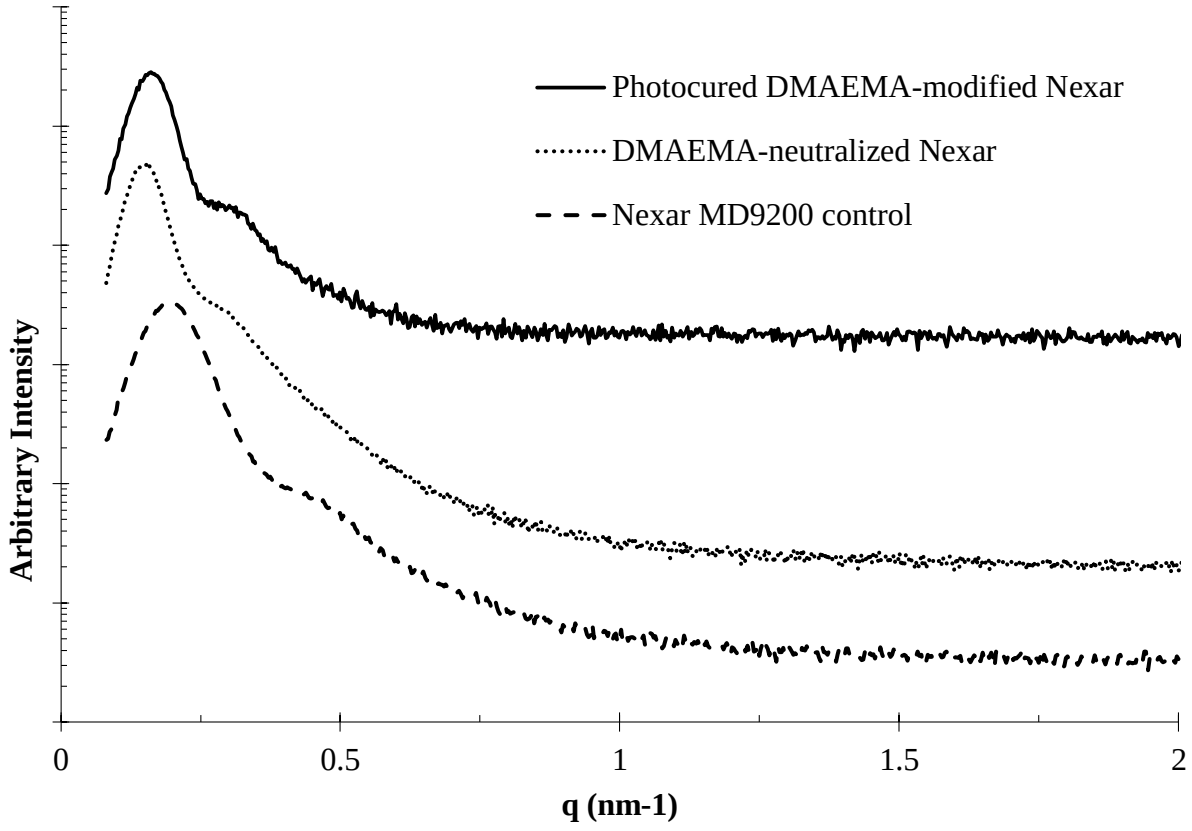

Figure 6.2. SAXS profiles of photocured DMAEMA-modified Nexar (solid line), the DMAEMA-neutralized but uncured Nexar (dotted line), and the unmodified control (dashed line) membranes. The profiles have been shifted vertically for clarity.

Previous studies also investigated the development of morphology in sulfonated pentablock copolymers. The micellar solution structure of Nexar in nonpolar solvents arose from aggregation of SS central blocks and good solvation of flanking HI blocks and terminal tBS blocks.[54-55] Casting micellar solutions led to the presence of similar ion-aggregated morphology in films.[56] Shull *et al* employed grazing incidence SAXS to directly observe in real time the evolution of morphology as solvent evaporated to form a thin film.[73] This investigation in particular supported the hypothesis that the morphology observed for unmodified Nexar remained largely unchanged after neutralization with DMAEMA, as the neutralized sample still retained the high volume fraction of the ionic block that drove the development of bicontinuous microphase-separation. This proved consistent with the observed increase in *d*-spacing for the ionic domains, ostensibly because the DMAEMA countercations are significantly larger in size than the proton of the unmodified sample. This increase in domain spacing displayed the opposite effect relative to trivalent aluminum cations that electrostatically crosslinked the SS domains.[60] The difference likely resulted from the retention of 1:1 cation to anion ratio in addition to the bulkier nature of the ammonium methacrylate countercation relative to Al^{3+}.

Photocuring further served to preserve this observed bicontinuous morphology by covalently linking through the countercations of the ionic domain. SAXS (**Figure 6.3**) demonstrated the marginal differences in scattering profiles for the modified membrane before and after a thermal annealing step. Both samples exhibited maxima in the scattering profile near 0.17 nm^{-1} and 0.32 nm^{-1}, indicating the retention of bicontinuous bulk morphology and *d*-spacing for the ionic domains. This further demonstrated the strong nature of the electrostatic interactions between the polymer-bound sulfonate groups and

covalently linked ammonium countercations. The preservation of the bulk morphology also indicated the efficiency of the photocuring step, as further thermal curing likely would have resulted in another decrease in ionic domain *d*-spacing like that observed for the photocuring step.

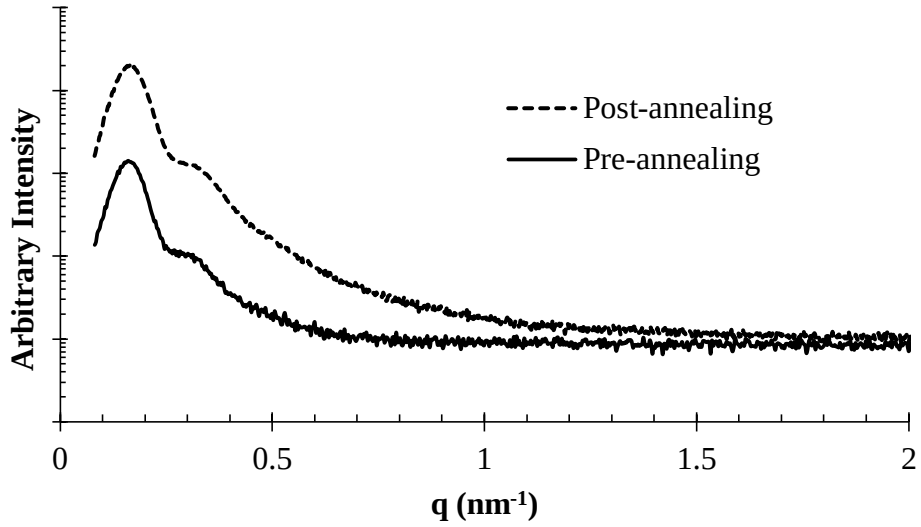

Figure 6.3. SAXS profiles of photocured DMAEMA-modified Nexar before (solid line) and after (dashed line) thermal annealing for 18 h at 130 °C *in vacuo*. The profiles have been shifted vertically for clarity.

6.4.3 Water uptake, WVTR, and NaCl permeability

Immersion of the modified Nexar membrane in deionized water determined its water uptake over time (**Table 6.2**). The photocured membrane demonstrated a significantly lower extent of water uptake compared to the control membrane. The experimentally determined water uptake for the control membrane of 83.7 ± 5.0 % agreed well with previous literature.[56] The reduction in water uptake for the modified membrane likely resulted from the increased hydrophobicity of the countercation compared to the unmodified polymer which counteracted the increased size of the ionic domains. WVTR

measurements further reflected this change in the ionic domains. Although the bicontinuous morphology favorable for high water vapor transport persisted in the modified film, the WVTR dropped by roughly an order of magnitude compared to the control film. The reduced water uptake and WVTR for crosslinked Nexar followed similar trends to those reported for Al^{3+}-crosslinked films, and the measured values for the unmodified polymer film agreed with reported values.[56, 60]

Modification of Nexar MD9200 and subsequent photocuring did not significantly affect the NaCl permeability of the membrane, as both films exhibited values approaching 10^{-7} cm^2 sec^{-1}. These measurements agreed well with a previous report that established the potential of sulfonated styrenic pentablock copolymers with varying IEC for desalination applications.[20] That study concluded that water swelling played a significant role in NaCl transport through the membrane and that further investigations were required to establish the transport mechanism. While probing the transport mechanism fell outside the scope of the present study, the reduced swelling capacity of the modified membrane without any consequential effect in the NaCl permeability proved encouraging for a more detailed investigation of photocured, DMAEMA-neutralized sulfonated styrenic pentablock copolymers as a platform for desalination applications.

Table 6.2. Water uptake, water vapor transportation rate, and NaCl permeability values for Nexar MD9200 control and the modified membrane.

Sample	Water uptake (wt%)	WVTR ($kg\ m^{-2}\ day^{-1}$)	NaCl Permeability ($cm^2\ sec^{-1}$)
Nexar MD9200	83.7 ± 5.0	24.4 ± 2.6	9.8×10^{-8}
Photocured DMAEMA-modified Nexar	17.1 ± 2.9	2.5 ± 0.1	9.7×10^{-8}

6.4.4 Healing of defects

Optical microscopy evaluated the healable nature of the membrane through close examination of a defect (**Figure 6.4**). The modified membrane demonstrated the ability to bridge 50 μm wide scratches upon heating to 170 °C with the application of a slight shear force (**Figure 6.4 A-B**). These results highlighted the importance of the electrostatic crosslinking with the cured countercations when compared to the tests performed at 210 °C (**Figure 6.4 C-D**). When the temperature exceeded the ion-dissociation temperature determined from DMA and DSC, the membrane exhibited no ability to heal. Similarly, the control membrane did not heal at 170 °C, likely due to the reduced electrostatic interactions. **Figure 6.4 E-F** reveals particularly well that the application of gentle shear at 170°C across the film indentation did not result in healing but rather further damage of the bulk film.

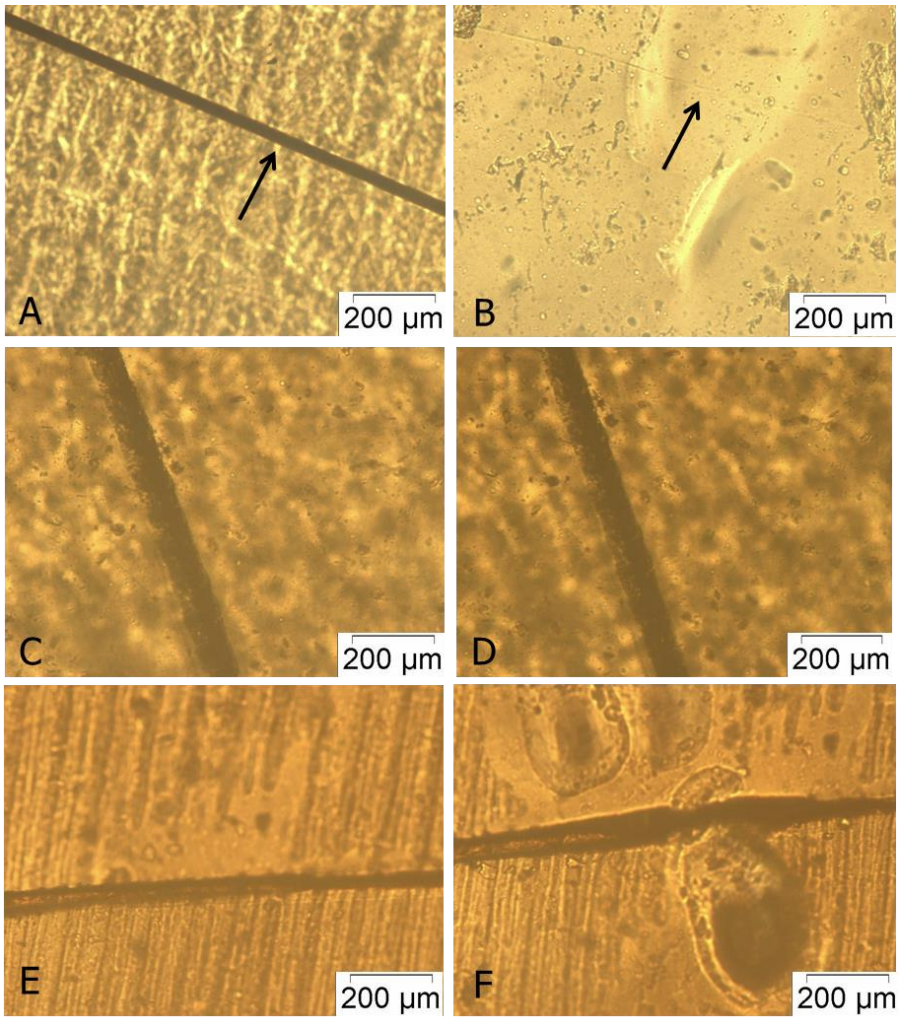

Figure 6.4. Healing micrographs of modified Nexar (A-D) and control membrane (E-F). Images on the left are of the membranes immediately after indentation, and images on the right are the membranes after heating to 210 °C (D) or 170 °C (B, F) and attempting to heal.

Tensile testing subsequently demonstrated the recovery of mechanical properties upon the healing of film defects. Indentation of the dumbbell-shaped samples with a razor blade perpendicular to the direction of extensional deformation imparted nominally 50 µm wide defects to the membrane as determined using optical microscopy (**Figure 6.4A**). Tensile testing of these damaged specimens exposed the reduced stress and strain behavior

of the samples as expected, confirming the weakening of the membrane upon introduction of the defect. Representative stress-strain profiles of the various samples clearly exhibit the recovery of mechanical properties for damaged and subsequently healed samples relative to samples that were indented but not healed (**Figure 6.5A**). For all three sample sets, Young's modulus remained consistent within error throughout the tensile experiments (**Figure 6.5B**). The healed sample demonstrated enhanced strain-at-break properties relative to the damaged samples (**Figure 6.5C**), further confirming the efficiency of the healing step to improve the material properties of the damaged polymer samples. Lastly, the healed samples exhibited a maximum stress within error of the modified, undamaged polymer samples, showing that the healing process afforded near complete recovery of maximum stress (**Figure 6.5D**).

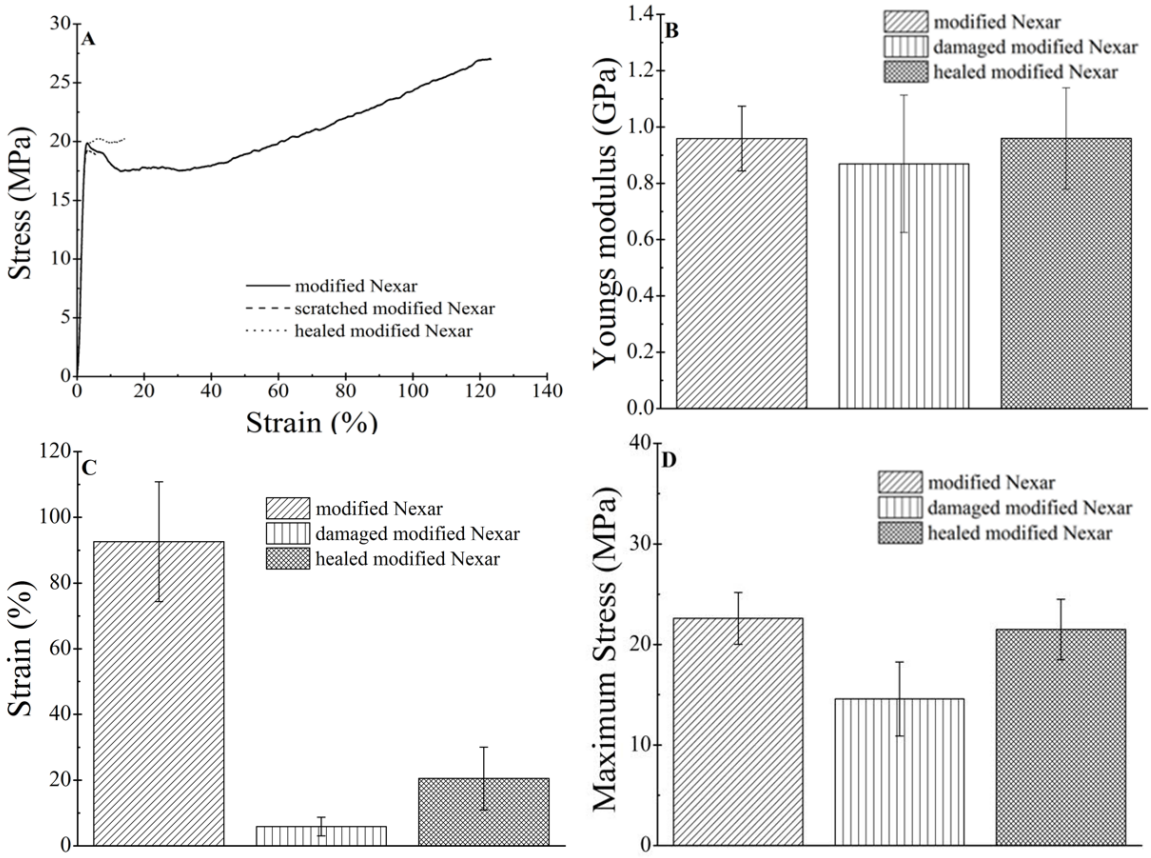

Figure 6.5. (A) Representative stress-strain tensile profiles and compiled average (b) Young's modulus, (c) strain at break, and (d) maximum stress for modified Nexar, damaged modified Nexar, and healed modified Nexar samples.

Table 6.3 compares the average mechanical properties to the unmodified control previously studied in literature.[60] Modification and subsequent photocuring increased the maximum stress of the sulfonate-containing pentablock copolymer. This modification of the polymer also caused a concurrent decrease in strain at break, however. Interestingly, the damaged modified samples also exhibited an average stress at break similar to that of the unmodified control. The healed samples displayed maximum stress roughly double that of the unmodified polymer, and served to further reinforce that modification resulted in improved mechanical strength.

Table 6.3. Tensile properties of photocured, DMAEMA-modified Nexar.

Sample	**Young's Modulus (GPa)**	**Strain (%)**	**Maximum Stress (MPa)**
Nexar MD9200 [a]	NR	250	11.5
Modified Nexar	0.96 ± 0.12	92.6 ± 18.2	22.6 ± 2.6
Damaged Modified Nexar	0.87 ± 0.24	5.9 ± 2.8	14.6 ± 3.7
Healed Modified Nexar	0.96 ± 0.18	20.5 ± 9.6	21.4 ± 3.0

[a] Values from Ref. 60; NR = not reported.

6.5 Conclusions

This report details for the first time the neutralization and subsequent photocuring of a sulfonated styrenic pentablock copolymer. The two-step, facile modification yielded an ion-containing block copolymer membrane with bicontinuous bulk morphology and

resulted in an extension of the service window by 70 °C. Water uptake decreased when measured gravimetrically by swelling, and WVTR decreased by roughly an order of magnitude upon modification; however, NaCl permeability through the membrane remained constant. Furthermore, the introduction of strongly associating ions with restricted mobility increased maximum stress and decreased strain and break in tensile experiments. However, such ionic aggregates proved crucial to the film's ability to heal defects. Optical microscopy revealed the ability to remove defects from the membrane below the ion dissociation temperature, which was not observed for the control polymer. Additional experiments compared the tensile properties of damaged and subsequently healed samples, and revealed the recovery of maximum stress and strain at break upon healing of the samples. These properties together represent the first example in the literature of a photocured, ion-containing healable block copolymer, and serve as a platform for further investigation of these kinds of polymers for various applications.

6.6 Acknowledgments

This work is based on work supported in part by Kraton Polymers, LLC. The authors acknowledge Mr. Nathan Carter for discussions regarding healing properties of films and Dr. Zhiyang Zhang for her insight with respect to salt permeability measurements.

6.7 References

1. Ye, Y.; Sharick, S.; Davis, E. M.; Winey, K. I.; Elabd, Y. A., High Hydroxide Conductivity in Polymerized Ionic Liquid Block Copolymers. *ACS Macro Letters* **2013,** *2* (7), 575-580.
2. Meek, K. M.; Sharick, S.; Ye, Y.; Winey, K. I.; Elabd, Y. A., Bromide and Hydroxide Conductivity–Morphology Relationships in Polymerized Ionic Liquid Block Copolymers. *Macromolecules* **2015,** *48* (14), 4850-4862.

3. Ye, Y.; Choi, J.-H.; Winey, K. I.; Elabd, Y. A., Polymerized Ionic Liquid Block and Random Copolymers: Effect of Weak Microphase Separation on Ion Transport. *Macromolecules* **2012,** *45* (17), 7027-7035.
4. Hemp, S. T.; Zhang, M.; Allen, M. H.; Cheng, S.; Moore, R. B.; Long, T. E., Comparing Ammonium and Phosphonium Polymerized Ionic Liquids: Thermal Analysis, Conductivity, and Morphology. *Macromolecular Chemistry and Physics* **2013,** *214* (18), 2099-2107.
5. Weber, R. L.; Ye, Y.; Banik, S. M.; Elabd, Y. A.; Hickner, M. A.; Mahanthappa, M. K., Thermal and Ion Transport Properties of Hydrophilic and Hydrophobic Polymerized Styrenic Imidazolium Ionic Liquids. *J. Polym. Sci., Part B: Polym. Phys.* **2011,** *49* (18), 1287-1296.
6. Evans, C. M.; Sanoja, G. E.; Popere, B. C.; Segalman, R. A., Anhydrous Proton Transport in Polymerized Ionic Liquid Block Copolymers: Roles of Block Length, Ionic Content, and Confinement. *Macromolecules* **2016,** *49* (1), 395-404.
7. Shen, H.; Eisenberg, A., Block Length Dependence of Morphological Phase Diagrams of the Ternary System of PS-b-PAA/Dioxane/H2O. *Macromolecules* **2000,** *33* (7), 2561-2572.
8. Weber, R. L.; Ye, Y.; Schmitt, A. L.; Banik, S. M.; Elabd, Y. A.; Mahanthappa, M. K., Effect of Nanoscale Morphology on the Conductivity of Polymerized Ionic Liquid Block Copolymers. *Macromolecules* **2011,** *44* (14), 5727-5735.
9. Tamami, M.; Williams, S. R.; Park, J. K.; Moore, R. B.; Long, T. E., Poly(propylene glycol)-based ammonium ionenes as segmented ion-containing block copolymers. *Journal of Polymer Science Part A: Polymer Chemistry* **2010,** *48* (19), 4159-4167.
10. Hemp, S. T.; Zhang, M.; Tamami, M.; Long, T. E., Phosphonium ionenes from well-defined step-growth polymerization: thermal and melt rheological properties. *Polymer Chemistry* **2013,** *4* (12), 3582-3590.
11. Abdulahad, A. I.; Jangu, C.; Hemp, S. T.; Long, T. E., Influence of Counterion on Thermal, Viscoelastic, and Ion Conductive Properties of Phosphonium Ionenes. *Macromolecular Symposia* **2014,** *342* (1), 56-66.
12. Choi, J.-H.; Ye, Y.; Elabd, Y. A.; Winey, K. I., Network Structure and Strong Microphase Separation for High Ion Conductivity in Polymerized Ionic Liquid Block Copolymers. *Macromolecules* **2013,** *46* (13), 5290-5300.
13. Moffitt, M.; Khougaz, K.; Eisenberg, A., Micellization of Ionic Block Copolymers. *Accounts of Chemical Research* **1996,** *29* (2), 95-102.
14. Pawar, G. M.; Lalancette, R. A.; Bonder, E. M.; Sheridan, J. B.; Jäkle, F., ROMP-Derived Pyridylborate Block Copolymers: Self-Assembly, pH-Responsive Properties, and Metal-Containing Nanostructures. *Macromolecules* **2015,** *48* (18), 6508-6515.
15. Nelson, A. M.; Long, T. E., Synthesis, Properties, and Applications of Ion-Containing Polyurethane Segmented Copolymers. *Macromolecular Chemistry and Physics* **2014,** *215* (22), 2161-2174.
16. Lee, A. L. Z.; Ng, V. W. L.; Wang, W.; Hedrick, J. L.; Yang, Y. Y., Block copolymer mixtures as antimicrobial hydrogels for biofilm eradication. *Biomaterials* **2013,** *34* (38), 10278-10286.
17. Park, D.; Finlay, J. A.; Ward, R. J.; Weinman, C. J.; Krishnan, S.; Paik, M.; Sohn, K. E.; Callow, M. E.; Callow, J. A.; Handlin, D. L.; Willis, C. L.; Fischer, D. A.;

Angert, E. R.; Kramer, E. J.; Ober, C. K., Antimicrobial Behavior of Semifluorinated-Quaternized Triblock Copolymers against Airborne and Marine Microorganisms. *ACS Applied Materials & Interfaces* **2010,** *2* (3), 703-711.
18. Hemp, S. T.; Allen, M. H.; Green, M. D.; Long, T. E., Phosphonium-Containing Polyelectrolytes for Nonviral Gene Delivery. *Biomacromolecules* **2011,** *13* (1), 231-238.
19. Grünauer, J.; Shishatskiy, S.; Abetz, C.; Abetz, V.; Filiz, V., Ionic liquids supported by isoporous membranes for CO2/N2 gas separation applications. *Journal of Membrane Science* **2015,** *494*, 224-233.
20. Geise, G. M.; Freeman, B. D.; Paul, D. R., Characterization of a sulfonated pentablock copolymer for desalination applications. *Polymer* **2010,** *51* (24), 5815-5822.
21. Kim, O.; Kim, S. Y.; Park, B.; Hwang, W.; Park, M. J., Factors Affecting Electromechanical Properties of Ionic Polymer Actuators Based on Ionic Liquid-Containing Sulfonated Block Copolymers. *Macromolecules* **2014,** *47* (13), 4357-4368.
22. Kim, O.; Shin, T. J.; Park, M. J., Fast low-voltage electroactive actuators using nanostructured polymer electrolytes. *Nat Commun* **2013,** *4*.
23. Pergushov, D. V.; Muller, A. H. E.; Schacher, F. H., Micellar interpolyelectrolyte complexes. *Chemical Society Reviews* **2012,** *41* (21), 6888-6901.
24. Suga, T.; Sakata, M.; Aoki, K.; Nishide, H., Synthesis of Pendant Radical- and Ion-Containing Block Copolymers via Ring-Opening Metathesis Polymerization for Organic Resistive Memory. *ACS Macro Letters* **2014,** *3* (8), 703-707.
25. Wang, Z.; Guo, L.; Wang, Y., Isoporous membranes with gradient porosity by selective swelling of UV-crosslinked block copolymers. *Journal of Membrane Science* **2015,** *476*, 449-456.
26. Ortiz-Negrón, A.; Suleiman, D., The effect of TiO2 nanoparticles on the properties of sulfonated block copolymers. *Journal of Applied Polymer Science* **2015,** *132* (41), n/a-n/a.
27. Park, M. J.; Kim, S. Y., Ion transport in sulfonated polymers. *Journal of Polymer Science Part B: Polymer Physics* **2013,** *51* (7), 481-493.
28. Kim, S. Y.; Lee, J.; Park, M. J., Proton Hopping and Diffusion Behavior of Sulfonated Block Copolymers Containing Ionic Liquids. *Macromolecules* **2014,** *47* (3), 1099-1108.
29. Fitzgerald, J. J.; Weiss, R. A., Synthesis, Properties, and Structure of Sulfonate Ionomers. *Journal of Macromolecular Science, Part C* **1988,** *28* (1), 99-185.
30. Mori, H.; Kudo, E.; Saito, Y.; Onuma, A.; Morishima, M., RAFT Polymerization of Vinyl Sulfonate Esters for the Controlled Synthesis of Poly(lithium vinyl sulfonate) and Sulfonated Block Copolymers. *Macromolecules* **2010,** *43* (17), 7021-7032.
31. Xie, W.; Cook, J.; Park, H. B.; Freeman, B. D.; Lee, C. H.; McGrath, J. E., Fundamental salt and water transport properties in directly copolymerized disulfonated poly(arylene ether sulfone) random copolymers. *Polymer* **2011,** *52* (9), 2032-2043.
32. Bae, B.; Kawamura, S.; Miyatake, K.; Watanabe, M., Synthesis and properties of sulfonated poly(arylene ether)s containing azole groups. *Journal of Polymer Science Part A: Polymer Chemistry* **2011,** *49* (17), 3863-3873.

33. Chu, J. Y.; Kim, A. R.; Nahm, K. S.; Lee, H.-K.; Yoo, D. J., Synthesis and characterization of partially fluorinated sulfonated poly(arylene biphenylsulfone ketone) block copolymers containing 6F-BPA and perfluorobiphenylene units. *International Journal of Hydrogen Energy* **2013,** *38* (14), 6268-6274.
34. Duong, P. H. H.; Chung, T.-S.; Wei, S.; Irish, L., Highly Permeable Double-Skinned Forward Osmosis Membranes for Anti-Fouling in the Emulsified Oil–Water Separation Process. *Environmental Science & Technology* **2014,** *48* (8), 4537-4545.
35. Blaiszik, B. J.; Kramer, S. L. B.; Olugebefola, S. C.; Moore, J. S.; Sottos, N. R.; White, S. R., Self-Healing Polymers and Composites. *Annual Review of Materials Research* **2010,** *40* (1), 179-211.
36. Herbst, F.; Döhler, D.; Michael, P.; Binder, W. H., Self-Healing Polymers via Supramolecular Forces. *Macromolecular Rapid Communications* **2013,** *34* (3), 203-220.
37. Varley, R., Ionomers as Self Healing Polymers. In *Self Healing Materials: An Alternative Approach to 20 Centuries of Materials Science*, Zwaag, S., Ed. Springer Netherlands: Dordrecht, 2007; pp 95-114.
38. Zhang, L.; Brostowitz, N. R.; Cavicchi, K. A.; Weiss, R. A., Perspective: Ionomer Research and Applications. *Macromolecular Reaction Engineering* **2014,** *8* (2), 81-99.
39. Aboudzadeh, M. A.; Muñoz, M. E.; Santamaría, A.; Marcilla, R.; Mecerreyes, D., Facile Synthesis of Supramolecular Ionic Polymers That Combine Unique Rheological, Ionic Conductivity, and Self-Healing Properties. *Macromolecular Rapid Communications* **2012,** *33* (4), 314-318.
40. Sundaresan, V. B.; Morgan, A.; Castellucci, M., Self-Healing of Ionomeric Polymers with Carbon Fibers from Medium-Velocity Impact and Resistive Heating. *Smart Materials Research* **2013,** *2013*, 12.
41. Kalista, S. J.; Pflug, J. R.; Varley, R. J., Effect of ionic content on ballistic self-healing in EMAA copolymers and ionomers. *Polymer Chemistry* **2013,** *4* (18), 4910-4926.
42. Grande, A. M.; Castelnovo, L.; Landro, L. D.; Giacomuzzo, C.; Francesconi, A.; Rahman, M. A., Rate-dependent self-healing behavior of an ethylene-co-methacrylic acid ionomer under high-energy impact conditions. *Journal of Applied Polymer Science* **2013,** *130* (3), 1949-1958.
43. Haase, T.; Rohr, I.; Thoma, K., Dynamic temperature measurements on a thermally activated self-healing ionomer. *Journal of Intelligent Material Systems and Structures* **2014,** *25* (1), 25-30.
44. Rahman, M. A.; Spagnoli, G.; Grande, A. M.; Di Landro, L., Role of Phase Morphology on the Damage Initiated Self-healing Behavior of Ionomer Blends. *Macromolecular Materials and Engineering* **2013,** *298* (12), 1350-1364.
45. Fall, R. A., Puncture Reversal of Polyethylene Ionomers-Mechanistic Studies. **2001**.
46. Kalista Jr, S. J., Self-healing of thermoplastic poly (ethylene-co-methacrylic acid) copolymers following projectile puncture. **2003**.
47. Baghdachi, J.; Provder, T., *Smart Coatings III*. American Chemical Society: 2010; Vol. 1050, p 0.

48. Bergman, S. D.; Wudl, F., Re-Mendable Polymers. In *Self Healing Materials: An Alternative Approach to 20 Centuries of Materials Science*, Zwaag, S., Ed. Springer Netherlands: Dordrecht, 2007; pp 45-68.
49. Chen, X.; Dam, M. A.; Ono, K.; Mal, A.; Shen, H.; Nutt, S. R.; Sheran, K.; Wudl, F., A Thermally Re-mendable Cross-Linked Polymeric Material. *Science* **2002,** *295* (5560), 1698-1702.
50. Hohlbein, N.; Shaaban, A.; Bras, A. R.; Pyckhout-Hintzen, W.; Schmidt, A. M., Self-healing dynamic bond-based rubbers: understanding the mechanisms in ionomeric elastomer model systems. *Physical Chemistry Chemical Physics* **2015,** *17* (32), 21005-21017.
51. Lei, Z. Q.; Xiang, H. P.; Yuan, Y. J.; Rong, M. Z.; Zhang, M. Q., Room-Temperature Self-Healable and Remoldable Cross-linked Polymer Based on the Dynamic Exchange of Disulfide Bonds. *Chemistry of Materials* **2014,** *26* (6), 2038-2046.
52. Hentschel, J.; Kushner, A. M.; Ziller, J.; Guan, Z., Self-Healing Supramolecular Block Copolymers. *Angewandte Chemie* **2012,** *124* (42), 10713-10717.
53. Willis, C. L.; Handlin, D. L., Jr.; Trenor, S. R.; Mather, B. D. Sulfonated block copolymers, method for their preparation, and their. WO2007010039A1, 2007.
54. Choi, J.-H.; Kota, A.; Winey, K. I., Micellar Morphology in Sulfonated Pentablock Copolymer Solutions. *Industrial & Engineering Chemistry Research* **2010,** *49* (23), 12093-12097.
55. Griffin, P. J.; Salmon, G. B.; Ford, J.; Winey, K. I., Predicting the solution morphology of a sulfonated pentablock copolymer in binary solvent mixtures. *Journal of Polymer Science Part B: Polymer Physics* **2016,** *54* (2), 254-262.
56. Choi, J.-H.; Willis, C. L.; Winey, K. I., Structure–property relationship in sulfonated pentablock copolymers. *Journal of Membrane Science* **2012,** *394–395*, 169-174.
57. Geise, G. M.; Falcon, L. P.; Freeman, B. D.; Paul, D. R., Sodium chloride sorption in sulfonated polymers for membrane applications. *Journal of Membrane Science* **2012,** *423–424*, 195-208.
58. Geise, G. M.; Freeman, B. D.; Paul, D. R., Sodium chloride diffusion in sulfonated polymers for membrane applications. *Journal of Membrane Science* **2013,** *427*, 186-196.
59. Geise, G. M.; Doherty, C. M.; Hill, A. J.; Freeman, B. D.; Paul, D. R., Free volume characterization of sulfonated styrenic pentablock copolymers using positron annihilation lifetime spectroscopy. *Journal of Membrane Science* **2014,** *453* (0), 425-434.
60. Geise, G. M.; Willis, C. L.; Doherty, C. M.; Hill, A. J.; Bastow, T. J.; Ford, J.; Winey, K. I.; Freeman, B. D.; Paul, D. R., Characterization of Aluminum-Neutralized Sulfonated Styrenic Pentablock Copolymer Films. *Industrial & Engineering Chemistry Research* **2013,** *52* (3), 1056-1068.
61. Zuo, J.; Shi, G. M.; Wei, S.; Chung, T.-S., The Development of Novel Nexar Block Copolymer/Ultem Composite Membranes for C2–C4 Alcohols Dehydration via Pervaporation. *ACS Applied Materials & Interfaces* **2014,** *6* (16), 13874-13883.
62. Thong, Z.; Han, G.; Cui, Y.; Gao, J.; Chung, T.-S.; Chan, S. Y.; Wei, S., Novel Nanofiltration Membranes Consisting of a Sulfonated Pentablock Copolymer

Rejection Layer for Heavy Metal Removal. *Environmental Science & Technology* **2014,** *48* (23), 13880-13887.
63. Schneider, N. S.; Zukas, W. S.; Pomerantz, N. L., Effect of cation exchange on dimethyl methylphosphonate permeation kinetics in a pentablock hydrocarbon ionomer and a perfluorocarbon ionomer. *Polymer* **2014,** *55* (1), 150-159.
64. Willis, C. L. Metal-neutralized sulfonated block copolymers, process for making them and their use. WO2011046709A1, 2011.
65. Willis, C. L. Amine-neutralized sulfonated block copolymers and method for making same. WO2011046708A1, 2011.
66. Gao, R.; Wang, D.; Heflin, J. R.; Long, T. E., Imidazolium Sulfonate-containing Pentablock Copolymer-Ionic Liquid Membranes for Electroactive Actuators. *J. Mater. Chem.* **2012,** *22* (27), 13473-13476.
67. Miranda, D. F.; Versek, C.; Tuominen, M. T.; Russell, T. P.; Watkins, J. J., Cross-Linked Block Copolymer/Ionic Liquid Self-Assembled Blends for Polymer Gel Electrolytes with High Ionic Conductivity and Mechanical Strength. *Macromolecules* **2013,** *46* (23), 9313-9323.
68. Kataoka, T.; Ishioka, Y.; Mizuhata, M.; Minami, H.; Maruyama, T., Highly Conductive Ionic-Liquid Gels Prepared with Orthogonal Double Networks of a Low-Molecular-Weight Gelator and Cross-Linked Polymer. *ACS Applied Materials & Interfaces* **2015,** *7* (41), 23346-23352.
69. Bara, J. E.; Hatakeyama, E. S.; Gabriel, C. J.; Zeng, X.; Lessmann, S.; Gin, D. L.; Noble, R. D., Synthesis and light gas separations in cross-linked gemini room temperature ionic liquid polymer membranes. *Journal of Membrane Science* **2008,** *316* (1–2), 186-191.
70. Altava, B.; Compañ, V.; Andrio, A.; del Castillo, L. F.; Mollá, S.; Burguete, M. I.; García-Verdugo, E.; Luis, S. V., Conductive films based on composite polymers containing ionic liquids absorbed on crosslinked polymeric ionic-like liquids (SILLPs). *Polymer* **2015,** *72*, 69-81.
71. Ahn, Y.; Kim, E.; Hyon, J.; Kang, C.; Kang, Y., Photoresponsive Block Copolymer Photonic Gels with Widely Tunable Photosensitivity by Counter-Ions. *Advanced Materials* **2012,** *24* (23), OP127-OP130.
72. Yasuda, H.; Ikenberry, L. D.; Lamaze, C. E., Permeability of solutes through hydrated polymer membranes. Part II. Permeability of water soluble organic solutes. *Die Makromolekulare Chemie* **1969,** *125* (1), 108-118.
73. Laprade, E. J.; Liaw, C.-Y.; Jiang, Z.; Shull, K. R., Mechanical and microstructural characterization of sulfonated pentablock copolymer membranes. *Journal of Polymer Science Part B: Polymer Physics* **2015,** *53* (1), 39-47.

Chapter 7: Cleavable Hydrogels from Microstereolithography

(*In preparation* for submission)

Evan Margaretta[a], Donald C. Aduba, Jr.[ab], Nicholas A. Chartrain[b], Allison M. Pekkanen[c], Robert Z. Haley[a], Christopher B. Williams[b], Timothy E. Long[ac*]

[a]*Department of Chemistry, Macromolecules Innovation Institute;* [b]*Department of Mechanical Engineering;* [c] *Department of Biomedical Engineering and Mechanics Virginia Tech, Blacksburg, VA, 24061*

*To whom correspondence should be addressed
E-mail: telong@vt.edu
TEL: (540) 231-2480
FAX: (540) 231-8517

Keywords: hydrogels, 3D printing, stimulus response, chemical degradation, microstereolithography

7.1 Abstract

Polyethylene glycol methacrylate (PEGMA) readily photocured in the presence of various amounts of different pH-labile crosslinkers to yield degradable covalent networks. Additive manufacturing with the microstereolithography technique afforded 3D-printed networks with good resolution and degradable functionalities. Tertiary alkyl esters provided acid sensitivity, poly(lactide-*co*-glycolide) ester bonds imparted hydrolytic instability, and a fluorinated aromatic ester was investigated for its base sensitivity. Thermogravimetric analysis, differential scanning calorimetry, and thermogravimetric sorption analysis probed the thermal properties and water uptake of the 3D-printed networks, establishing their suitability as hydrogels. Evaluation of the 3D-printed objects for their degradability demonstrated full degradation as quickly as 6 h.

7.2 Introduction

Polymer networks or gels represent attractive targets for researchers owing to their design versatility and tunable properties. Careful selection of crosslinker and monomer enable control over the physicochemical properties of the network. Similarly, the crosslinker content of the network composition adjusts inherent material properties such as degree of swelling and modulus.[1-2] Their inherent insolubility and enhanced toughness relative to linear polymers restrict their processability and recyclability.[3] However, these same properties also facilitate a variety of applications such as separations, long-term controlled release, dental resins, solid state aerospace fuels, and structural adhesives.[2, 4-9]

Two main synthetic routes lead to network formation: post-polymerization modification to covalently link multiple chains, and polymerization in the presence of a multifunctional crosslinker.[10-14] Researchers often extend the latter strategy towards photopolymerization of acrylates, methacrylates, and acrylamide monomers in the presence of a difunctional crosslinker.[15-16] The UV-curing method extends well into three dimensions through the mask projection stereolithography (SL) process, which fabricates objects through sequential curing of individual layers. Advances in SL technology resulted in feature sizes < 10 μm with drastically decreased fabrication times, leading to a branch of the field known as microstereolithography (μSL).[17-18] μSL represents just one of several additive manufacturing or 3D-printing techniques, but also proves suitable for a wide variety of resin compositions, providing they exhibit suitable viscosity. End-functionalized oligomers, known as photopolymers, often meet this criteria, and find widespread use for the 3D-printing of crosslinked networks for cell scaffolding and novel polymeric electrolytes.[19-20]

Networks that demonstrate a change in physicochemical properties upon exposure to an external stimulus represent an attractive target for researchers.[21] pH proves a particularly attractive stimulus due to the variety of known and stable physiological conditions. Thus, many reports exist of pH-responsive networks.[22-28] Tertiary alkyl esters demonstrate both thermally-induced and acid lability in polymer networks and in core-crosslinked star polymers, allowing conversion of insoluble networks to soluble linear polymers.[13, 29-30] Theato *et al.* demonstrated that fluorinated phenyl esters also show pH-sensitivity, degrading to liberate the corresponding phenol in the presence of basic species such as amines.[31-33] Poly(lactide-*co*-glycolide) (PLGA) exhibits hydrolytic sensitivity widely studied for controlled release applications.[34-36] The hydrolysis of the polymer chain liberates lactic and glycolic acid and thus proves autocatalytic under neutral or physiological conditions.[37] However, the literature lacks reports that include known cleavable groups into compositions for μSL to achieve 3D-printed objects with inherently designed degradable properties. While more attention lies with incorporating a functional monomers into the μSL process, continued progress in crosslinker synthesis will serve to further enhance the tunability of the resulting objects' properties.

This manuscript details for the first time the fabrication of three-dimensional networks that feature stimuli-labile linkages through μSL. Crosslinkers based on a tertiary alkyl diacrylate, tetrafluorophenyl-1,4-diacrylate, and PLGA-based urethane-containing dimethacrylate provided network structure with poly(ethylene glycol) methacrylate (PEGMA) reactive diluent. To the authors' best knowledge, this report is the first example of PLGA additive manufacturing with μSL. The present work further demonstrates the

degradation response of the 3D-printed objects, with implications for fields such as manufacturing and tissue engineering.

7.3 Experimental

7.3.1 Materials

Acryloyl chloride, triethylamine (TEA), pyridine, 2,5-dimethyl hexane-2,5-diol, tetrafluorohydroquinone (TFHQ), dimethoxyacetophenone (DMPA), phenylbis(2,4,6-trimethylbenzoyl)phosphine oxide (PPO) and poly(ethylene glycol) methacrylate (PEGMA, average molecular weight 500 g/mol) were purchased from Sigma Aldrich and used as received. Glycolide (≥ 99%) and D/L-lactide (98%) were purchased from Sigma Aldrich and dried *in vacuo* at 45 °C for several days prior to use. 2-isocyanatoethyl methacrylate (IEM) was purchased from TCI America and used as received. Dibutyltin dilaurate (DBTDL) and stannous ethylhexanoate ($Sn(Oct)_2$) were purchased from Sigma Aldrich and used as received. Polyethylene glycol (PEG, average molecular weight 400 g/mol) was received from Procter & Gamble and dried at 80 °C *in vacuo* prior to use. All solvents were purchased from Spectrum Chemical and used as received.

7.3.2 Analytical Methods

^{1}H and ^{19}F nuclear magnetic resonance spectroscopies were performed on an Agilent U4-DD2 spectrometer operating at 400 MHz and ambient temperature in $CDCl_3$ or D_2O. Thermogravimetric analysis (TGA) was performed on a TA Instruments Q500 operating at 10 °C/min temperature ramp under nitrogen atmosphere. Differential scanning calorimetry (DSC) was performed on a TA Instruments Q2000 operating under nitrogen atmosphere at a 10 10 °C/min heating rate. Transitions were determined on the second heat after a quench cool. Photocalorimetry experiments (PhotoDSC) were

performed at 25 °C on a TA Instruments Q1000 equipped with a TA Q Series PCA photoirradiation attachment operating over a spectral range of 250-650 nm at an intensity of 22 mW/cm^2 from an Omnicure S2000 UV source. Samples of mass 20 ± 2 mg and nominal thickness 2 mm were analyzed in an open pan under a nitrogen atmosphere.

Water sorption values were determined by thermogravimetric sorption analysis (TGASA) at 25 °C using a relative humidity (RH) stepwise ramp on a TA Instruments Q5000. Each sample was dried as part of the instrumental procedure at 0% RH at 25 °C until the sample weight equilibrated. The instrument increased RH in 5% increments and maintained each step until the sample weight exhibited < 0.01% change in weight for 10 min. The upper RH bound of the experiment was 95%. Water sorption was calculated based on the weight gain of sample.

7.3.3 Synthesis of acid-cleavable crosslinker

Synthesis of the acid-cleavable diacrylate crosslinker was adapted from previous literature procedure. 2,5-dimethyl hexane-2,5-diol (50.0 g, 0.342 mol), TEA (143 mL, 1.026 mol), and 400 mL DCM were charged to a clean, dry, 1 L, round-bottomed flask equipped with a magnetic stir bar and placed in an ice water bath. Acryloyl chloride (61.1 mL, 0.752 mol) was added dropwise over 90 min and the reaction was allowed to warm to room temperature and proceeded for 18 h. Triethylammonium chloride (TEACl) precipitate was collected by vacuum filtration. The filtrate was concentrated under rotary evaporation and filtered again to further remove TEACl. In a separatory funnel, the filtrate was washed twice with DI H_2O to remove TEACl and twice with aqueous NaOH (5% w/w) to neutralize and remove acrylic acid. Rotary evaporation to remove the remaining solvent afforded a dark yellow oil in 88% yield. ^{1}H NMR: δ (ppm) 6.15 (2H), 5.90 (2H), 5.60 (2H), 1.71 (4H), 1.34 (12H).

7.3.4 Synthesis of base-cleavable crosslinker

Synthesis of the base-cleavable diacrylate crosslinker was adapted from previous literature. TFHQ (5.0 g, 30 mmol), pyridine (4.8 mL, 60 mmol), and 100 mL DCM were charged to a clean, dry, 250 mL, round-bottomed flask equipped with a magnetic stir bar and placed in an ice water bath. Acryloyl chloride (5.5 mL, 65 mmol) was added dropwise over 90 min and the reaction was allowed to warm to room temperature and proceeded for 18 h. Pyridinium chloride precipitate was removed by vacuum filtration. The filtrate was concentrated under rotary evaporation and washed twice with 75 mL DI H_2O in a separatory funnel. The DCM phase was dried over Na_2SO_4 before the solvent was removed under rotary evaporation to afford colorless crystals in 68% yield. ^{1}H NMR: δ (ppm) 6.70 (2H), 6.35 (2H), 6.15 (2H). ^{19}F NMR: δ (ppm) -153.31

7.3.5 Synthesis of PLGA-based dimethacrylate

Synthesis of the hydrolytically unstable polyester diol was adapted from previous literature. Briefly, glycolide (4.46 g, 0.038 mol) and D/L-lactide (5.54 g, 0.038 mol) were added under nitrogen to a flame-dried, 50 mL, round-bottomed flask equipped with a magnetic stir bar. The flask was immersed in an oil bath thermostated to 130 °C and the monomers were allowed to melt completely. The temperature was reduced to 120 °C, and PEG (10.00 g, 0.025 mol) and $Sn(Oct)_2$ catalyst (1 wt% in toluene, 200 ppm) was added by syringe under nitrogen. The reaction was allowed to proceed for 24 h, upon which time the flask was removed from heat. The product was dissolved in chloroform and washed repeatedly with a 9:1 mixture by volume of hexanes and methanol. Chloroform was removed under rotary evaporation and the resulting viscous liquid was dried to constant weight *in vacuo* at 70 °C. The PLGA-based diol (9.5 g, 0.11 mol) was then added under

nitrogen to a 50 mL, two-neck round-bottomed flask equipped with magnetic stirring and a water condenser. DBTDL (1 wt% in $CHCl_3$, 100 ppm) was added by syringe, along with IEM (4.0 mL, 0.28 mol). The reaction flask was then immersed in an oil bath thermostated to 40 °C and the reaction proceeded for 12 h. The product was washed twice with hexanes, and dried under rotary evaporation, yielding difunctional PLGA-based urethane methacrylate (PLGA-UM) as a clear, viscous liquid in 97% yield. ^{1}H NMR: δ (ppm) 6.12 (2H), 5.60 (2H), 5.22 (2H), 4.73 (6H), 4.32 (2.3 H), 4.23 (4H), 3.70 (4H), 3.64 (32 H), 3.51 (4H), 1.95 (6H), 1.54 (7.7 H).

7.3.6 Additive manufacturing

An Autodesk Ember 3D desktop printer and accompanying Print Studio CAD software was used to design and print the desired parts containing the acid-cleavable or base cleavable crosslinkers. During the print process, a LED ultraviolet light source with emission wavelength of 405 nm and intensity of 20 mW/cm^2 was emitted to pass through a series of conditioning optics to ensure efficient and even distribution of light projected onto the photopolymer resin. Subsequently, UV light reflected off an array of mirrors through a digital micro-mirror device (DMD) located below and in parallel with the resin vat, which digitally patterned two-dimensional sliced layers transmitted from the three-dimensional file designed by the CAD software. The DMD was a DLP® 0.45" WXGA with a microarray size of 912 x 1140 with mirrors spaced 7.6 microns apart.

For PEGMA-based cubic lattices with 1 mol% acid-labile or base-labile crosslinker printed with 2 wt% PPO photoinitiator, the pattern then passed through a set of imaging optics before projection onto the resin vat's optical window where photopolymer resin was selectively cured into crosslinked layers for 15 s each with a layer thickness set to 250 μm.

After curing of each layer onto the build platform, the resin vat rotated 60 degrees away from the optical window at a rate of 1 rpm to allow recoat before the curing of the next layer. This layer-by-layer process was repeated until the completion of the part, upon which the part was immersed in isopropyl alcohol to remove any residual uncured monomer. For a PEGMA-based colosseum with 45 mol% acid-labile crosslinker, the layer cure time was 30 s, with a cure depth of 100 μm initiated by 1 wt% PPO. 0.025 wt% avobenzone was incorporated as a UV blocker to improve resolution.

Parts containing PLGA-UM and PEGMA were fabricated using a custom-built mask projection μSL machine consisting of a UV light source, conditioning optics, a mirror, a dynamic mask connected to a computer, imaging optics, and a resin container with a stage mounted on a linear actuator as previously described.[19-20] Briefly, a LightningCure LC-L1V3 UV LED system by Hamamatsu was chosen as a source of ultraviolet light. The conditioning optics (Edmund Optics) ensured that the entire dynamic mask was illuminated by UV light while the imaging optics focus the patterned light onto the resin surface and reduce the image dimensions by a factor of two. The dynamic mask, consists of a DLP 0.65 1080p DMD from Texas. The DMD is a 1920 x 1080 array of aluminum micromirrors that measures 0.65-inch along the diagonal. Each square micromirror has a side length of 7.56 μm. The imaging optics reduce the image dimensions by a factor of 2 so the effective projection area of each micromirror on the surface of the photopolymer surface is 3.78 μm x 3.78 μm. Due to the optics of the system, the maximum part size in the XY plane is 4 mm by 6 mm. The maximum dimension in the Z direction is 36mm. A linear actuator (Zaber NA11B60) was used to control the movement of a custom stage fabricated using fused deposition modeling.

For resins containing PLGA-UM, PEGMA, 2 wt% DMPA and 0.05 wt% avobenzone, 100 μm layers were exposed for 5.5 seconds at an exposure of 7.5 mW/cm^2. Between layers, the build stage was dipped 3 mm below the resin surface for a duration of 3 seconds and after the stage was raised to the build location for the subsequent layer, the resin was allow to settle for 6 seconds. Scaffolds up to 8 mm tall were fabricated. After printing, the parts were removed from the build platform using a razor blade and excess resin was carefully blotted off. The parts were then cleaned by sonication in isopropanol. The parts were subsequently post-cured by irradiating them with a handheld UV lamp.

7.4 Results and Discussion

7.4.1 Synthesis of the crosslinkers for the networks

Straightforward synthetic routes yielded three various degradable crosslinkers (**Figure 7.1**) Acryloyl chloride readily imparted photocurable functionality to 2,5-dimethylhexane-2,5-diol and to tetrafluorohydroquinone (TFHQ). The reaction proceeded readily under common conditions utilizing dichloromethane solvent and an amine to scavenge liberated HCl. In the case of the acid-labile tertiary alkyl diacrylate (compound A), the reaction provided a high yield. The synthetic strategy for the TFHQ diacrylate (compound B) resulted in similar yields compared to previous literature, but lower relative to the acid-labile crosslinker. This likely resulted from excess pyridine partially degrading the product.[31] The final crosslinker investigated in the present study featured hydrolyzable ester linkages and urethane methacrylate endgroups. Difunctional PEG 400 initiated ring opening polymerization (**Scheme 7.1**) of an equimolar mixture of D/L-lactide and glycolide with $Sn(Oct)_2$, a composition which suppresses crystallinity.[35] The PEG-initiated, PLGA-based diol then readily reacted with 2-isocyanatoethyl methacrylate to

provide photocurable end-functionality (PLGA-UM). ^{1}H NMR indicated the molecular weight of PLGA-UM to be 1180 g mol^{-1}, with n = 3.6 on average.

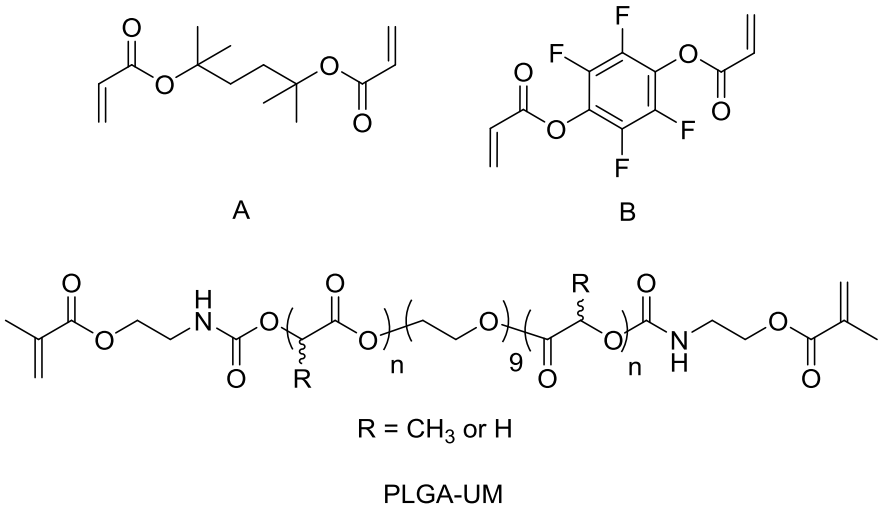

Figure 7.1. Structures of acid-labile crosslinker (A); base-labile crosslinker (B); and PEG-based, PLGA-containing crosslinker (PLGA-UM).

7.4.2 Photocalorimetry of acid-labile networks

Photocalorimetry investigated resin compositions with varying extent of photoinitiator (DMPA) or acid-labile crosslinker incorporation. The thermograms (**Figure 7.2**) revealed differences in curing behavior of resin compositions. In all cases, the irradiation source turned on after 1 min, leading to an immediate and significant exotherm that resulted from curing of acrylate or methacrylate polymerization. The exotherm signal then decreased and decayed to a flat baseline, indicating that no further polymerization occurred. The trial continued for a minimum of 2 min after reaching this baseline. The baseline after the photocuring experiment did not return to 0 W/g heat flow due heat generated from the irradiation source. Varying the amount of crosslinker at a constant

photoinitiator concentration (**Figure 7.2A**) led to slight changes in the breadth of the exotherm peak as well as initial slope. Varying the photoinitiator content of the resin mixture also affected the polymerization response to UV. A resin mixture of 99 mol% PEGMA with 1 mol% A and 3 wt% DMPA demonstrated an exotherm with a faster initial slope and narrower peak breadth than the same resin composition with 2 wt% DMPA (**Figure 7.2B**). In all cases investigated, the exotherm peaked within a minute of UV exposure, indicating suitability for a layer-by-layer curing process with reasonable print times.

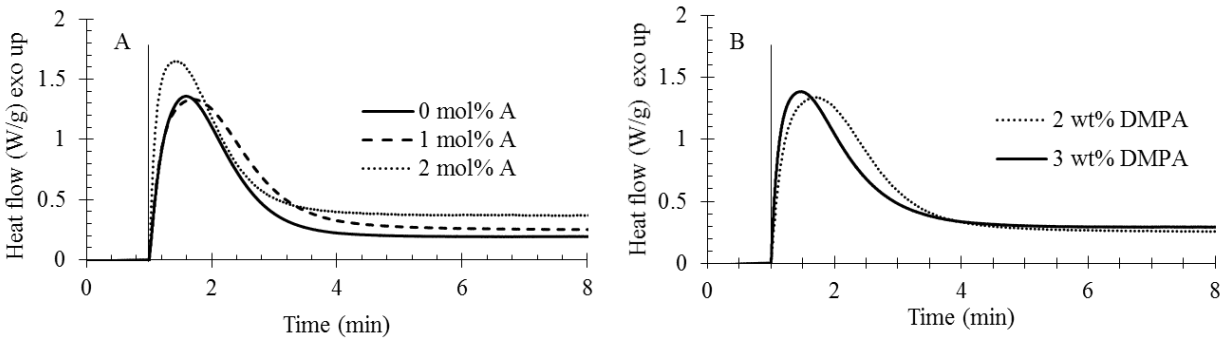

Figure 7.2. Photocalorimetry traces of (A) PEGMA with various mol% incorporation of A using 2 wt% DMPA and (B) PEGMA with 1 mol% A with varied photoinitiator concentration. Vertical lines at time = 1 min correspond to start of irradiation.

7.4.3 Additive manufacturing

µSL readily fabricated hydrogels through layer-by-layer UV irradiation of PEGMA-based mixtures with incorporated crosslinker (**Scheme 7.2**). This process enabled printing of parts that featured 1 or 45 mol% A, 1 mol% of B, or 10 or 30 mol% PLGA-UM with PEGMA as a reactive diluent to qualitatively tailor resin viscosity and mechanical

robustness of the parts. SEM images (**Figure 7.3**) of the parts that contain 1 mol% A or B revealed their resolution. Both cubic lattices demonstrated cure-through as a result of the depth of penetration of the UV irradiation. Resins with relatively low amounts of incorporated crosslinker required longer exposure times per layer to produce an object that could support its own weight during the printing process, which resulted in cure-through and reduced the resolution of the obtained part relative to the desired part (**Figure 7.3C**)

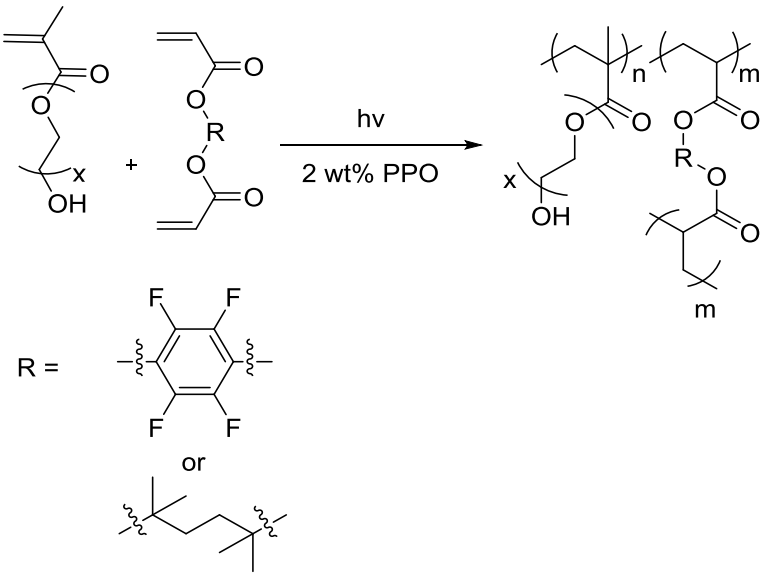

Scheme 7.2. µSL photocuring of PEGMA with cleavable diacrylate crosslinkers.

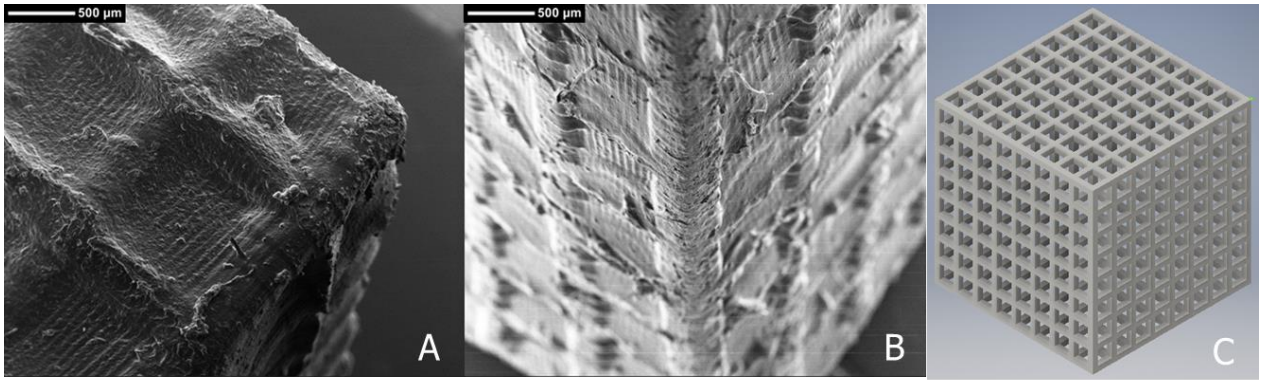

Figure 7.3. SEM images of 1 cm^3 cubic lattices of PEGMA printed with (A) 1 mol% acid-labile crosslinker or (B) 1 mol% base-labile crosslinker. Also provided is an image (C) of the CAD model used for the printing process.

Increasing the amount of acid-labile crosslinker from 1 mol% to 45 mol% enabled printing of a colosseum with better resolution (**Figure 7.4**). The greater crosslink density in the resulting network imparted more robust mechanical properties to the network layers, which minimized object damage from the shearing step of the printing process. The incorporation of 0.025 wt% avobenzone as a UV absorber also afforded good resolution of the part with 100 μm layer thickness (**Figure 7.4B**).

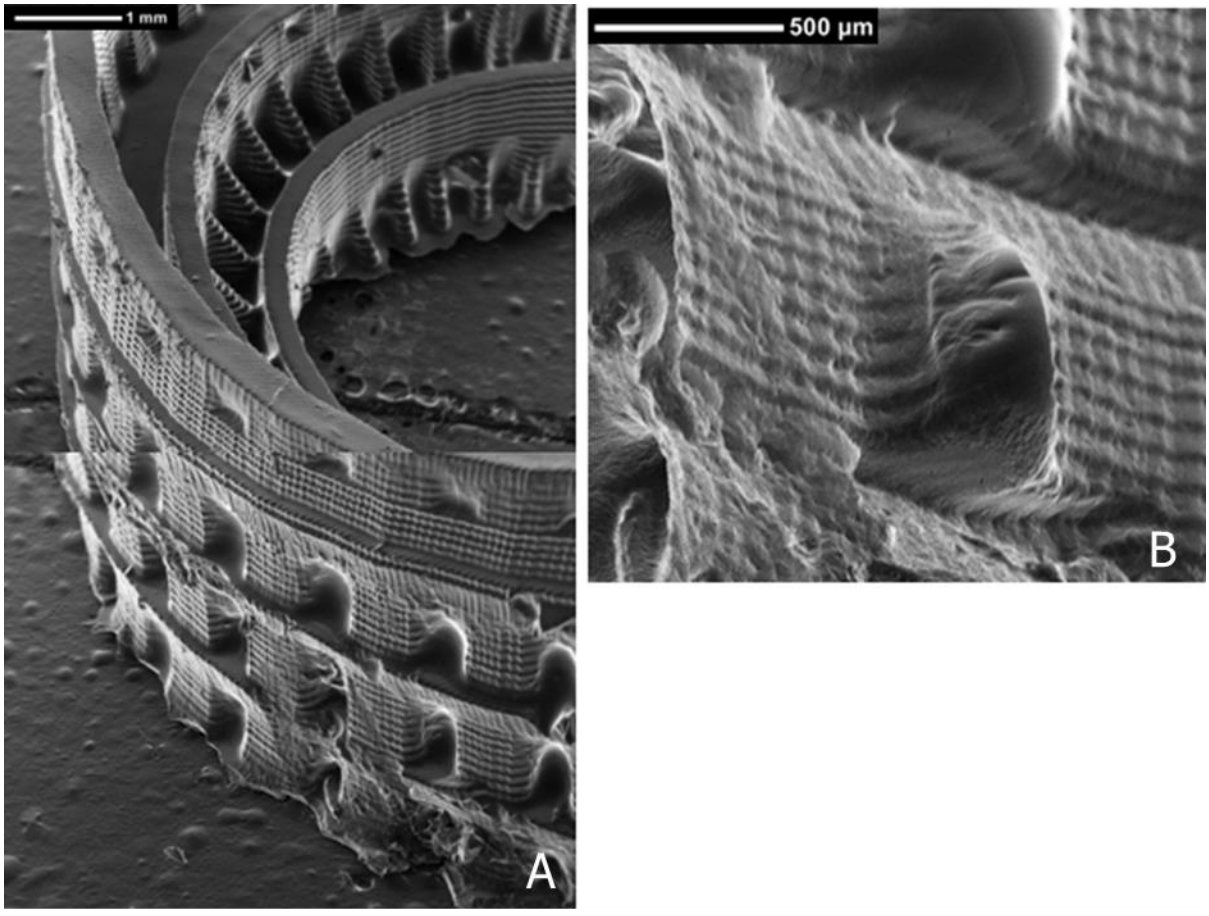

Figure 7.4. SEM images of a colosseum printed with 45 mol% acid-labile crosslinker with PEGMA in the presence of 0.025 wt% avobenzone.

Printing a mixture of PLGA-UM and PEGMA using 2 wt% DMPA also afforded parts (**Scheme 7.3**). Pure PLGA-UM resin exhibited a viscosity high enough to prohibit effective printing using μSL. Thus, PEGMA served to tune resin viscosity as a reactive monofunctional diluent. When the PEGMA resin contained 30 mol% PLGA-UM, printing a cubic lattice (**Figure 7.5A-B**) yielded a structure that exhibited good resolution in each layer but significant cure-through between layers. Further decreasing the amount of PLGA-UM to 10 mol% in the PEGMA resin served minimize layer cure-through (**Figure 7.5C-D**). This permitted printing of a lattice structure with rectangular windows that remained well-defined relative to those obtained from the composition with 30 mol% crosslinker.

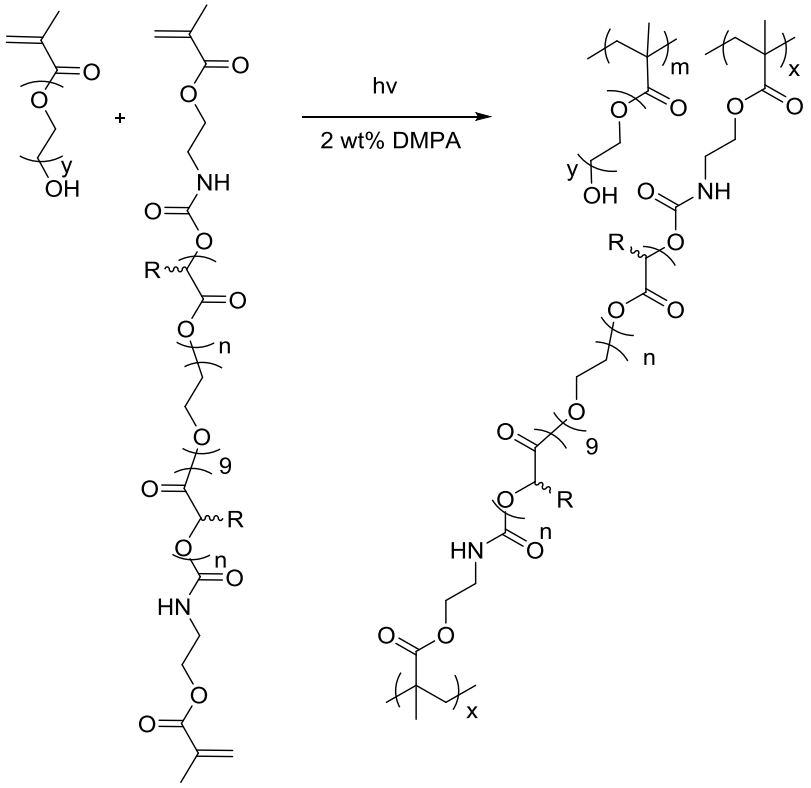

Scheme 7.3. μSL photocuring of PLGA-UM with PEGMA.

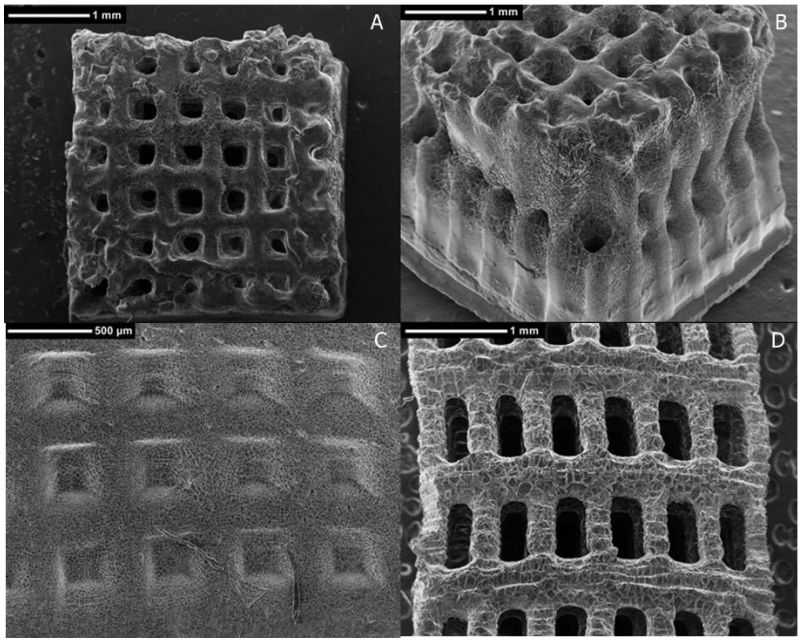

Figure 7.5. SEM images of cubic lattices printed from a mixture of (A-B) 30 mol% or (C-D) 10 mol% PLGA-UM with PEGMA. Images A and C are of the object in the X,Y-print direction, while images B and D show object resolution in the Z direction.

7.5.4 Thermal properties and water uptake

TGA investigated the thermal properties of the 3D printed parts (**Figure 7.6**). The temperature at which the sample lost 5% of its mass was deemed the degradation temperature ($T_{d,5\%}$). Because all the parts printed included PEGMA, the differences in degradation profile resulted from the relative amounts and the chemical structure of the crosslinker. Parts containing the acid-labile crosslinker demonstrated an overall greater thermal stability than parts containing the base-cleavable crosslinker or PLGA-UM (**Table 7.1**). The $T_{d,5\%}$ for parts containing the acid cleavable crosslinker decreased upon greater

incorporation of the crosslinker, due to the known thermal decomposition of tertiary alkyl esters.[38]

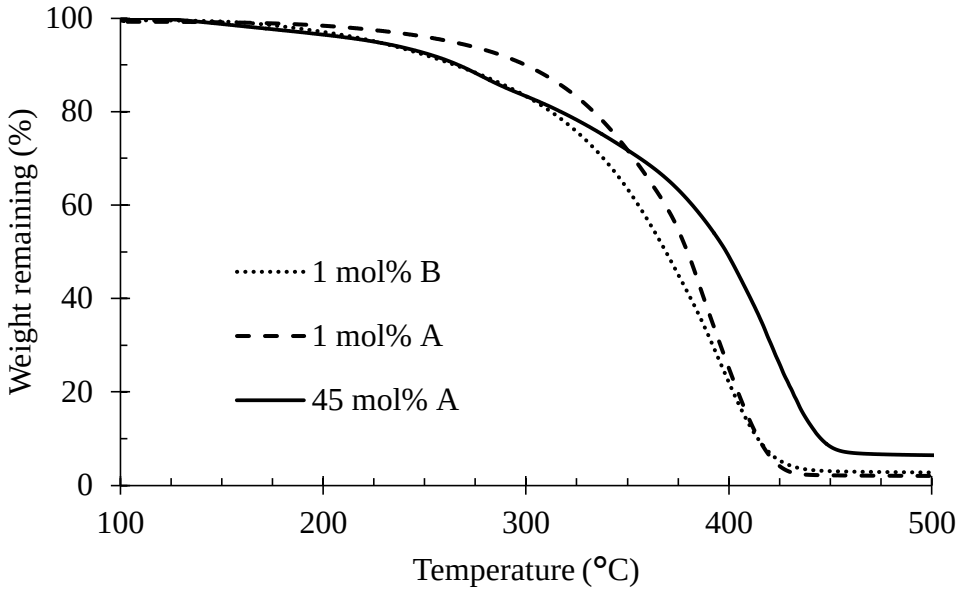

Figure 7.6. TGA weight loss profiles of 3D-printed objects containing PEGMA and a synthesized, degradable crosslinker.

DSC (**Figure 7.7**) further investigated the thermal properties of the PEGMA-based printed parts. The PEG side-chains of PEGMA prove crystallizable at appropriate temperatures. The samples each exhibit crystallization exotherms and melting endotherms in the second heating steps. The glass transition temperature (T_g) remained consistent (**Table 7.1**) near -60 °C. The qualitatively soft nature of the obtained parts proved consistent with T_m and T_g values below room temperature.

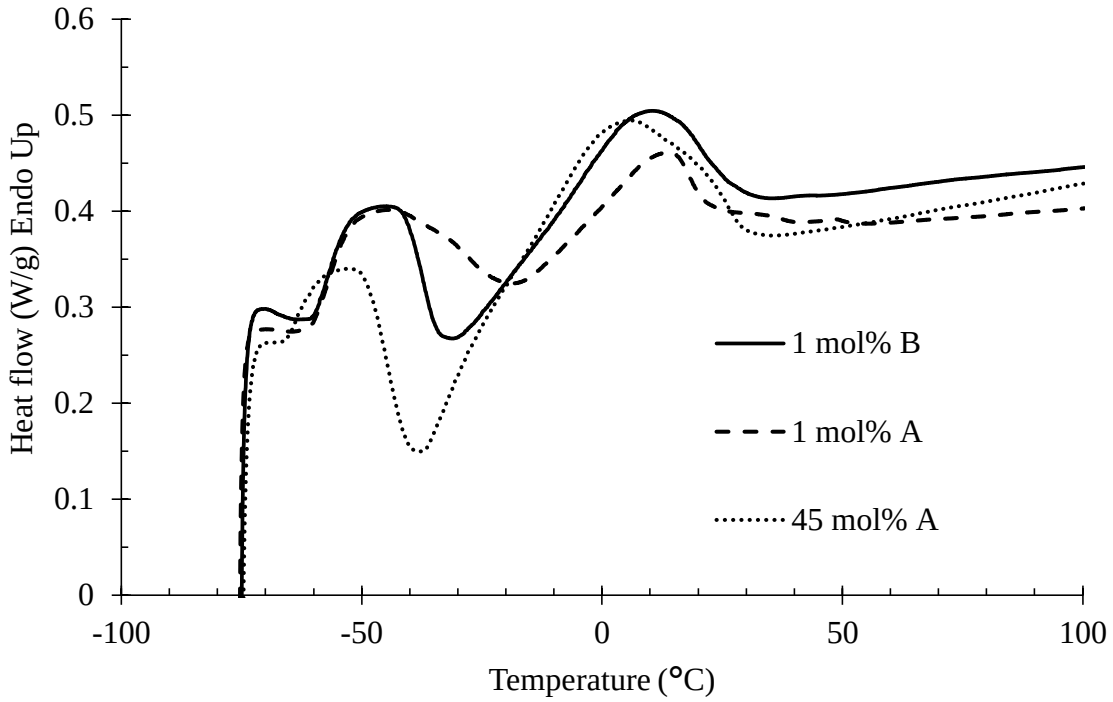

Figure 7.7. DSC thermograms of parts 3D-printed from PEGMA and a synthesized cleavable crosslinker.

Table 7.1. Thermal properties of investigated 3D-printed parts and photocured networks.[a]

Sample	$T_{d,5\%}$ (°C)	T_g (°C)	T_c (°C)	T_m (°C)	Weight gain at 95 % RH (%)	Dissolution time (d)
1 mol% B in PEGMA	224	-57	-32	10	57	ND
1 mol% A in PEGMA	264	-57	-18	13	57	0.25
45 mol% A in PEGMA	224	-60	-38	4	46	16
10 mol% PLGA-UM in PEGMA	222	-60	-38	0	53	1
30 mol% PLGA-UM in PEGMA	223	-32	ND	ND	34	1
PLGA-UM	211	-5	ND	ND	7	20

[a] ND = not determined

DSC also compared the properties of PEGMA-based, PLGA-UM-containing 3D-printed parts with those of a photocured network comprised of pure PLGA-UM. The photocured film of PLGA-UM exhibited a T_g at -5 °C. DSC revealed no T_m or T_c from either PEG or PLGA crystallites. This observation proved consistent with the low molecular weight of the PLGA repeating segments, as well as the lactide and glycolide composition chosen to suppress crystallinity.[35] Similarly, the 9 average repeat units present in the PEG 400 portion of the PLGA-UM proved too low to form crystallites. The PEGMA-containing part with 30 mol% PLGA-UM similarly exhibited no crystallization exotherm or melting endotherm in the DSC thermogram (**Figure 7.8**). The T_g occurred at -32 °C, which agreed well with the Fox equation value of -31 °C predicted for the 50:50 wt% composition of PEGMA and PLGA-UM. Further decreasing the PLGA-UM content to 10 mol% caused the T_g to reduce to -60 °C. The network exhibited crystallizability, with an observed T_c at -38 °C and observed T_m at 0 °C. These transitions correlated well with those observed for the PEGMA-based networks discussed above.

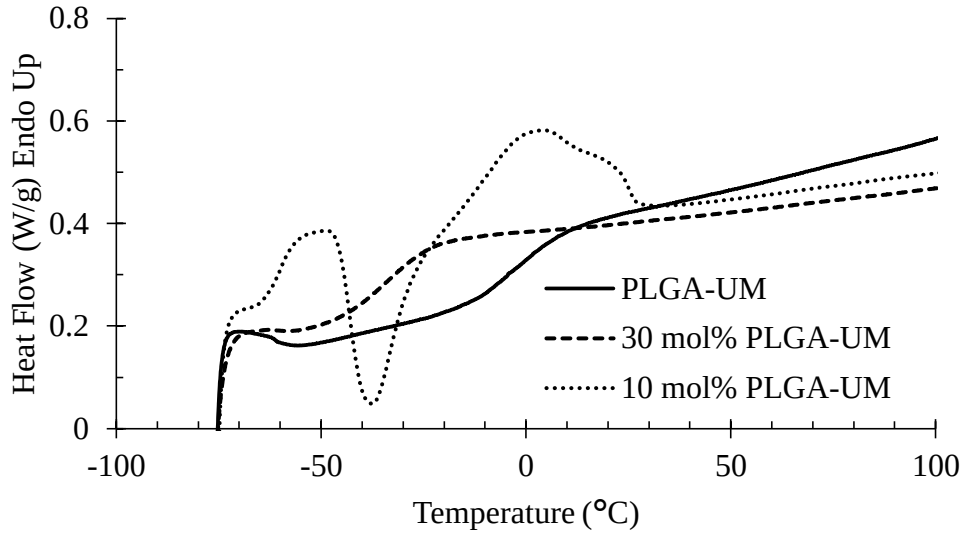

Figure 7.8. DSC thermograms of crosslinked PLGA-UM and a network containing 30 mol% PLGA-UM and 70 mol% PEGMA.

Thermogravimetric sorption analysis (TGASA) probed the water uptake of the networks at constant 25 °C with increasing RH (**Figure 7.9**). The samples all exhibited exponentially increasing water uptake at higher relative humidity. Objects fabricated from μSL with 99 mol% PEGMA demonstrated nearly 57% weight gain at 95% RH, regardless of whether the crosslinker contained the acid-labile alkyl linker or the base-cleavable tetrafluorophenyl linker. This further supported the hypothesis that at low amounts of crosslinker content, the resulting object displayed thermal and uptake properties similar to the PEGMA homopolymer. As the amount of A increased to 45 mol%, the water uptake decreased to 46 wt%, owing to the increased crosslink density and more hydrophobic nature of the network with higher content of A.

The network photocured from 100 mol% PLGA-UM exhibited only roughly 7% weight gain at 95% RH, likely due to the higher crosslink density of the network. When PLGA-UM content decreased from 100 to 30 mol% and then to 10 mol%, the equilibrium weight gain from water uptake increased to 33.7 wt% and 52.9 wt%, respectively. This probably resulted from the increased hydrophilicity of the networks on account of having increased PEGMA content. As PEGMA content decreased, water sorption decreased in all cases evaluated.

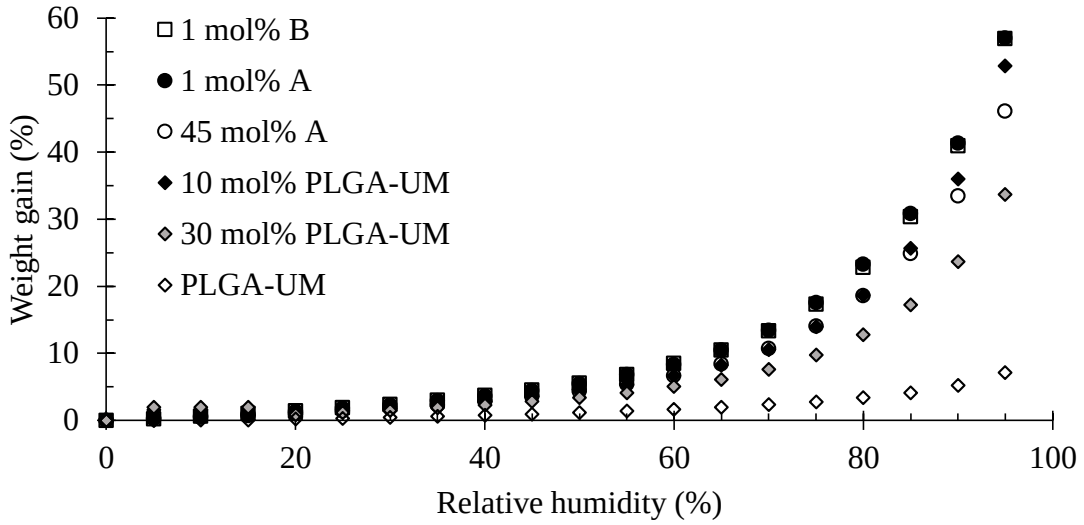

Figure 7.9. Sorption isotherms at 25 °C revealed water uptake of the networks.

7.4.4 Part degradation

Immersion of 3D-printed parts that featured incorporated base-cleavable crosslinker in *n*-butyl amine or aqueous 10 M KOH investigated the degradability of the parts. Soaking the network in *n*-butyl amine caused no noticeable degradation over a time period of two weeks, in contrast to similar gels investigated in the literature previously that degraded within minutes.[31] Employing 10 M KOH as a strong base solution did not dissolve the network. Increasing temperature to 70 °C and allowing the solution to stir for 12 h caused a visible change in the appearance of the 3D-printed lattice structure (**Figure 7.10**). However, the part remained intact.

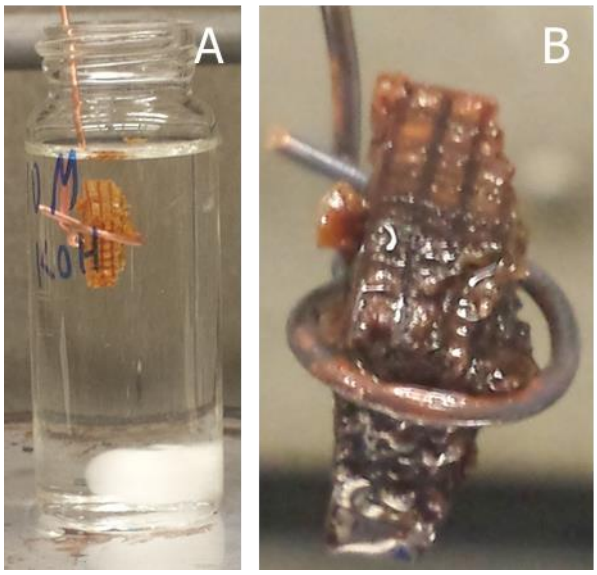

Figure 7.10. PEGMA-based network with 1 mol% B (A) immediately upon immersion in 10 M aqueous KOH at 70 °C and (B) after 12 h.

While incorporation of B did not impart alkine-cleavability to the 3D-printed objects, objects containing A proved readily degradable. A PEGMA-based cubic lattice containing 1 mol% A dissolved fully in concentrated HCl at room temperature. The part exhibited significant and visible degradation after 30 minutes, and was fully degraded at 6 h (**Figure 7.11**). Increasing the amount of crosslinker present in the 3D-printed object to 45 mol% further increased the time to complete degradation of the part to 16 d.

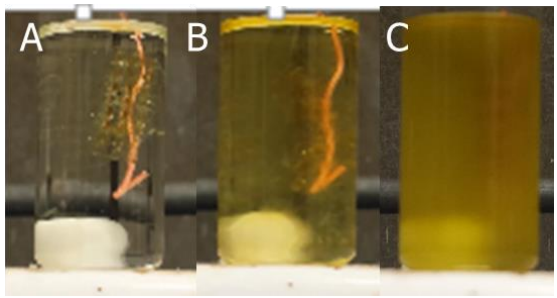

Figure 7.11. Degradation of a 3D-printed lattice structure that contained 1 mol% A (A) immediately upon, (B) 30 min after, and (C) 6 h after immersion in concentrated HCl.

Immersion of the PLGA-UM-containing 3D-printed networks in concentrated HCl demonstrated the cleavability of the crosslinker PLGA segments. Parts that featured 30 mol% or 10 mol% PLGA-UM degraded fully within 24 hours of immersion (**Figure 7.12**). The observed yellow color exhibited for the part with 10 mol% PLGA-UM after degradation likely resulted from the higher content of PEGMA, which has a yellow color, in the network (**Figure 7.12B**). The network with no PEGMA required a significantly longer time (20 d) to fully degrade. This likely resulted from the drastically higher crosslink density and markedly reduced water uptake of the network.

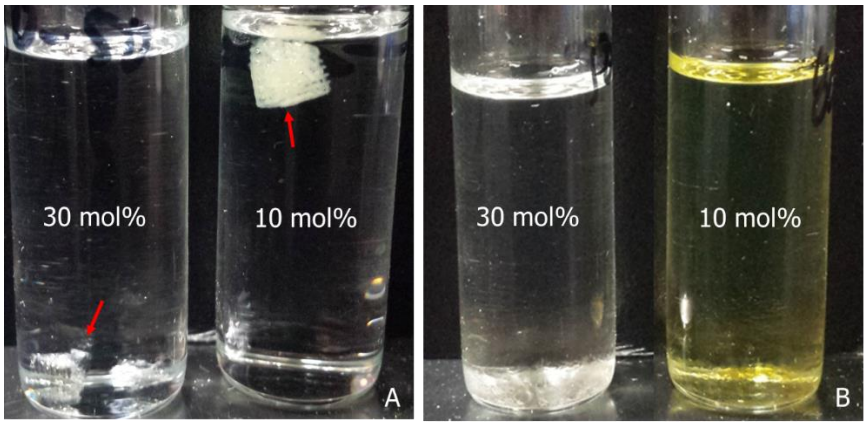

Figure 7.12. 3D-printed lattice structures (A) immediately upon and (B) 24 h after immersion in concentrated HCl.

7.5 Conclusions

Previous literature established precedence for difunctional, cleavable compounds to serve as crosslinking agents in polymer networks. For the first time, the present work extended these networks into three dimensions using µSL to 3D-print degradable objects. Tertiary alkyl esters, fluorinated phenyl esters, or hydrolyzable PLGA esters imparted inherent stimuli response into the 3D-printed objects, the first time that PLGA was printed using µSL. Thermal characterization and water sorption analysis enabled construction of

structure-property relationships of the objects. Exposure to strong acid resulted in complete degradation and dissolution of the 3D-printed parts that featured the tertiary alkyl esters or PLGA esters, representing the first example of chemically-degradable 3D-printed networks.

7.6 Acknowledgments

The authors acknowledge Procter & Gamble for material and financial support, the Macromolecular Materials Discovery Center at Virginia Tech for instrument support, and Miss Mariam Badawi for TGASA instrumentation support.

7.7 References

1. Gökçeören, A. T.; Şenkal, B. F.; Erbil, C., Effect of crosslinker structure and crosslinker/monomer ratio on network parameters and thermodynamic properties of Poly (N-isopropylacrylamide) hydrogels. *Journal of Polymer Research* **2014,** *21* (3), 1-12.
2. Dragan, E. S., Design and applications of interpenetrating polymer network hydrogels. A review. *Chemical Engineering Journal* **2014,** *243*, 572-590.
3. Long, T. E., Toward Recyclable Thermosets. *Science* **2014,** *344* (6185), 706-707.
4. *Structural Adhesives: Chemistry and Technology*. Springer US: 1986.
5. Davis, K. A.; Anseth, K. S., Controlled Release from Crosslinked Degradable Networks. **2002,** *19* (4-5), 39.
6. Buwalda, S. J.; Boere, K. W. M.; Dijkstra, P. J.; Feijen, J.; Vermonden, T.; Hennink, W. E., Hydrogels in a historical perspective: From simple networks to smart materials. *Journal of Controlled Release* **2014,** *190*, 254-273.
7. Uhrich, K. E.; Cannizzaro, S. M.; Langer, R. S.; Shakesheff, K. M., Polymeric Systems for Controlled Drug Release. *Chemical Reviews* **1999,** *99* (11), 3181-3198.
8. Campos, L. M. d. P.; Boaro, L. C.; Ferreira, H. P.; dos Santos, L. K. G.; dos Santos, T. R.; Parra, D. F., Evaluation of polymerization shrinkage in dental restorative experimental composites based: BisGMA/TEGDMA, filled with MMT. *Journal of Applied Polymer Science* **2016,** *133* (24), n/a-n/a.
9. Tanver, A.; Huang, M.-H.; Luo, Y.; Khalid, S.; Hussain, T., Energetic interpenetrating polymer network based on orthogonal azido-alkyne click and polyurethane for potential solid propellant. *RSC Advances* **2015,** *5* (79), 64478-64485.
10. Bonner, D. K.; Zhao, X.; Buss, H.; Langer, R.; Hammond, P. T., Crosslinked linear polyethylenimine enhances delivery of DNA to the cytoplasm. *Journal of Controlled Release* **2013,** *167* (1), 101-107.
11. Han, S.-C.; He, W.-D.; Li, J.; Li, L.-Y.; Sun, X.-L.; Zhang, B.-Y.; Pan, T.-T., Reducible polyethylenimine hydrogels with disulfide crosslinkers prepared by

michael addition chemistry as drug delivery carriers: Synthesis, properties, and in vitro release. *Journal of Polymer Science Part A: Polymer Chemistry* **2009,** *47* (16), 4074-4082.
12. Zhou, C.; Deng, L.; Yao, F.; Xu, L.; Zhou, J.; Fu, G. D., A Well-Defined Amphiphilic Polymer Conetwork from Sequence Control of the Cross-Linking in Polymer Chains. *Industrial & Engineering Chemistry Research* **2014,** *53* (49), 19239-19248.
13. Mather, B. D.; Williams, S. R.; Long, T. E., Synthesis of an Acid-Labile Diacrylate Crosslinker for Cleavable Michael Addition Networks. *Macromolecular Chemistry and Physics* **2007,** *208* (18), 1949-1955.
14. Halpern, J. M.; Urbanski, R.; Weinstock, A. K.; Iwig, D. F.; Mathers, R. T.; von Recum, H. A., A biodegradable thermoset polymer made by esterification of citric acid and glycerol. *Journal of Biomedical Materials Research Part A* **2014,** *102* (5), 1467-1477.
15. Schmidt, C.; Scherzer, T., Monitoring of the shrinkage during the photopolymerization of acrylates using hyphenated photorheometry/near-infrared spectroscopy. *Journal of Polymer Science Part B: Polymer Physics* **2015,** *53* (10), 729-739.
16. Karikari, A. S.; Edwards, W. F.; Mecham, J. B.; Long, T. E., Influence of Peripheral Hydrogen Bonding on the Mechanical Properties of Photo-Cross-Linked Star-Shaped Poly(d,l-lactide) Networks. *Biomacromolecules* **2005,** *6* (5), 2866-2874.
17. Bertsch, A.; Lorenz, H.; Renaud, P., 3D microfabrication by combining microstereolithography and thick resist UV lithography. *Sensors and Actuators A: Physical* **1999,** *73* (1–2), 14-23.
18. Bertsch, A.; Zissi, S.; Jézéquel, Y. J.; Corbel, S.; André, C. J., Microstereophotolithography using a liquid crystal display as dynamic mask-generator. *Microsystem Technologies 3* (2), 42-47.
19. Sirrine, J. M.; Pekkanen, A. M.; Nelson, A. M.; Chartrain, N. A.; Williams, C. B.; Long, T. E., 3D-Printable Biodegradable Polyester Tissue Scaffolds for Cell Adhesion. *Australian Journal of Chemistry* **2015,** *68* (9), 1409-1414.
20. Schultz, A. R.; Lambert, P. M.; Chartrain, N. A.; Ruohoniemi, D. M.; Zhang, Z.; Jangu, C.; Zhang, M.; Williams, C. B.; Long, T. E., 3D Printing Phosphonium Ionic Liquid Networks with Mask Projection Microstereolithography. *ACS Macro Letters* **2014,** *3* (11), 1205-1209.
21. Sood, N.; Bhardwaj, A.; Mehta, S.; Mehta, A., Stimuli-responsive hydrogels in drug delivery and tissue engineering. *Drug delivery* **2016,** *23* (3), 1-23.
22. Gillies, E. R.; Fréchet, J. M. J., pH-Responsive Copolymer Assemblies for Controlled Release of Doxorubicin. *Bioconjugate Chemistry* **2005,** *16* (2), 361-368.
23. Gillies, E. R.; Goodwin, A. P.; Fréchet, J. M. J., Acetals as pH-Sensitive Linkages for Drug Delivery. *Bioconjugate Chemistry* **2004,** *15* (6), 1254-1263.
24. Kwon, Y. J.; Standley, S. M.; Goodwin, A. P.; Gillies, E. R.; Fréchet, J. M. J., Directed Antigen Presentation Using Polymeric Microparticulate Carriers Degradable at Lysosomal pH for Controlled Immune Responses. *Molecular Pharmaceutics* **2005,** *2* (1), 83-91.

25. Murthy, N.; Thng, Y. X.; Schuck, S.; Xu, M. C.; Fréchet, J. M. J., A Novel Strategy for Encapsulation and Release of Proteins: Hydrogels and Microgels with Acid-Labile Acetal Cross-Linkers. *Journal of the American Chemical Society* **2002,** *124* (42), 12398-12399.
26. Bilalis, P.; Varlas, S.; Kiafa, A.; Velentzas, A.; Stravopodis, D.; Iatrou, H., Preparation of hybrid triple-stimuli responsive nanogels based on poly(L-histidine). *Journal of Polymer Science Part A: Polymer Chemistry* **2015**, n/a-n/a.
27. Bal, A.; Özkahraman, B.; Özbaş, Z., Preparation and characterization of pH responsive poly(methacrylic acid-acrylamide-N-hydroxyethyl acrylamide) hydrogels for drug delivery systems. *Journal of Applied Polymer Science* **2016,** *133* (13), n/a-n/a.
28. García, J. M.; Jones, G. O.; Virwani, K.; McCloskey, B. D.; Boday, D. J.; ter Huurne, G. M.; Horn, H. W.; Coady, D. J.; Bintaleb, A. M.; Alabdulrahman, A. M. S.; Alsewailem, F.; Almegren, H. A. A.; Hedrick, J. L., Recyclable, Strong Thermosets and Organogels via Paraformaldehyde Condensation with Diamines. *Science* **2014,** *344* (6185), 732-735.
29. Kilian, L.; Wang, Z.-H.; Long, T. E., Synthesis and cleavage of core-labile poly(alkyl methacrylate) star polymers. *Journal of Polymer Science Part A: Polymer Chemistry* **2003,** *41* (19), 3083-3093.
30. Palmieri, F.; Adams, J.; Long, B.; Heath, W.; Tsiartas, P.; Willson, C. G., Design of Reversible Cross-Linkers for Step and Flash Imprint Lithography Imprint Resists. *ACS Nano* **2007,** *1* (4), 307-312.
31. Metz, N.; Theato, P., Synthesis and Characterization of Base Labile Poly(N-isopropylacrylamide) Networks Utilizing a Reactive Cross-Linker. *Macromolecules* **2009,** *42* (1), 37-39.
32. Son, H.; Jang, Y.; Koo, J.; Lee, J.-S.; Theato, P.; Char, K., Penetration and exchange kinetics of primary alkyl amines applied to reactive poly(pentafluorophenyl acrylate) thin films. *Polym J* **2016,** *48* (4), 487-495.
33. Eberhardt, M.; Théato, P., RAFT Polymerization of Pentafluorophenyl Methacrylate: Preparation of Reactive Linear Diblock Copolymers. *Macromolecular Rapid Communications* **2005,** *26* (18), 1488-1493.
34. Tan, H. Y.; Widjaja, E.; Boey, F.; Loo, S. C. J., Spectroscopy techniques for analyzing the hydrolysis of PLGA and PLLA. *Journal of Biomedical Materials Research Part B: Applied Biomaterials* **2009,** *91B* (1), 433-440.
35. Gilding, D. K.; Reed, A. M., Biodegradable polymers for use in surgery—polyglycolic/poly(actic acid) homo- and copolymers: 1. *Polymer* **1979,** *20* (12), 1459-1464.
36. John, G.; Morita, M., Synthesis and Characterization of Photo-Cross-Linked Networks Based on l-Lactide/Serine Copolymers. *Macromolecules* **1999,** *32* (6), 1853-1858.
37. Tsuji, H., Autocatalytic hydrolysis of amorphous-made polylactides: effects of l-lactide content, tacticity, and enantiomeric polymer blending. *Polymer* **2002,** *43* (6), 1789-1796.
38. Rudy, C. E.; Fugassi, P., The Thermal Decomposition of Tertiary Butyl Acetate. *J. Phys. Colloid Chem.* **1948,** *52* (2), 357-363.

Chapter 8: Photocured Poly(Vinyl Alcohol)-Based Hydrogels

(*In preparation* for submission)

Evan Margaretta, Justin M. Sirrine, Charles S. Carfagna, Jr., Timothy E. Long*

Department of Chemistry, Macromolecules Innovation Institute
Virginia Tech, Blacksburg, VA, 24061

*To whom correspondence should be addressed
E-mail: telong@vt.edu
TEL: (540) 231-2480
FAX: (540) 231-8517

Keywords: hydrogels, photorheology, poly(vinyl alcohol)

8.1 Abstract

Acid-catalyzed transacetalization of an acrylamide dimethylacetal compound with the hydroxyls of poly(vinyl alcohol) (PVOH) afforded PVOH with varied amounts of photocurable pendant acrylamide groups. Photocuring revealed the influence of acrylamide concentration, solvent presence, and photoinitiator presence on curing efficiency, as examined using Soxhlet extractions. Addition of poly(ethylene glycol) diacrylate (PEGDA) served to increase the concentration of curable functionality in the solution. Photocalorimetry and photorheology tracked the curing process and revealed the effects of increasing PEGDA content as well as the complex dynamics of the process.

8.2 Introduction

Polymer networks demonstrate a range of properties widely applicable for many applications. Networks that swell in water, or hydrogels, prove useful in areas such as separations, as cell scaffolding, or for controlled release.[1-4] Because of their immense design versatility, hydrogels prove attractive additions to the synthetic toolkit for researchers attempting to solve a variety of problems.[5] Parameters such as crosslink

density, porosity, and hydrophobicity or hydrophilicity of composition readily tune properties such as extent of water uptake, particle diffusion, and release profiles.[6-9] The size and shape of hydrogels also play important roles in optimizing their suitability for various applications.[10-12]

Additive manufacturing, or 3D-printing, enables production of objects with precise control over material arrangement in three-dimensional space. Several types of additive manufacturing exist suitable for a wide array of materials such as metals, ceramics, composites, and polymers.[13-16] These various techniques include extrusion-based techniques such as fused deposition modeling and direct-write printing; powder bed strategies such as selective laser sintering, selective laser melting, and binder jetting; and photoirradiation processes such as stereolithography (SLA) and microstereolithography (μSL).[13, 17-25] Optimization of the process to minimize defects and reduce production times serves to reduce manufacturing costs and enables custom fabrication of parts for applications such as personalized biomedical devices.[26-31]

By far, the largest application for 3D-printed hydrogels is as cell scaffolding for tissue engineering. Employing additive manufacturing processes to fabricate these parts generally utilizes jetting or stereolithograpy techniques.[23] In most cases, the hydrogel formation occurs in the absence of water, and the resulting part is then post-swelled, which may lead to loss of feature resolution or changed mechanical properties.[32-33] One notable exception from Zhang *et al.* exploited the lower critical solution temperature and shear thinning behavior of poly(isopropyl glycidyl ether-*b*-ethylene oxide-*b*-isopropyl glycidyl ether) in water for direct-write printing of non-covalent hydrogels.[34] The limitations and suitability of various techniques for hydrogel printing are well reviewed in the literature.[35-

[37] However, the literature lacks reports of printing already-swollen hydrogels from aqueous solutions using SLA or μSL.

Poly(vinyl alcohol) (PVOH) results from the hydrolysis of poly(vinyl acetate) (PVA) and demonstrates water solubility. The hydroxyl group present in each repeat unit provides a reactive handle for polymer modification to further enable a range of applications from fuel cells, heavy metal adsorbents, and biomedical materials.[38-39] PVOH modified with pendant acrylamide groups previously provided the bases for contact lenses when photopolymerized in conjunction with other hydrophilic monomers.[40-45] In one particular case, the photopolymerized networks encapsulated pristine unmodified PVOH and demonstrated time-dependent release profiles with implications for delivery of therapeutics from contact lenses.[41] That study demonstrated the feasibility of photocuring aqueous PVOH solutions with high efficiency. However, no reports exist wherein this strategy extends into three dimensions, as enabled with stereolithographic techniques.

The present study details the evaluation of photocured hydrogels for potential extension into μSL fabrication techniques. Decoration of poly(vinyl alcohol) (PVOH) with pendant acrylamide groups through acid-catalyzed transacetalization afforded a water soluble, photocurable matrix. Curing an aqueous solution of the modified PVOH with increasing poly(ethylene glycol) diacrylate (PEGDA) content afforded pre-swollen gels. Photocalorimetry examined the thermodynamics of the curing process, and photorheology served to characterize mechanical properties of the hydrogels during and after curing.

8.3 Experimental

8.3.1 Materials

Poly(vinyl alcohol) (PVOH, M_w = 9,000-10,000 g/mol, 80% hydrolyzed), acryloyl chloride, aminoacetaldehyde dimethyl acetal, triethylamine (Et_3N), hydroquinone, Iragcure-2959, and poly(ethylene glycol) diacrylate (PEGDA, average molecular weight 575 g/mol) were purchased from Sigma Aldrich and used without further purification. All other solvents were purchased from Spectrum Chemical and used without further purification.

8.3.2 Analytical Methods

^{1}H NMR spectroscopy was performed on a Varian 400 MHz spectrometer at ambient temperature in D_2O or $CDCl_3$. Thermogravimetric analysis (TGA) was performed on a TA Instruments Q500 operating under a nitrogen atmosphere at a 10 °C/min temperature ramp. Differential scanning calorimetry was performed on a TA Instruments Q2000 differential scanning calorimeter operating under a constant 50 mL/min nitrogen purge. A heat/cool/heat procedure was performed from -80 °C to 150 °C at a 10 °C/min heating ramp and 100 °C/min cooling rate. Gel fractions were determined by Soxhlet extraction with water as the extraction solvent. Photocalorimetry experiments (PhotoDSC) were performed at 25 °C on a TA Instruments Q1000 equipped with a TA Q Series PCA photoirradiation attachment operating over a spectral range of 250-650 nm at an intensity of 22 mW/cm^2 from an Omnicure S2000 UV source. Samples of mass 20 ± 1 mg and nominal thickness 2 mm were analyzed in an open pan under a nitrogen atmosphere. The same UV source and intensity were used to perform photorheology on a TA Instruments Discovery HR-2 operating in oscillation mode at 0.3% strain, 10 Hz, and 25 °C using 20 mm parallel plate geometry and Smart Swap™ UV curing accessory.

8.3.3 Synthesis of acrylamide modifier

Synthesis of the acrylamide modifier was performed according to the following procedure. Aminoacetaldehyde dimethyl acetal (20.0 g, 0.19 mol), Et_3N (64 mL, 0.46 mol), and dichloromethane (DCM, 50 mL) were added to a clean, dry 250 mL, round-bottomed flask equipped with magnetic stirring and placed in an ice water bath. Acryloyl chloride (18.4 mL, 0.23 mol) was added dropwise slowly over 90 min and the reaction was allowed to warm to room temperature and subsequently proceeded for 18 h. Triethylammonium chloride precipitate was removed from the reaction mixture by vacuum filtration. The filtrate was concentrated under rotary evaporation, then washed in a separatory funnel twice with DI H_2O and once with aqueous NaOH (5% w/w). The resulting DCM phase was dried over Na_2SO_4 and the solvent was removed by rotary evaporation, yielding a yellow liquid in 80.3% yield. ^{1}H NMR δ (ppm) 6.28 (1H), 6.12 (1H), 5.67 (1H), 4.41 (1H), 3.50 (2H), 3.38 (6H)

8.3.4 Modification of PVOH

The transacetalization of PVOH with the acrylamide modifier was adapted from an established procedure and performed as follows.[40] 80.0 mL H_2O was added to 25.0 g PVOH in a clean, dry, 250 mL, round-bottomed flask equipped with magnetic stirring. The mixture was heated to 90 °C to facilitate dissolution of PVOH, then cooled to room temperature. 20.0 g HCl and 60 mL additional H_2O were added to flask along with 250 mg hydroquinone inhibitor, and the mixture was stirred until homogenous in a room temperature water bath. The desired amount of acrylamide modifier was then added directly to the reaction vessel, which was allowed to stir for 24 h. The modified PVOH product was isolated by dropwise precipitation into a large excess of acetone with vigorous stirring. The supernatant was decanted and the precipitate was washed thoroughly with

ethanol to remove any lingering acid and dried. The product and 500 mg hydroquinone were dispersed in a minimal amount of H_2O at room temperature with vigorous stirring. The final dispersion was 7.7 wt% polymer in water.

8.4 Results and discussion

8.4.1 Modification of PVOH

The acryloyl chloride reaction with the primary amine of aminoacetaldehyde dimethyl acetal yielded the acrylamide dimethyl acetal modifier in good yield (**Scheme 8.1**). The solubility of the acrylamide-containing product in water reduced the isolated yield from the crude reaction product, but overall isolated, purified yield still exceeded 80% of the theoretical yield. The acrylamide dimethyl acetal product readily underwent acid-catalyzed transacetalization with the hydroxyl groups of PVOH (**Scheme 8.2**). Selection of PVOH with M_w = 9-10 kg/mol served to decrease polymer dissolution time and to reduce solution viscosity. The modification reaction conditions also served to cleave simultaneously any residual acetate groups on the parent polymer. Sufficiently dilute conditions mitigated the possibility of interchain transacetalization and therefore crosslinking. Similarly, the presence of hydroquinone radical inhibitor prevented the premature curing of the acrylamide functionalities.

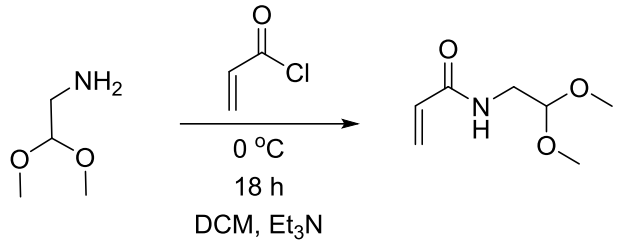

Scheme 8.1. Synthesis of acrylamide dimethyl acetal modifier.

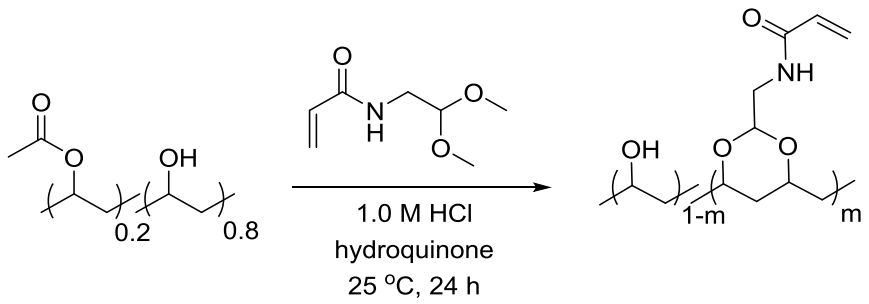

Scheme 8.2. Transacetalization modification of acrylamide dimethyl acetal compound with PVOH.

Intrachain transacetalization likely favored the reaction of adjacent hydroxyls due to the favorable thermodynamics of forming a six-membered ring rather than larger cyclics.[46-47] ^{1}H NMR spectroscopy determined the extent of the modification reaction, revealing compositions that featured 2.4, 4.3, and 11.7 acrylamide units on average per polymer chain. These acrylamide-bearing PVOH samples were designated as PVOH-A_x, where x represented the average number of acrylamide functional groups per polymer chain.

8.4.2 Photocuring of PVOH-based solutions

Addition of 2 wt% of the water-soluble photoinitiator Irgacure-2959 (PI) to the aqueous solutions of acrylamide-decorated PVOH enabled photocuring with a 365 nm lamp operating at 22 mW/cm^2 (**Scheme 8.3**). PVOH-$A_{2.4}$ and PVOH-$A_{4.3}$ exhibited no qualitative changes after 10 min exposure to UV irradiation. The lack of curing likely resulted from the abundance of water, which exhibits strong absorbance bands in the UV spectral range; the presence of hydroquinone which prevented premature curing; and the low concentration of acrylamide units in the solution. However, the PVOH-A_{11} solution demonstrated significant curing evidenced by the formation of a cured gel after only 5 min irradiation. The obtained held its own weight, but did not exhibit the mechanical strength

required for additive manufacturing. This was likely due to relatively low concentration of polymer in solution, only 7.7 wt% solids.

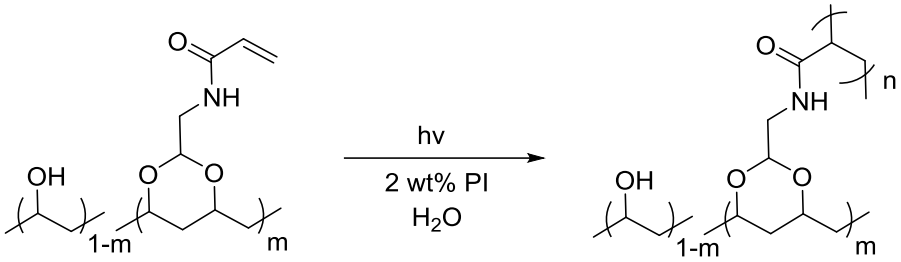

Scheme 8.3. Photocuring of PVOH-A_x aqueous solutions to afford hydrogels.

Then, a more in-depth study revealed the importance of both PI and water on the curing process. Irradiation of PVOH-$A_{11.7}$ with and without solvent, and with and without PI generated four polymer networks. Soxhlet extractions of the dried films with water determined the gel fractions, and therefore the efficiency of the photocrosslinking step (**Table 8.1**). In the presence of both water and PI, the resulting network demonstrated 98% gel fraction, while a similar solution with no PI crosslinked to yield a network with 72% gel fraction. Casting a PVOH-$A_{11.7}$ solution with 2 wt% PI yielded a heterogeneous film with visible PI crystals in a PVOH-$A_{11.7}$ matrix. Irradiating this film provided a network with only 56% gel fraction, a significant decrease from the solution phase samples. In the presence of neither PI nor solvent, the curing step only achieved 22% gel content. These results highlighted the relevance of each component for attaining efficient crosslinking. Water provided chain mobility and allowed pendant acrylamides to exist in close proximity in the solution state, while PI increased radical concentration and therefore curing efficiency. Immersion of extracted films of PVOH-$A_{11.7}$-based networks in water for 72 h further evaluated their water uptake. The network obtained by irradiating a solution of

PVOH-$A_{11.7}$ with PI demonstrated 477 wt% uptake of water, while the film obtained from the solution with no PI exhibited 434 wt% uptake of water.

Table 8.1. Effects of photoinitiator and water content on gel fraction for PVOH-$A_{11.7}$ networks.[a]

Photoinitiator	Water	Gel fraction (wt%)	Water uptake (wt%)
+	+	98	477
+	−	56	ND
−	+	72	434
−	−	22	ND

[a] + present, − absent; ND = not determined

Because the cured hydrogel of PVOH-$A_{11.7}$ failed to hold its own weight, addition of poly(ethylene glycol) diacrylate (PEGDA) served to increase the crosslink density and weight fraction of the gel relative to water. Adding an increasing amount of PEGDA to the PVOH-$A_{11.7}$ solution revealed an upper limit of homogeneity at 15 wt% PEGDA relative to the total solution, at which time PVOH-$A_{11.7}$ precipitated. Three ternary compositions of PEGDA, PVOH-$A_{11.7}$, and water were made and photocured (**Scheme 8.4**) with 2 wt% PI relative to the total solids (**Table 8.2**). All compositions exhibited visible photocuring evidenced by the formation of mechanically robust gels with high gel fractions.

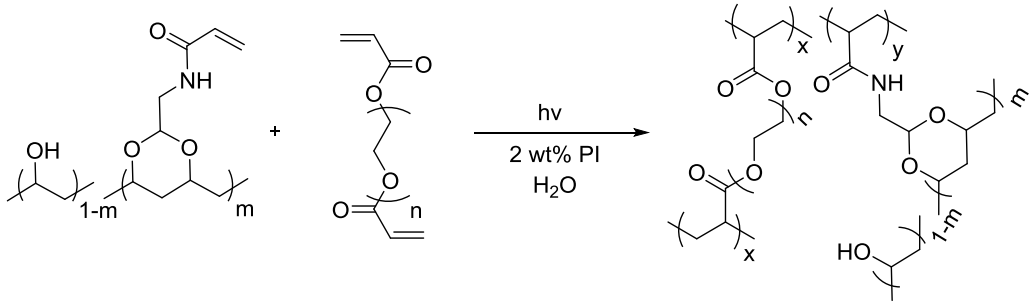

Scheme 8.4. Photocured hydrogels containing both PVOH-$A_{11.7}$ and PEGDA.

Table 8.2. Summary of ternary hydrogel compositions and properties.

Sample	PVOH-$A_{11.7}$ content (wt%)[a]	PEGDA content (wt%)[a]	Total solids (wt%)[b]	Water content (wt%)[b]	Gel fraction (wt%)[c]	$T_{d,5\%}$ (°C)[c]

PVOH-$A_{11.7}$-1	100	0	7.7	92.3	98	248
PVOH-$A_{11.7}$-2	55.5	44.5	13.1	86.9	97	247
PVOH-$A_{11.7}$-3	39.3	60.7	17.5	82.5	98	251
PVOH-$A_{11.7}$-4	33.3	66.7	20.0	80.0	99	255

[a] Relative to total solids; [b] relative to hydrogel, [c] determined for dehydrated gels

8.4.3 Photocalorimetry and photorheology

Photocalorimetry of the PVOH-$A_{11.7}$ solutions with increasing PEGDA content revealed the increasing intensity of the curing exotherm with increasing PEGDA incorporation (**Figure 8.1**). As the double bond concentration increased in the sample solution, the exotherm increased. For PVOH-$A_{11.7}$-3 and PVOH-$A_{11.7}$-4, multiple small exotherms were observed after the initial curing exotherm. This likely resulted from sample shrinkage away from the edges of the calorimeter pan as the sample cured, leading to the exposure of uncured resin to UV around the edges. All liquid solutions filled the bottom of the sample pan; however, after the calorimetry experiments, the PVOH-$A_{11.7}$-3 and PVOH-$A_{11.7}$-4 samples were solids that did not cover the bottom of the pan. A second irradiation step at the 19 min mark clearly revealed the lack of further photocuring in the experiments.

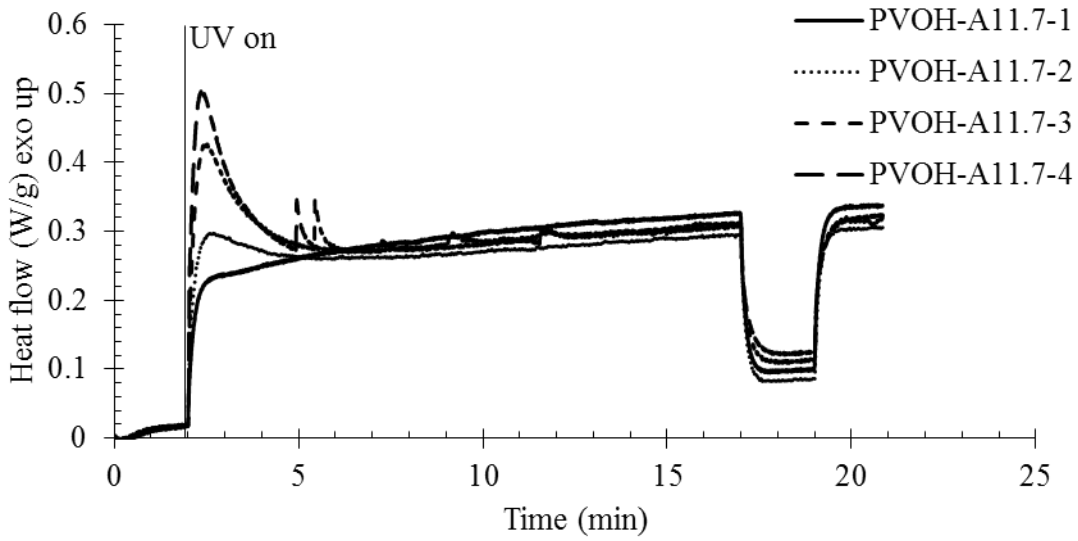

Figure 8.1. Photocalorimetry of aqueous solutions of PVOH-$A_{11.7}$ with increasing PEGDA.

Replication of the photocalorimetry experiments for PVOH-$A_{11.7}$-3 and PVOH-$A_{11.7}$-4 served to reveal the variability of the observed multiple exotherms (**Figure 8.2**). The secondary exotherms appeared at different times and with different intensities, pointing to the complicated dynamics of photocuring in solution. However, for µSL applications, the cure times for individual layers generally do not exceed 30 s. Minimizing exposure to UV during the manufacturing process could further mitigate shrinkage of the fabricated part.

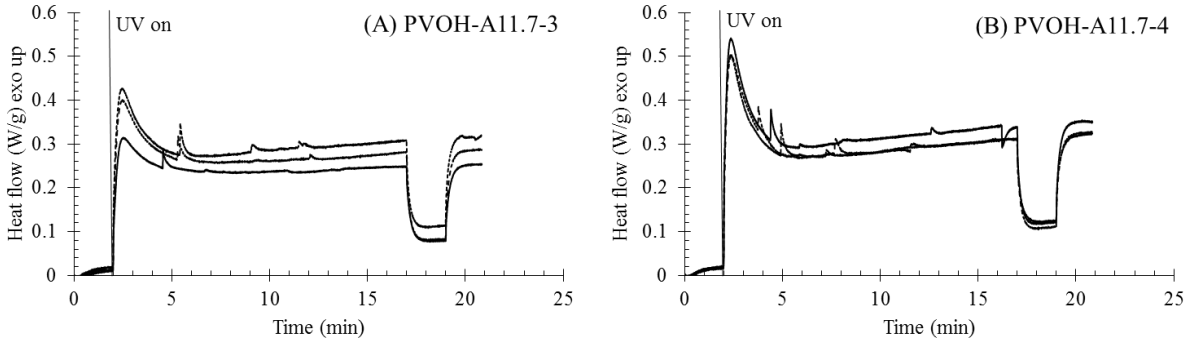

Figure 8.2. Variability in multiple exotherms observed using photocalorimetry for (A) PVOH-$A_{11.7}$-3 and (B) PVOH-$A_{11.7}$-4.

Photorheology confirmed the trend of increasing photocuring extent with increasing PEGDA content by demonstrating the more rapid storage modulus response to UV irradiation upon increasing the PEGDA content and therefore wt% total solids. The initial slopes of the modulus upon irradiation corresponded to the rate of the photocuring process, demonstrating that as PEGDA increased, the photocuring of the solution occurred faster. Similarly, the plateau moduli remained relatively constant over time for the samples containing PEGDA, while the sample without any additional PEGDA crosslinker present exhibited a continually rising modulus. The rising modulus after a low initial modulus increase regime likely resulted from inefficient but slowly continuing curing. The PEGDA-containing samples reached a consistent plateau modulus and remained there, likely indicating the lack of further curing over time. Similarly, the PEGDA-containing samples exhibited increasing storage moduli with increasing PEGDA-content, consistent with a higher degree of crosslinking. Discontinuities in the storage modulus plateau over time likely resulted from slipping of the rheometer upper plate as the experiment proceeded, perhaps as a consequence of sample contraction upon photocuring.

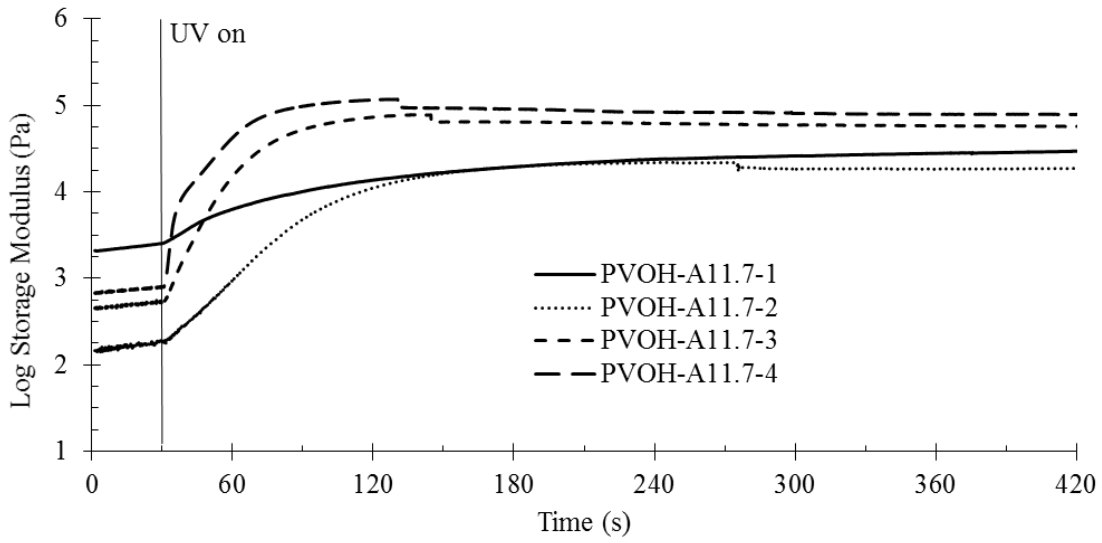

Figure 8.3. Photorheology of aqueous solutions containing PVOH-$A_{11.7}$ and PEGDA. The vertical line at t = 30 s corresponds to the start of UV irradiation.

Sample contraction and polymerizable group concentration played a large role in the photocuring process. Further investigations into the direct fabrication of hydrogels by additive manufacturing must consider volumetric and geometric changes in part dimensions; the relative amount of excluded solvent upon curing, the mechanical strength of the part to support its hydrated weight, and the efficiency and extent of photocuring. Exclusion of water during the photocuring process will reduce the concentration of polymerizable groups in the remaining resin and therefore change cure kinetics. The present study served to highlight and underscore the importance of these factors for employing μSL to fabricate hydrogels.

8.5 Conclusions

Poly(vinyl alcohol) served as the basis for hydrogels photocured directly from solution. Synthesis of an acrylamide dimethylacetal modifier enabled facile acid-catalyzed transacetalization to provide PVOH with varied extents of pendant, photocurable

acrylamide groups. Photocuring solutions of acrylamide-modified PVOH revealed the formation of a hydrogel only in PVOH-$A_{11.7}$, which was selected for further investigation. Adding PEGDA changed the concentration of photocurable groups in the solution, which changed the dynamics of the curing process. Photocalorimetry and photorheology more closely examined the effects of adding PEGDA on the curing process, and revealed the effects of complicated dynamics on the curing process.

8.6 Acknowledgments

This work is supported in part by Procter & Gamble. The authors acknowledge the Macromolecular Materials Discovery Center at Virginia Tech for instrument support.

8.7 References

1. Hoare, T. R.; Kohane, D. S., Hydrogels in drug delivery: Progress and challenges. *Polymer* **2008,** *49* (8), 1993-2007.
2. Mellati, A.; Dai, S.; Bi, J.; Jin, B.; Zhang, H., A biodegradable thermosensitive hydrogel with tuneable properties for mimicking three-dimensional microenvironments of stem cells. *RSC Advances* **2014,** *4* (109), 63951-63961.
3. Wang, K. L.; Burban, J. H.; Cussler, E. L., Hydrogels as separation agents. In *Responsive Gels: Volume Transitions II*, Dušek, K., Ed. Springer Berlin Heidelberg: Berlin, Heidelberg, 1993; pp 67-79.
4. Buwalda, S. J.; Boere, K. W. M.; Dijkstra, P. J.; Feijen, J.; Vermonden, T.; Hennink, W. E., Hydrogels in a historical perspective: From simple networks to smart materials. *Journal of Controlled Release* **2014,** *190*, 254-273.
5. Hennink, W. E.; van Nostrum, C. F., Novel crosslinking methods to design hydrogels. *Advanced Drug Delivery Reviews* **2002,** *54* (1), 13-36.
6. Ahmed, E. M., Hydrogel: Preparation, characterization, and applications: A review. *Journal of Advanced Research* **2015,** *6* (2), 105-121.
7. Deligkaris, K.; Tadele, T. S.; Olthuis, W.; van den Berg, A., Hydrogel-based devices for biomedical applications. *Sensors and Actuators B: Chemical* **2010,** *147* (2), 765-774.
8. Hoffman, A. S., Hydrogels for biomedical applications. *Advanced Drug Delivery Reviews* **2002,** *54* (1), 3-12.
9. Nuttelman, C. R.; Henry, S. M.; Anseth, K. S., Synthesis and characterization of photocrosslinkable, degradable poly(vinyl alcohol)-based tissue engineering scaffolds. *Biomaterials* **2002,** *23* (17), 3617-3626.
10. Talei Franzesi, G.; Ni, B.; Ling, Y.; Khademhosseini, A., A Controlled-Release Strategy for the Generation of Cross-Linked Hydrogel Microstructures. *Journal of the American Chemical Society* **2006,** *128* (47), 15064-15065.
11. Bulmus, V.; Chan, Y.; Nguyen, Q.; Tran, H. L., Synthesis and Characterization of Degradable p(HEMA) Microgels: Use of Acid-Labile Crosslinkers. *Macromolecular Bioscience* **2007,** *7* (4), 446-455.

12. Murthy, N.; Thng, Y. X.; Schuck, S.; Xu, M. C.; Fréchet, J. M. J., A Novel Strategy for Encapsulation and Release of Proteins: Hydrogels and Microgels with Acid-Labile Acetal Cross-Linkers. *Journal of the American Chemical Society* **2002,** *124* (42), 12398-12399.
13. Kenzari, S.; Bonina, D.; Marie Dubois, J.; Fournée, V., Complex metallic alloys as new materials for additive manufacturing. *Science and Technology of Advanced Materials* **2014,** *15* (2), 024802.
14. Zhang, X.; Jiang, X.; Sun, C., Micro-stereolithography of polymeric and ceramic microstructures. *Sens Actuators A: Phys* **1999,** *77*.
15. Dul, S.; Fambri, L.; Pegoretti, A., Fused deposition modelling with ABS–graphene nanocomposites. *Composites Part A: Applied Science and Manufacturing* **2016,** *85*, 181-191.
16. Matsuzaki, R.; Ueda, M.; Namiki, M.; Jeong, T.-K.; Asahara, H.; Horiguchi, K.; Nakamura, T.; Todoroki, A.; Hirano, Y., Three-dimensional printing of continuous-fiber composites by in-nozzle impregnation. *Scientific Reports* **2016,** *6*, 23058.
17. Wendel, B.; Rietzel, D.; Kühnlein, F.; Feulner, R.; Hülder, G.; Schmachtenberg, E., Additive Processing of Polymers. *Macromolecular Materials and Engineering* **2008,** *293* (10), 799-809.
18. Yap, C. Y.; Chua, C. K.; Dong, Z. L.; Liu, Z. H.; Zhang, D. Q.; Loh, L. E.; Sing, S. L., Review of selective laser melting: Materials and applications. *Applied Physics Reviews* **2015,** *2* (4), 041101.
19. Zein, I.; Hutmacher, D. W.; Tan, K. C.; Teoh, S. H., Fused deposition modeling of novel scaffold architectures for tissue engineering applications. *Biomaterials* **2002,** *23*.
20. Kitson, P. J.; Glatzel, S.; Chen, W.; Lin, C.-G.; Song, Y.-F.; Cronin, L., 3D printing of versatile reactionware for chemical synthesis. *Nat. Protocols* **2016,** *11* (5), 920-936.
21. Mohamed, O. A.; Masood, S. H.; Bhowmik, J. L., Optimization of fused deposition modeling process parameters: a review of current research and future prospects. *Advances in Manufacturing* **2015,** *3* (1), 42-53.
22. Farahani, R. D.; Chizari, K.; Therriault, D., Three-dimensional printing of freeform helical microstructures: a review. *Nanoscale* **2014,** *6* (18), 10470-10485.
23. Chia, H. N.; Wu, B. M., Recent advances in 3D printing of biomaterials. *Journal of Biological Engineering* **2015,** *9* (1), 1-14.
24. Bertsch, A.; Lorenz, H.; Renaud, P., 3D microfabrication by combining microstereolithography and thick resist UV lithography. *Sensors and Actuators A: Physical* **1999,** *73* (1–2), 14-23.
25. Bertsch, A.; Zissi, S.; Jézéquel, Y. J.; Corbel, S.; André, C. J., Microstereophotolithography using a liquid crystal display as dynamic mask-generator. *Microsystem Technologies 3* (2), 42-47.
26. Dawood, A.; Marti, B. M.; Sauret-Jackson, V.; Darwood, A., 3D printing in dentistry. *Br Dent J* **2015,** *219* (11), 521-529.
27. Noort, R., The future of dental devices is digital. *Dent Mater* **2012,** *28*.
28. Odde, D. J.; Renn, M. J., Laser-guided direct writing of living cells. *Biotechnol Bioeng* **2000,** *67*.
29. Jose, R. R.; Rodriguez, M. J.; Dixon, T. A.; Omenetto, F.; Kaplan, D. L., Evolution of Bioinks and Additive Manufacturing Technologies for 3D Bioprinting. *ACS Biomaterials Science & Engineering* **2016**.
30. He, Y.; Xue, G.-h.; Fu, J.-z., Fabrication of low cost soft tissue prostheses with the desktop 3D printer. *Scientific Reports* **2014,** *4*, 6973.
31. Norotte, C.; Marga, F. S.; Niklason, L. E.; Forgacs, G., Scaffold-free vascular tissue engineering using bioprinting. *Biomaterials* **2009,** *30*.
32. Studart, A. R., Additive manufacturing of biologically-inspired materials. *Chemical Society Reviews* **2016,** *45* (2), 359-376.

33. Skoog, S.; Goering, P.; Narayan, R., Stereolithography in tissue engineering. *Journal of Materials Science: Materials in Medicine* **2014,** *25* (3), 845-856.
34. Zhang, M.; Vora, A.; Han, W.; Wojtecki, R. J.; Maune, H.; Le, A. B. A.; Thompson, L. E.; McClelland, G. M.; Ribet, F.; Engler, A. C.; Nelson, A., Dual-Responsive Hydrogels for Direct-Write 3D Printing. *Macromolecules* **2015,** *48* (18), 6482-6488.
35. Billiet, T.; Vandenhaute, M.; Schelfhout, J.; Vlierberghe, S.; Dubruel, P., A review of trends and limitations in hydrogel-rapid prototyping for tissue engineering. *Biomaterials* **2012,** *33*.
36. Stanton, M. M.; Samitier, J.; Sanchez, S., Bioprinting of 3D hydrogels. *Lab on a Chip* **2015,** *15* (15), 3111-3115.
37. Kirchmajer, D. M.; Gorkin Iii, R.; in het Panhuis, M., An overview of the suitability of hydrogel-forming polymers for extrusion-based 3D-printing. *Journal of Materials Chemistry B* **2015,** *3* (20), 4105-4117.
38. Moulay, S., Review: Poly(vinyl alcohol) Functionalizations and Applications. *Polymer-Plastics Technology and Engineering* **2015,** *54* (12), 1289-1319.
39. Anseth, K. S.; Metters, A. T.; Bryant, S. J.; Martens, P. J.; Elisseeff, J. H.; Bowman, C. N., In situ forming degradable networks and their application in tissue engineering and drug delivery. *Journal of Controlled Release* **2002,** *78* (1–3), 199-209.
40. Kennedy, J. P.; Subramanyam, U., Polymer networks, process for producing same, and products made therefrom. Google Patents: 2010.
41. Winterton, L. C.; Lally, J. M.; Sentell, K. B.; Chapoy, L. L., The elution of poly (vinyl alcohol) from a contact lens: The realization of a time release moisturizing agent/artificial tear. *Journal of Biomedical Materials Research Part B: Applied Biomaterials* **2007,** *80B* (2), 424-432.
42. Mühlebach, A.; Müller, B.; Pharisa, C.; Hofmann, M.; Seiferling, B.; Guerry, D., New water-soluble photo crosslinkable polymers based on modified poly(vinyl alcohol). *Journal of Polymer Science Part A: Polymer Chemistry* **1997,** *35* (16), 3603-3611.
43. Müller, B. Photocrosslinked polymers. 5508317, 1996.
44. Müller, B. Photocrosslinked polymer. 5789464, 1998.
45. Müller, B. Photocrosslinked polymers. 5849810, 1998.
46. Galli, C.; Illuminati, G.; Mandolini, L., Ring-closure reactions. I. Kinetics of lactone formation in the range of seven- to twelve-membered rings. *Journal of the American Chemical Society* **1973,** *95* (25), 8374-8379.
47. Casadei, M. A.; Galli, C.; Mandolini, L., Ring-closure reactions. 22. Kinetics of cyclization of diethyl (ω-bromoalkyl)malonates in the range of 4- to 21-membered rings. Role of ring strain. *Journal of the American Chemical Society* **1984,** *106* (4), 1051-1056.

Chapter 9: Overall Conclusions

Controlled radical polymerization using the reversible addition-fragmentation chain transfer (RAFT) polymerization technique afforded synthesis of a library of ABA triblock copolymers. The central acrylic block readily underwent post-polymerization modification to yield a triblock copolymer with reinforcing polystyrene A blocks and poly(methylimidazolium acrylate) B blocks. Incorporation of ionic liquid (IL) induced a drastic morphology change, which resulted in enhanced ionic conductivity. The IL-containing membrane demonstrated a mechanical response to applied electric potential and proved suitable for use as an actuator.

A systematic examination of the influence of ionic liquid choice on the thermal properties of binary IL-sulfonated polymer mixtures generated structure-property relationships. Similarly, investigation of lithium bis(trifluoromethylsulfonyl)imide's ($LiTf_2N$) influence on the physicochemical properties of the corresponding IL 1-ethyl-3-methylimidazolium bis(trifluoromethylsulfonyl)imide (EMIm Tf_2N) upon addition in varying amounts. Anionic polymerization and subsequent post-polymerization modification afforded poly(*t*-butyl styrene-*b*-styrene-4-lithium sulfonate-*b*-*t*-butyl styrene). Using the relationships observed for the two binary mixtures allowed generation of ternary block copolymer electrolytes that featured poly(*t*-butyl styrene-*b*-styrene-4-lithium sulfonate-*b*-*t*-butyl styrene) as the polymeric component enabled evaluation of sulfonated styrenic block copolymers as a platform for ternary polymer electrolytes in battery applications.

Neutralization with 2-(dimethylamino)ethyl methacrylate (DMAEMA) of a commercially available sulfonated styrenic pentablock copolymer yielded a product with

similar microphase-separated morphology and photocurable counterions. UV irradiation secured this morphology and imparted covalent linking of the ammonium countercations to each other. The resulting membrane exhibited an extended service window of thermomechanical properties, reduced water uptake and water vapor transport rate, and similar NaCl permeability when compared to the sulfonic acid-containing parent polymer. The presence of ionic interactions also allowed the material to heal physical defects. Optical microscopy directly imaged the healing of indentations on the surface of the films, and tensile testing demonstrated the recovered mechanical properties of samples upon a healing step. The simple two-step modification strategy therefore resulted in significantly enhanced properties and imparted healing capability to the material.

The rational design and facile synthesis of stimulus-responsive crosslinkers enabled fabrication of 3D-printed parts by microstereolithography μSL. Crosslinkers featured acid-labile functionalities as tertiary alkyl esters or hydrolytically instable poly(lactide-*co*-glycolide) (PLGA) ester bonds. Varying the amount of functional crosslinker present in a poly(ethylene glycol) methacrylate (PEGMA)-based resin changed the properties and degradation profiles of the fabricated objects. The timeframe of degradation ranged from 6h to 20 d. These stimulus-responsive objects may ultimately prove relevant as support materials for other additive manufacturing techniques. Furthermore, the PLGA-based objects could demonstrate use as degradable tissue scaffolds.

Modification of poly(vinyl alcohol) (PVOH) yielded a series of water-soluble polymers with varied amounts of photocurable pendant acrylamide groups. Increasing the acrylamide concentration resulted in more facile and efficient photocuring of the solutions. Addition of poly(ethylene glycol) diacrylate (PEGDA) to the solutions served to enhance

the mechanical strength of the hydrogels. Photocalorimetry and photorheology demonstrated the change in curing kinetics, and also demonstrated the various factors requiring consideration for directly photocuring hydrogels in three dimensions from aqueous solutions.

Chapter 10: Suggested Future Work

10.1 Ionic crosslinkers for microstereolithography

To date, efforts in developing materials to enhance additive manufacturing techniques focus largely on engineering thermoplastics for fused deposition modeling or hot melt extrustion. Microstereolithography (μSL), however, represents an exciting opportunity for polymer chemists to explore. As a greater emphasis is placed on green chemistry, researchers continue to investigate light as a reagent to induce chemical changes, such as polymerization or crosslinking, to the benefit of μSL. While more attention lies with incorporating a functional monomers into the μSL process, continued progress in crosslinker synthesis will serve to further enhance the tunability of the resulting objects' properties.

In that vein, ionic crosslinkers in particular prove interesting. A previous literature example featured up to 10 wt% of styrenic ionic liquid monomer crosslinked with 90 wt% of uncharged diacrylate.[1] Objects printed with ionic crosslinkers in addition to ionic liquid monomers should exhibit higher conductivity. As μSL technology increases to yield smaller feature sizes and improved resolution, tunable ionic resin properties may enable additive manufacturing of circuits in three dimensions, which would be an exciting advancement within the field.

Ammonium, phosphonium, pyridinium, and imidazolium ions receive much attention in the literature. Employing commonly used monomers as functional quaternizing agents would enable synthesis of difunctional crosslinkers. Acrylate- or methacrylate-containing monomers represent promising building blocks due to the photosensitivity of those functionalities under UV curing conditions relative to styrenic compounds. **Figure**

10.1 below shows the structures of some functional quaternizing agents and quaternizable monomers, all of which are commercially available. Quaternizing agents include 2-bromoethyl acrylate and 4-vinylbenyzl chloride. Quaternizable monomers include 1-vinylimidazole, DMAEMA, diphenylphosphinostyrene, and 4-vinylpyridine. Combination of these monomers would yield structures as shown in **Figure 10.2**. The synthesis of the divinyl crosslinkers would proceed in a single quaternization step, which may prove useful for potential commercialization. Subsequent anion exchange offers another variable to finely tune glass transition and melting temperatures of the resulting ionic crosslinkers.

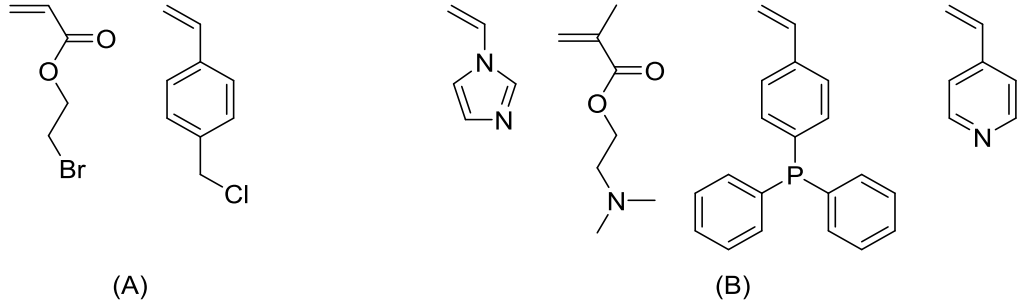

Figure 10.1. Structures of (A) monomeric quaternizing agents and (B) quaternizable monomers.

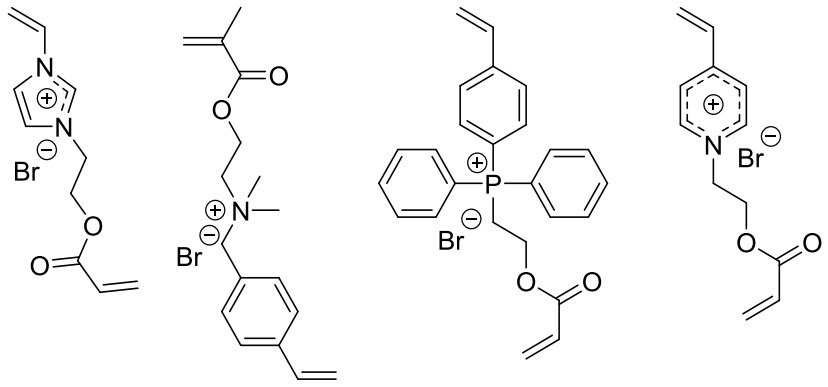

Figure 10.2. Structures of several potential difunctional crosslinkers that each feature at least one acrylate or methacrylate functionality.

Doubly-charged difunctional crosslinkers represent another subgroup of ionic crosslinkers. Similar chemistry would see the two quaternizable monomers linked by an alkyl dihalide according to **Scheme 10.1**. While DMAEMA is shown here, 4-vinylpyridine and 1-vinylimidazole may exhibit similar reactivity to yield doubly-charged divinyl crosslinkers. **Scheme 10.2** demonstrates the potential synthesis of a doubly-charged diacrylate beginning with a DABCO ditertiary amine and an acrylic quaternizing agent. Research on DABCO-containing monomers has proceeded for a few years in our group, and the reactivity towards quaternization is well established. Similarly, the thermal degradation pathway of the diquaternized product is well understood and ion exchange to more bulky, less basic counteranions serves to increase its thermal stability and depress glass transition and melting temperatures. In all of the examples listed in this section, ion exchange exists as a valuable tool for adjusting the thermal properties of the compound for μSL compatibility, as well as the thermal, electrochemical, and conductivity properties of the printed object.

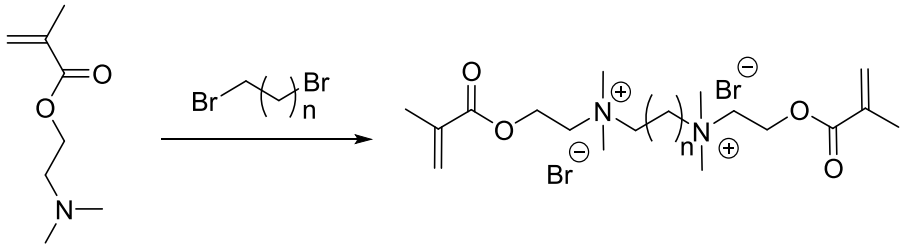

Scheme 10.1. The reaction of a quaternizable monomer with an alkyl dibromide to yield a doubly-charged crosslinker.

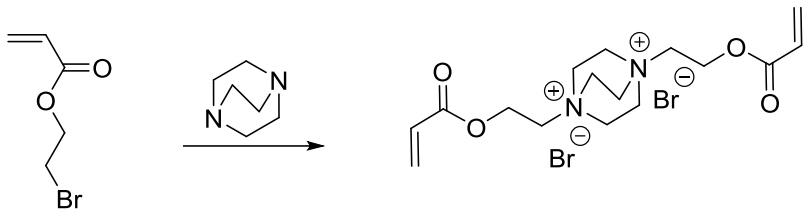

Scheme 10.2. The reaction of a DABCO with 2-bromoethyl acrylate to afford a proposed doubly-charged diacrylic crosslinker.

Another potential route for ion-containing crosslinkers to improve μSL lies in the association of ionic groups between the uncured recoat layer and the previous printed layer. These ionic interactions could improve layer adhesion at the interface. Because hydrogen bonding also affects the mechanical strength of cured networks, the interplay and potential synergy of hydrogen bonding and ionic interactions to afford enhanced interlayer adhesion represents an interesting avenue of exploration.[2] One potential monomer exploits an imidazolium-based diol and further reacts it with an isocyanate-containing methacrylate to afford a small molecule crosslinker with potential for both ionic and hydrogen bonding interactions to improve interlayer adhesion in the μSL process (**Scheme 10.3**).[3]

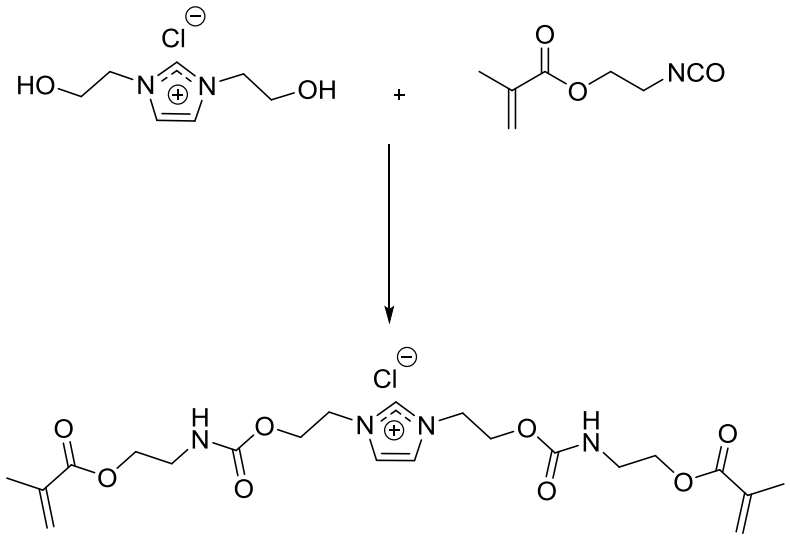

Scheme 10.3. Proposed difunctional urethane methacrylate crosslinker that features the imidazolium functionality.

10.2 Direct fabrication of hydrogels from microstereolithography

As discussed previously, many factors must be considered in the direct fabrication of pre-swollen hydrogels from μSL. Judicious crosslinker selection and resin formulation should account for the concentration of polymerizable groups, the volume of excluded water upon crosslinking, resin viscosity, and curing kinetics. To that end, simplifying the crosslinker structure to multifunctional poly(ethylene glycol) (PEG) acrylates would provide a starting point for streamlining resin formulation. Similarly, a more highly crosslinked network with low molecular weight between crosslinks will likely exclude more water than one with greater molecular weight between crosslinks. A looser network should more readily host water. To achieve this, water-soluble PEG diacrylate (PEGDA) with PEG molecular weight ≥ 1 kg/mol may provide sufficient molecular weight between crosslinks to prevent significant exclusion of water. Because it holds that acrylate concentration will decrease given increasing PEGDA molecular weight with constant polymer concentration, the acrylate concentration could be further tuned with the inclusion of a smaller, multifunctional acrylate such as Sartomer SR 494 or trimethylolpropane ethoxylate triacrylate (**Figure 10.3**).

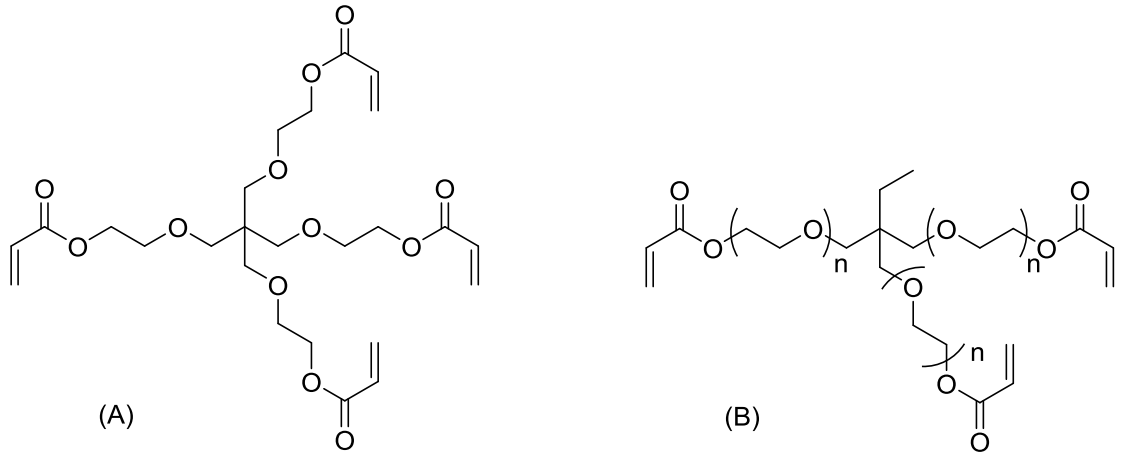

Figure 10.3. Structures of (A) Sartomer SR 494 and (B) trimethylolpropane ethoxylate triacrylate multifunctional water-soluble acrylates.

10.3 References

1. Schultz, A. R.; Lambert, P. M.; Chartrain, N. A.; Ruohoniemi, D. M.; Zhang, Z.; Jangu, C.; Zhang, M.; Williams, C. B.; Long, T. E., 3D Printing Phosphonium Ionic Liquid Networks with Mask Projection Microstereolithography. *ACS Macro Letters* **2014,** *3* (11), 1205-1209.
2. Karikari, A. S.; Edwards, W. F.; Mecham, J. B.; Long, T. E., Influence of Peripheral Hydrogen Bonding on the Mechanical Properties of Photo-Cross-Linked Star-Shaped Poly(d,l-lactide) Networks. *Biomacromolecules* **2005,** *6* (5), 2866-2874.
3. Gao, R.; Zhang, M.; Wang, S.-W.; Moore, R. B.; Colby, R. H.; Long, T. E., Polyurethanes Containing an Imidazolium Diol-Based Ionic-Liquid Chain Extender for Incorporation of Ionic-Liquid Electrolytes. *Macromolecular Chemistry and Physics* **2013,** *214* (9), 1027-1036.